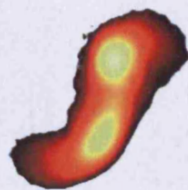


Things that go bump in the night: the dynamics & hydrodynamics of stellar clusters



A thesis submitted for the degree of
Doctor of Philosophy
at the University of Leicester.

by

Timothy James Adams

Theoretical Astrophysics Group
Department of Physics and Astronomy
University of Leicester

July 2003

UMI Number: U493795

All rights reserved

INFORMATION TO ALL USERS

The quality of this reproduction is dependent upon the quality of the copy submitted.

In the unlikely event that the author did not send a complete manuscript and there are missing pages, these will be noted. Also, if material had to be removed, a note will indicate the deletion.



UMI U493795

Published by ProQuest LLC 2013. Copyright in the Dissertation held by the Author.
Microform Edition © ProQuest LLC.

All rights reserved. This work is protected against
unauthorized copying under Title 17, United States Code.



ProQuest LLC
789 East Eisenhower Parkway
P.O. Box 1346
Ann Arbor, MI 48106-1346

©Tim Adams 2003.

**This Thesis is copyright material and no quotation from it may be
published without proper acknowledgement.**

**Things that go bump in the night:
the dynamics and hydrodynamics of stellar clusters.
Timothy James Adams**

Abstract

I examine some of the dynamical interactions which occur in stellar clusters. I examine how a population of brown dwarfs will evolve within a cluster, in an attempt to explain the discrepancy between observational results and theoretical models regarding the number of brown dwarfs in a stellar cluster. I find that it is unlikely that the entire brown dwarf population could be expelled from the cluster in less than many dynamical relaxation times. Instead I propose that it is likely that the majority of the brown dwarfs are instead in binary systems with brighter companions which hide them from view.

I have also modelled the formation of blue stragglers through the collision of two main-sequence stars. I propose that the angular momentum problem that other authors have found with blue stragglers formed via off-axis collisions can be resolved by considering the angular momentum loss associated with a stellar wind or locking to a disc. I show that both can quickly reduce the angular momentum of the merged object to the point where it can contract down to the main-sequence.

I have examined the possibility of explaining the apparent paucity of red giants in the cores of post-core-collapse globular clusters through collisions with binary systems and with single stars. I show that such collisions often result in a bound system, where the red giant envelope acts as a common envelope and is eventually dispersed. I also show that such collisions can remove up to 17% of the red giant population.

I have developed a new implementation of the SPH technique which allows particles of very different masses to be included in the same simulation. I perform tests with particles with masses differing by a factor of 10^9 and find the method to be robust.

In memory of my father, who didn't quite manage to see me finish...

Thomas William Adams, 15-12-1925 – 16-9-2001

Acknowledgements

First and foremost I must thank my supervisor Melvyn Davies. His boundless optimism for the various bits of work presented here have ensured that they were finished. He was an excellent supervisor, and any student would be lucky to work with him. A thank you must also go to Alison Sills, my oft referred to Canadian collaborator.

I must say thank you to all the people whom I have had the pleasure of working with (either directly or indirectly), if I were to try and list them all here this thesis would get even bigger, and frankly it's long enough already!

Thank you to all the people who I have had the pleasure of sharing an office with over the past three years; Fraser, Anna, Mike, Louise, Owen, Sam, Dave, Jon, Yohann and Rosie.

A huge thank you to all my family who have helped me through my university career, showing interest even if they didn't have a clue as to what I was blathering on about! Thank you to Mum, aunty Marj and uncle Tom. Thank you to those who are no longer with us, my father, my aunty Anne and my uncle Fred. I suppose I should thank my sister as well, wonder what for? 😊

Thank you to those who I have lived with over the past three years, namely Steve and Louise. Thank you for providing me with something else to do other than work.

I'd like to thank the computer staff here at the university, in particular Dr Chris Rudge and Stuart Poulton for all their efforts. The simulations presented here were performed on UKAFF, HEX (funded through the EPSRC strategic equipment initiative) and the theoretical astrophysics group Linux cluster, supported a PPARC rolling grant, The Royal Society, AMD, 3-com and Crucial.

Financial support in the form of a PPARC studentship is gratefully acknowledged.

I'd better do one last blanket thank you to all those whom I haven't mentioned directly. This doesn't mean you're not appreciated, it just means that I need to try and keep the number of pages of thesis down!

Declaration

I hereby declare that this thesis has not been submitted either in full or in part for any other degree at this or any university. All work has been performed either on my own, or in collaborations where I put in the majority of the work.

The following papers have resulted from the work presented here:

Chapter 2

Brown dwarf populations in open clusters

Adams, Davies, Jameson & Scally. *MNRAS* 2002

Chapter 4

High-resolution simulations of stellar collisions between equal-mass main-sequence stars in globular clusters

Sills, Adams, Davies & Bate *MNRAS* 2002

Blue stragglers as stellar collision products: The angular momentum question

Sills, Adams & Davies *MNRAS* 2003 in prep

Chapter 5

On the origin of red giant depletion by means of low velocity collisions

Adams, Davies & Sills *MNRAS* 2003

A handwritten signature in black ink, appearing to read 'Tim Adams', with a stylized flourish at the end.

Tim Adams

July 2003

Contents

1	Introduction	17
1.1	Introduction	17
1.2	Open clusters	18
1.3	Globular Clusters	21
1.4	Generalised Dynamics	24
1.4.1	Virial equilibrium	25
1.4.2	Timescales within a cluster	29
1.4.3	Close encounters	34
1.4.4	Two-body scattering	36
1.4.5	Density profiles	36
1.4.6	Core collapse	38
1.4.7	Staving off core collapse	39
1.5	Stellar collisions	40
1.6	Thesis Overview	43
2	Brown dwarfs	47
2.1	Introduction	47
2.2	Theory	50

2.2.1	Dynamics of the Cluster	50
2.2.2	Binary population dynamics	51
2.3	Initial Conditions	54
2.3.1	Stellar population	54
2.3.2	Brown dwarf population	55
2.3.3	Binary population	55
2.3.4	Length scales in the N-Body code	57
2.4	Numerical Results	59
2.4.1	Overall evolution of the cluster	59
2.4.2	Comparison to the Pleiades cluster	67
2.4.3	Future evolution	67
2.5	Discussion	70
2.5.1	Evolution of the Cluster	70
2.5.2	Evolution of the binary population	70
2.5.3	Brown dwarf - brown dwarf binaries	77
2.5.4	Binary system visibility	78
2.5.5	Brown dwarf cooling & the binary second sequence	80
2.5.6	Probabilities of finding a brown dwarf	81
2.6	Conclusions	85
3	Oil-on-water	89
3.1	Introduction	89
3.2	Theory	91
3.2.1	The Kernel function W	93
3.2.2	SPH application	94

3.2.3	Artificial viscosity	96
3.2.4	The problem with SPH	97
3.3	Numerical Methods	101
3.4	Testing the method	103
3.4.1	Initial testing	103
3.4.2	Single star	104
3.4.3	Rotating star	104
3.4.4	Wide binary	107
3.4.5	Eccentric binary	111
3.4.6	Permanent Roche lobe overflow in an eccentric system	115
3.4.7	Circular systems	118
3.5	Astrophysical uses	125
4	Blue stragglers	129
4.1	Introduction	129
4.2	Theory	132
4.2.1	Stellar models	133
4.3	Resolution	134
4.3.1	Convection zones	138
4.3.2	Effects of rotation	140
4.4	Off-axis collisions	140
4.4.1	Simulation parameters	142
4.5	Results	144
4.6	Evolution	151
4.6.1	Mass and angular momentum loss	152

4.7	Another way?	161
4.8	Conclusions	166
5	Red-giant depletion	169
5.1	Introduction	169
5.2	Observations	171
5.3	Theory	172
5.3.1	Possible outcomes of red-giant binary collisions	172
5.3.2	Common envelopes	177
5.3.3	Knock outs	183
5.3.4	Collision probabilities	184
5.3.5	Red giant models	186
5.4	Numerical Methods	186
5.4.1	4-body code	187
5.4.2	Hydrodynamical simulations	188
5.5	Results	189
5.5.1	Determination of interaction timescales	189
5.5.2	Detailed hydrodynamics	192
5.6	Subsequent evolution	199
5.7	Other methods	200
5.8	Conclusions	205
6	Conclusions and future work	209
6.1	Future work	209

SPECIAL NOTE

**ITEM SCANNED AS SUPPLIED
PAGINATION IS AS SEEN**

The CD-ROM provided at the end of this thesis contains a number of animations of the computer simulations described in this text. The CD itself is of the CD-R format and cannot be overwritten. The animations are in the .mpeg formats: they can be played by most movie-playing software packages on any major platform and operating system. A CD icon appears at the relevant points in the thesis text, with a description of each movie.

Whilst every effort has been taken to ensure that the CD is free from any defects and faults, including computer viruses, the author does not take any responsibility for the same. Use of the CD is entirely at the user's risk. The author does not take any responsibility whatsoever for any loss of whatever nature which may be incurred as a result of using this CD.

Chapter 1

Introduction to stellar clusters

1.1 Introduction

The night sky presents us with an interesting question. Why do some stars have very few neighbours, perhaps just a binary companion or sometimes none at all (the majority of stars do at least have a binary companion see for example (Richichi, Leinert, Jameson & Zinnecker 1994)) whilst other stars are seen to be in amalgamations with other stars where the number of neighbours can run into the hundreds of thousands? The populations are in-fact related. Stars, such as our own sun, seldom form in isolation. Instead they are formed in groups of a few (such as ρ Ophiuchus (Klose 1986)), or sometimes in groups of many thousands of stars such as M80 (Harris & Racine 1974). Stars are formed through the collapse of a part of a giant molecular cloud (Jeans 1902, Spitzer 1949). The more massive the part of the cloud which is collapsing, the more stars we are likely to get.

Star formation seems to be an intrinsically inefficient process. Only a few percent of the mass which was in the initial gas cloud goes into forming stars (see for example Wilking & Lada (1983)). The rest of the mass tends to get blown away by the winds of the newly formed stars. The efficiency of the star formation will determine some of the subsequent evolution of the stars. If over 50% of the original gas mass is lost, then the stars will not be bound together, thus the stars will move away from one another. If

less of the initial gas mass is lost, the stars which were formed together will tend to stay together.

If the stars are within one of these bound structures, how do they go to being relatively isolated in the field. Within this bound group the stars move around on orbits, and will occasionally undergo interactions with their neighbours. These interactions will change the kinetic energy of the two stars. Eventually, after a sufficient number of interactions it is possible for a star to climb out of the potential well of the cluster and become unbound. It will then go on to form part of the galactic disc.

These bound groups of stars are referred to as stellar clusters. In this thesis, I am going to look at some of the interactions which occur within these clusters. I will not be looking at unbound stellar groups like ρ Ophiuchus. I'm going to try to explain some of the observations made of clusters. Before I do that, I need to lay down the framework of what a cluster is, and how it evolves. That is the purpose of this chapter. I will give a more in-depth introduction to each problem that I look at the start of each subsequent chapter.

1.2 Open clusters

There are two types of clusters: open clusters and globular clusters. Open clusters contain, typically, a few thousand stars in a loosely bound amalgamation. The fact that these clusters are loosely bound mean that they tend to dissociate on a relatively short time scale. Interactions between the stars within the cluster result in stellar members being ejected from the system and going off to become part of the galactic disk. Most open clusters are relatively young, with very few seen with ages over a Gyr (Binney & Tremaine 1987).

It is within such an environment that our own star was born and subsequent interactions led to it being expelled from its cluster and it becoming a member of the galactic disc.

There are some 10^5 open clusters in our galaxy, virtually all are contained within the



FIGURE 1.1. A picture of the Pleiades cluster located some 110 pc away from the Earth. The Pleiades cluster is a fairly typical open cluster, it is still quite young (around 125 million years old). It has served as a good hunting ground for objects known as brown dwarfs as I shall discuss more in chapter 2. Image courtesy of Astroscopic Labs, [http : //www.lichta.de/AstroWeb/gallery_fullsize.php3?iSOId = 5&iBPId = 109](http://www.lichta.de/AstroWeb/gallery_fullsize.php3?iSOId=5&iBPId=109)

galactic plane (Binney & Tremaine 1987). This means that a great many are obscured from view by dust in the plane and the galactic bulge. In chapter 2, I present a table detailing the properties of some of the nearby open clusters (page 71).

Much work has been done on the evolution of open clusters, both through observations and numerical modelling of the processes which go on within them. Terlevich (1987) demonstrated the use of n-body modelling techniques, when she successfully modelled the evolution of a set of small open clusters right through to their evaporation. Since this time both our understanding and the increased performance of computing facilities have enabled us to perform simulations of stellar clusters which are more realistic in terms of the numbers of stars that a cluster contains. Indeed we are now in a position where we are able to model the collapse of a small gas cloud and watch the formation of stars and brown dwarfs (Bate, Bonnell & Bromm 2003). These simulations have started to confirm observations of features such as the shape of the initial mass function (IMF) (i.e. how many stars of a particular mass are created within a cluster). Work by Luhman, Rieke, Young, Cotera, Chen, Rieke, Schneider & Thompson (2000) has demonstrated a strong similarity between the Initial mass functions (IMF) of the Trapezium, Pleiades and M35 open clusters. They performed sensitive, high-resolution imaging of the central portion of the Trapezium cluster utilising the Near-Infrared Camera and Multi-Object Spectrometer (NICMOS) aboard the Hubble Space telescope, as well as performing ground based observations to take K-band spectra for many of their sources. Their methodology allowed observations of objects well below the hydrogen burning limit and so we are now beginning to get a full explanation of the galactic field IMF. Confirmation of the IMF of clusters has forced us to confront one of the more awkward questions with regard to open clusters; what has happened to the all the brown dwarfs? Brown dwarfs are failed stars. As they were being formed within the cluster, their mass never became high enough to start hydrogen burning in their cores. Theory predicts that many brown dwarfs should be formed within open clusters, however, observations are finding only a relatively small number within sampled clusters (Pinfield, Jameson & Hodgkin 1998, Hambly, Hodgkin, Cossburn & Jameson 1999, Pinfield, Hodgkin, Jameson, Cossburn, Hambly & Devereux 2000, Gizis, Reid & Monet 1999, Reid &

Mahoney 2000). I look into this question and put forward a number of suggestions for a solution to this conundrum in Chapter 2. Much of the observational work on looking for Brown dwarfs has focused on a relatively near by open cluster known as the Pleiades (an image of the cluster is shown in Fig. 1.1).

Due to its young age and proximity, the Pleiades cluster is an excellent hunting ground for brown dwarfs. Many surveys have been made of this cluster; Hambly et al. (1999) performed a survey in the I and R bands and identified nine distinct single brown dwarf candidates. Further surveys have yielded more brown dwarf candidates within the cluster, notably a recent survey (Pinfield et al. 2000) has identified 30 possible brown dwarfs in a six square degree survey of the cluster. Of particular interest is the work of Pinfield et al. (1998). Their examination of the dynamics of the Pleiades cluster lead them to believe that there could be as many as several thousand unseen brown dwarfs. If this is the case it is important to understand why so few brown dwarfs have been found within the central portions of the cluster which have been so well studied. The young age of the cluster means that it is relatively unlikely that the brown dwarfs could have cooled to a point far beyond detection, instead one tends to look for a more dynamical explanation for their apparent depletion. In chapter 2, I detail my extensive modelling of a population of brown dwarfs in a cluster very similar in structure to the Pleiades. I also go on to consider how age will further hamper efforts to find brown dwarfs in older, yet closer, open clusters such as the Hyades.

1.3 Globular Clusters

Globular clusters are much more massive than open clusters. They contain around $10^5 - 10^6$ stars and those of our galaxy represent some of the oldest objects in the universe. They are made up of population II stars (i.e. those with a very low metallicity) indicating that they were formed before any appreciable nuclear burning of the hydrogen formed during the creation of the universe had taken place. In some interacting galaxies (for instance NGC 7714), we see a population of globular clusters which are actually relatively young (10^8 yrs or so (Lançon & Boily 2000).)

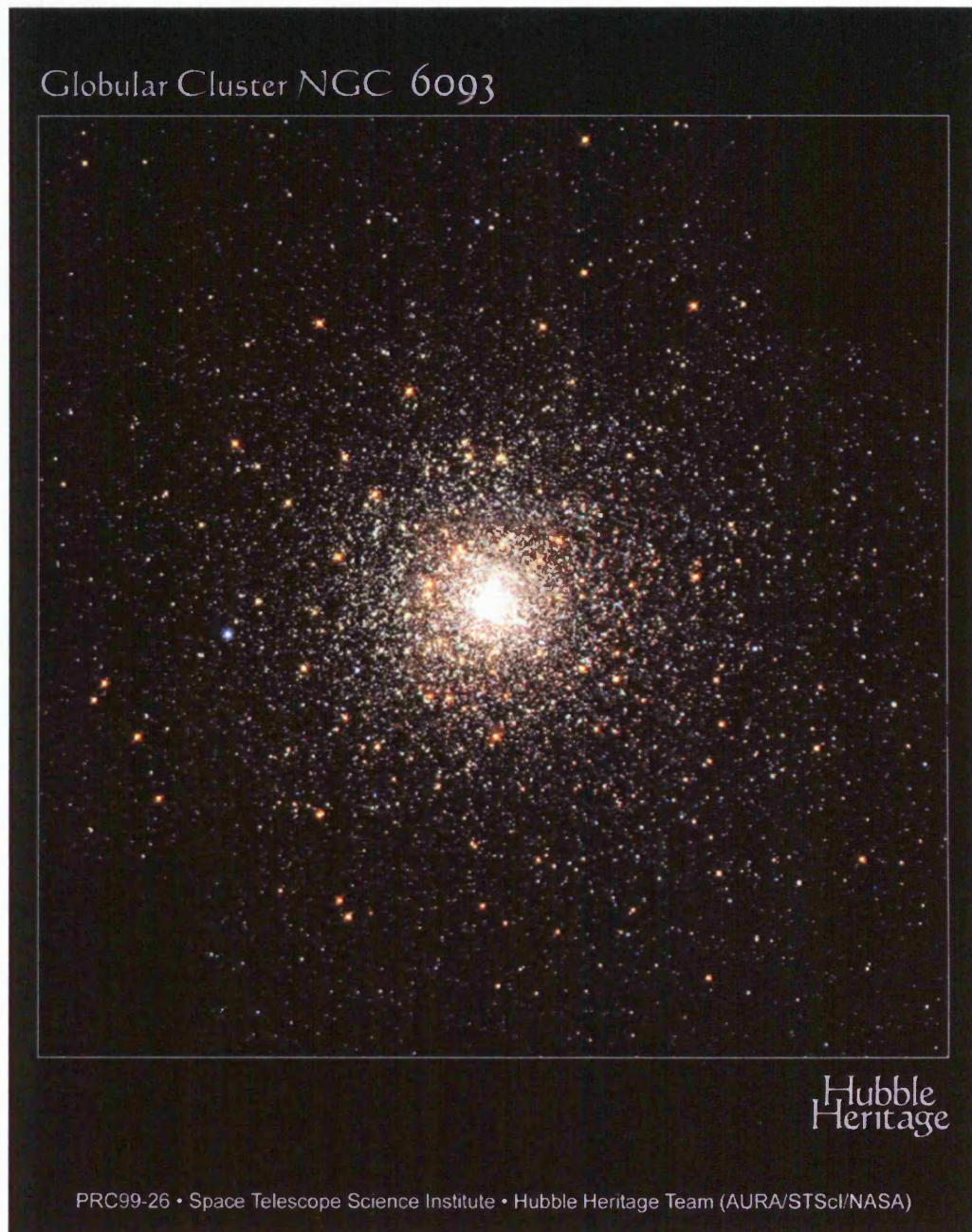


FIGURE 1.2. An image of the globular cluster M80. M80 is one of the densest globular clusters within our galaxy. It lays approximately 8 kpc from the Earth and has an age of around 15 billion years. Image courtesy of STScI, funded under grant NAS5-26555.

As can be seen in Fig. 1.2 a globular cluster has a large range in its surface brightness as a function of its radius. For most globular clusters there is a central region where the brightness of the cluster levels off to a fairly constant level. In some globular clusters however, we find that the surface brightness continues to increase down to the smallest resolvable radius (King 1985). Such clusters are said to have central cusps. These cusps are believed to be related to the process of core collapse which I shall discuss in Section 1.4.6.

The Milky Way has some 150-200 globular clusters, over half of these are contained within 10kpc of the galactic centre. The rest are spread out around the galaxy, with some at around 50kpc from the galactic centre (Harris & Racine 1979). Many of these globular clusters lie outside of the galactic plane, in relative isolation from the rest of the galaxy. Due to their much higher mass, globular clusters are more resistant to breaking up (i.e. losing stars from their outer boundaries) than open clusters. Although they can be disrupted, there is theoretical evidence to believe that the number of globular clusters used to be much higher (Gnedin & Ostriker 1997). Indeed, we see globular clusters dissociating today (Odenkirchen *et al.* 2001).

The ages of globular clusters are determined by examining their Hertzsprung-Russell diagrams. A globular cluster represents essentially an instantaneous burst of star formation with all the stars in the cluster formed at the same time. This means that the cluster should have a sharp turn-off on the main sequence. It is then a question of understanding stellar evolution to calculate the age of the cluster in question. Although globular clusters are supposed to have a sharp turn-off on the main sequence, observations have shown that in most globular clusters there exists a population of stars which exist beyond this turn-off point, this means that they appear bluer than the rest of the stellar population and for this reason they are known as blue stragglers (Sandage 1953). These blue straggler stars apparently have a mass higher than they should for the cluster age, so the question is how do they still exist? Stellar evolution cannot readily explain the existence of a population of stars heavier than the turn off mass of a cluster still being on the main sequence, and it is highly unlikely that there could have been a second wave of star formation within the cluster as any free gas would likely have been expelled by the

winds of the original stellar population. Instead there have been attempts to explain this population through collisions and subsequent mergers of lower mass stars. In chapter 4 I examine the possibility of forming blue stragglers through direct collisions between stars. It is easy to show that stellar collisions are inevitable within a dense environment like a globular cluster, what we need to do is understand the outcomes of these collisions.

The presence of blue stragglers within the HR diagram is not the only apparent stellar evolution oddity for globular clusters. Observations of post-core-collapse clusters have indicated that there is some proportion, maybe as high as 50% (Djorgovski & Piotto 1993) of the clusters' red giant population missing. It is believed that this depletion is a genuine effect and not related to observational techniques (i.e. only being able to view some fraction of the cluster). This effect is not seen in non-post-core-collapse clusters. I investigate some possible mechanisms for destroying a proportion of the red giant population in chapter 5.

At one time, it was believed that globular clusters didn't contain any binary stars (Gunn & Griffin 1979). This was to change when globular clusters were examined in the X-ray part of the electromagnetic spectrum. Satellite observations of several globular clusters revealed a population of X-ray sources, recognised to be interacting binary systems (see Verbunt & Hut (1987)). The discovered sources were relatively bright, low-mass X-ray binaries. These are composed of a neutron star (or black hole) which is accreting material from a low-mass main-sequence star and they have typical luminosities of 10^{36-38} erg/s. With more sensitive detectors, observations have found a population of cataclysmic variables within globular clusters (see for example Grindlay, Heinke, Edmonds, Murray & Cool (2001)). Globular clusters contain more interacting binary systems per unit mass than the disc of the galaxy. This suggests that there must be some environmental factor in a globular which is beneficial to the creation of interacting binaries.

1.4 Generalised Dynamics

Both open and globular clusters have their evolution dominated by Newtonian gravity. As a result the equation of motion for all of the stars within a cluster is simply:

$$\ddot{\mathbf{r}}_i = -G \sum_{j=1, j \neq i}^N m_j \frac{\mathbf{r}_i - \mathbf{r}_j}{|\mathbf{r}_i - \mathbf{r}_j|^3} \quad (1.1)$$

This one equation determines many of the characteristics of a cluster. It tells us how a cluster will evolve and how long it will take, it also tells us about how the stars will be distributed within the cluster. There are some effects which alter the cluster that Eqn. 1.1 doesn't tell us about. For instance, it doesn't deal with the evolution of the stars within the cluster, and it doesn't allow for tidal dissipation events. There are external factors which can influence the evolution of a cluster. The external potential due to the host galaxy can lead to shock heating of a cluster (Spitzer & Chevalier 1973), and this can alter the internal dynamics of the cluster.

As the stars within the cluster orbit around the centre of the cluster's potential, they will occasionally undergo interactions with one another (these interactions are described in subsequent sections). These interactions lead to a redistribution of the energy within the cluster. The lighter stars tend to pick up energy and move further away from the centre of the cluster, whilst the heavier stars tend to lose energy and sink toward the core of the cluster. These interactions will lead to a change in the stellar distribution within the cluster, with most of the heavy stars being concentrated toward the core and the lighter stars being further out.

1.4.1 Virial equilibrium

The Virial theorem can be used to describe the distribution of energies within a bound system like a cluster of stars. A derivation can be made by considering the quantity:

$$Q = \sum_i \mathbf{p}_i \cdot \mathbf{r}_i \quad (1.2)$$

where \mathbf{p}_i is the linear momentum and \mathbf{r}_i is the position vector for particle i in a system of particles. If the time derivative of Q is taken, we get:

$$\frac{dQ}{dt} = \sum_i \left(\frac{d\mathbf{p}_i}{dt} \cdot \mathbf{r}_i + \mathbf{p}_i \cdot \frac{d\mathbf{r}_i}{dt} \right) \quad (1.3)$$

We can consider this expression one term at a time. The left hand side may be rewritten as:

$$\begin{aligned} \frac{dQ}{dt} &= \frac{d}{dt} \sum_i m_i \frac{d\mathbf{r}_i}{dt} \cdot \mathbf{r}_i \\ &= \frac{d}{dt} \sum_i \frac{1}{2} \frac{dm_i r_i^2}{dt} \end{aligned} \quad (1.4)$$

If we use the definition of the moment of inertia for the system:

$$I = \sum_i m_i r_i^2 \quad (1.5)$$

then Eqn. 1.4 may be expressed as:

$$\frac{dQ}{dt} = \frac{1}{2} \frac{d^2 I}{dt^2} \quad (1.6)$$

So we can now re-express Eqn. 1.3 as:

$$\frac{1}{2} \frac{d^2 I}{dt^2} - \sum_i \mathbf{p}_i \cdot \frac{d\mathbf{r}_i}{dt} = \sum_i \frac{d\mathbf{p}_i}{dt} \cdot \mathbf{r}_i \quad (1.7)$$

Now we can consider the second term on the left hand side of this expression. We may expand it thus:

$$\begin{aligned} \sum_i \mathbf{p}_i \cdot \frac{d\mathbf{r}_i}{dt} &= \sum_i m_i \mathbf{v}_i \cdot \mathbf{v}_i \\ &= 2 \sum_i \frac{1}{2} m_i v_i^2 \\ &= 2U \end{aligned} \quad (1.8)$$

i.e. this second term is simply twice the kinetic energy of the system. We can now look at the right hand side of Eqn. 1.7. If we use Newton's second law, we may rewrite it as:

$$\frac{d\mathbf{p}_i}{dt} \cdot \mathbf{r}_i = \sum_i \mathbf{F}_i \cdot \mathbf{r}_i \quad (1.9)$$

where \mathbf{F}_i is the total force on particle i . If we consider how this force is made up, i.e. look at all the contributions from other particles (j), then:

$$\sum_i \mathbf{F}_i \cdot \mathbf{r}_i = \sum_i \left(\sum_{j, j \neq i} \mathbf{F}_{ij} \right) \cdot \mathbf{r}_i \quad (1.10)$$

recalling Newton's third law allows us to rewrite this as:

$$\begin{aligned} \sum_i \mathbf{F}_i \cdot \mathbf{r}_i &= \frac{1}{2} \sum_i \left(\sum_{j, j \neq i} (\mathbf{F}_{ij} - \mathbf{F}_{ji}) \cdot \mathbf{r}_i \right) \\ &= \frac{1}{2} \sum_i \left(\sum_{j, j \neq i} \mathbf{F}_{ij} \cdot (\mathbf{r}_i - \mathbf{r}_j) \right) \end{aligned} \quad (1.11)$$

The force due to each particle in the system may be expressed as:

$$\mathbf{F}_{ij} = \frac{Gm_i m_j}{|\mathbf{r}_i - \mathbf{r}_j|^2} \hat{\mathbf{r}}_{ij} \quad (1.12)$$

where $\hat{\mathbf{r}}_{ij}$ is the unit vector between particles i and j . Thus Eqn. 1.11 may be expressed as:

$$\begin{aligned} \sum_i \mathbf{F}_i \cdot \mathbf{r}_i &= \frac{1}{2} \sum_i \left(\sum_{j, j \neq i} \frac{Gm_i m_j}{|\mathbf{r}_i - \mathbf{r}_j|^3} (\mathbf{r}_i - \mathbf{r}_j)^2 \right) \\ &= \frac{1}{2} \sum_i \sum_{j, j \neq i} \frac{Gm_i m_j}{|\mathbf{r}_i - \mathbf{r}_j|} \end{aligned} \quad (1.13)$$

where the right hand side of this expression is clearly the total gravitational potential energy (the factor of 1/2 takes account of the double counting associated with the double sum), Ω of the system.

Eqn. 1.7 can thus now be expressed as (if we consider time averaged quantities):

$$\left\langle \frac{1}{2} \frac{d^2 I}{dt^2} \right\rangle - 2 \langle U \rangle = \langle \Omega \rangle \quad (1.14)$$

In the case of a bound orbit (as is appropriate for stars within a cluster) the change in the moment of inertia is zero. Thus we may express the Virial theorem as:

$$2U + \Omega = 0 \quad (1.15)$$

The Virial theorem applies to any gravitationally bound system and has some important consequences. The total energy of the cluster will be given by the sum of the potential and gravitational energy:

$$E_{\text{tot}} = U + \Omega \quad (1.16)$$

we can replace Ω by using equation 1.15, thus:

$$E_{\text{tot}} = -U \quad (1.17)$$

Let's consider what happens when the cluster loses energy over time:

$$\frac{dE_{\text{tot}}}{dt} = -\frac{dU}{dt} \quad (1.18)$$

So as the cluster loses energy, the kinetic energy of the stars increases, or in simple terms; as the cluster loses energy its stars move faster. Any gravitationally bound system exhibits this negative heat capacity (Binney & Tremaine 1987). This negative heat capacity has serious consequences for the cluster and will be described in section 1.4.6.

1.4.2 Timescales within a cluster

The interactions mentioned in the previous section are associated with various timescales. In turn the evolution of cluster is then determined by these timescales.

Crossing time

The simplest timescale for a cluster is its crossing time. This simply refers to how long it takes a star to travel from one point in a cluster to another. Typically we look at two versions of the crossing time, the cluster crossing time (the period taken to go from one side to the other) and the half-mass crossing time (the time to move across the part of the cluster containing half the total cluster mass.) Thus the crossing time may be expressed as:

$$t_{\text{cross}} = \frac{R}{v} \quad (1.19)$$

where R is the appropriate radius and v is the velocity dispersion within the cluster, or:

$$t_{\text{half}} = \frac{R_{\text{half}}}{v} \quad (1.20)$$

where R_{half} is the half mass radius for the cluster.

In the case of open clusters such as the Pleiades, the cluster crossing time is of order 10-15 million years. Whilst for a globular cluster where the velocity dispersion is much higher the crossing time is of order 10^5 years (Binney & Tremaine 1987).

Relaxation time

The relaxation time may be defined as the period it takes for a star within a cluster to undergo a sufficient number of scatterings (see Section 1.4.4) that it forgets what its original velocity was; i.e. $|\delta v| = |\underline{v}|$.

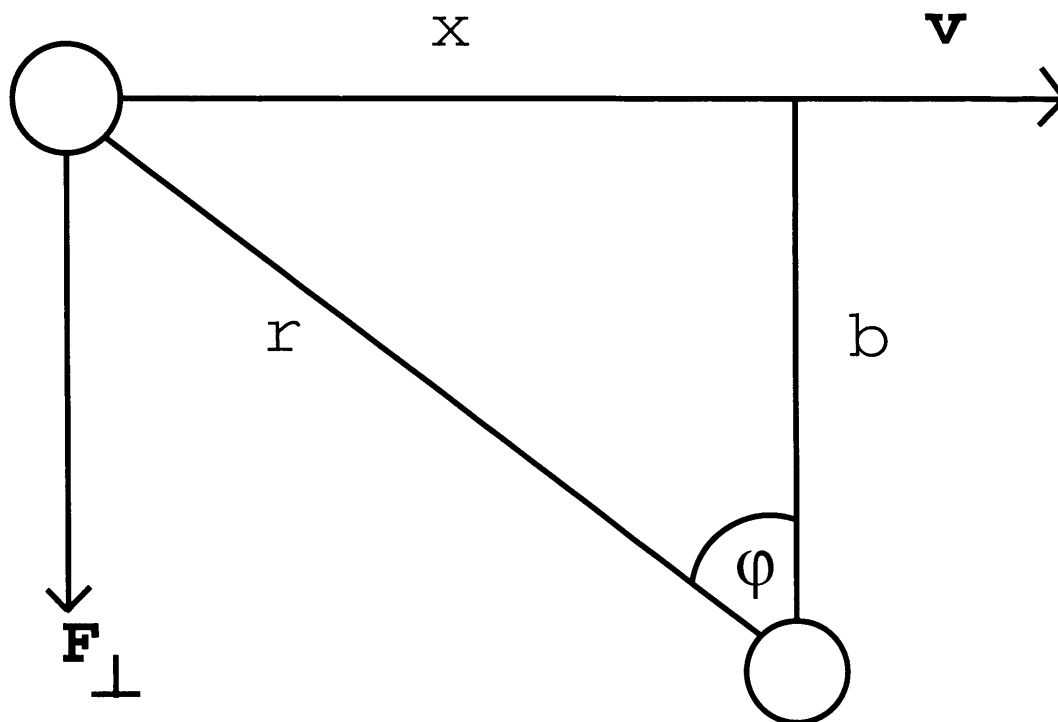


FIGURE 1.3. Schematic for the derivation of the relaxation time in a cluster. As two stars pass, their paths are deflected by their mutual gravitational attraction, this deflection is known as scattering. After a sufficient number of scattering events the star “forgets” what its initial velocity was, this leads to the definition of the relaxation time.

One may make a derivation based on Fig. 1.3. As two stars pass one another within a cluster, they both experience a force component which is perpendicular to their direction of motion. This force causes a change in their velocity. If we consider just the perpendicular component of the force, then:

$$\begin{aligned}
 F_{\perp} = m\dot{v}_{\perp} &= \frac{Gm_1m_2}{r^2} \cos \varphi \\
 &= \frac{Gm_1m_2}{b^2 + x^2} \cos \varphi \\
 &= \frac{Gm_1m_2b}{(b^2 + x^2)^{\frac{3}{2}}}
 \end{aligned} \tag{1.21}$$

x is the distance travelled by a star in a time t at a velocity v . If we assume for the sake of simplicity that $m_1=m_2$ then Eqn. 1.21 may be rewritten as:

$$F_{\perp} = \frac{Gm^2}{b} \left[1 + \left(\frac{vt}{b} \right)^2 \right]^{-\frac{3}{2}} \tag{1.22}$$

thus the change in v_{\perp} is simply:

$$\dot{v}_{\perp} = \frac{Gm}{b^2} \left[1 + \left(\frac{vt}{b} \right)^2 \right]^{-\frac{3}{2}} \tag{1.23}$$

To find the total change in perpendicular velocity for a star, we need to integrate this expression over all time:

$$\begin{aligned}
 \delta v_{\perp} &= \int_{-\infty}^{\infty} \frac{Gm}{b^2} \left[1 + \left(\frac{vt}{b} \right)^2 \right]^{-\frac{3}{2}} dt \\
 &= \frac{2Gm}{bv}
 \end{aligned} \tag{1.24}$$

This is only for an interaction with a single star. In reality there will be many interactions each contributing δv_{\perp} which combine to form an over all change of Δv_{\perp} . If we

assume a constant number density distribution of stars, then the surface density distribution presented to the incoming stars is of order:

$$n_{\star} = \frac{N}{\pi R^2} \quad (1.25)$$

where N is the number of stars and R is some descriptive radius of the cluster, such as the half mass radius.

The number of stars that then come within some radius, b of the interloping star is of order:

$$\begin{aligned} \delta n &= n_{\star} 2\pi b \delta b \\ &= \frac{2N}{R^2} b \delta b \end{aligned} \quad (1.26)$$

Looking at the sum of the squares of δv_{\perp} gives:

$$\begin{aligned} \delta v_{\perp, tot}^2 &= \delta v_{\perp}^2 \delta n \\ &= \frac{8G^2 N m^2}{b v^2 R^2} \delta b \end{aligned} \quad (1.27)$$

To find the total change in v_{\perp}^2 we need to integrate this expression over all impact parameters, b :

$$\begin{aligned} \Delta v_{\perp}^2 &= \int_{b_{\min}}^R \frac{8G^2 N m^2}{v^2 R^2} \frac{db}{b} \\ &= 8N \left(\frac{Gm}{vR} \right)^2 \ln \left[\frac{R}{b_{\min}} \right] \end{aligned} \quad (1.28)$$

Making use of the Virial theorem, we can replace Gm/R and get:

$$\Delta v_{\perp}^2 = \frac{8}{N} v^2 \ln \left[\frac{R}{b_{\min}} \right] \quad (1.29)$$

Thus the number of crossings that a star has to make across a cluster to ensure relaxation is:

$$\begin{aligned} n_{\text{relax}} &= \frac{v^2}{\Delta v_{\perp}^2} \\ &= \frac{N}{8 \ln \left[\frac{R}{b_{\text{min}}} \right]} \end{aligned} \quad (1.30)$$

Thus the relaxation time of the cluster is:

$$\begin{aligned} t_{\text{relax}} &= n_{\text{relax}} t_{\text{cross}} \\ &= \frac{N}{8 \ln \left[\frac{R}{b_{\text{min}}} \right]} t_{\text{cross}} \end{aligned} \quad (1.31)$$

To make this expression more useful, we need to replace the logarithm in the denominator of this expression. To do this we simply equate the kinetic and potential energies of a star during the closest passage to give:

$$\begin{aligned} b_{\text{min}} &= \frac{2Gm}{v^2} \\ &= \frac{2R}{N} \end{aligned} \quad (1.32)$$

where I have made use of the Virial theorem to replace the v^2 term. Thus Eqn. 1.31 maybe rewritten as:

$$t_{\text{relax}} = \frac{N}{8 \ln \left(\frac{N}{2} \right)} t_{\text{cross}} \quad (1.33)$$

Typically we find that most of the important dynamical processes (such as mass segregation (Spitzer 1940)) occur on the relaxation time scale of the cluster. The stars don't have to undergo extremely close interactions to forget what their original velocity is, instead the cumulative effects of many small interactions can have exactly the same effect. This is taken into account in the derivation of t_{relax} .

This time scale is quite long, for instance in the case of the Pleiades cluster the relaxation time is of order 100 million years (see chapter 2). Whilst for an average milky-way globular cluster the half mass relaxation time is of order several billion years (Harris 1996).

1.4.3 Close encounters

Within this chapter, I have mentioned that the evolution of a cluster is influenced by having stars interact with one another over some length scale. I've given timescales for the crossing and relaxation time of a cluster, but how long do we have to wait for two stars to come within some specified distance of one another?

This timescale has a similar background to the collision time in a gas. If we treat each of the stars in a cluster as a gas particle, then the timescale for two stars to pass within some specified distance of one another is:

$$t = \frac{1}{n\sigma v} \quad (1.34)$$

where n is the number density of stars and v is the velocity dispersion within the cluster. σ is the cross-section for the interaction.

If one were to rely purely on chance for two stars to come within a distance r_{min} of one another, the timescale for such interactions would be quite long. However, the mass of the stars involved in the interaction means that gravity can act to deflect the paths of the two stars and bring more distant stars closer together during an interaction.

Put simply, the mutual gravity of the two stars serves to pull them together, thus increasing the initial separation they can be at yet still undergo a collision. To derive this cross-section we start off by considering the conservation of energy and angular momentum at two points, where the stars are infinitely far apart and when they come within the desired minimum distance, r_{min} :

$$\frac{1}{2}m_r v_\infty^2 = \frac{1}{2}m_r v^2(r_{\min}) - \frac{Gm_1 m_2}{r_{\min}} \quad (1.35)$$

$$r_{\min} v(r_{\min}) = b v_\infty \quad (1.36)$$

where m_r is the reduced mass, b is the impact parameter and v_∞ is the relative velocity at infinity. If we eliminate $v(r_{\min})$ between equations 1.36 and 1.35 we can show:

$$\begin{aligned} b^2 &= \left(1 + \frac{2Gm_1 m_2}{m_r v_\infty^2 r_{\min}}\right) r_{\min}^2 \\ &= \left(1 + \frac{v^2}{v_\infty^2}\right) r_{\min}^2 \end{aligned} \quad (1.37)$$

which now allows us to write the cross-section for the interaction as:

$$\begin{aligned} \sigma &= \pi b^2 \\ &= \pi r_{\min}^2 \left(1 + \frac{v^2}{v_\infty^2}\right) \end{aligned} \quad (1.38)$$

Clearly in regions where v_∞ is high (10^2 - 10^3 km/s, such as in the centre of the galaxy), the focusing term in this equation is going to be negligible. In slower velocity regimes, such as in clusters (≈ 70 km/s for globular clusters and 1km/s for open clusters) the focusing term is far more important and can significantly reduce the time for a collision to occur. In a low velocity dispersion environment the collision time scale may be estimated by (Binney & Tremaine 1987):

$$t_{\text{coll}} = 7 \times 10^{10} \text{yr} \left(\frac{10^5 \text{pc}^{-3}}{n}\right) \left(\frac{v_\infty}{10 \text{km/s}}\right) \left(\frac{R_\odot}{R_{\min}}\right) \left(\frac{M_\odot}{m}\right) \quad (1.39)$$

where n is the number density of single stars of mass m . Interesting encounters start to occur when $R_{\min} \approx 3R_\odot$ (Rasio & Shapiro 1991, Davies, Benz & Hills 1992), at this distance tides can be raised in the two stars and energy dissipated. For the core of a globular cluster where $v_\infty \approx 10$ km/s and $n \approx 10^5 \text{pc}^{-3}$, the collision time is around 10^{11} yrs.

1.4.4 Two-body scattering

There are two forms of two-body scattering, strong and weak. I shall consider each in turn.

Strong two-body scattering occurs when we have two stars come relatively (in a cluster sense) close together. As this happens the gravitational pull of one star on the other is sufficient to severely deflect the paths of both stars. Such strong scattering is largely responsible for the escape of stars from a cluster. When a light star undergoes a strong scattering with a heavy star, the light star picks up energy from the heavier star. This increase in energy can be sufficient to allow the lighter star to escape from the cluster.

Weak two body scattering is basically the same as strong scattering, except that it occurs over a larger separation. As a result of the larger separation between the two stars the deflection that they suffer is commensurately less.

This two body scattering is responsible for the relaxation of the cluster that was discussed in section 1.4.2. The strong scattering occurs for separations which are close to b_{\min} , whilst the weak scattering is for the larger separations. Collisions with larger impact parameters are for more likely than those at b_{\min} . As a result it is the weak scattering which dominates the relaxation, as it overwhelms the strong scattering through sheer number of events.

As the scattering takes place, the cluster moves toward an equipartition of energy. As a result the lighter stars then to pick up energy during the collisions and heavier stars tend to loose energy. This causes heavy stars to move inwards toward the centre of the cluster, whilst the lighter stars move outwards. This is known as mass segregation.

1.4.5 Density profiles

If we are to be sure that the theories describing the evolution of a cluster are correct, we require some method of comparing theoretical predictions to observational data. There are the obvious methods, such as just looking at a cluster and saying that a particular

population of stars lies in a particular place, for example looking at the depletion of red giants in the core of a globular cluster. Sometimes, however, we require tests which are somewhat more robust. The evolution of a cluster should drive its density profile to some shape, this shape should be the same in observations and in theoretical models.

One of the most successful models of a cluster's density function is the King model (King 1966). The King model starts off with a distribution function which is a lowered isothermal model. The distribution function tells us about the energy distribution of the stars within a cluster. It is lowered because it allows for the fact that at some velocity a star can escape from the cluster. The distribution function in terms of the stars relative energy, ε , is:

$$f(\varepsilon) = \begin{cases} \rho_1(2\pi\sigma^2)^{-\frac{3}{2}}(e^{\frac{\varepsilon}{\sigma^2}} - 1) & \varepsilon > 0; \\ 0 & \varepsilon \leq 0; \end{cases} \quad (1.40)$$

where σ is the velocity dispersion of the cluster and ρ_1 is a characteristic density (the core density). The relative energy of a star is related to its velocity and its relative potential within the cluster:

$$\varepsilon = \Psi - \frac{1}{2}v^2 \quad (1.41)$$

Equation 1.40 can be integrated over all energies, or equivalently over all velocities to find the density distribution in terms of Ψ

$$\begin{aligned} \rho(\Psi) &= \frac{4\pi\rho_1}{2\pi\sigma^2} \left[\int_0^{\sqrt{2\Psi}} \left(v^2 e^{\frac{\Psi - \frac{1}{2}v^2}{\sigma^2}} - 1 \right) dv \right] \\ &= \frac{4\pi\rho_1}{2\pi\sigma^2} \left[e^{\frac{\Psi}{\sigma^2}} \int_0^{\sqrt{2\Psi}} v^2 e^{-\frac{1}{2}\frac{v^2}{\sigma^2}} dv - \frac{(2\Psi)^{\frac{3}{2}}}{3} \right] \end{aligned} \quad (1.42)$$

On performing the remaining integration and application of the limits, the density as a function of the potential is given by:

$$\rho(\Psi) = \rho_1 \left[\sqrt{\frac{4\Psi}{\pi\sigma^2}} \left(1 + \frac{2\Psi}{3\sigma^2} \right) \right] + \rho_1 \operatorname{erf} \left(\frac{\sqrt{\Psi}}{\sigma} \right) e^{\frac{\Psi}{\sigma^2}} \quad (1.43)$$

A further two integrations using Poisson's equation are required to take this density based on the cluster potential to a density based on the radial co-ordinate, and this is usually done numerically.

The King profile has served particularly well when applied to the majority of globular clusters in our galaxy. Some, however, do show deviations from the expected profile within their core regions. It is believed that these clusters have undergone the process of core collapse which is discussed in Section 1.4.6.

1.4.6 Core collapse

For globular clusters, the mass segregation which results from the two body scattering events can lead to a substantial build up of heavy stars within their cores. Over a sufficiently long period of time (a few relaxation times) this build up in density can become quite severe.

As the heavy stars move into the core, the evolutionary timescales within the core get shorter and shorter. Eventually a point is reached where the evolution of the core toward a dynamical equilibrium becomes independent of the surrounding halo, because the timescales in the two regions are so different. Although the core is dynamically independent of the halo, it is still in thermal contact with it. This means that the core can lose energy to the halo. As this happens, the negative heat capacity of the core means that it will actually heat up. The contraction of the core continues with energy being passed out to the halo via the ejection of core stars after strong two body scattering events, or interactions with hard binary systems. Early models of the evolution of globular clusters (Cohn 1979) suggested that the runaway mass segregation going on within the core would eventually lead to the formation of a region of infinite density. This process is known as core collapse.

This core collapse has a distinct observational characteristic. In an un-collapsed cluster the surface brightness tends to flatten off around the core. In a collapsed cluster this flattening off is not seen, instead the density continues to increase down to the smallest resolvable radius. However, an infinite core density is not seen.

1.4.7 Staving off core collapse

Observations of globular clusters do show that some do exhibit strange brightness profiles within their cores, but there is no evidence for an infinite density. The models which had predicted the formation of this region are somewhat too simple. They neglect the presence of binary systems, they also neglect dissipative interactions between stars.

To stop core collapse, a cluster requires some input of energy within the core which can offset the loss of energy to the halo. A prime source for this energy is a population of binary systems. Broadly speaking, there are two types of binary systems, hard and soft¹. A hard binary is one which is resilient to breaking up during an interaction with a third body, any interaction it undergoes can only make it harder (Heggie 1972). In the process of making it harder, energy is released from the binary and given to the star that it is interacting with. This acts as a source of heat for the cluster, which because of the negative heat capacity causes the core to cool down and start to expand.

An obvious question is, what is the source of these binary systems? These binaries can come from three sources; they could be a primordial population that were formed at the same time as the cluster was formed. They could be formed through two body interactions or through three body interactions.

Two body binaries can be formed when two stars come close enough to raise tides on the surface of one another. These tides can dissipate some of the kinetic energy of the two stars leaving them in a bound binary system. Three body binaries, rely on the coming together of three single stars. During the interaction of the three stars, it is possible for one of the stars to take away a significant fraction of the kinetic energy of the three bodies, this leaves the other two stars in a bound binary system.

¹A soft binary is one which isn't resilient to breakup, and so can't help to save the core from collapse.

Each of the hard binaries can only supply a finite amount of energy to the core. Each scattering that a binary system undergoes imparts some kinetic energy to it and sends it out in increasingly large orbits, additionally the binary can get ground down to the point where the next interaction involves a direct physical collision between one of the components and the interloping star.

The supply of energy from the hard binary system effectively halts the core collapse. The amount of energy that the core releases can be enough to cause the core to re-expand to some extent. As the core expands and cools it can meet up with the halo that it had heated earlier. At this point the core can actually be cooler than this halo. This leads to a temperature inversion (Heggie & Hut 2003) and energy passes from the halo into the core, causing the core to expand further. Eventually the core expands to a point where the temperature inversion disappears and the expansion of the core stops. Once this stage has been reached, the binary systems in the core are no longer supplying sufficient energy to keep the core in this expanded state. Thus the core starts to contract again, doomed to repeat its failure in trying to collapse time and time again. This process of collapse and re-expansion is known as gravothermal oscillation.

1.5 Stellar collisions

When one is talking in cluster parlance, a collision usually refers to an interaction where stars come close enough together to significantly deflect each others flight paths. This distance is still many times the diameter of each of the stars involved and so we do not get a direct physical collision. However, in some clusters (most notably globular clusters) the density of stars is sufficiently high (10^5 stars/pc³ in their cores) that direct physical collisions between stars can actually happen with an appreciable frequency.

It is not only collisions between single stars that take place. Collisions can also occur between binary systems, typically such collisions will lead to the formation of a new binary or higher hierarchy system. We can also have collisions between main-sequence / turn-off stars and degenerate bodies such as white dwarfs and neutron stars.

What might collisions be able to explain?

Direct physical collisions between stars are currently used to explain a number of observational features.

Blue straggler stars

As mentioned in Section 1.3 globular clusters are seen to have a population of stars which have masses beyond the turn-off mass of the cluster. If these stars were formed with the rest of the stellar population, then they should have already evolved off onto the giant and horizontal branch, not on the main sequence. One possible mechanism for forming these stars is to have two lower mass main-sequence stars collide and form a merged object which goes on to form the blue straggler that we see today. Such a formation channel has been considered by several authors (Benz & Hills 1987, Lombardi, Rasio & Shapiro 1996a, Procter Sills, Bailyn & Demarque 1995). I have examined the details of these collisions with the highest resolution simulations performed to date. The results are presented in Chapter 4.

Red giant depletion

Also as mentioned in Section 1.3 observations seem to indicate that the cores of post-core collapse globular clusters have an apparent paucity in their population of red-giant stars. The red giant phase occurs toward the end of the stellar evolution cycle. The star swells up and has a radius much larger than that of when it was on the main sequence. This increased radius coupled to the high number density of bodies within the core hint that there could be a dynamical explanation for the absence of these red giants. If the red giant were to undergo a direct physical collision with another star, then the red giant could be effectively destroyed (Rasio & Shapiro 1990, Davies, Benz & Hills 1991). I consider the effects of such collisions in Chapter 5.

Low mass X-ray binaries

A low-mass X-ray binary consists of a neutron star or black hole in a binary system with a low-mass main-sequence star. The orbit is sufficiently close that the main-sequence star fills its Roche lobe and transfers material to the companion. This transfer

of material leads to the formation of an accretion disc around the primary and as this is slowly accreted, energy is released in the form of X-rays. The reason collisions are important for LMXBs is that some mechanism is required to shrink an otherwise wide orbit down and bring the two components into contact. The timescales associated with gravitational radiation and magnetic braking are too long to bring the stars into contact, instead scattering events and binary exchanges can lead to the binary becoming harder and coming into contact. This is why more LMXBs per unit mass are seen in globular clusters compared to the field.

Millisecond pulsars

Observations of globular clusters have revealed a population of rapidly rotating neutron stars, known as millisecond pulsars (MSPs). MSPs are formed when a neutron star is in a binary system and accretes material from the secondary. The angular momentum of the material being accreted causes the neutron star to spin up to millisecond periods. It would seem therefore that millisecond pulsars would likely be associated with the low-mass X-ray binaries that I previously mentioned. There is a problem with this assumption, there are far more MSPs than there are LMXBs. A solution to this problem is to consider what has happened in the past for a cluster (Davies & Hansen 1998). It is entirely possible that neutron stars could have interacted with a binary system and replaced one of the components. As a result the neutron star could be in a binary system with an intermediate mass star ($1.5-3M_{\odot}$). This star would have evolved and the binary system would have come into contact. Thus mass and angular momentum could have been transferred to the neutron star, spinning it up. This mass transfer would have happened in the past and would not be visible today, thus we are left with a millisecond pulsar in a binary system.

Cataclysmic variables

Cataclysmic variables are binary systems in which mass is being accreted from a low mass main-sequence star onto a white dwarf. For CVs to be produced, we initially have to start off with a relatively wide binary system composed of two main-sequence stars. The heavier of the two components evolves and expands and starts to pass mass to the

other component in the binary system. This mass transfer is likely to be unstable and a common envelope phase results. Within the common envelope, the separation of the two components decreases as orbital energy and angular momentum are removed. This leaves the now white-dwarf main-sequence star in a tight binary which can then come into contact and allow mass to pass from the main-sequence star to the white dwarf. In the core of a globular cluster the wide binaries that would go on to form CVs are unlikely to survive interactions with other stars. To explain the CV population seen in the cores of most globular clusters we rely on mass segregation moving some of the halo CV population into the core (Davies 1997) and we also can get a second generation of CVs produced through collisions. When a white dwarf comes with $\approx 3R_*$ of a main-sequence star, tides can be raised in the star and sufficient energy dissipated that the two become bound. This binary will naturally be quite close and will come in to contact in a relatively short period of time.

1.6 Thesis Overview

The intent of this thesis is to examine some of the phenomena which I have alluded to in this chapter. Each chapter is essentially a self contained unit where I lay out a problem and detail my attempts to solve it.

In Chapter 2, I present the results of multiple simulations of open clusters, modelling the dynamics of a population of brown dwarf members. I investigate whether it is possible that a large population of brown dwarfs could be formed and subsequently ejected in a short period of time. I consider the effects of a large range of primordial binary populations, including the possibilities of having brown dwarf members contained within a binary system. I also examine the effects of various cluster diameters and masses. My examination of a population of wide binary systems containing brown dwarfs, reveals evidence for exchange reactions whereby the brown dwarf is ejected from the system and replaced by a heavier main-sequence star. I find that it is unlikely that all of the brown dwarf population could be ejected from the cluster in a period less than several relaxation times. Instead I show that there exists the possibility of hiding a large fraction

of the brown dwarfs within a primordial binary population. I conclude that it is probable that the majority of brown dwarfs are contained within such primordial binary systems which then hides a large proportion of them from detection.

In Chapter 3, I describe a new adaptation of the smooth particle hydrodynamics method that I have developed. It allows two populations of very different mass particles to be used in the same simulation. A very light population of particles can sit on top of a population of heavy particles (the tested mass difference is 9 orders of magnitude) via the use of a pseudo-force based on the number density of the heavy particles. I perform a series of test simulations looking at the response of the method to various situations, and explain some of the possible future uses. This actually represents the last piece of work I have performed. The chapter is placed here because it provides details on the SPH method which I use within the subsequent chapters.

In Chapter 4, I examine the formation and evolution of blue stragglers produced through direct collisions between stars. I start by identifying the optimum resolutions for performing the runs. In doing so I present the highest resolution of a stellar collision formed to date. I show that a resolution of 100,000 particles is sufficient to understand the properties of the merged object and to act as a starting point for the stellar evolution code.

I then go on to consider a series of off-axis collisions between various-mass main-sequence stars. As was previously found, the resultant merged object initially possesses too much angular momentum to allow it to contract down to the main sequence. Although no evidence for discs or surface convection zones are found in the immediate post-collision object, I postulate about possible angular momentum loss methods which will allow the merged objects to contract down to the main-sequence.

Finally I consider the results of Davies, Piotto & De Angeli (submitted) and show that the dynamical population of blue stragglers is likely to only account for 1/6 of the total population seen in globular clusters. Thus, attention should now be focused on the production of blue stragglers through binary system evolution.

In Chapter 5, I investigate a means of explaining the apparent paucity of red giant

stars within post core collapse globular clusters. I propose that collisions between the red giants and binary systems can lead to the destruction of some proportion of the red giant population by either knocking out the core of the red giant or by forming a common envelope system which will lead to the dissipation of the red giant envelope. Treating the red giant as two point masses, one for the core and another for the envelope (with an appropriate force law to take account of the distribution of mass), and the components of the binary system also treated as point masses, I utilise a four-body code to calculate the timescales on which the collisions will occur. I then perform a series of smooth particle hydrodynamics runs to examine the details of mass transfer within the system. In addition I show that collisions between single stars and red giants lead to the formation of a common envelope system which will destroy the red giant star. I find that low velocity collisions between binary systems and red giants can lead to the destruction of up to 13% of the red giant population. This could help to explain the colour gradients observed in PCC globular clusters. I also find that there is the possibility that binary systems formed through both sorts of collision could eventually come into contact perhaps producing a population of cataclysmic variables.

Chapter 2

Brown dwarf populations in open clusters.

2.1 Introduction

Brown dwarfs are essentially failed stars; they formed within a stellar nebula just like any other star, but they failed to reach a mass that generates sufficiently high central temperatures and pressures to induce the process of hydrogen fusion. As a result of the lack of fusion, brown dwarfs are naturally very dark objects. The little light that they do put out is normally at the Infrared end of the spectrum and is typically left over energy from the accretion process.

The identification of brown dwarfs is a difficult process; their inherently faint magnitudes make them both difficult to locate and to classify. Classification of brown dwarf status relies on the identification of spectral features from the object which couldn't have come from a low-mass star. The primary identifier of a brown dwarf is the presence of a lithium resonance doublet at 6708 \AA . This feature up until recently proved very difficult to locate and the existence of isolated brown dwarfs was a subject of some controversy.

The first confirmed identification of a brown dwarf within the Pleiades cluster was by Basri, Marcy & Graham (1996) Teide 1. They successfully identified, spectroscopically, the lithium feature in a brown dwarf candidate first discovered by Stauffer, Hamilton &

Probst (1994). Since this first identification the assignment of brown dwarf status has been given to many more candidate objects, particularly in the Pleiades cluster.

Due to its young age and proximity, the Pleiades cluster is an excellent hunting ground for brown dwarfs. Many surveys have been made of this cluster; (Hambly et al. 1999) performed a survey in the I and R bands and identified nine distinct single brown dwarf candidates. Further surveys have yielded more brown dwarf candidates within the cluster, notably a recent survey (Pinfield et al. 2000) has identified 30 possible brown dwarfs in a six square degree survey of the cluster. Of particular interest is the work of Pinfield et al. (1998). Their examination of the dynamics of the Pleiades cluster lead them to believe that there could be several thousand unseen brown dwarfs. If this is the case it is important to understand why so few brown dwarfs have been found within the central portions of the cluster which have been so well studied.

The discovery of Gliese 229B (a brown dwarf contained within a binary system) by Nakajima, Oppenheimer, Kulkarni, Golimowski, Matthews & Durrance (1995) (see also Golimowski, Burrows, Kulkarni, Oppenheimer & Bruckardt (1998), Basri & Martín (1999)) poses the interesting possibility of containing cluster brown dwarfs within a primordial binary population. Since this first discovery of a binary containing a brown dwarf, a further six have been identified through the use of data from the 2MASS survey (Gizis (2000), Skrutskie, Beichman, Capps, Carpenter, Chester, Cutri, Elias, Elston, Huchra, Liebert, Lonsdale, Monet, Price, Schneider, Seitzer, Stiening, Strom & Weinberg (1995)). Martín, Brandner, Bouvier, Luhman, Stauffer, Basri, Zapatero Osorio & Barrado y Navascués (2000) performed near-infrared photometry on very low-mass members of the Pleiades cluster. They failed to detect any resolved binary systems with a separation of more than 0.2 arcsec; however they do manage to identify CFHT-P1-16 as a brown dwarf binary of separation 0.08 arcsecs (equivalent 11 AU) by use of HST data. They also detect the presence of a binary second sequence within the colour magnitude diagram (Haffner & Heckmann (1937), Hurley & Tout (1998) for a discussion). However, they conclude that there is a deficiency in the population of wide binary systems (those with a separation greater than 27 AU); I consider this issue in this chapter.

Another cluster of interest is the Hyades. This is located at about 46 pc from the sun,

and is considerably older than the Pleiades (≈ 650 Myrs as opposed to the Pleiades age of ≈ 120 Myrs). Observations of this cluster reveal a deficit in low mass objects and brown dwarfs (Gizis et al. 1999), although recent observations (Reid & Mahoney 2000) have identified a binary system, which may possibly contain a brown dwarf. However, in other regards it appears to be quite similar to the Pleiades, just older.

Work by Luhman et al. (2000) has demonstrated a strong similarity between the initial mass functions (IMFs) of the Trapezium, Pleiades and M35 open clusters. They performed sensitive, high-resolution imaging of the central portion of the Trapezium cluster utilising the Near-Infrared Camera and Multi-Object Spectrometer (NICMOS) aboard the Hubble Space telescope, as well as performing ground based observations to take K-band spectra for many of their sources. Their methodology allowed observations of objects well below the hydrogen burning limit and so we are now beginning to get a full explanation of cluster IMFs. Within the several hundred objects identified within the Trapezium cluster, around 50 have been classified as brown dwarf candidates. The derived Trapezium IMF is found to be similar to mass functions measured in other young star forming regions, *e.g.* IC 348 (Luhman, Rieke, Lada & Lada 1998) and ρ Oph (Luhman & Rieke 1998). Indeed this work lends credence to the idea of a universal IMF, at least in the case of open clusters¹. If this is true, a consistent model of brown dwarf dynamics within a cluster should explain observed differences.

I seek to model the evolution of a cluster of stars which also contains a population of brown dwarfs, in an effort to predict what happens to the brown dwarf contingent that star clusters are predicted to have. Stellar clusters may be modelled either through Fokker-Plank codes or direct n-body integrators. It is this latter technique that I apply. The use of n-body codes to simulate open cluster evolution has become common place with more advanced codes allowing more detailed study. The work of Terlevich (1987) demonstrated the use of n-body simulations; she successfully modelled the evolution of several clusters to their evaporation (*i.e.* their total dissipation) and examined the process of mass segregation within the cluster.

Earlier work by de la Fuente Marcos & de la Fuente Marcos (2000) began the ex-

¹there appear to be fundamental differences between these IMF's and those of globular clusters.

amination of brown dwarf evolution in open clusters. They utilised the *Nbody5* code by Sverre Aarseth and examined the evolution of 8 separate cluster models which varied in their stellar make up. They conclude for their models the relative percentages of brown dwarfs to normal stars at older cluster ages is strongly dependent on the IMF used at the start of their simulations. I seek to further this work via the use of the more advanced code NBODY 6 also by Sverre Aarseth (see Hurley, Tout, Aarseth & Pols (2001) for a review of the NBODY 6 code). I examine the affects of various cluster diameters, masses and density profiles. I also examine the implications of various binary fractions and the effects they can have on a brown dwarf population or at least appear to have.

2.2 Theory

2.2.1 Dynamics of the Cluster

The motion of the objects within the cluster leads to the definition of two important timescales. The first of these timescales is the cluster crossing time, t_{cross} , which defines how long it takes a star or brown dwarf to move across the cluster. It is defined by the equation:

$$t_{\text{cross}} = \frac{R_{\text{hm}}}{v} \quad (2.1)$$

where R_{hm} is the half-mass radius of the cluster and v is the velocity dispersion.

The second timescale is the relaxation time, t_{relax} . As the stars and brown dwarfs move within the cluster they undergo gravitational interactions with each other. The relaxation time refers to the period taken for a star to undergo sufficient interactions with various other bodies exchanging energy and have a resultant change in velocity of order $|\delta v| = |v|$. One may estimate the relaxation time of a cluster based on the two-body relaxation time as defined in Section 1.4.2:

$$t_{\text{relax}} = \frac{N}{8 \ln N} t_{\text{cross}} \quad (2.2)$$

where N is the number of stars within the cluster.

The exchange of energy during the two-body interaction is a very important driving force for the cluster. During an interaction between two stars, energy is transferred from the heavier to the lighter one, until the cluster reaches a state of equipartition of energy. This results in the heavy star falling deeper into the cluster potential, namely toward the core of the cluster. This leads to the phenomena of mass segregation, whereby one finds the heaviest stars within a cluster migrating toward the core regions. Bonnell & Davies (1998) demonstrate that the timescale for mass segregation within a cluster is well fitted by t_{relax} (as was predicted by Spitzer 1940). Hence systems which are older than their t_{relax} should be mass segregated.

Whilst the heavy stars have lost energy during two body interactions, the lighter stars (or brown dwarfs) have gained energy. As a result the body's velocity naturally increases and so it can move further out into the cluster. After a sufficient number of interactions, it is possible that the light star, or brown dwarf, may have a velocity which exceeds the escape speed of the cluster. This leads to the process of evaporation, whereby the cluster may lose mass via the escape of energetic stars.

2.2.2 Binary population dynamics

Within the cluster environment there is likely to be a population of binaries. These provide another important mechanism for driving the evolution of the cluster; interactions between binary systems and single stars provide another method of energy transfer within the system as I now briefly describe.

There are two types of binary system, hard and soft. The definition of hard and soft arise when a binary system undergoes an interaction with a third star. One has to consider the ratio of the total kinetic energy of the three bodies and the binding energy of the binary. If the kinetic energy of the system is greater than the binding energy, then there exists the possibility that energy can be passed into the binary and cause it to break up; this is referred to as a soft binary system. Whilst if the kinetic energy of the three body event is less than the binding energy of the binary, the binary is said to be hard. In

this case energy is transferred to the interloping star and the binary becomes tighter, or harder. This transfer in energy then alters the energy budget of the cluster. The dividing line between the hard and soft regimes occurs when the total kinetic energy is just equal to the binding energy of the binary and so leads to the definition of the critical velocity;

$$V_{\text{crit}}^2 = \frac{2GM_1M_2[M_1 + M_2 + M_3]}{M_3(M_1 + M_2)} \frac{1}{d} \quad (2.3)$$

where M_1 , M_2 are the masses of the two stars within the binary system and M_3 is the mass of the third star, whilst d is the binary separation. If we equate the resulting kinetic energy of the system to the binary system's binding energy, we can write the resulting definition of the hard soft boundary limit:

$$d_{\text{h/s}} = 1744 \frac{M_1M_2}{M_3v^2} \left(\frac{M_1 + M_2}{M_1 + M_2 + M_3} \right) \text{ AU} \quad (2.4)$$

where v is now simply the relative velocity of the interloping star in kms^{-1} and the masses are in solar units. Clearly we now see that the hard soft boundary of a star is now a function of the interloping star's mass. Thus a system might be hard to one interaction whilst being soft to another one.

As already mentioned, if a hard binary system were to undergo an interaction, it is expected to get harder; in doing so energy has to be transferred from the binary system to the third star. This results in an increase in the third star's velocity and can ultimately lead to its evaporation from the cluster. Alternatively, if the interloping star has a mass greater than one of the components within the binary, then the two may be exchanged, with a hardening of the new binary system. A trivial calculation, based on a binary system with components of $0.6 M_{\odot}$ and $0.05 M_{\odot}$, undergoing an interaction with a $0.4 M_{\odot}$ star and forming a new binary which is 20 per cent harder than the original system results in a kick velocity to the $0.05 M_{\odot}$ body (a brown dwarf) of 4.9 kms^{-1} . The escape velocity of my clusters is of order 2.5 kms^{-1} , so clearly if such an interaction were to take place, the ejected brown dwarf would soon escape from the cluster.

The interaction timescale for bodies within the cluster may be defined as:

$$\tau = \frac{1}{n\sigma v} \quad (2.5)$$

where n is the number density of stars, v is the relative stellar velocity and σ is the interaction cross-section. The clusters within my simulations all initially have a constant velocity dispersion, which is allowed to evolve with the cluster. As a consequence the interaction cross-section may be estimated as:

$$\sigma = \pi r_{\text{col}}^2 \left(1 + \frac{2G(M_1 + M_2 + M_3)}{v^2 r_{\text{col}}} \right) \quad (2.6)$$

where v is the relative velocity of the binary and the interloping stars and r_{col} is the distance of closest approach for the system.

As stellar clusters evolve they are subject to tidal forces from the galaxy within which they reside. These forces lead to perturbations on the orbits of the stars within the cluster. For simplicity I model the motion of clusters moving on a circular orbit about the centre of our galaxy at a radius equivalent to that of the sun from the galactic centre ($R_G=8.5\text{kpc}$), this yields Oorts constants of $A = 14.5 \pm 1.5 \text{ kms}^{-1}\text{kpc}^{-1}$ and $B = -12 \pm 3 \text{ kms}^{-1}\text{kpc}^{-1}$. With the addition of tidal forces to the calculations, the equations of motion for the stars within the cluster become (Giersz & Heggie 1997);

$$\ddot{x} = F_x + 2\omega_G \dot{y} + 3\omega_G^2 x \quad (2.7)$$

$$\ddot{y} = F_y - 2\omega_G \dot{x}$$

$$\ddot{z} = F_z - \omega_G^2 z$$

where ω_G is the angular velocity about the centre of the galaxy defined by:

$$\omega_G = \sqrt{\frac{GM_G}{R_G^3}} \quad (2.8)$$

with M_G is the mass of the galaxy contained within a distance R_G .

One of the most obvious effects of the tidal field is the existence of a tidal radius for the cluster. This is the point at which the gravitational forces due to the cluster and the galaxy balance; it is defined by:

$$r_{\text{tidal}} = \left(\frac{GM_c}{4A(A-B)} \right)^{\frac{1}{3}} \quad (2.9)$$

where M_c is the total mass of the open cluster. Once past this radius a star is no longer considered to be bound to the cluster and moves off to become a part of the galactic disk. Throughout all the simulations the effects of an external tidal field on the cluster are included with tidal radii calculated with the Oort constants as measured in the solar neighbourhood.

2.3 Initial Conditions

2.3.1 Stellar population

Stellar masses for the population of stars within the simulations were produced by two methods. The first method was to simply utilise a catalogue of stellar masses for the objects currently present within the Pleiades. To this catalogue I added a population of 100 low-mass stars which were simply produced by doubling up the population of low mass bodies in the catalogue. This allowed me to model the well studied inner portions of the cluster. The addition of a further 100 bodies was decided on via numerical experiments that we performed.

The second method of producing stellar masses was to use the mass function by Kroupa, Tout & Gilmore (1993). With this function I produced a distribution of stars with an upper limit on mass of $10 M_{\odot}$ and a lower mass of $0.08 M_{\odot}$ (the hydrogen burning limit). Evolution of the stellar population was accomplished via the use of fitting formulae Eggleton, Fitchett & Tout (1989). In using the IMF by Kroupa, Tout & Gilmore (1993) I extended my investigations by looking at clusters of different masses, with stellar numbers ranging between 1000 and 3000.

In addition to examining two different mass profiles I also investigate the effects of two different initial density distributions. The first is the Plummer distribution pattern which is commonly used in N-body simulations due to the fact that it's simple and fairly realistic. The second set of models examined the evolution of a uniform spherical distribution, which is preferred by some authors (e.g. de la Fuente Marcos & de la Fuente Marcos (2000)) as a model for open clusters.

2.3.2 Brown dwarf population

Within my simulations I added to the cluster a population of 1500 brown dwarfs, each of which had a mass of $0.05 M_{\odot}$ and positions and velocities determined in the same manner as for the stellar population. Investigations were made into using a brown dwarf IMF and populations with a constant mass other than $0.05 M_{\odot}$; however the choice of brown dwarf mass had very little effect on the evolution of the cluster or of the brown dwarf populations themselves.

2.3.3 Binary population

Within the simulations performed between 0 and 500 primordial binary systems were added to the cluster. The binary systems were composed of stars all ready contained within the cluster, thereby conserving the total mass of the cluster between the simulations. In the cases where the Pleiades masses have been used the components of the binary systems have been randomly paired (Leinert, Zinnecker, Weitzel, Christou, Ridgway, Jameson, Haas & Lenzen (1993), Kroupa, Petr & McCaughrean (1999), Kroupa (2000), although for a differing view see for example Mazeh & Goldberg (1992)). For the other simulations, the IMF used produced the required binary components. In each simulation a discrete fraction of the binary population was forced to have a brown dwarf as a secondary. Three numbers which result from this treatment are the fraction of stars in binary systems, f_s , the fraction of brown dwarfs contained within binaries, f_{bd} and the fraction of objects (*i.e.* brown dwarfs and stars) contained within binaries, f_{bin} :

$$f_s = \frac{N_b}{N_b + N_s} \quad (2.10)$$

$$f_{bd} = \frac{N_{bd,bin}}{N_{bd,bin} + N_{bd}} \quad (2.11)$$

$$f_{bin} = \frac{N_b + N_{bd,bin}}{N_{bd,bin} + N_{bd} + N_b + N_s} \quad (2.12)$$

where N_s , N_b , N_{bd} and $N_{bd,bin}$ are the number of single stars, the number of stars contained in binary systems, the number of brown dwarfs and the number of brown dwarfs contained in binary systems. The various fractions considered are listed in Table 2.1. These were chosen so that I might investigate the effects that the different binary populations had on the evolution of the cluster.

The positions of the binary systems were set to be consistent with the distribution of stars in the particular cluster. The eccentricities of the systems were selected from a thermalised distribution (Jeans 1929), whilst the nodes and inclinations were randomly selected.

The separations of the binary components were chosen so that they were uniformly distributed in $\log d$. This was accomplished using the following;

$$d = d_0 10^{-x} \quad (2.13)$$

$$x = A \log R \quad (2.14)$$

where d_0 is the upper limit of the binary separation, A is a random number chosen from a uniform distribution between 0 and 1 and R is a quantity known as the range. The range determines the spread in binary separations between the upper limit and d_0/R . A low value of R constrains the majority of the binary population to tight orbits whilst a high value leads to a greater spread in d . Both scenarios of high and low R were examined for the clusters in these simulations.

The separation of the binary components helps to determine what happens during a binary single encounter. When a tight binary undergoes an interaction, the energies involved tend to be much higher than during a corresponding interaction with a wide binary. However, the probability of a tight binary undergoing an interaction, is much lower than that of a wide system; this is simply because it presents a much smaller cross section. To investigate the possible differences between the tight and wide systems, two distinct upper limits on the binary separation were examined within the simulations. One, with $d_0=90$ AU, produced a tight population of binaries whilst the other, $d_0=900$ AU, produced a wider set (both with $R=100$). Interactions involving the tighter binary population should lead to a change in the energy makeup of the cluster. Either the population will harden or the lighter member of the binary system (which could be a brown dwarf) will be ejected with a substantial velocity which may be sufficient for it to escape the cluster. Interactions involving the wider binaries are more likely to result in the ionisation of the binary system. The associated kicks given to the binary components will be less than in the previous scenario, consequently it is possible that brown dwarfs released from these soft systems remain within the cluster. Our upper and lower limits on d allow us to investigate two important scenarios and see what effect they have on the evolution of the brown dwarf population. Some argument could be made for selecting an even larger upper limit for the separation of the binary components. Work by Gizis, Kirkpatrick, Burgasser, Reid, Monet, Liebert & Wilson (2001) demonstrates that the population of very wide systems ($d > 1000$ AU) is non-negligible; however, the chosen separations should allow me to investigate the interesting effects within the cluster.

Table 2.1 details the properties of the binary populations within the simulations I have run.

2.3.4 Length scales in the N-Body code

Within the N-body code there exists a characteristic length scale $\overline{\mathcal{R}}$. This is a quantity which is fed into the simulation at the start and then all length scales during the simulation are scaled by this value. This distance maybe linked to the characteristic length

Model	d_0	R	f_{bin}	f_s	f_{bd}
I	0.001	100	0.08	0.2, 0.18, 0.15, 0.13, 0.1	0, 0.017, 0.033, 0.05, 0.066
II	0.001	100	0.16	0.4, 0.35, 0.3, 0.25, 0.2	0, 0.03, 0.06, 0.1, 0.13
III	0.001	100	0.24	0.6, 0.53, 0.45, 0.38, 0.3	0, 0.05, 0.1, 0.15, 0.2
IV	0.001	100	0.32	0.8, 0.7, 0.6, 0.5, 0.4	0, 0.066, 0.133, 0.2, 0.266
V	0.001	100	0.4	1.0, 0.88, 0.75, 0.63, 0.5	0, 0.083, 0.166, 0.25, 0.333
VI	0.0001	100	0.08	0.2, 0.1	0, 0.066
VII	0.0001	100	0.16	0.4, 0.2	0, 0.133
VIII	0.0001	100	0.24	0.6, 0.3	0, 0.2
IX	0.0001	100	0.32	0.8, 0.4	0, 0.266
X	0.0001	100	0.40	1.0, 0.5	0, 0.333
XI	0.001	10	0.08	0.2, 0.1	0, 0.066
XII	0.001	10	0.40	1.0, 0.5	0, 0.333
XIII	-	-	-	-	-

Table 2.1. Properties of the binary systems in some of the simulations. Here R is the range used within the simulation to determine the binary properties, f_{bin} , f_s and f_{bd} are the fractional numbers of objects, stars and brown dwarfs contained within a binary population. The separations quoted are in model units.

scale associated with the Plummer model, b , which gives the space density as a function of radial distance from the centre of the cluster as:

$$\rho(r) = \frac{3M_c}{4\pi b^3} \left(1 + \frac{r^2}{b^2}\right)^{-\frac{5}{2}} \quad (2.15)$$

via the formula (Anderson 2001):

$$\bar{\mathfrak{R}} = \frac{16}{3\pi} b \quad (2.16)$$

During the simulations detailed values of $\bar{\mathfrak{R}}$ between 1.0 and 6.0 parsecs were investigated for both types of distribution pattern.

2.4 Numerical Results

2.4.1 Overall evolution of the cluster

I begin by giving a brief overview of my results before giving a greater discussion about each of the salient points.

Through my simulations I have found that the presence of a brown dwarf population, regardless of their individual masses or numbers, has a minimal impact on the evolution of the cluster as a whole. More massive stars experience mass segregation toward the centre of the cluster, whilst the lighter stars and brown dwarfs move to the outer parts of the cluster.

As the lighter stars and brown dwarfs move outward, some fraction of them gain a sufficient velocity to escape from the gravitational potential of the cluster. Clusters which were initially more centrally condensed (*i.e.* those with small values of $\bar{\mathfrak{R}}$) had higher velocity dispersions and as a result evaporated faster than those less tightly bound (*i.e.* those clusters with large values of $\bar{\mathfrak{R}}$).

For all the models investigated, I found that during the early part of the cluster evolution (a few t_{cross}) the escape rates of brown dwarfs was virtually identical to that of the low-mass stars. At later epochs some difference in the two rates would present itself; however, this was dependent on the binary fraction of the simulation as I shall discuss later.

I also found that both the initial density distributions evolve toward a similar state. That is to say, that the clusters that we initially set up with a uniform density rapidly evolved (within a few t_{cross}) to a state similar to the equivalent Plummer model system. The major difference between the two initial density distribution relates to the number of bodies within the cluster at a given time. It was found that the Plummer model tended to undergo an early phase of mass loss where a fraction of the cluster was lost; however, this rapid loss only took place for a short period of time. Past a few t_{cross} the loss rates for the two distributions became essentially equivalent, which is not overly surprising given the evolution of the uniform sphere and the Plummer models toward a similar King Profile.

Examinations of various cluster sizes demonstrated, that qualitatively, the evolution remains the same; however, the timescales over which the processes occurred showed variation with the initial cluster properties. Clusters with smaller values of $\bar{\mathcal{R}}$ took a shorter period (in years) to evaporate and tended to evaporate more uniformly, with stars and brown dwarfs being lost at roughly the same rates. For $\bar{\mathcal{R}}$ values below four, the loss of brown dwarfs from the Plummer and spherical model clusters were virtually identical; however, for larger $\bar{\mathcal{R}}$ values the Plummer models tended to lose roughly twice as many brown dwarfs as the equivalent spherical system at early cluster ages.

The first diagnostic commonly used to observe cluster evolution within a simulation is to look at the process of mass segregation. Fig 2.1 shows how three different mass bins contribute to the make up of four shells within the cluster, as a function of time. The three mass bins considered were $0-0.05 M_{\odot}$, $0.05-1.0 M_{\odot}$ and $M > 1 M_{\odot}$. As can be seen, initially all three mass bins are evenly distributed within the cluster; however, mass segregation is seen to take place rapidly.

By the time the cluster has evolved to the age of $10 t_{\text{cross}}$ (which in the case of a cluster with $\bar{\mathcal{R}}=4.5$ is 125 Myr, the age of the Pleiades cluster), we already see an increase in the fractional number of large (*i.e.* $M \geq M_{\odot}$) mass stars within the inner parts of the cluster, with a corresponding decrease in the fractional numbers of brown dwarfs. Whilst in the outer parts of the cluster there is a build up in the number of brown dwarfs.

This pattern continues on throughout the lifetime of the cluster. The last of the four plots represents the cluster when it has reached an age of $43 t_{\text{cross}}$. Here we note that the fractional number of heavy stars appears to increase over the entire cluster; what is really happening is that the lighter stars and brown dwarfs are being lost preferentially to the heavy stars and so the fraction of heavy stars within the cluster, as a whole, is seen to increase.

Fig 2.2 shows how the number of brown dwarfs and stars contained within the cluster varies as a function of time for a simulation which initially contained 500 primordial binary systems, each of which had a brown dwarf as a secondary. These two figures help us to understand the apparent increase in heavy star population present in Fig 2.1. At the start of the simulation the normal stars are outnumbered 3:2 by brown dwarfs,

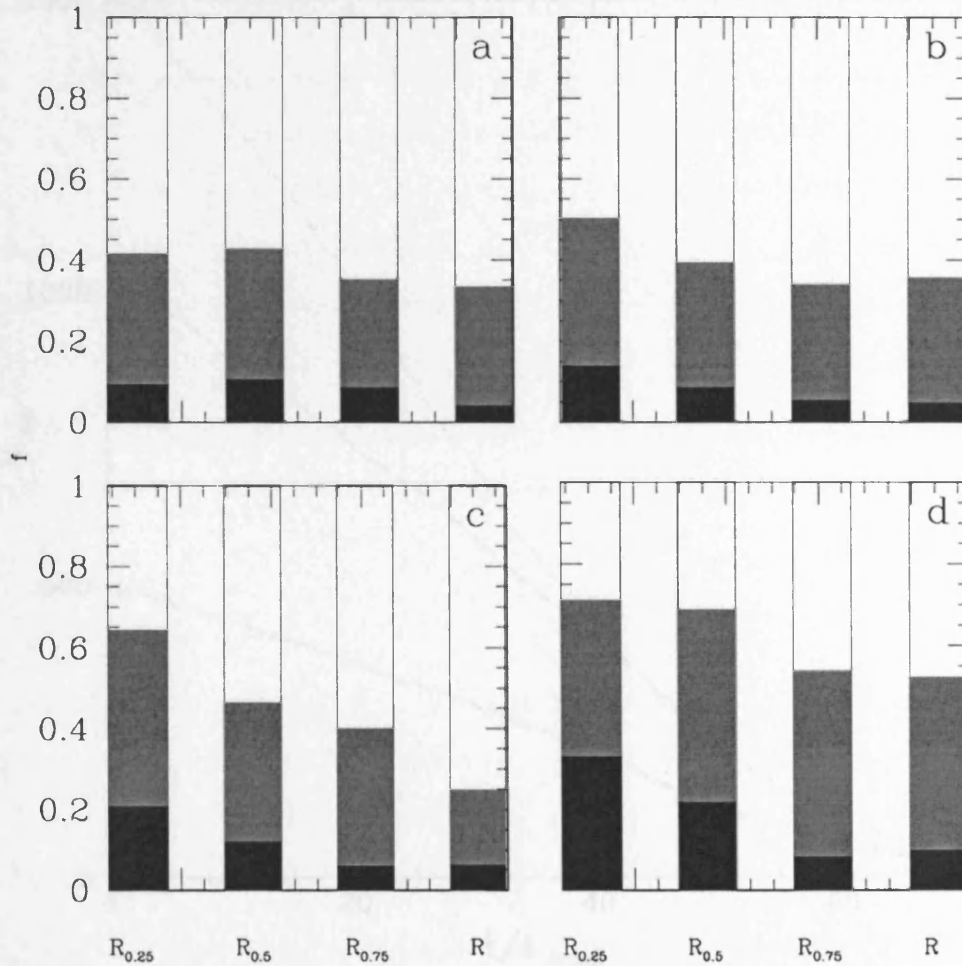


FIGURE 2.1. Plots of how the populations of stars within a given region change as a function of time. The above plots show how three different mass bins contribute to the make up of a region. The black part of the histogram represents the heavier stars $M \geq 1M_{\odot}$, the grey represents the lighter stars of the cluster $0.05 M_{\odot} < M < M_{\odot}$ whilst the plain area represents the brown dwarf population of the cluster. The four regions considered were all fractions of the tidal radius, R_T . Namely, $0 \leq R_{0.25} < R_T/4$, $R_T/4 \leq R_{0.5} < R_T/2$, $R_T/2 \leq R_{0.75} < 3R_T/4$ and $3R_T/4 \leq R < R_T$. The four boxes represent, (a) the initial dispersal, (b) the dispersal after ≈ 125 Myr ($\approx 10t_{\text{cross}}$, the age of the Pleiades), (c) ≈ 300 Myr and (d) the dispersal after 650 Myr ($\approx 43 t_{\text{cross}}$, the age of the Hyades cluster).

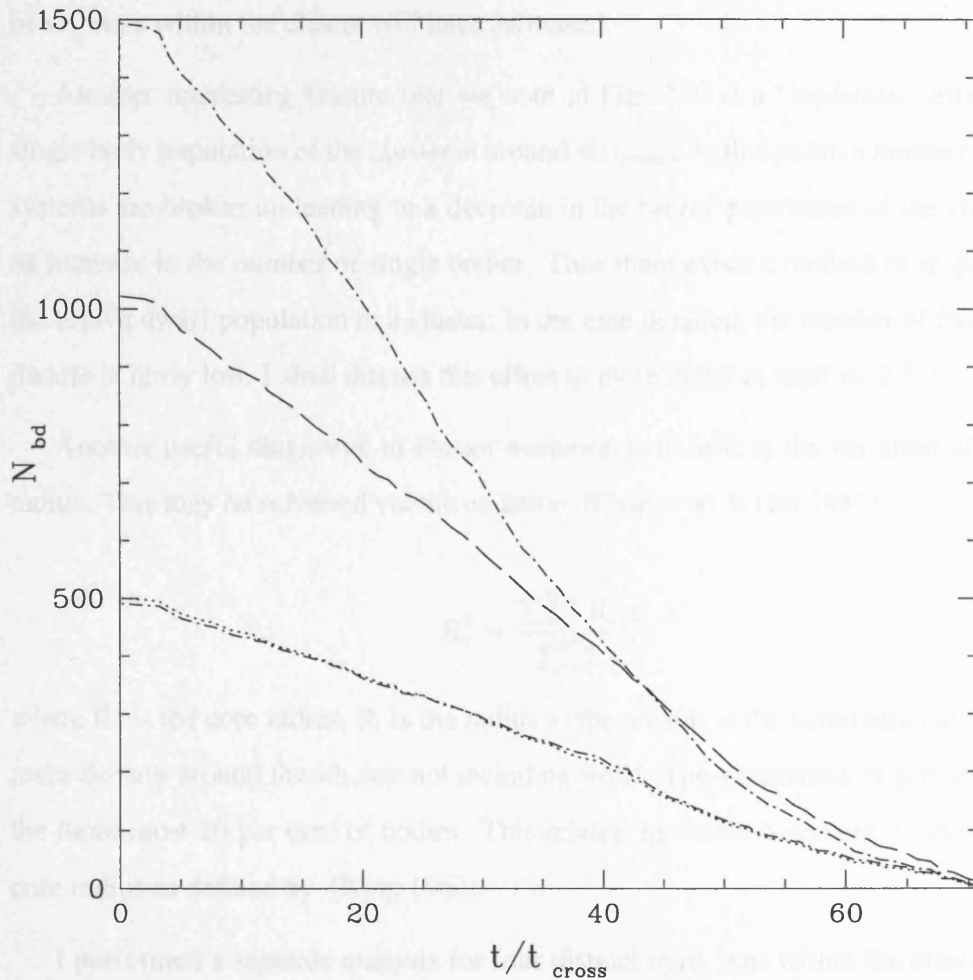


FIGURE 2.2. Evolution of the populations of the stellar and brown dwarf populations within a simulation that contained 500 primordial binaries each of which had a brown dwarf as the secondary, *i.e.* a simulation where $f_{bd} = 0.333$ (see section 2.3.3 for a full definition of f_{bd}). The dotted with long-dash line represents the single population of brown dwarfs, the long dashed line represents the population of single stars. The dotted line represents the brown dwarf population which is contained within a binary system with another cluster member and finally the dotted with short-dash line represents the stellar population contained within binary systems. Note that the number of objects in this figure are cumulative, *i.e.* there are 500 brown dwarfs tied up in binary systems and a further 1000 free brown dwarfs at the start of the simulation.

consequently the heavy star population initially makes up a very small fraction of the entire population. However, when the cluster is $\approx 35 t_{\text{cross}}$ old we see that there is a near 1:1 relation between the brown dwarf and star numbers. Thus the fractional number of heavy stars within the cluster will have increased.

Another interesting feature that we note in Fig 2.2, is a “repletion” effect in the single body population of the cluster at around $40 t_{\text{cross}}$. At this point, a number of binary systems are broken up leading to a decrease in the binary population of the cluster, but an increase in the number of single bodies. Thus there exists a method of re-populating the brown dwarf population in a cluster. In the case detailed, the number of freed brown dwarfs is fairly low. I shall discuss this effect in more detail in section 2.5.2

Another useful diagnostic of cluster evolution is to look at the variation of the core radius. This may be achieved via the equation (Casertano & Hut 1985);

$$R_c^2 = \frac{\sum_{i=1}^{N_{20}} R_i^2 \rho_i^2}{\sum_{i=1}^{N_{20}} \rho_i^2} \quad (2.17)$$

where R_c is the core radius, R_i is the radius to the i th star in the summation and ρ_i is the mass density around the i th star not including itself. The summation is performed over the inner most 20 per cent of bodies. This relates, to within 6 percent, to the observed core radius as defined by (King 1962).

I performed a separate analysis for four distinct mass bins within the cluster. These are shown in Fig 2.3. The core radius of the heavy stars ($M \geq 2 M_{\odot}$) is denoted by the dotted line and as can be seen it decreases from its initial value as the stars sink toward the deepest parts of the cluster potential. The brown dwarfs (solid line) in contrast have a core radius which increases with time. This corresponds to their outward motion, following interactions with heavier bodies. Between these two extremes we see that the overall trend is for an increased core radius, with stars gradually moving out from the cluster centre before they eventually evaporate from the environment.

An important diagnostic for my investigation is to look at the surface density profiles of the brown dwarfs. Fig 2.4 shows the profiles for two simulations, once they had reached an age of $10 t_{\text{cross}}$. Both of these simulations contained 500 primordial binary

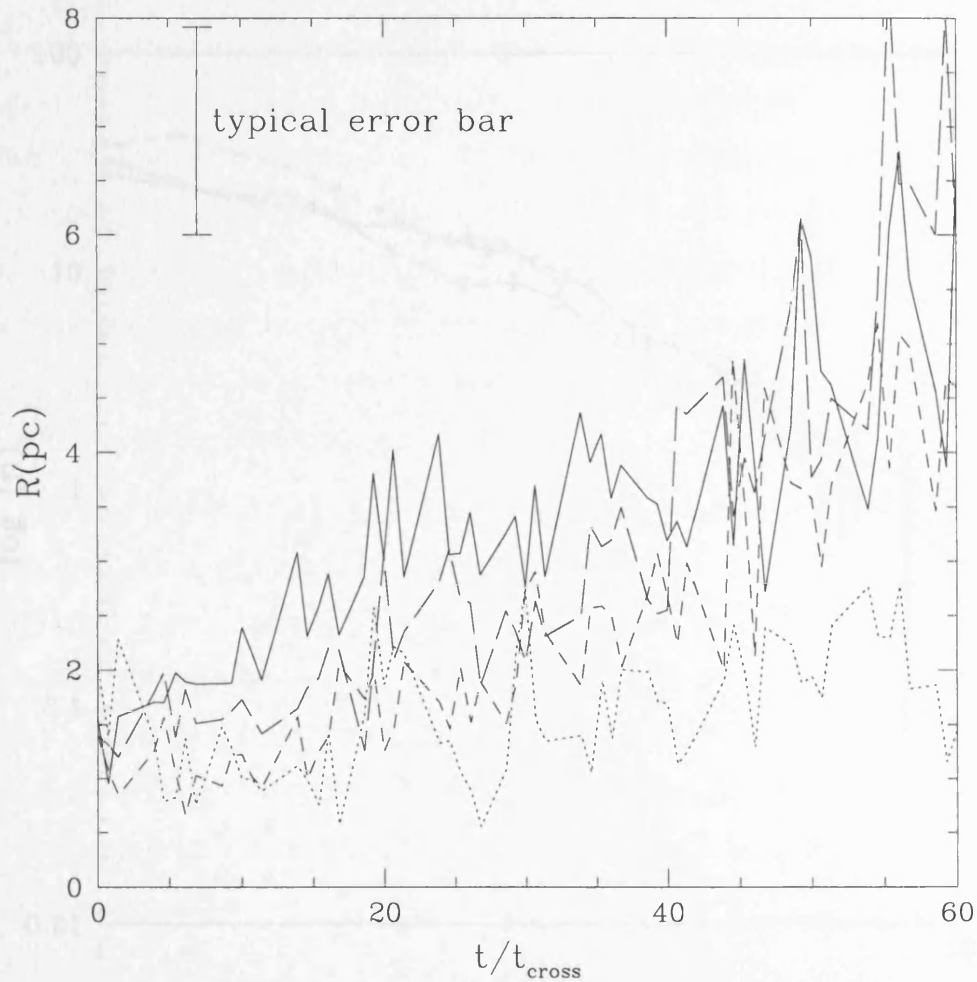


FIGURE 2.3. The time averaged variation of the core radii (in pc) for the brown dwarf population (solid line) and various stellar populations. The dotted line represents the heaviest stars within the cluster, with a mass greater than $2 M_{\odot}$. The shortest dashed line, represents stars with a mass between 1 and $2 M_{\odot}$, whilst the longer dashed line represents stars with masses between 0.6 and $1 M_{\odot}$. The rest of the stellar population hasn't been plotted for diagram clarity. However, it followed the general trend of the low mass stars and brown dwarfs. Error bars in this and all other plots are based on the standard deviation between different realisations of a particular set of cluster parameters.

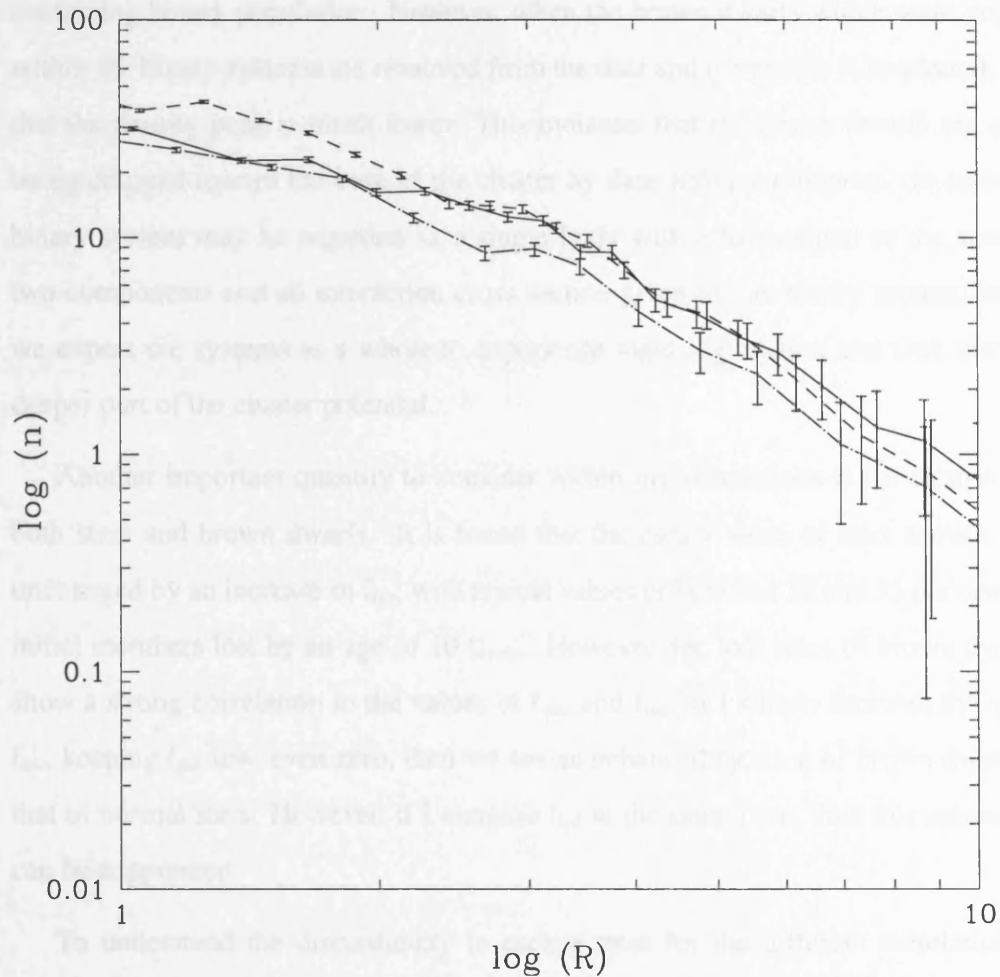


FIGURE 2.4. A comparison of the brown dwarf surface density profiles (number pc^{-2}) as a function of the cluster radius R (in pc) at the age of the Pleiades. The solid line represents the profile of a cluster which contained 500 primordial binaries, none of which had a brown dwarf member. The dashed line represents the profile of a cluster which contained 500 primordial binaries, each of which had a brown dwarf member. The dashed and dotted line is for the same cluster, but this time the binary brown dwarf components have been removed from the analysis.

systems; one set of binaries contained only stellar members, whilst the other simulation had a brown dwarf secondary in all of the systems. This second simulation is denoted by the dashed line on Fig 2.4. As can be seen, within the core regions of the cluster the brown dwarf surface density is much increased in comparison to the non-brown dwarf containing binary population. However, when the brown dwarfs which were contained within the binary systems are removed from the data and the profile is re-plotted, we see that the density peak is much lower. This indicates that the brown dwarfs are actually being dragged toward the core of the cluster by their heavier primaries. In essence the binary system may be regarded as a single body with a mass equal to the sum of its two components and an interaction cross section given by the binary separation. Thus we expect the systems as a whole to experience mass segregation and sink toward the deeper part of the cluster potential.

Another important quantity to consider within my simulations is the escape rate of both stars and brown dwarfs. It is found that the escape rates of stars remain largely unchanged by an increase in f_{bin} with typical values of between 10 and 35 per cent of the initial members lost by an age of $10 t_{\text{cross}}$. However, the loss rates of brown dwarfs do show a strong correlation to the values of f_{bin} and f_{bd} . If I simply increase the value of f_{bin} keeping f_{bd} low, even zero, then we see an enhanced ejection of brown dwarfs over that of normal stars. However, if I increase f_{bd} at the same time, then this enhancement can be suppressed.

To understand the discontinuity in escape rates for the different simulations, one must consider the timescale over which an interaction between a binary system and a single body will lead to the exchange of a body or the splitting up of the binary, t_{enc} . For a binary system that is at the hard-soft boundary, this timescale turns out to be well matched by the local relaxation timescale, t_{relax} ; however, for a binary system with a separation much less than $d_{\text{h/s}}$ we find $t_{\text{enc}} \gg t_{\text{relax}}$. Within my simulations, a number of the brown dwarf containing binaries are hard to an interaction with an intruder of $0.6 M_{\odot}$. Hence, one expects the brown dwarf binary population to exist within the cluster for a period in excess of the relaxation time. This then explains why we see a higher population of brown dwarfs within the high f_{bd} clusters at later cluster ages.

I also found that the escape rates of both the stars and the brown dwarfs are dependent on the initial cluster size and the cluster distribution pattern. As is expected, clusters which had smaller values of $\bar{\mathcal{R}}$ evaporated in a shorter period (in years) compared to clusters with larger values of $\bar{\mathcal{R}}$. For clusters with an $\bar{\mathcal{R}}$ less than four the evaporation rates of the Plummer and uniform distribution patterns were almost identical; however, for larger values of $\bar{\mathcal{R}}$ it was found that the Plummer models underwent an enhanced mass loss at early cluster ages ($10\text{--}15 t_{\text{cross}}$) relative to the same size uniform distribution pattern. At later cluster ages the loss rates for the two models become more even; however, the Plummer model is obviously more depleted than the uniform model.

2.4.2 Comparison to the Pleiades cluster

A comparison can be made between the properties of some of my simulations and the Pleiades cluster. I make a comparison between the Pleiades and my simulations which had an $\bar{\mathcal{R}}$ of 4.5 parsecs. Perhaps the most obvious comparison is shown in Fig 2.5. In this figure I compare the stellar surface number density profile of the Pleiades cluster to that of a simulation containing 100 binary systems, each of which was made up of two stars, and another simulation which also had 100 binary systems but with each of these containing a brown dwarf as a secondary. As can be seen, over the majority of the cluster, the three profiles match remarkably well, with the only region where the simulations show an appreciable difference being the core.

In Table 2.2 I make a comparison between the properties of some of our simulations and data for the Pleiades cluster. As can be seen, I closely match many of the physical parameters describing the cluster, in particular the core radius and the crossing times.

2.4.3 Future evolution

Evolution of the cluster beyond the age of the Pleiades ($\approx 10 t_{\text{cross}}$; for $\bar{\mathcal{R}} = 4.5$ this is equivalent to 125 Myr) is shown on many of the figures presented in this chapter. For instance in Fig 2.1 I show the continuation of mass segregation. The lower right hand

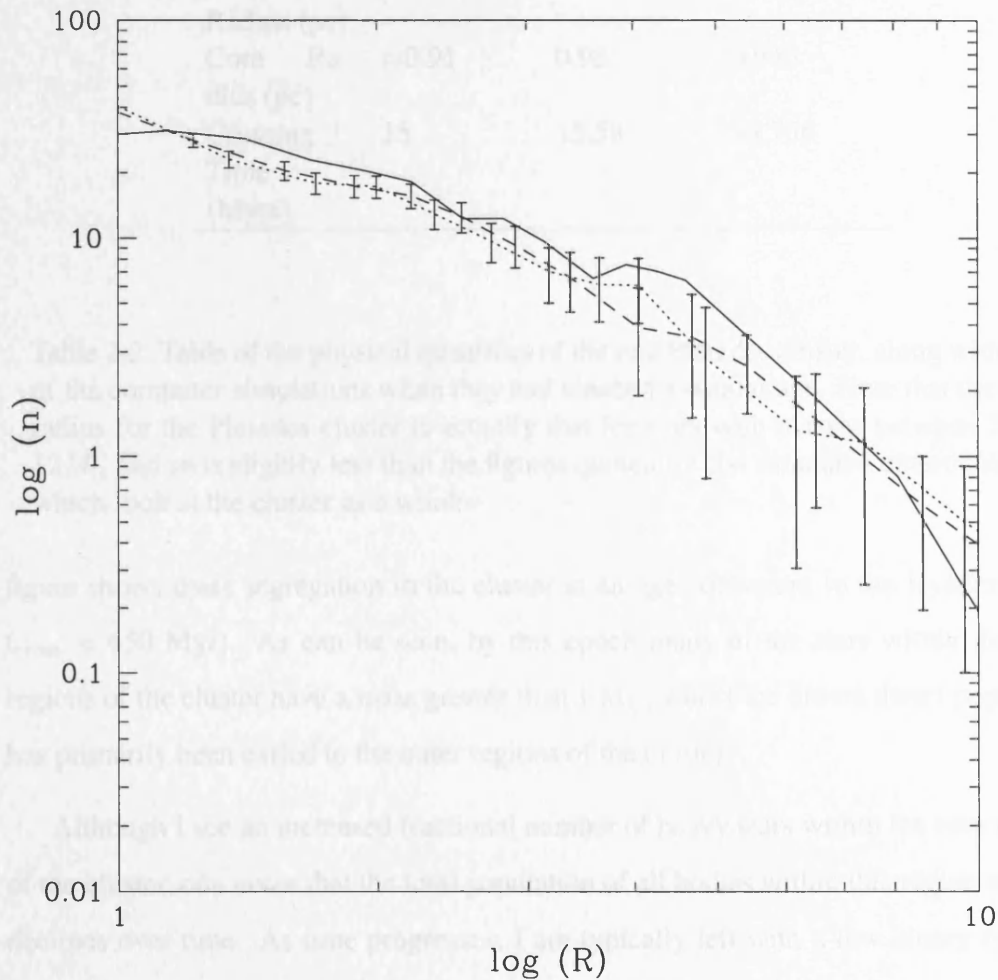


FIGURE 2.5. A comparison of the surface stellar density (all masses), n , as a function of radius (in parsecs) for the real Pleiades cluster (solid line) and two simulations. Both the simulations contained 100 primordial binaries; the dotted line had both members of the binary system as main sequence stars, whilst the dashed line represents a cluster where all the binary systems had a brown dwarf component.

Property	Real Pleiades cluster	Simulated cluster with no brown dwarfs	Simulated cluster with 1000 brown dwarfs
No. of stars	≈ 900	1013	920
Tidal Radius (pc)	13.1	12.15	13.05
Core Ra- dius (pc)	≈ 0.91	0.92	0.945
Crossing Time (Myrs)	15	15.58	14.756

Table 2.2. Table of the physical quantities of the real Pleiades cluster, along with two of the computer simulations when they had reached a similar age. Note that the core radius for the Pleiades cluster is actually that for stars with masses between 3 and $12M_{\odot}$ and so is slightly less than the figures quoted for the simulated environments, which look at the cluster as a whole.

figure shows mass segregation in the cluster at an age equivalent to the Hyades (≈ 43 $t_{\text{cross}} \approx 650$ Myr). As can be seen, by this epoch many of the stars within the inner regions of the cluster have a mass greater than $1 M_{\odot}$, whilst the brown dwarf population has primarily been exiled to the outer regions of the cluster.

Although I see an increased fractional number of heavy stars within the core regions of the cluster, one notes that the total population of all bodies within this region actually declines over time. As time progresses, I am typically left with a few binary systems, containing relatively heavy stars in tight orbits, in the core region, whilst the rest of the stellar population moves out wards and eventually evaporates from the cluster.

The most important result is regarding the evaporation of the brown dwarfs from the cluster. For the first few crossing times (10—15) the evaporation of brown dwarfs had been fairly similar to that of the lower mass stars within the simulation, with a loss of both types being in the region of 5 to 35 per cent. However, once past this point the ejection rate of the brown dwarfs may drastically increase. By $50 t_{\text{cross}}$ one observes differences between the two escape rates of up to 25 per cent in our most extreme simulations.

This increased escape rate is linked to the interaction between the binary population and the single bodies in the cluster. Virtually all the binaries will be hard to an interaction with a brown dwarf and so the result of a brown-dwarf binary encounter will be an increased velocity for the brown dwarf. This increased velocity will eventually lead to the evaporation of the brown dwarf from the cluster. We never completely lose all the brown dwarfs from the cluster; however, their numbers are drastically reduced in comparison to the stellar content.

2.5 Discussion

2.5.1 Evolution of the Cluster

We have seen that mass segregation takes place within the cluster, with the brown dwarfs being moved out of the cluster's central regions, to be replaced by heavier stars. Along with this mass segregation, I have also found an enhanced escape rate for the brown dwarfs, compared to the stellar population, at later cluster ages.

This preferential escape rate, at older cluster ages, may be very important in explaining the lack of brown dwarf observations in older clusters, such as the Hyades, although this is not the only explanation for a lack of observations of brown dwarfs in old clusters, as I shall discuss later. The loss of many of the brown dwarfs relatively early in the evolution of the cluster, would allow them to move many degrees away from the cluster of interest. A trivial calculation shows that a velocity of 1 kms^{-1} , over a period of a million years, leads to a displacement of 1 pc. This being the case, if a brown dwarf is to be within, say, four tidal radii (which is $\approx 13 \text{ pc}$ for the Pleiades cluster) then it can't have left the cluster any more than 52 Myrs ago.

2.5.2 Evolution of the binary population

Within the cluster, some of the most important interactions will be between single stars and binary systems.

Name	d	t_{cluster}	t_{cross}	t_{rel}	M	r_{tide}	r_{core}	f	references
NGC 2516	373	110	9	220	1000	13.0	-	0.89	Abt & Levey (1972), Dachs & Kabus (1989), Hawley <i>et al.</i> (1999)
Pleiades	135	125	15	90	≈ 1000	13.1	0.91	0.88	Pinfield <i>et al.</i> (1998)
NGC 2287	655	160 - 200	-	-	≥ 120	6.3	-	0.78 - 0.84	Harris <i>et al.</i> (1993), Ianna <i>et al.</i> (1987), Cox (1954)
Praesepe	174	400 - 900	19.4	370	1160	12.0	2.8	0.56 - 0.02	Andrievsky (1989), Jones & Shaffer (1991), Mermilliod & Mayor (1999), Mer- milliod <i>et al.</i> (1990), Hodgkin <i>et al.</i> (1999)
Hyades	46	625	18	390	500 - 1000	10.3	2.6	0.1 - 0.27	Perryman <i>et al.</i> (1998), Reid & Hawley (1999)
NGC 2660	2884	900 - 1200	22.8	315	≥ 400	9.6	1.5	0.08 - 0	Frandsen <i>et al.</i> (1989), Hartwick & Hesser (1971), Sandrelli <i>et al.</i> (1999)
NGC 3680	735	1450	7.5	28	≥ 100	4.3	0.6	0	Hawley <i>et al.</i> (1999), Nordström <i>et al.</i> (1997, 1996)

Table 2.3. Table listing the physical properties of some of the nearby open clusters. The individual columns describe; the distance to the cluster in parsecs, d; the age of the cluster in Myrs, t_{cluster} ; the half mass relaxation time of the cluster in Myrs, t_{relax} ; estimated total mass of the cluster in M_{\odot} , M; the tidal radius in parsecs, r_{tide} ; the core radius in parsecs, r_{core} . The penultimate column lists the fractional number of brown dwarfs left within my simulated clusters when they had reached an age equivalent to that of the real cluster. Whilst the final column gives references to papers where information has been gathered from. Columns 2 through 7 adapted from Zwart *et al.* 2001.

When a single star encounters a hard binary system the binary becomes harder and the released potential energy is converted to kinetic energy, for both the binary system and the single star. The kinetic energy given to the single star may result in it having a velocity which exceeds the escape velocity of the cluster; if this happens then the single star will eventually evaporate from the cluster.

An examination of the simulation data revealed that relatively few binary systems had undergone any significant interaction by the age of the Pleiades. A few systems did demonstrate signs of softening and a few had undergone an exchange interaction, whereby the lighter star in the binary was exchanged for a heavier intruder. The number of interactions and exchanges were dependent on the upper size of the binary, d_o , and the range, R , used. The number of exchanges was also dependent on the brown dwarf binary fraction f_{bd} .

To understand why only a few binaries have undergone interactions by the age of the Pleiades, one needs to examine Eqn. (2.5) and (2.6). By rearrangement of these two equations and substitution of the cluster age, τ , one may obtain an expression for the maximum size of a binary that has yet to undergo an interaction;

$$R_{\max} = \frac{1}{2} \left(-\frac{GM_{\text{tot}}}{v^2} + \sqrt{\left(\frac{GM_{\text{tot}}}{v^2}\right)^2 + \frac{4}{n\nu\pi\tau}} \right) \quad (2.18)$$

where, $M_{\text{tot}} = M_1 + M_2 + M_3$ and v is the relative velocity between the binary and the intruder star. As with the hard-soft boundary, we see that this is a function of the intruder mass. This formula assumes we have a constant velocity dispersion throughout the cluster. As the cluster evolves, this will no longer be the case and the formula will need to be modified. Any binary with a separation less than R_{\max} will not have undergone an interaction and so its properties should remain unchanged.

If I substitute into this formula for properties appropriate to the Pleiades cluster, $n \approx 150 \text{ pc}^{-3}$, $M_1 = M_{\odot}$, $M_3 = 0.6 M_{\odot}$ and $v = 2 \text{ kms}^{-1}$ we obtain Fig 2.6.

As marked, the figure may be broken into four distinct regions. The first region, region 1, extends from the y axis up to the solid line (which represents the maximum size of a binary yet to undergo an interaction) and lies above the dashed line (which represents

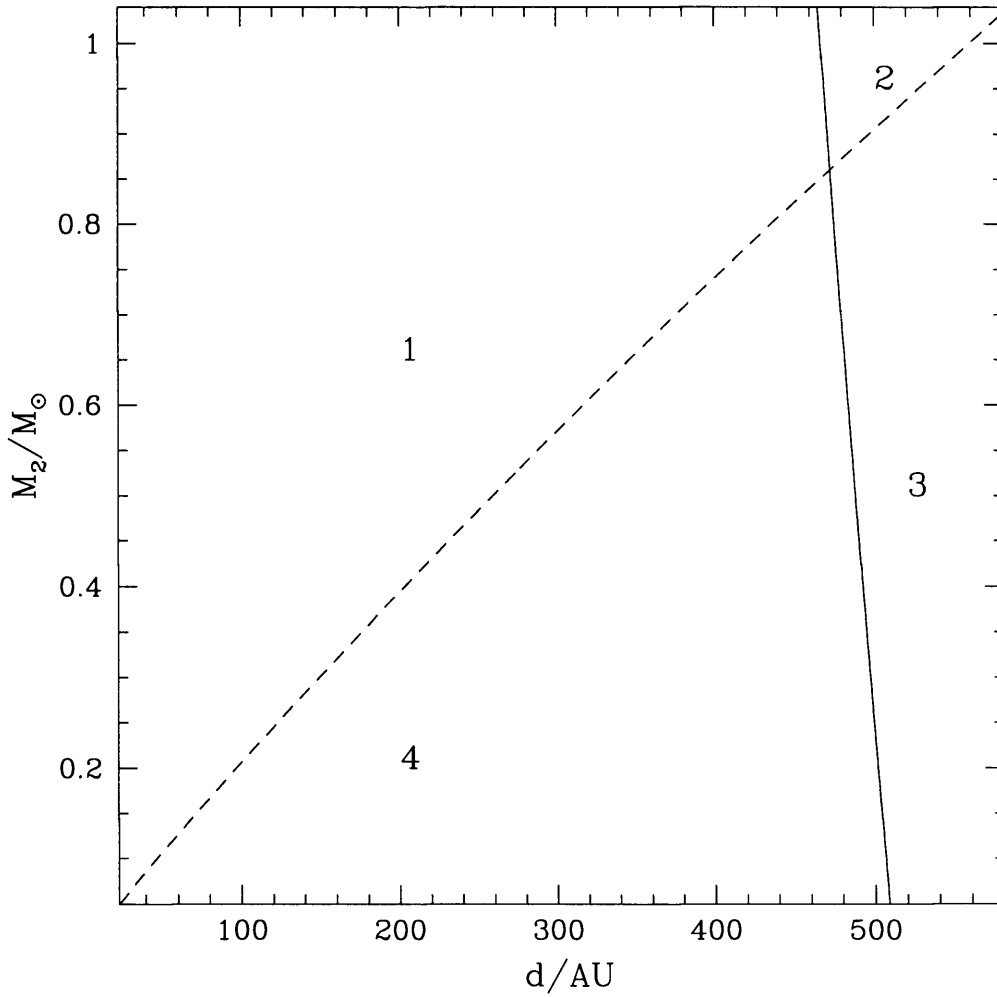


FIGURE 2.6. Comparison of the hard-soft boundary (dashed line) of a binary with the maximum size that a binary can have before it will interact with another star (solid line) both in AU, for a variety of secondary masses (in M_\odot). The plot is for a primary mass of $1 M_\odot$ with a velocity dispersion of 2 kms^{-1} .

the hard soft boundary); binaries which occupy this region may be regarded as safe within the cluster environment. Statistically, they shouldn't undergo an interaction within the cluster environment. The second region, region 2, denotes hard binaries that will undergo interactions within the time allotted. These interactions will lead to either a hardening of the binary or an exchange of members. The third region, region 3, represents soft binaries which will undergo interactions. These binaries will either become softer or be broken up. The fourth region, region 4, represents soft binaries which shouldn't interact within the period allotted.

We can investigate what Eqn.s (2.4) and (2.18) mean for the binary systems within my simulations. Fig 2.7 shows a plot of the binary separations against the product of the two components masses; the different symbols used represent which region the binary systems occupy on Fig 2.6. In this figure I show how the populations of two different simulations may be regarded at two different epochs, plot (i) and (ii) represent clusters at an age similar to that of the Pleiades cluster, whilst plots (iii) and (iv) are results calculated for a cluster with an age similar to that of the Hyades cluster. Plots (i) and (iii) represent a simulation where a primordial population of 500 binaries were forced to take a brown dwarf as a secondary, whilst plots (ii) and (iv) are representative of a simulation where again 500 primordial binaries were present but this time they were only made up of main-sequence stars. Both populations of binary systems were set up with an upper limit to their separations of $d_0=900$ AU and $R=100$. Within these four plots it is possible to reconstruct the four regions of Fig 2.6. Within Fig 2.7 the following symbols have been used to denote what region a binary system would occupy in Fig 2.6: open triangles represent region 1, filled triangles denote region 2, filled circles are equivalent to region 3 and open circles denote region 4. In each plot a line has been drawn; this may be thought of as denoting the hard soft boundary line of Fig 2.6. It is then possible to see that the four different types of binary system are clumped together in distinct regions. This indicates that the interactability of a binary system is determined by its binding energy, the higher the binding energy, the harder the binary, and the less likely it is to interact. It can be seen that, the number of binary systems that may be regarded as interactable increases with time, just as one would expect from Eqn. (2.18). However, it is interesting to note

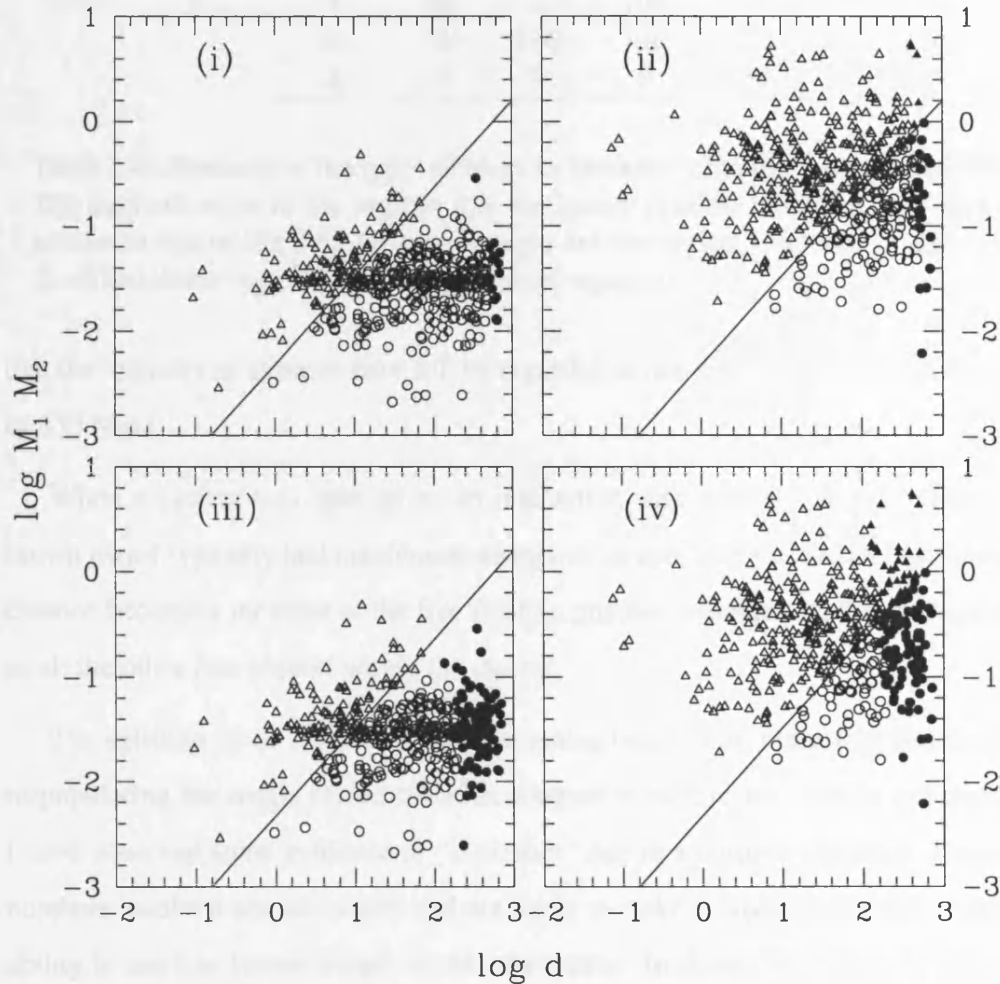


FIGURE 2.7. Demonstration of how the binary systems within two simulations may be regarded, in terms of Eqn.s (2.4) and (2.18), at different times (d in AU, M_1 and M_2 in solar units). The top row represent clusters with an age similar to that of the Pleiades, whilst the lower row represents clusters at the age of the Hyades. Two separate simulations were considered. Plots (i) and (iii) represent a primordial population of 500 binary systems in which each of the systems were forced to have a brown dwarf as a secondary; plots (ii) and (iv) represent a population where the binary systems were only made up of main sequence stars. Open triangles represent binary systems which may be regarded as hard and non-interacting within the allotted time period, filled triangles denote binary systems which are hard and may interact within the given period. Open circles represent non-interacting soft systems and filled circles show soft interacting systems.

symbol	plot i	plot ii	plot iii	plot iv
○	340	155	246	86
●	14	22	108	91
△	146	318	146	285
▲	0	5	0	38

Table 2.4. Numbers of the types of binaries present within the four plots of Fig 2.7. The symbols refer to the regions that the binary systems would occupy on a plot similar to that of Fig 2.6. An open triangle denotes region 1, a filled triangle region 2, a filled circle region 3 and an open circle region 4.

that the majority of systems may still be regarded as non-interactable even after a period of 650 Myrs.

When a system was split up by an interaction with a third star, the ejected star or brown dwarf typically had insufficient energy to escape from the cluster. As a result it in essence became a member of the free floating population subject to the same conditions as all the other free objects within the cluster.

The splitting up of a brown-dwarf containing binary, has interesting possibilities for re-populating the single brown dwarf contingent in the cluster. Within my simulations I have observed some evidence of “*repletion*” late in a clusters evolution; however the numbers involved are very small and not likely to make an appreciable difference in our ability to see free brown dwarfs within the cluster. In theory, we might be able to tune the binary separations, so that instead of following a description of being uniform in $\log d$, they instead have a peak in separations which cause them to become interactable all at roughly the same time. In doing so we might be able to induce a sizable “*repletion*” effect within the cluster. In actual observations this “*repletion*” effect would be seen as an increased brown dwarf population compared to what I predict should be present at a given time.

d_0	R	f_{bin}	$f_{2\text{BD}}$
0.001	100	0.40	0.16
0.001	100	0.40	0.33
0.001	100	0.40	0.50
0.001	100	0.40	0.66

Table 2.5. Details of the additional runs performed (along with those detailed in Table 2.1), to investigate the effects of a population of binaries made up solely of brown dwarfs. Within the table, d_0 is the maximum separation between the binary components, R is the Range of the binary orbits *i.e.* it defines the spread in binary orbits, see section 2.2.2 for full details. f_{bin} is the fraction of objects within the cluster that are contained in binaries, and $f_{2\text{BD}}$ is the fraction of brown dwarfs contained within binaries with other brown dwarfs.

2.5.3 Brown dwarf - brown dwarf binaries

Prompted by the discovery of several brown dwarf - brown dwarf binary systems within the Pleiades cluster, a set of simulations were run within which a distinct fraction of the brown dwarfs were forced to be in a binary system with another brown dwarf, along with a population of binary systems composed solely of stars. This fraction, which I refer to as the double brown dwarf fraction, is defined so that;

$$f_{2\text{BD}} = \frac{N_{\text{bd,bd}}}{N_{\text{bd,bin}} + N_{\text{bd}}} \quad (2.19)$$

where, $N_{\text{bd,bd}}$ is the number of brown dwarfs contained within a binary system with another brown dwarf. In all the simulations I kept the total number of binary systems constant.

The overall evolution of the cluster isn't effected by the population of brown dwarf - brown dwarf binaries; however, the number of exchanges within the cluster is sensitive to the value of $f_{2\text{BD}}$. As the fraction of binaries containing only brown dwarfs rises, the number of interactions where one member of a binary system is replaced by a heavier interloper falls. This may initially seem contradictory, after all the binding energy of a double brown dwarf system is much lower than that of a similar system made up with a main sequence star; however, the reason for the decreased exchange rate lies within

Eqn. (2.18). Within this equation we see that the total mass of the system is important in determining the maximum size of a binary which has not yet interacted. This mass term arises because of the effects of gravitational focusing, whereby the mass of the binary system actually draws the interloping star toward it. In the case of a brown dwarf - brown dwarf binary system, the total mass of the binary is relatively low and so the effects of focusing are negligible. Consequently, the maximum size of a binary, made up only of brown dwarfs, not to have undergone an interaction at some epoch is much greater than that of a system which contains a main-sequence star.

As a result one expects the brown dwarf containing binary population to exist within the cluster environment throughout much of the clusters lifetime. The brown dwarf - brown dwarf binary, presents possibly the best opportunity for detecting brown dwarfs. In such a system, we don't have to worry about glare effects since both components have roughly the same luminosity. Another advantage is that the pair of brown dwarfs will move onto the binary second sequence with a brighter apparent magnitude than a single brown dwarf, aiding their detection.

2.5.4 Binary system visibility

If we are to detect the two components within a binary system, an important consideration is their separation. With an *HST* angular resolution of 0.1 arcsec, one can trivially calculate the minimum binary orbit that we should be able to resolve; this turns out to be 13.5 AU for the Pleiades cluster which is 135 pc from the Earth. This is of course for a binary system lying perpendicular to the line of sight (*i.e.* an inclination of 0 degrees.) The natural inclination of the system to our line of sight means that many systems which have a separation of greater than 13.5 AU are still unresolvable.

One can show that the fraction of circular binary systems visible despite the effects of inclinations is described by the formula (see the appendix for a derivation):

$$f(x) = \sqrt{1 - x^2} \quad (2.20)$$

where x is the ratio of the true binary separation to the minimum separation required for resolution.

If one were to consider my wider binary population (*i.e.* a maximum binary separation of 900 AU) one can show that when observations are made of a cluster at the Pleiades distance with ground based telescopes (which have their resolution limited to 1 arcsec by seeing effects in the atmosphere) approximately 65 percent of the systems would remain unresolved into two distinct sources. The situation would become better with the use of the HST with approximately 14 percent of the systems remaining unresolved; however, the cost in telescope resources means that this is most unlikely to take place.

In addition to the problems associated with inclination effects, there is another method of hiding a brown dwarf from direct observation within a binary system. The low luminosity of a brown dwarf means that it is possible to hide it via the glare of the primary. A reasonable estimate for the difference in fluxes that would prevent resolution of two distinct components is of order 10:1. This problem can be overcome to some extent by making observations within infra-red bands where brown dwarfs emit much of their energy, for instance in the K band, thus ensuring the highest ratio of fluxes possible. With the 10:1 constraint on the relative fluxes, it is possible to calculate the required angular separation between the two components of a binary system if they are to be resolved optically. For a low mass main sequence dwarf as the primary, the minimum required angular separation is of order $0.7''$ for a heavy ($0.07 M_{\odot}$) brown dwarf and is of order $2.35''$ for a lighter ($0.01 M_{\odot}$), hence cooler, brown dwarf. Whilst for a primary like the Sun the minimum angular separation for a heavy brown dwarf and the primary is $1.35''$ and for the lighter brown dwarf it is $2.65''$. These angular separations can then be interpreted in terms of the minimum physical separation between the binary pair. Clearly in the case of my softer binary population (upper separation of 900 AU) located at the distance of the Pleiades, observations with a ground based telescope would then only resolve between 12 and 27 percent of the entire binary population.

Even if the binary systems are not directly resolvable, it is still possible to discover the existence of a population of binaries. The main method of detecting an unresolved population is to look for the existence of a binary second sequence in the cluster's colour

magnitude diagram as I shall discuss in the next section.

2.5.5 Brown dwarf cooling & the binary second sequence

Brown dwarfs have no renewable source of energy; that which they radiate comes from reserves built up during the original accretion from the nebula and subsequent contraction. As a result, brown dwarfs are continually cooling down and become gradually dimmer.

This cooling is important in hiding brown dwarfs from sight. There are a number of papers describing models of brown dwarfs, for example Baraffe, Chabrier, Allard & Hauschildt (1998). They find that a $0.05 M_{\odot}$ brown dwarf will have a magnitude in the I band of 19.56 at the age and distance of the Pleiades cluster, this is still within the limits of most modern surveys. However, if one were to take into account the spectrum of brown dwarf masses resulting from the tail of the IMF one finds that the Pleiades observations, with a limiting I band magnitude of 20 (which corresponds to a lower detectable brown dwarf mass of $\approx 0.04 M_{\odot}$), will fail to detect some 50 per cent of the brown dwarf population (assuming brown dwarfs have masses between 0.02 and $0.075 M_{\odot}$ described by the IMF of Kroupa (1995)). In the case of the older Hyades cluster (≈ 650 Myr) the fraction of brown dwarfs missed by a similar survey would be about the same, the greater brown dwarf age offset by the clusters proximity to us. More recent surveys extend the depths of observations through to $I=22$, in the case of the Pleiades and Hyades this should result in only ≈ 35 per cent of the brown dwarf population being missed.

The previous arguments can only be applied to isolated brown dwarfs. Those within a binary system will be subject to different conditions. As was mentioned in the previous section, the presence of a binary population, which isn't directly resolvable, may be betrayed by the existence of a second sequence on the colour magnitude diagram.

A binary system has a luminosity equal to the sum of the two components, but a colour which is redder than the equivalent star of the same luminosity (Haffner & Heckmann 1937, Hurley & Tout 1998). This leads to the formation of a second se-

quence lying ≈ 0.75 mag above the main sequence on the colour magnitude diagram. This relative height of the second sequence is true for binary systems with non-extreme mass ratios ($q = M_2/M_1$); however, in the cases where brown dwarfs are the secondary, an extreme mass ratio is likely to occur. These systems tend to move away from the second sequence and occupy the gap between it and the main sequence line.

If the mass ratio is particularly extreme, then the redness of the low mass companion is insufficient to move the system onto the second sequence. In this case the system lies either somewhere between the two lines or very close to the main sequence. The most extreme mass ratio that one expects to find lying on the second sequence is of order, $q=0.33$ (this is within the I, I-K plane Steele & Jameson (1995)). If q is less than this, the binary moves away from the second sequence. In the case where a brown dwarf is the companion, a low value of q is quite probable, unless we also have a fairly low mass primary.

Clearly even for a massive brown dwarf ($\approx 0.07 M_\odot$) if the binary system is to lie on the second sequence then the primary can be no more massive than $\approx 0.2 M_\odot$. Within my simulated data I find that from all the binary systems still present at the age of the Pleiades between 2 and 6 per cent fulfilled the condition of $q \geq 0.33$; clearly the vast majority of binary systems will not be detectable in this manner. As I have previously discussed, brown dwarfs cool as they get older. This results in their magnitudes becoming fainter and as a consequence of this, a system which was initially on the binary second sequence will move away from it. Thus, in old clusters, it is possible that a population of brown dwarfs contained in binaries may be entirely hidden from view.

Observations of the Pleiades cluster (Steele & Jameson 1995) have shown some evidence of a second sequence at very low stellar masses, thus indicating the existence of a brown dwarf population in binary systems.

2.5.6 Probabilities of finding a brown dwarf

I have detailed many methods by which brown dwarfs are lost from observations; these range from dynamical depletion to hiding the brown dwarf in a binary system. What do

these losses imply for the probability of observing a brown dwarf within a cluster?

It is trivial to find out how many brown dwarfs are left in the various simulations at various epochs, a general trend shows that the more brown dwarfs which were initially contained within a binary systems the greater the number still contained within the cluster at later epochs. However, it is not merely a question of how many brown dwarfs are present within the cluster, but rather how many can be seen. As I have said, at later epochs there tends to be a higher number of brown dwarfs in the clusters which have a high f_{bd} , this is because the brown dwarfs in binaries are retained by the cluster. Unfortunately, as I have discussed, a high proportion of binary systems are hidden via inclination effects. Despite this, one still expects to be able to see more brown dwarfs in these high f_{bd} clusters at very old cluster ages compared to clusters which had fewer brown dwarfs initially contained in binary systems.

We see, in Fig 2.8, that at the age of the Pleiades ($\approx 10 t_{cross}$), the simulated cluster still contains nearly 90 per cent of its original brown dwarf members. The most up to date observations, however, have only revealed 30 brown dwarfs within the real cluster (this is in part due to the fact that only a modest fraction of the whole cluster has been surveyed to the required depth to find brown dwarfs). When we look at a time closer to the Hyades age, 650 Myrs ($\approx 43 t_{cross}$), we see that within the more pessimistic simulation where no brown dwarfs were contained within binary systems only 10 per cent of the original brown dwarfs are retained within the cluster. The most optimistic simulation indicated that, at the age of the Hyades, the cluster would contain only 30 per cent of the original brown dwarf population.

Combination of the data within Fig 2.8 and the various effects which hide brown dwarfs (*i.e.* cooling, being contained within a binary system), shows that at the age of the Pleiades ($\approx 10 t_{cross}$) anywhere between 40 and 50 per cent of the original brown dwarf population should, in principle, be viewable (this is with an I band magnitude limit of 20, surveys limited to $I=22$ should be able to find up to 65 per cent of the brown dwarf population); whilst at the age of the Hyades ($\approx 43 t_{cross}$) this figure falls off to between 3 and 16 per cent. Thus, the probability of finding a brown dwarf in an old cluster like the Hyades is very small.

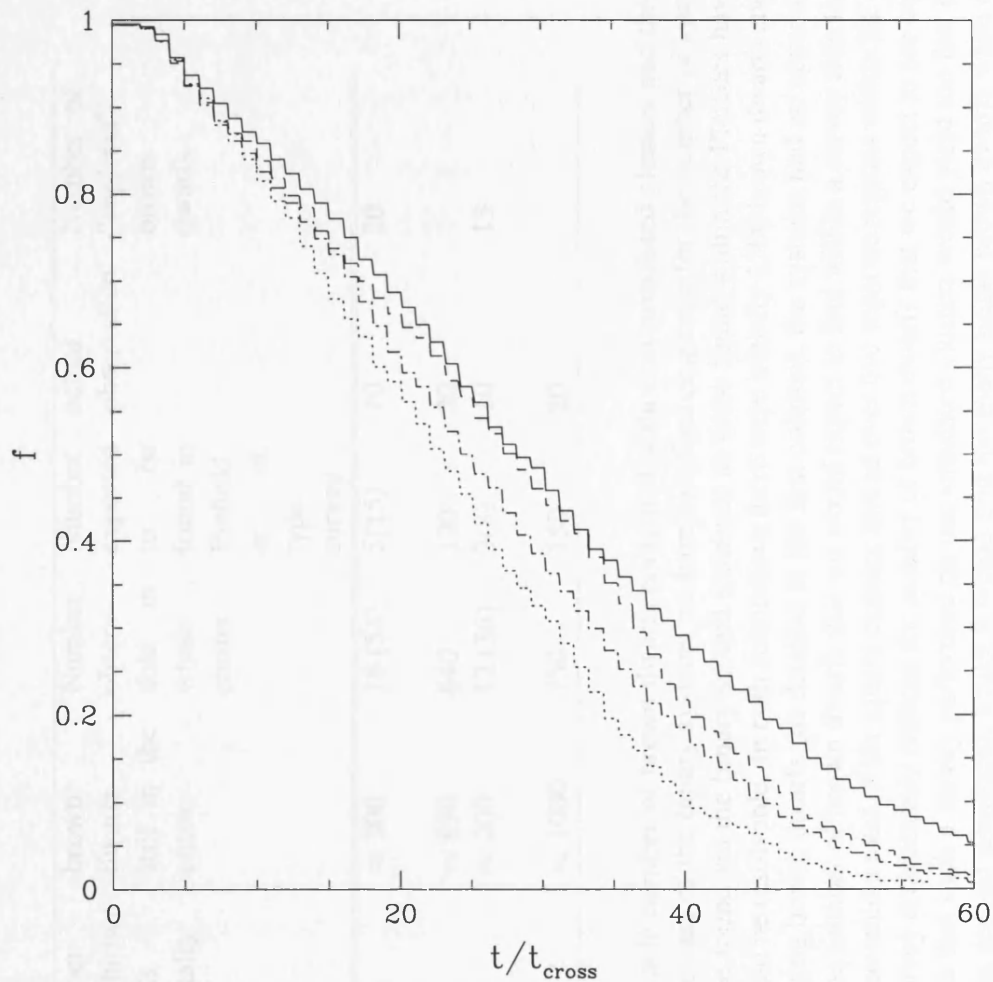


FIGURE 2.8. The fraction of the original brown dwarf population still contained within the cluster as a function of the cluster crossing time for a number of my simulations. The solid line represents a simulation containing 500 primordial binaries each of which had a brown dwarf secondary, whilst the short dashed line is for a similar simulation, except that this time no brown dwarfs were in binary systems. The long dashed line represents a simulation containing 100 primordial binaries, each of which has a brown dwarf secondary, whilst the dotted and dashed line represents the same simulation, except no brown dwarfs were contained within a binary systems. All these simulations were performed with an $\bar{R}=4.5$.

	Number of brown dwarfs originally	brown dwarfs still in the cluster	Number observ- able in whole cluster	Number expected to be found in Pinfield <i>et al.</i> type survey	actual observation	Number of “repleted” brown dwarfs
binary sys- tems	500	≈ 300	18 (54)	5(15)	10	20
single	1000	≈ 850	640	120	20	
binary sys- tems	250	≈ 200	12 (36)	3(8)	10	13
single	1250	≈ 1000	750	180	20	

Table 2.6. A comparison of the observable number of brown dwarfs contained within my simulated clusters and the current observations of the Pleiades cluster. In the case of the binary systems we have two figures quoted for the number of systems visible. The first refers to those which should be found via the binary second sequence as those found within the Pleiades have been. The second figure refers to those which should be resolvable. In both simulations there were initially 1500 brown dwarfs and 500 binary systems with a discrete fraction containing brown dwarfs (as detailed in the first column), the systems had an upper separation of 900 AU. In the fifth column we detail the number of brown dwarfs that we would expect to find within a survey akin to that carried out by Pinfield *et al.* 2000. This survey covered a total of six square degrees spread over five separate regions within the central parts of the cluster. As can be seen such a survey dramatically reduces the number of brown dwarfs that we expect to see compared to a survey of the cluster as a whole. We see that such a survey performed on our simulated clusters would yield too few brown dwarf containing binary systems (found via the second sequence), whilst it would find too many single brown dwarfs when compared to observations of the real Pleiades cluster.

2.6 Conclusions

Through my simulations I have been able closely to match the observed stellar surface density distribution, as well as other key properties of the Pleiades cluster, for a varied number of brown dwarfs within the cluster environment. This indicates that the presence of a brown dwarf population is unlikely to be betrayed by the observed stellar population.

I have demonstrated that, in the case of the Pleiades and Hyades clusters, the cooling of the brown dwarfs on their own should be insufficient to hide them from view.

However, if they are contained within a primordial binary population, then the difference in luminosity between the primary and brown dwarf companion might be enough to make the companion unobservable, due to equipment limitations. Observations lend credence to the existence of a primordial binary population within the Pleiades. In particular the discovery of a binary second sequence by Steel & Jameson (1994) indicates that there are many unresolved binary systems within the Pleiades cluster, all of which have the potential to hide brown dwarfs. The work by Richichi et al. (1994) indicates that around half of the observed stars in the sky must actually be unresolved binary systems. This again lends credence to some of the high binary fractions used in some of my simulations.

My multiple realisations of the cluster have shown that the effects of different brown dwarf binary fractions are minimal. The dynamics of the cluster remain largely unchanged with key features such as the stellar surface density profile and the loss rates of stars remaining almost the same for a particular cluster size. Containing a contingent of brown dwarfs within a primordial binary population has two key effects; first, the larger this contingent the greater the population of brown dwarfs present within the cluster at later cluster epochs. Second, by containing the brown dwarfs within a binary system we have an effective method of hiding them from view, both in terms of inclination effects and their continual cooling.

In the case of the Pleiades cluster I have demonstrated via the combination of Figs 2.4 & 2.8, that the effects of dynamical depletion of brown dwarfs is insufficient to explain the low number of single brown dwarfs observed in the well studied central portions of

the cluster (≈ 30 strong brown dwarf candidates in total, a third of which are in binary systems with low mass companions). However, in the case of the much older Hyades cluster, depletion effects become far more important, with perhaps two thirds, or more, of the initial brown dwarf population lost from the cluster; and a greater proportion hidden from view by effects associated with binary systems. This quite clearly helps to explain why there are no confirmed brown dwarf sightings within the Hyades cluster.

Of concern, however, is the relatively low number of brown dwarf observations within the well studied central portions of the Pleiades cluster. The data from my simulations would seem to indicate that the surface number density of brown dwarfs within the central parts of the cluster would lend themselves to detection. This being the case, there are a number of possibilities for explaining the disparity between observation and our results:

- 1) The number of brown dwarfs within the cluster has been over estimated. This seems likely as the work of Rabound & Mermilliod (1998) demonstrates the extreme uncertainties as regards the mass of the Pleiades cluster. They use three distinct methods of predicting the cluster mass; namely the use of the tidal radius, the virial theorem and a proposed IMF, and get three different results with very large confidence bands.
- 2) The cluster contains a population of very low mass brown dwarfs. As a result of their low mass these brown dwarfs have quickly cooled to a point below our detection threshold.
- 3) A greater proportion of the brown dwarfs are contained within moderately tight binary systems and so are not optically resolvable. Brown dwarfs contained in systems with a low-mass primary (such that the mass ratio of the system is greater than a third) will be detectable via the binary second sequence on the CMD. Brown dwarfs contained in systems with heavy primaries ($M > 0.2 M_{\odot}$) may be detectable via the radial shifts in the light from the primary, in much the same way as the search for extra-solar planets is being conducted.

It is this later theory that I favour. The observed number of single brown dwarfs compared to our predictions is so small it seems unlikely that such a large single popu-

lation exists within the cluster. The effects of mass segregation cannot move a sufficient fraction of the single brown dwarfs out of the well studied central region of the Pleiades cluster to account for the low numbers observed. I have shown that the majority of brown dwarfs contained within a binary system are virtually undetectable without a massive search looking for radial shifts in the light of the primary. We also see that my simulated data predicts too few binary systems would be observed on the binary second sequence, this would strongly suggest a much higher binary fraction within the cluster (which is of course necessary to explain the main sequence star-star binary systems we observe as well) providing a method of hiding a substantial population of brown dwarfs within the cluster. Further, an examination of my simulations demonstrates that a considerable fraction of the currently single brown dwarfs may actually have initially been in binary systems which were broken up, *i.e.* the single population is, in part, made up by the *repletion* effects that I discussed in section 2.5.1. This would remove the need for a large single population of brown dwarfs to be present within the newly formed cluster.

Chapter 3

Oil-on-water: A multiphase SPH method to model mass transfer in binary systems

3.1 Introduction

Smooth Particle Hydrodynamics (henceforth SPH) was conceived by Lucy (1977) and Gingold & Monaghan (1977). In essence it is a Lagrangian averaging scheme; the properties at a point are determined by the properties of the surrounding points. It has been successfully used over the past two and a half decades to model many astrophysical phenomena and has proved extremely robust.

Lucy developed the SPH technique whilst investigating the possibility that binary systems might be formed via a fission process of a rotating proto-star (Lucy 1977). Since these early days the method has been refined and with the increased computing power available to us more spectacular simulations have been performed. Simulations of colliding stars regularly been performed with increasing resolution, see for example Benz & Hills (1987), Davies et al. (1991), Sills, Adams, Davies & Bate (2002). Simulations of colliding neutron stars have been performed by Rosswog & Davies (2002). Whilst Bate, Bonnell & Bromm (2003) have recently performed a simulation of a collapsing star for-

mation region. They have resolved down to the opacity limit and witnessed the formation of many stars and brown dwarfs, making important inroads into the understanding of the initial mass function of stellar clusters.

SPH does however have its limitations, whilst these are not entirely inherent to the method they are related to computing. Computers can only process information to a limited accuracy, if we are dealing with numbers which are beyond the accuracy limit of the computer, then we start to get spurious results. As I will detail in Section 3.2, each of the SPH equations is a function of the masses of the particles in the simulation, if we have particles of wildly differing mass (by this I mean many orders of magnitude) the limits on computational accuracy mean that the method no longer works as the properties of very light particles become dominated by their heavier neighbours.

For this reason, until now, modellers have been forced into performing simulations where the SPH particles have masses which vary by no more than a couple of orders of magnitude. This has effectively ruled out performing a full simulation of an accreting binary system, as the mass transferred per orbit is small (of order $10^{-12} M_{\odot}$ per orbit) we would need a large number of particles (10^{12} or so, whilst the current limit is 10^6) to model the secondary star. Instead one injects particles into the disc of the primary in place of having the secondary as reservoir (see for example Truss (2002)). This has also prevented a full simulation of the onset of a common envelope system (although, attempts have been made (Rasio & Livio 1996), leaving us with no choice but to parameterise the problem in an attempt to gain an understanding of what happens during the very important process (see Chapter 5).

In this chapter, I detail my attempts to develop a new technique, firmly based on the SPH method, which might allow us to start making inroads into the understanding of the aforementioned onset of common envelope, or the beginnings of mass transfer.

I allow a population of heavy SPH particles to form the majority of a star, and then cover these in a population of very light particles. These two populations each have independent hydrodynamic interactions. The only interaction between the two populations is through the force of gravity, and a pseudo-force acting on the lighter population based on the number density of particles in the heavier particle population below it. Although

this doesn't allow for a full modelling of the system, it does allow us to start investigating unusual geometries in mass transfer systems and it should allow an understanding of the processes which occur at the start of the mass transfer process.

3.2 Theory

SPH is a very versatile method, not wasting time integrating over empty space as grid based methods inherently do. To derive the equations behind SPH we first need to gain some understanding of the interpolation scheme which underpins it. If we have some function, $f(r)$, then a smoothed approximation to the function may be expressed as:

$$\langle f(r) \rangle = \int_{all\ space} f(r')W(r - r', h)dr' \quad (3.1)$$

where W satisfies the condition:

$$\int_{all\ space} W(r, h)dr = 1 \quad (3.2)$$

W is known as the kernel, its width is parameterised by the smoothing length, h , and as $h \rightarrow 0$ we return to:

$$\langle f(r) \rangle \rightarrow f(r) \quad (3.3)$$

Normally the kernel function is selected so that it is strongly peaked at $r = 0$ and as a consequence as h tends to zero the kernel becomes a delta function, $\delta(r)$. In this case it is possible to expand the function $f(r)$ in a Taylor series about r as a power series in h :

$$\langle f(r) \rangle = f(r) + O(h^2) \quad (3.4)$$

where O maybe regarded as the error term in the approximation. Thus we see we may replace the function $f(r)$ by its smoothed approximation to within the accuracy of the smoothing process.

For a discrete set of points, with masses:

$$m_i = \rho_i dr_i \quad (3.5)$$

the integral interpolant (Eqn. 3.1) may be replaced by a summation:

$$\langle f(r) \rangle = \sum_{j=1}^N f(r_j) \frac{1}{n_j} W(r - r_j, h) \quad (3.6)$$

$$\langle f(r) \rangle = \sum_{j=1}^N f(r_j) \frac{m_j}{\rho(r_j)} W(r - r_j, h) \quad (3.7)$$

Within the scheme, each point with its associated mass is known as an SPH particle. Eqn 3.7 is the corner stone of the SPH method, it allows us to find a smoothed approximation to the physical properties of the fluid. The easiest example is to look for an expression of the fluid density. If we substitute $f(r) = \rho(r)$ into Eqn. 3.7 we get:

$$\langle \rho(r) \rangle = \sum_{j=1}^N m_j W(r - r_j, h) \quad (3.8)$$

It is also important that we have some way of calculating the derivative of a particular function. As one might expect we may write the value of the differential as:

$$\frac{df(r)}{dr} = \int_{\text{allspace}} \frac{df(r')}{dr'} W(r, r', h) dr' \quad (3.9)$$

if we integrate the right-hand side by parts we get:

$$\begin{aligned} \frac{df(r)}{dr} &= [f(r)W(r, r', h)]_{\text{allspace}} - \\ &\int_{\text{allspace}} f(r') \nabla W(r, r', h) dr' \end{aligned} \quad (3.10)$$

The kernel function is normally selected so that it tends to zero at the limits of the integral. This has the effect of removing the first term of Eqn. 3.10. We can eliminate the remaining negative sign by simply reversing the limits of our integral. Hence:

$$\frac{df(r)}{dr} = \int_{all\ space} f(r') \nabla W_i(r, r', h) dr' \quad (3.11)$$

as before we may replace the integral by summing over a fixed number of points. Thus the derivative of a function may be expressed as:

$$\langle \nabla f(r) \rangle = \sum_j \frac{m_j}{\rho_j} f(r_j) \nabla W_i(r_i, r_j, h) \quad (3.12)$$

3.2.1 The Kernel function W

As mentioned earlier, W is known as the kernel; the simplest way of understanding this function is to regard it as a weighting. If we consider the fluid as a series of particles, then it is clear that particles which are close together will have a larger impact on each others' evolution, compared to those which are further apart. This is what the kernel models within a simulation. For physically realistic results it is best to assume that the kernel function takes on some Gaussian shape, this is because we require the kernel along with its first and second derivative to be both smooth and continuous. For example, in one dimension one could have the following as a kernel function:

$$W(x_i, x_j, h) = \kappa e^{-\frac{|x_i - x_j|^2}{h^2}} \quad (3.13)$$

Where the multiplicative constant, κ , is chosen such that the kernel sums to one when integrated over all space. Included within the definition of the kernel function is a the quantity h , the smoothing length.

The smoothing length tells us about how far the influence of a particular particle extends. It is customary to truncate the kernel so that particles which are more than $2h$ away from one another have no hydrodynamical effect on each other.

For the simulations detailed within this thesis a kernel function based on a cubic spline has been used (Monaghan & Lattanzio 1985):

$$W(r, h) = \frac{1}{\pi h^3} \begin{cases} 1 - \frac{3}{2}\nu^2 + \frac{3}{4}\nu^3 & \text{if } \nu \leq 1 \\ \frac{1}{4}(2 - \nu)^3 & \text{if } 1 < \nu \leq 2 \\ 0 & \text{otherwise} \end{cases} \quad (3.14)$$

where ν is simply:

$$\nu = \frac{r}{h} \quad (3.15)$$

The advantage that the cubic spline has over the Gaussian kernel is that it has compact support (i.e. it goes to zero at finite ν).

3.2.2 Application of the SPH method to the fluid equations

Here I shall give an overview of the use of the SPH method with regard to fluid dynamics. For a more detailed derivation of all the SPH equations, the interested reader is directed to Benz (1990) or Monaghan (1992).

To use the SPH method with a fluid, we may begin by considering the equation of momentum conservation:

$$\frac{dv}{dt} = -\frac{\nabla P}{\rho} \quad (3.16)$$

where ρ is the mass density of the material, v is the fluid velocity and P is the pressure within the material.

If we were to simply apply the SPH formalism to this equation we would find that momentum wouldn't be conserved. To prevent this we re-express the right hand of Eqn. 3.16 thus:

$$\frac{dv_i}{dt} = - \left[\nabla_i \left\langle \frac{P_i}{\rho_i} \right\rangle + \frac{P_i}{\rho_i^2} \nabla_i \langle \rho \rangle \right] \quad (3.17)$$

Then, using the definition supplied by Eqn. 3.12 we can say:

$$\frac{dv_i}{dt} = - \left[\sum_j \frac{P_j}{\rho_j} \frac{m_j}{\rho_j} \nabla_i W(r, h) + \frac{P_i}{\rho_i^2} \sum_j \frac{m_j}{\rho_j} \rho_j \nabla_i W(r_{ij}, h) \right] \quad (3.18)$$

which clearly condenses to:

$$\frac{dv_i}{dt} = - \left[\sum_j \left(\frac{P_i}{\rho_i^2} + \frac{P_j}{\rho_j^2} \right) m_j \nabla_i W(r, h) \right] \quad (3.19)$$

This expression tells us about the evolution of a particle's velocity as a function of time and location.

In a similar manner one may derive the equations of energy conservation within SPH by starting with the first law of thermodynamics for an inviscid, ideal gas:

$$\frac{du}{dt} = - \frac{P}{\rho} \nabla \cdot v \quad (3.20)$$

If one then follows the same principles as for the momentum equation (or see (Benz 1990)) one can show that the evolution of the particles internal energy is governed by:

$$\frac{du_i}{dt} = \frac{P_i}{\rho_i^2} \sum_{j=1}^N m_j v_{ij} \cdot \nabla_i W(r, h) \quad (3.21)$$

where $v_{ij} = v_i - v_j$.

3.2.3 Artificial viscosity

Thus far the equations of SPH have only been derived in the inviscid form. That is, there is no method of transferring kinetic energy of the fluid into heat. This means that the equations wouldn't be suitable for performing simulations in which there were shocks present. In a real fluid the presence of viscosity allows for the conversion of kinetic energy from shocks to be converted into heat the this heat in turn can be dissipated. Fortunately in astrophysical simulations the natural intermolecular viscosity is so small is to be ignorable. Within SPH, viscous dissipation is achieved via the use of two standard artificial viscosity terms. These terms mimic the viscous pressures between two interacting particles (Gingold & Monaghan 1983):

$$P_\alpha = \Pi_\alpha \rho^2 = -\alpha \rho l c_s \nabla \cdot v \quad (3.22)$$

and

$$P_\beta = \Pi_\beta \rho^2 = \beta \rho l^2 (\nabla \cdot v)^2 \quad (3.23)$$

where α and β are free parameters determining the strength of the viscosity and l is a characteristic length scale over which the shock is spread.

Eqn. 3.22 is a bulk viscosity term, it quenches subsonic oscillations after a shock. Eqn. 3.23 is a Von Neumann-Richtmyer-type viscosity which is more important in the supersonic regime to eliminate particle inter-penetration in high-Mach-number shocks. Typical values for the two free parameters are $\alpha \approx 1$ and $\beta \approx 2$.

The artificial viscosities used within the SPH code are included in the momentum equation (Eqn 3.19) thus:

$$\frac{dv_i}{dt} = - \left[\sum_j m_j \left(\frac{P_i}{\rho_i^2} + \frac{P_j}{\rho_j^2} + \Pi_{ij} \right) \nabla_i W(r_{ij}, h) \right] \quad (3.24)$$

as well as the energy conservation equation:

$$\frac{du_i}{dt} = \frac{P_i}{\rho_i^2} \sum_{j=1}^N m_j v_{ij} \cdot \nabla_i W(r, h) + \frac{1}{2} \sum_{j=1}^N m_j \Pi_{ij} v_{ij} \nabla W(r, h) \quad (3.25)$$

For the simulations presented in this thesis I have utilised the most common approach to artificial viscosity. This was first used by Monaghan and Gingold (1983) and combines both the shear and bulk viscosities.

$$\Pi_{ij} = \begin{cases} (-\alpha c_s \mu_{ij} + \beta \mu_{ij}^2) / \rho_{ij} & v_{ij} \cdot r_{ij} \leq 0 \\ 0 & v_{ij} \cdot r_{ij} > 0 \end{cases} \quad (3.26)$$

where $\rho_{ij} = (\rho_i + \rho_j) / 2$ and

$$\mu_{ij} = \frac{h v_{ij} \cdot r_{ij}}{r_{ij}^2 + \eta^2} \quad (3.27)$$

where $v_{ij} = v_i - v_j$. The quantity $\eta^2 = 0.01 h^2$, is included to avoid divergence for small separations between neighbouring particles. This formulation for the viscosity has been shown to reproduce shocks well Monaghan and Gingold (1983).

3.2.4 The problem with SPH

Within each of the SPH equations we see that the mass of the neighbour is an important quantity. It is this dependence on mass that causes the method to fail in the case of very different mass particles. Perhaps the easiest quantity to see how these problems arise is the density. In Fig. 3.1 I show schematically how the slight movement of a very heavy particle can take it in and out of the “*sphere of influence*” of a light particle. If we suppose that the heavy particle is many orders of magnitudes heavier than the light particle (say a mass difference of 10^4) then if the heavy particle were to just come within the sphere of influence of the light particle then despite the presence of the weighting

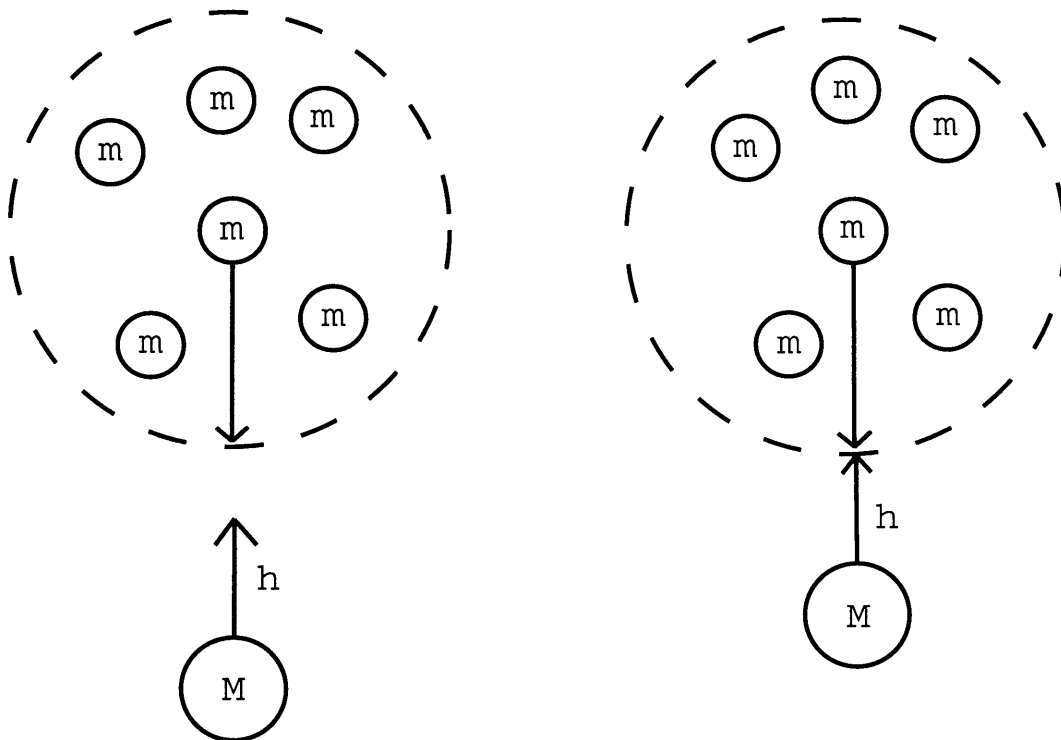


FIGURE 3.1. A diagrammatic explanation of why SPH goes wrong. Suppose the two diagrams above represent two time steps in a simulation. In the first step, the massive particle, M , is outside of the smoothing kernel for the light particle, m . Thus the density of the light particle is determined only by its surrounding similar massed particles. In the next time step, the heavy particle has come closer to the light particle. This means that it will be included in the calculation of the small particles mass. Whilst still at the very edge of the kernel function, its mass is so large it dominates the calculation of the smaller particles density and so we get erroneous results.

function it would still dominate the estimation of the light particle's density. Specifically, if we look at the kernel that has been used in this work, if we have $r/h = 1.99$ with a smoothing length of 0.05, the kernel still has a value of $\approx 10^{-4}$. With this multiplied by a large mass the density is radically altered for a light particle. This would in-turn lead to erroneous calculations of the force experienced by the particle, which then leads to energy conservation problems and the simulation results will be meaningless.

Instead we must find a way of having the light and heavy particles (henceforth oil and water, due to the similarity of a floating layer of oil on a bed of water) interacting in such a way that the oil particles are levitated on top of the water particles. With the only interaction between them being through their gravitational effects and some force

pushing the oil particles up against the pull of gravity. To do this, I have investigated the use of a pseudo force based on the number density of the water particles beneath the oil particles. Other than this pseudo-force and the effects of gravity there are no other interactions between the two species of particle.

This pseudo-force is added to the momentum equation thus:

$$\frac{dv_i}{dt} = -\sum_j m_j \left[\frac{P_i}{\rho_i^2} + \frac{P_j}{\rho_j^2} + \Pi \right] \nabla W(r, h) - \nabla \Phi - k \nabla n_{water} \quad (3.28)$$

where only particles of the same type are allowed to interact hydro-dynamically with one another.

An argument could be made for using a boundary condition to represent the surface of the star and having the oil particles laying on top of this. However, boundary conditions are notoriously difficult within the SPH method. Further, when one considers possible geometries (for instance the distorted shape of a star in a close binary system) it is clear that the existence of an analytic expression for the boundary is not guaranteed.

In Fig. 3.2 I give a diagrammatic explanation of what the ∇n force is doing. The advantage that this method has over a boundary condition is that the shape of a distorted star can be readily calculated by having a low resolution “water” star, this eliminates any need for complex boundary conditions.

The number density gradient, ∇n , of water below the oil particles is given simply by the summation over the kernel:

$$\nabla n_i = \sum_{j=1}^N \nabla_i W(r_{ij}, h_{ij}) \quad (3.29)$$

The value of the constant k was found through a series of numerical tests, I compared the number density gradient to the gravitational potential and the pressure of material above the oil layer. This meant that k would vary depending on the number of oil particle I used, with larger values required for more particles.

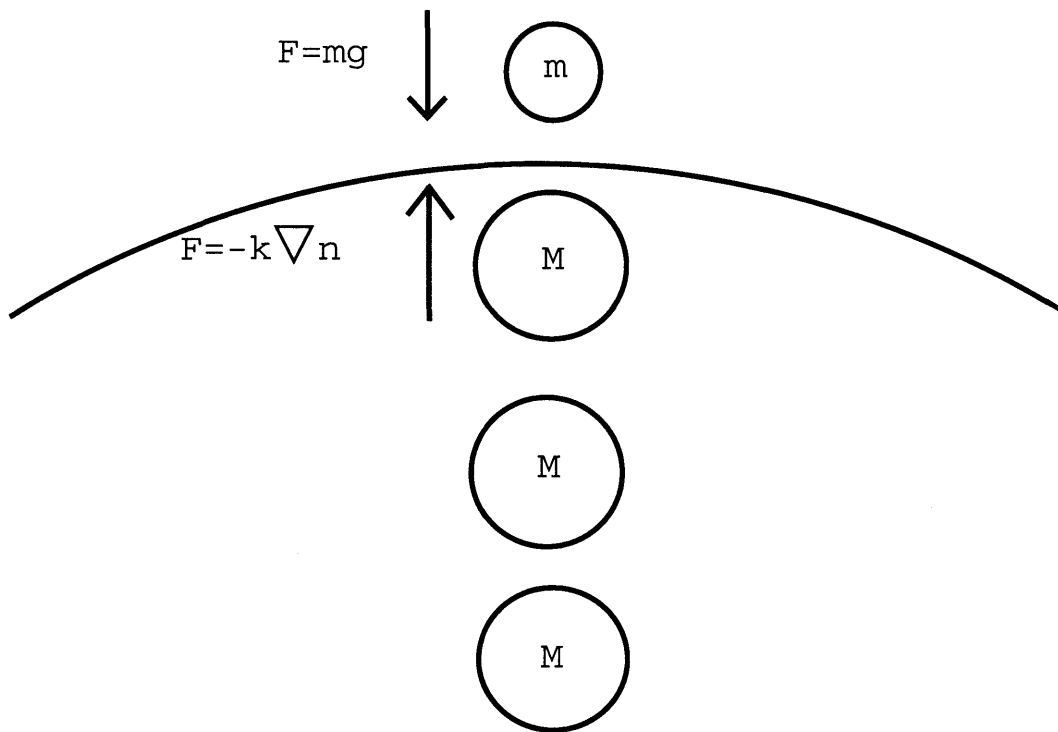


FIGURE 3.2. The concept behind the oil-on-water idea. A very light particle sits atop a body of heavy particles. It feels the gravity from the heavy particles, but does not interact with them through conventional SPH means. Instead it experiences an upward force based on the number density of particles below it. This allows a layer of oil to cover any arbitrarily shaped surface.

An alternative method of performing simulations with wildly different particle masses is to avoid substituting for $\langle n(r) \rangle$ in Eqn. 3.7. I briefly investigated this method and found that it still didn't resolve all the difficulties associated with large mass differences. However, Ott & Schnetter (2003) have investigated this method in more depth and propose some adaptations which produce some promising results.

3.3 Numerical Methods

The initial stellar model of a $0.6 M_{\odot}$ star was formed on a face centred cubic lattice. In order to minimise the number of water particles required in a simulation (thereby decreasing integration time) I remapped the initial particle distribution so that more particles were in the outer regions of the star. I used a power law to remap the particles and then used a neighbour list to construct new smoothing lengths for each of the particles. Particles were grouped so that those which initially had similar radii, all had similar radii after the remapping process. The underlying stellar models used were produced with the YREC code (Guenther, Demarque, Pinsonneault & Kim 1992). These were allowed to relax in their own potentials until the model reached an equilibrium condition.

I implemented the new formulation for SPH within the framework set out by the 3D SPH code by Benz (1990). A number of additions were made to the code to allow for the $-k\nabla n$ force. The first was the calculation of the ∇n quantity, this quantity was resolved along the three Cartesian co-ordinates so that it acted normally to the surface of the star. In addition I had to create new neighbour lists which contained neighbours of either any type of particle, or of particles only of the same type.

The code is multi-time stepping to save on computer time required for integration. To ensure the accuracy of the integration the oil particles were integrated on either their own unique time-step or on the shortest time step of the water particles, whichever was shortest.

Where simulations of binary systems have been performed, the primary has been represented as a point mass. This could represent, for example, a white dwarf companion

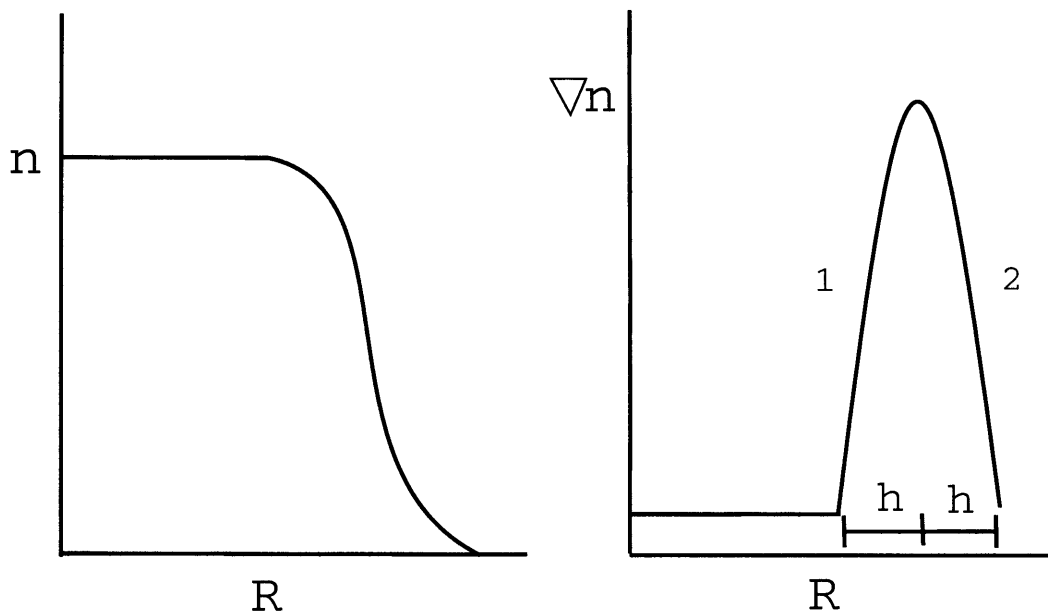


FIGURE 3.3. A diagrammatic explanation of the instability in the oil-on-water method. An initially uniformly distributed set of particles will relax to a distribution similar to that shown on the left hand side of this figure. The oil on water method relies on the derivative of the number density of the water particles. The shape of the derivative of the distribution is illustrated on the right-hand side of the figure. This breaks down in to two regions. Any oil particles in region 1 will be unstable, if they move just slightly to the left of the central peak, the ∇n becomes smaller and so the oil particle quickly sinks to the middle of the star. Oil particles in region 2 are stable. Any attempt to sink into the star are met with an increased ∇n force, and the particles are pushed back toward an equilibrium position.

or indeed a neutron star. The point mass interacted with both oil and water particles only through gravity.

A layer of oil is added to a pre-evolved stellar model. This layer is constructed by using the same face-centred cubic structure as the stellar model was created with, except that the smoothing length can be smaller. This meant that the number density of oil particles could be much higher than the number density of water particles at a particular radius. If the smoothing length of the oil particles is made too small, the oil can start to penetrate the water layer. Eventually the penetrating oil particle experiences sufficient force to expel it from the star, this can cause a disturbance in the rest of the oil layer. To counter this, it is possible to make the boundary “stiffer” by increasing the value of k . Although, too high a value of k can result in the oil layer sitting too high above the water surface.

There does exist an instability within the oil-on-water method. In Fig. 3.3 I show how the distribution of water particles leads to a spike in the derivative of n . Oil particles lying in region 2 of this diagram are stable, as any attempts to move inward are countered by an increasing ∇n force. However, Oil particles in region 1 are unstable, if they move towards the centre of the star, the ∇n force becomes smaller and the oil particles are free to move deeper into the star. Thus, to ensure the oil layer is stable, it is essential that it sits in region 2 of this diagram. This could lead to a large separation between the top of the water layer and the bottom of the oil-layer. To counter this one can simply only use a fraction of the waters smoothing length when calculating ∇n . This reduces the width of the spike in Fig. 3.3 and allows the oil to sit closer to the surface of the star.

3.4 Testing the method

To determine the usefulness of the oil-on-water technique, a number of tests have been performed. The zeroth order test was to use the code without any oil particles to ensure that the underlying SPH method had not been compromised. These tests compared the SPH evolution of a main-sequence star. The results from the oil-on-water code and a standard SPH code were identical, indicating that the underlying SPH method was still functioning correctly. I shall now concentrate on examining how well the method worked with oil particles included. In the following tests, the oil particles each had a mass of $1 \times 10^{-14} M_{\odot}$. There is no reason why the oil particles couldn't have either a lower mass or indeed a range of masses.

3.4.1 Initial testing

The first test was to examine whether the $k\nabla n$ force could balance a particle above the surface of the star. A single oil particle was placed above the surface of the star. Once a suitable value of k had been identified the oil particle remained above the stars surface.

The next test was to cover the star in oil particles, but not to have any inter-oil interactions. Again the layer was found to remain above the stars surface. There was a

degree of noise within the layer, with particles being scattered as they tried to reach an equilibrium.

I then added oil-oil interactions to the code. The details of the tests performed follow in the next sections.

3.4.2 Single star

The first test is to see how well the method can work with an isolated star. To an evolved model various numbers of oil particles were added. Tests have been conducted with anywhere between 4000 and 33,000 oil particles on top of a 15,000 particle star. It was found that the method became less noisy with additional layers of oil particles. This is because a deeper layer of oil served to damp out any initial fluctuations which occurred as the layer tried to settle to an equilibrium state.

In Fig. 3.4 I show a plot of those particles contained with $2h$ of the $z=0$ surface for a simulation with a single star with a layer of 15,000 oil particles on its surface. As can be seen, the oil covers the surface of the star completely. The initially equally spaced particles relax to an equilibrium configuration and go on to form a stable layer above the star.

In Fig. 3.5 a particle plot from a simulation with 33,000 oil particles is shown. In comparison with Fig. 3.4 we see that there is very little difference in terms of the height of the atmosphere of oil above the surface of the star. Instead, we have the oil layer sitting slightly closer to the surface of the star and the oil is somewhat more dense (in terms of number density).

All the models were allowed to evolve for an extended period of time (periods equivalent to several days-weeks) to ensure that the method was stable.

3.4.3 Rotating star

The next test for the method is to see how well it deals with rotation. This rotation could be imparted, for example, during a close passage of two stars, or it might be an intrinsic

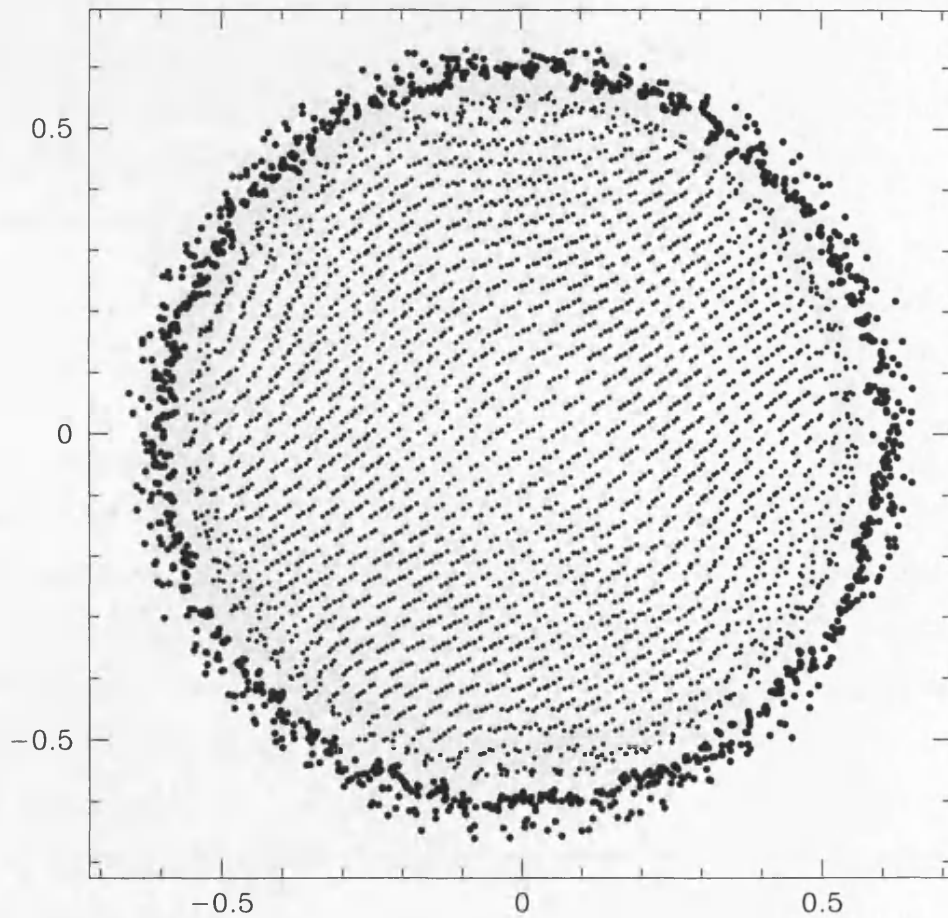


FIGURE 3.4. A $2h$ plot of a 15,000 particle star covered in a further 15,000 oil particles. This was one of the first purposeful tests done with the oil-on-water method. A stellar model was allowed to relax in its own potential before a layer of oil particles were added to its surface and the system allowed to continue evolving. The oil particles were initially equally spaced, but relaxed to a stable equilibrium within a short period of time.

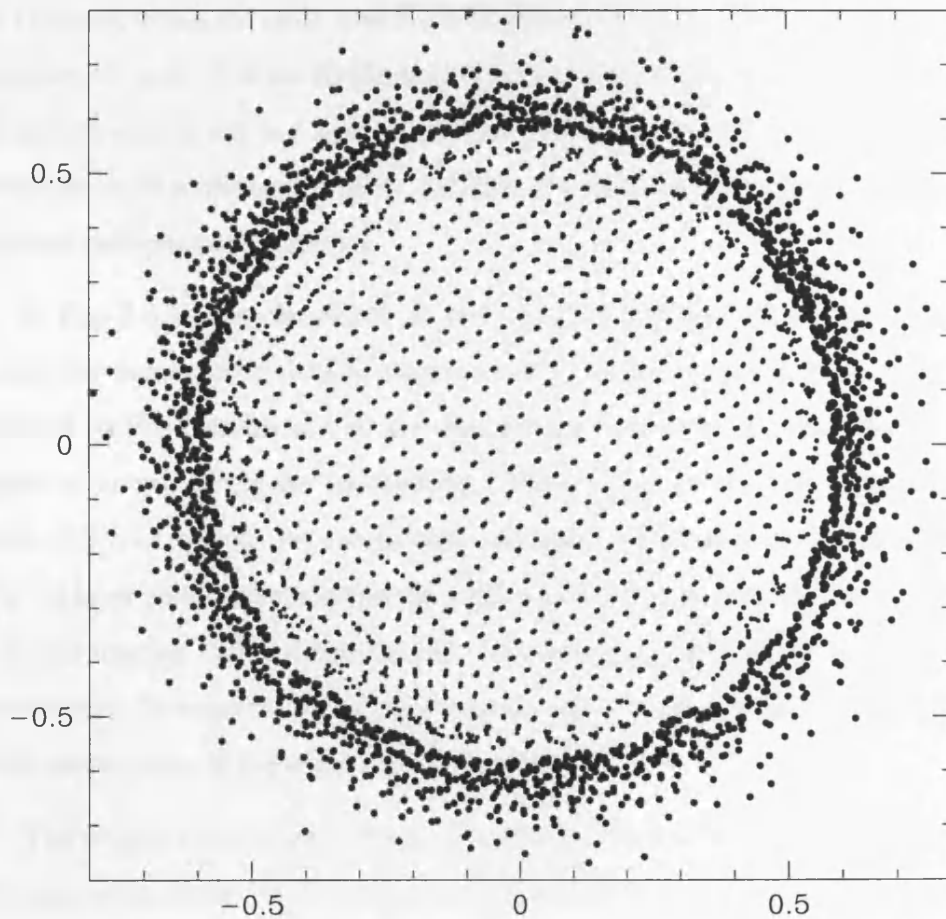


FIGURE 3.5. A $2h$ plot of a 15,000 particle star covered in a further 33,000 oil particles. Having found that the oil-on-water method could indeed support a layer of oil, it was the obvious next step to add more oil particles to the simulation. In order to ensure the particles remained balanced on the surface the value of k had to be increased slightly above that used in the lower resolution tests. As can be seen, there is very little difference in terms of the height of the atmosphere above the surface when compared to Fig. 3.4.

property of the star.

I took a relaxed oil covered star and gave all of its particles an instantaneous acceleration to some rotational velocity Ω . The star was then allowed to relax in its own potential. I considered two rotational velocities. One gave the star a surface spin period of 12 hours, whilst the other gave it a spin period of 6 hours. These two spin periods are between $1/6$ and $1/3$ of the Kepler period at the surface of the star. If we were to scale to properties appropriate to a neutron star (say $R \approx 10$ km, $M \approx 1.4 M_{\odot}$) these spin periods would be in the millisecond region. Thus this test should be sufficient for all but the most extreme astrophysical situations.

In Fig. 3.6 I show the effects of these rotation periods, along with a non-rotating model for comparison. I have taken a $2h$ slice in the y - z plane, with water particles denoted by filled circles and oil particles denoted by filled triangles. The top left hand figure is a non-rotating star for reference. The top right hand figure is the star spinning with a 12 hour period. As can be seen, the star has only become very slightly oblate. The oil layer still closely matches the surface contour of the star. The lower panel shows a model rotating with a 6 hour period. This time the oblateness of the model is more pronounced. In addition, the oil layer has become somewhat more disturbed, although it does remain close to the surface of the star.

The models were, again, allowed to run for an extended period of time to ensure that they remained stable. After an initial settling period the internal properties (for example the internal energy) of the oil was found to remain stable to the level of the integrator. The settling period for the rotating models was quite long. This could be reduced by slowly spinning up the star, rather than giving it an instantaneous spin.

3.4.4 Wide binary

The most common use for the oil-on-water method will be to examine the processes which occur within a binary system. Therefore it is important to examine the response of the oil-on-water method to the presence of an additional gravitational field.

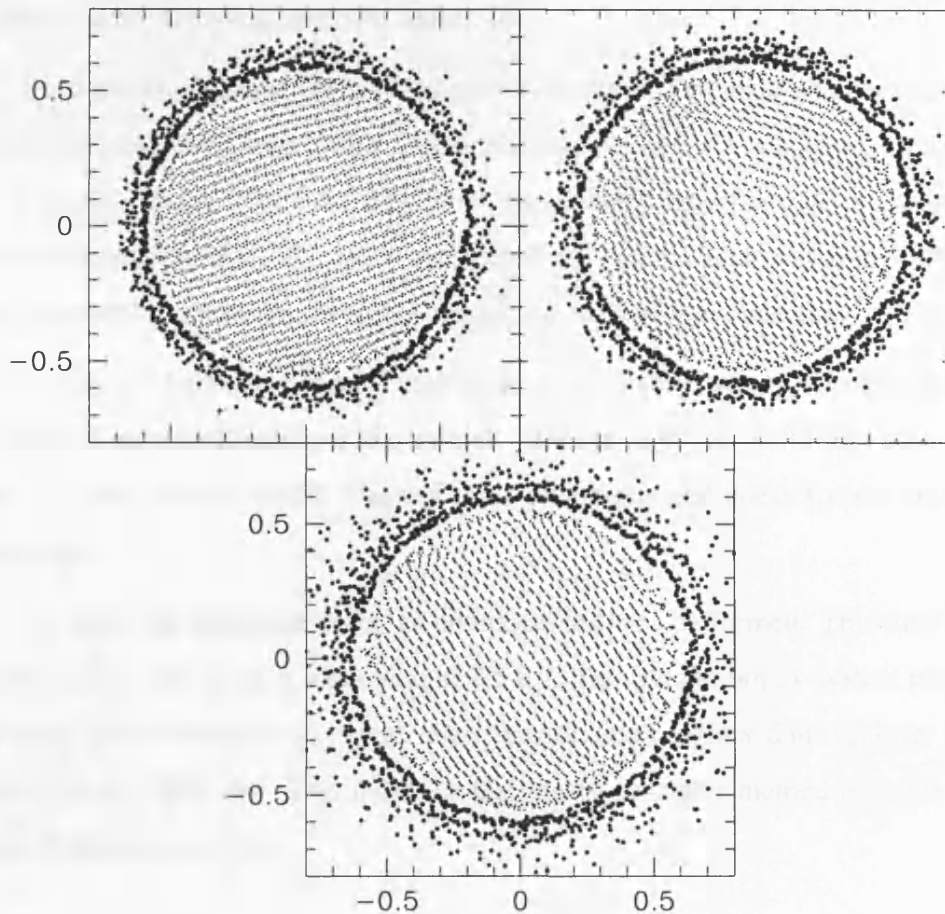


FIGURE 3.6. Plots of the effects of rotation on an oil covered star. In the top left hand panel I show a stationary model for comparison. This is a plot in the y - z plane of particles laying within $2h$ of the $x=0$ surface. In the top right hand panel I show a model which has been given a rotational velocity equivalent to a 12 hour period, we can see some distortion in the star and this is also traced out by the oil layer. In the lower figure I show a model which has been given a 6 hour period rotation velocity. As can be seen, the star is now more deformed as one would expect, but still the oil layer traces the outer boundary of the star.

For all of the binary system simulations, I placed the oil covered star in a binary with a point mass. I initially relaxed the two components in a co-rotating frame and applied a damping force to all the SPH particles to ensure that the relaxation process wasn't too violent. Once the system had relaxed the binary was moved back into a centre of mass frame and the damping force was turned off.

For a preliminary test, I selected properties which would create a binary system which would be non-Roche lobe filling. A $0.6 M_{\odot}$ oil covered main-sequence star was placed in a binary system with a $1.0 M_{\odot}$ point mass (which could represent a white dwarf) with a separation of $3.5 R_{\odot}$ and zero eccentricity. Within such a system we expect the main-sequence star to remain stable against the onset of mass transfer.

In Fig. 3.7 I show a series of snap shots of the binary system during several orbits. Clearly, as expected, mass transfer doesn't set in between the two components. Further, the oil layer remains firmly attached to its parent star and doesn't show any signs of distortion.

To stress the technique more, an additional test was performed. This time the same components were given a separation of $2.5 R_{\odot}$. This put the binary system much closer to being Roche lobe filling. Again, mass transfer didn't set in and the oil layer remained bound to the SPH star. This indicates that the oil-on-water method is stable within a detached binary system.

Eggletons formula for the Roche lobe size

To determine whether one of two stars in a binary system will be Roche lobe filling we need to consider the size of the stars Roche lobe . Eggleton (1983) produced an analytic approximation for the size of a Roche lobe .

$$r_L = \frac{0.49q^{\frac{2}{3}}}{0.6q^{\frac{2}{3}} + \ln\left(1 + q^{\frac{1}{3}}\right)} a \quad (3.30)$$

where q is the mass ratio of the system ($q=m_2/m_1$, where m_2 is the mass of the donor and m_1 is the mass of the primary) and a is the semi-major axis of the binary system. This de-

describes the volume displaced by an exponentially-spherical particle has the same properties as the inner Lagrangian point in a binary system. When a secondary particle is fixed in time, the primary star has expanded at a point after the volume is filled with water instead.

This is proven to give an idea of when a star is the most likely to be a star.

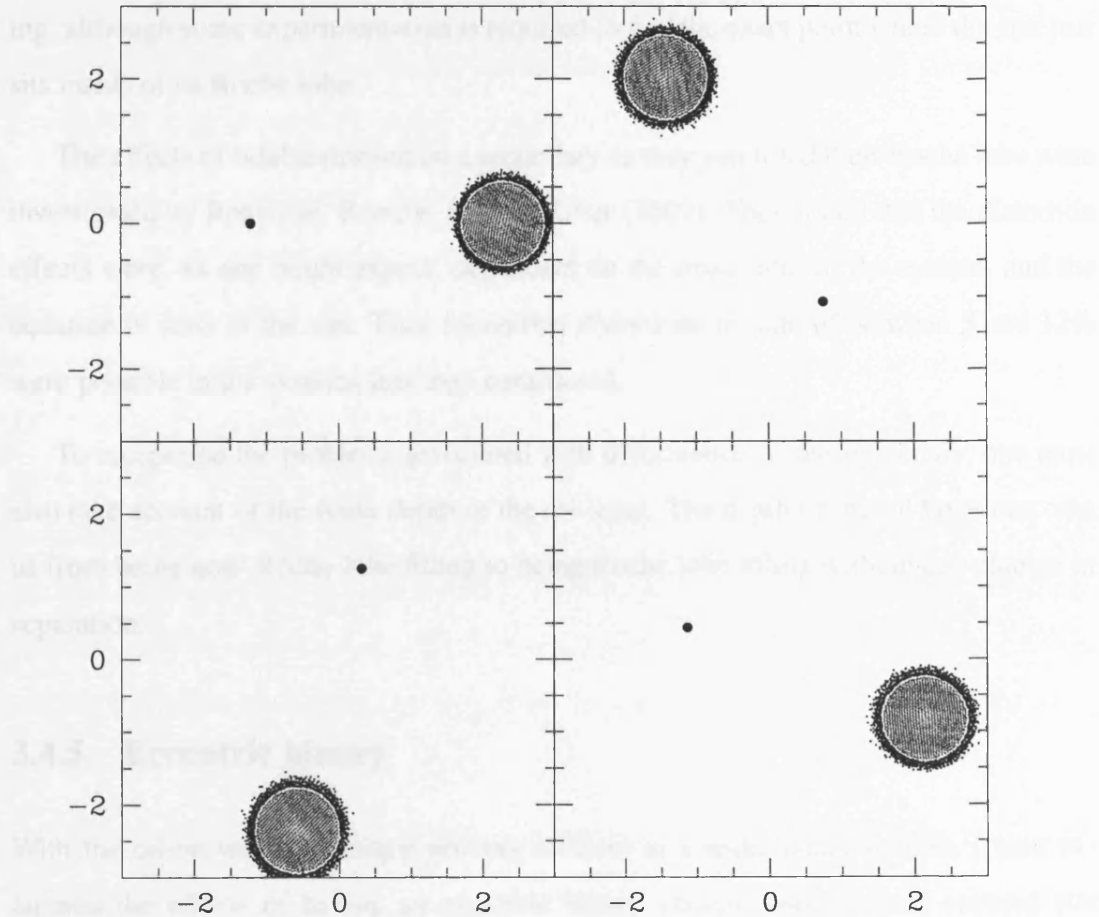


FIGURE 3.7. A time-series plot of a wide binary system. Only particles contained within $2h$ of the $z=0$ plane are plotted. Water particles are denoted by small dots, oil particles by slightly larger filled circles and the largest circle represents the point mass. The binary system was allowed to execute several orbits, during which no mass was transferred between the two components.

scribes the volume enclosed by an equipotential surface which has the same potential as the inner Lagrangian point in a binary system. When a binary system is Roche lobe filling the secondary star has expanded to a point where the volume described by r_L is filled with stellar material.

This expression gives an idea of when a star in the simulations should be Roche lobe filling, although some experimentation is required to find the exact point where the star just sits inside of its Roche lobe .

The effects of tidal distortion on a secondary as they just filled their Roche lobe were investigated by Renvoizé, Baraffe, Kolb & Ritter (2002). They found that the distortion effects were, as one might expect, dependent on the mass ratio of the system, and the equation of state of the star. They found that distortions in radii of between 5 and 12% were possible in the systems that they considered.

To compound the problems associated with deformation of the secondary, one must also take account of the finite depth of the oil-layer. The depth of the oil layer can take us from being non- Roche lobe filling to being Roche lobe filling without any change in separation.

3.4.5 Eccentric binary

With the oil-on-water technique proving resilient in a wide binary system, I next examined the effects of having an eccentric binary system where the oil covered star was Roche lobe filling at periastron and non-Roche lobe filling at apastron. Again the binary system was initially relaxed in a co-rotating frame at the periastron separation. Once the relaxation had completed the two components were given velocities consistent with an eccentric orbit:

$$v_{\text{app1}} = m_2 \sqrt{\frac{G(1-e)}{m_{\text{tot}}(1+e)a}} \quad (3.31)$$

with the subscripts interchanged for the velocity of the secondary.

In the test simulations I have used a $0.6 M_{\odot}$ secondary star covered in light particles, with a $1 M_{\odot}$ primary represented by a point mass. I found that for the secondary to be non-Roche lobe filling we required a binary separation of $2.5 R_{\odot}$ or more. For the eccentric binary test I set up the two stars with a separation of $2.5 R_{\odot}$ and an initial eccentricity of 0.2. This brought the secondary into and out of contact at peri and apastron respectively. Thus in theory we expect to see the mass transfer start during parts of the orbit and stop at others. This should lead to waves of mass moving from the secondary, through the L1 point and into a disc around the primary.

In Fig. 3.8 I show a series of snapshots from an orbit of the eccentric binary system. The oil particles are represented by the intermediate sized dots. In this figure the two stars are at periastron when the main-sequence star is on the right-hand side of the plot. At apastron we clearly see that the oil-covered main-sequence star is contained within its Roche lobe and so mass transfer doesn't set in. As the stars progress on their orbit and move toward periastron, the main-sequence star becomes Roche lobe filling and material starts to flow over the L1 point toward the primary. At periastron, we see a well developed stream of material passing to the primary. Then, as the stars start to move away from one another, back toward apastron, the main-sequence star is no longer Roche lobe filling and so the stream of material passing from the secondary to the primary breaks down and mass transfer stops.

This on-off mass transfer continues through all of the subsequent orbits. In Fig. 3.9 I show first how the separation of the two components of the binary system varies as a function of time. Then in the top panel I show how much mass is lost from the secondary as a function of time. This figure has been plotted so that both quantities are synchronised in time. Clearly, we can see that as expected mass transfer starts and stops dependent on the phase of the binary orbit. At periastron, the secondary is Roche lobe filling and so mass can pass through the L1 point to the primary. At apastron, the secondary is contained within its Roche lobe, thus material stops flowing through L1.

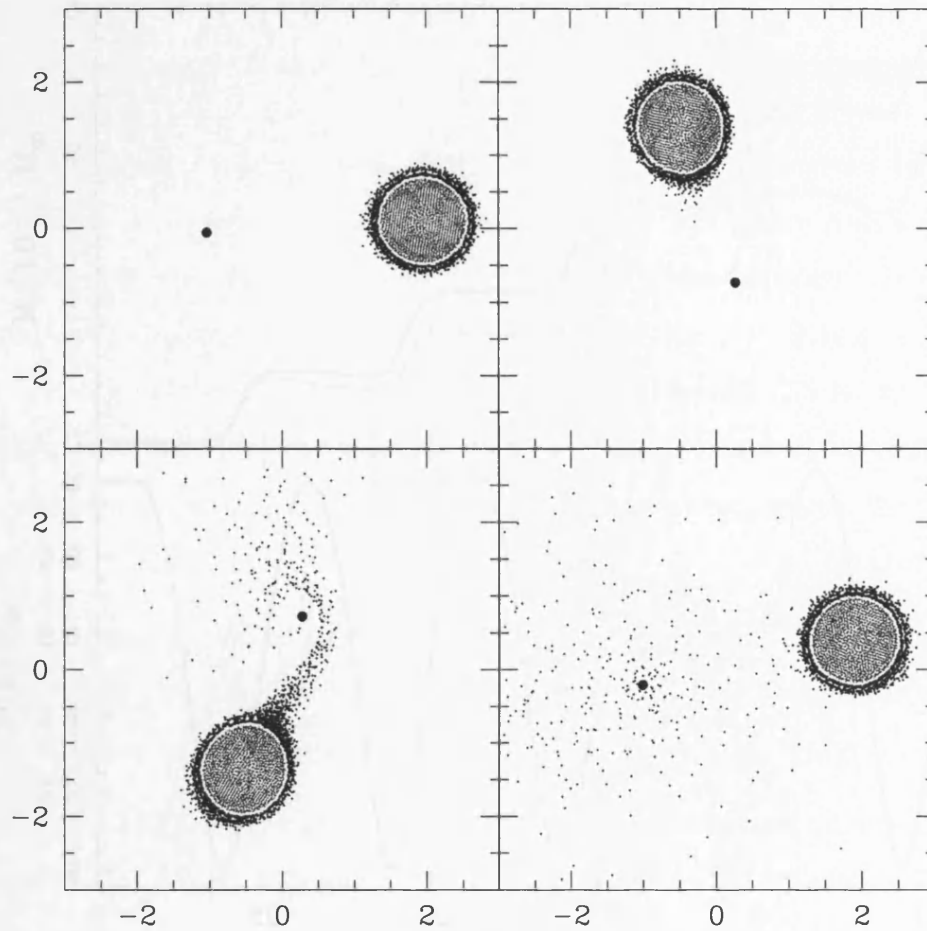


FIGURE 3.8. A time series of images from a simulation with an eccentric binary. Only particles within $2h$ of the $z=0$ plane have been plotted for clarity. The binary system was set up so that it was Roche lobe filling at periastron, but not at apastron. As can be seen in these plots we get a mass transfer stream forming as we move toward periastron, and as we move away this stream turns off, only the first orbit is presented here for clarity. This process continues throughout all the subsequent orbits as can be seen in Fig. 3.9.

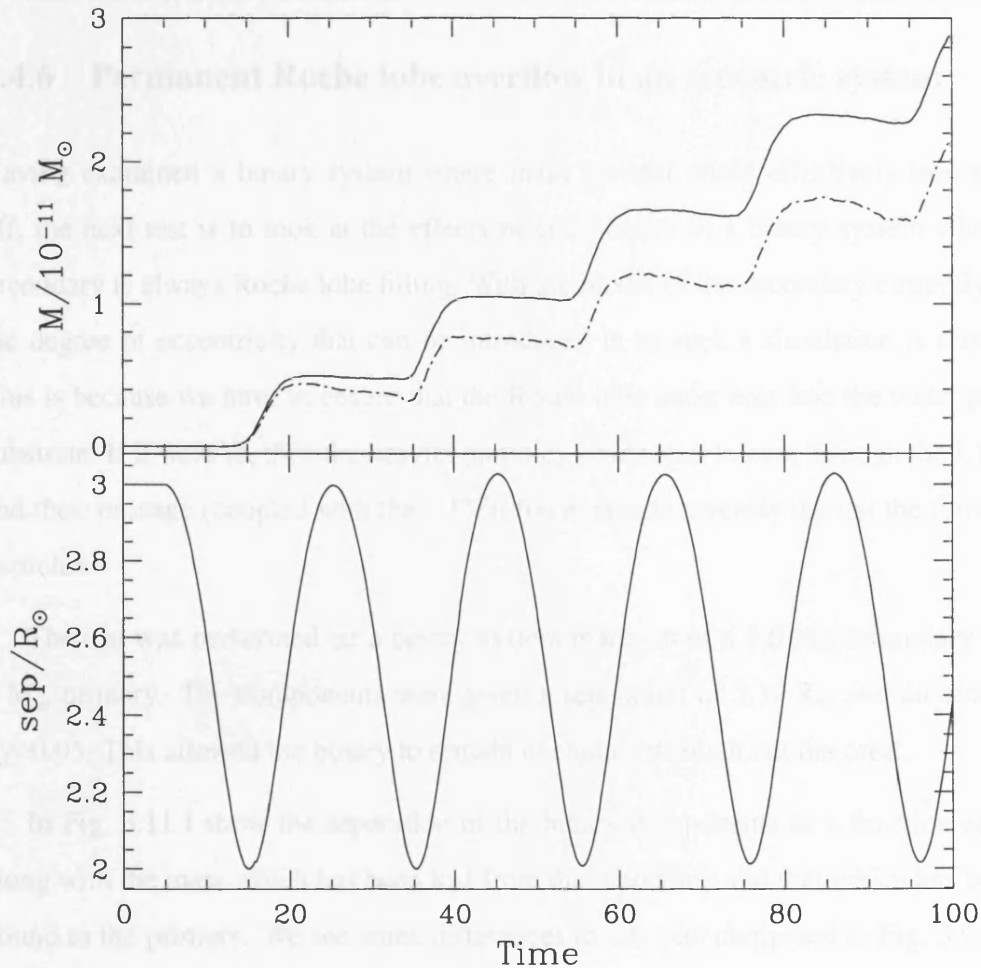
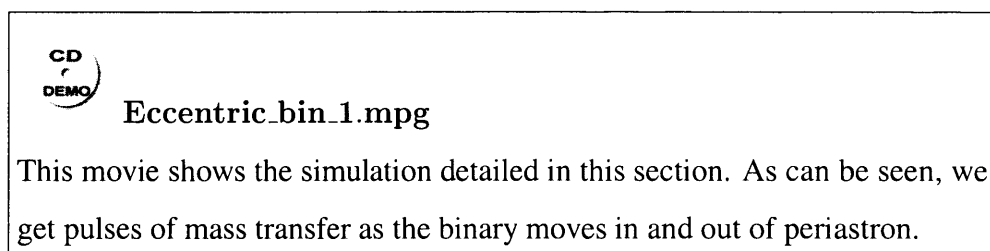


FIGURE 3.9. A plot showing how the separation of the two binary components varies with time (in solar units), whilst in the top panel I show how much mass is lost from the secondary as a function of time (solid line, in units of $10^{-11} M_{\odot}$) and how much mass is bound to the primary (dashed and dotted line). As can be seen the mass loss increases in pulses, which are representative of the phases in the binary orbit. Clearly, as we move to periastron we see that mass transfer begins removing mass from the secondary, whilst as we move back to apastron the mass transfer stops.



3.4.6 Permanent Roche lobe overflow in an eccentric system

Having examined a binary system where mass transfer could effectively turn on and off, the next test is to look at the effects of eccentricity in a binary system where the secondary is always Roche lobe filling. With the model of the secondary currently used, the degree of eccentricity that can be introduced in to such a simulation is restricted. This is because we have to ensure that the Roche lobe never eats into the water particle substrate. If it were to, then the heavier particles would start to pass through the L1 point and their passage (coupled with the $-k\nabla n$ force) would severely disrupt the flow of oil particles.

The test was performed on a binary system made up of a $0.6 M_{\odot}$ secondary with a $1 M_{\odot}$ primary. The components were given a separation of $2.19 R_{\odot}$ and an eccentricity=0.05. This allowed the binary to remain in contact through out the orbit.

In Fig. 3.11 I show the separation of the binary components as a function of time, along with the mass which has been lost from the secondary and that which has become bound to the primary. We see some differences in this plot compared to Fig. 3.9. First, the overall mass transfer rate in this simulation is higher than in the previous case, this is not unexpected given that the two components of the binary are closer together. Second, we see that the mass transfer never completely turns off during the orbit, although it is dramatically reduced as we pass to apastron.

The fluctuation in mass transfer will also lead to period variations in the torque applied to the components of the binary. The fluctuation will also likely be observable as pulses in the light curve of the binary, such as those seen in some low mass X-ray binaries.

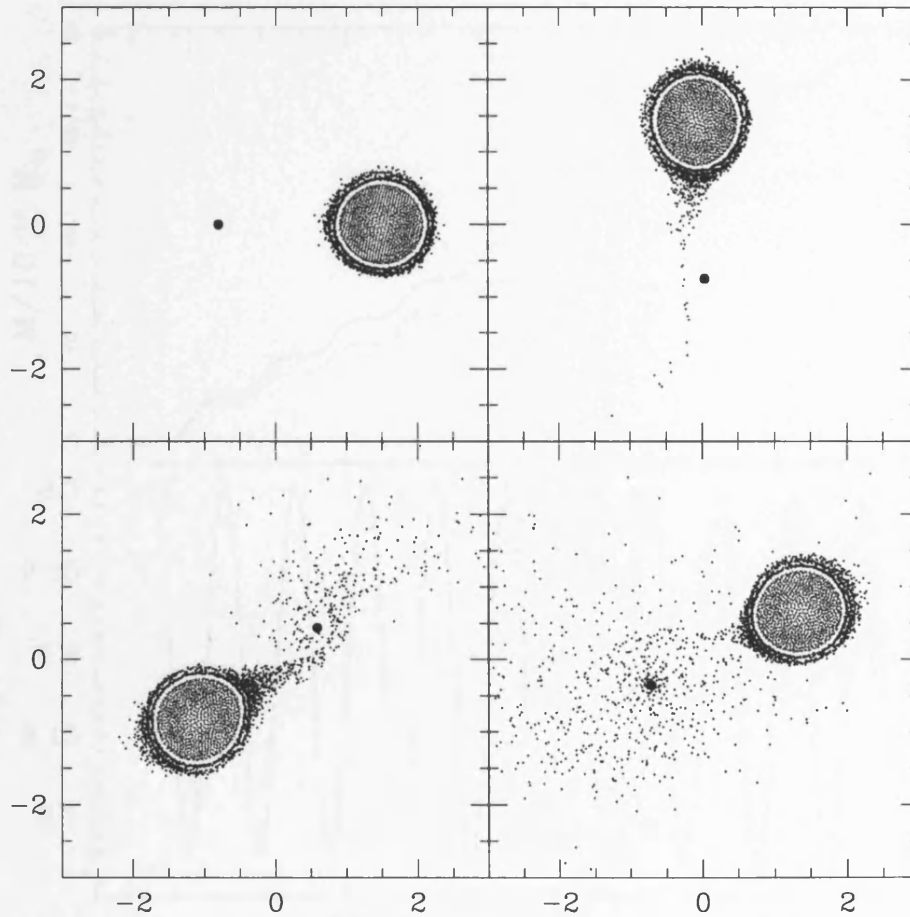


FIGURE 3.10. A time series of images from a simulation where the binary was eccentric, but always over filling its Roche lobe to some degree. Only particles within $2h$ of the $z=0$ plane have been plotted for clarity. As the binary system approaches periastron, we see a well developed mass transfer stream, and the beginnings of a disc. Moving away from periastron the star doesn't fill its Roche lobe to the same degree so the mass transfer rate drops. As a result the accretion stream loses a lot of its definition. Only the first orbit is shown here, the subsequent orbits follow the same pattern as can be seen in Fig. 3.11.

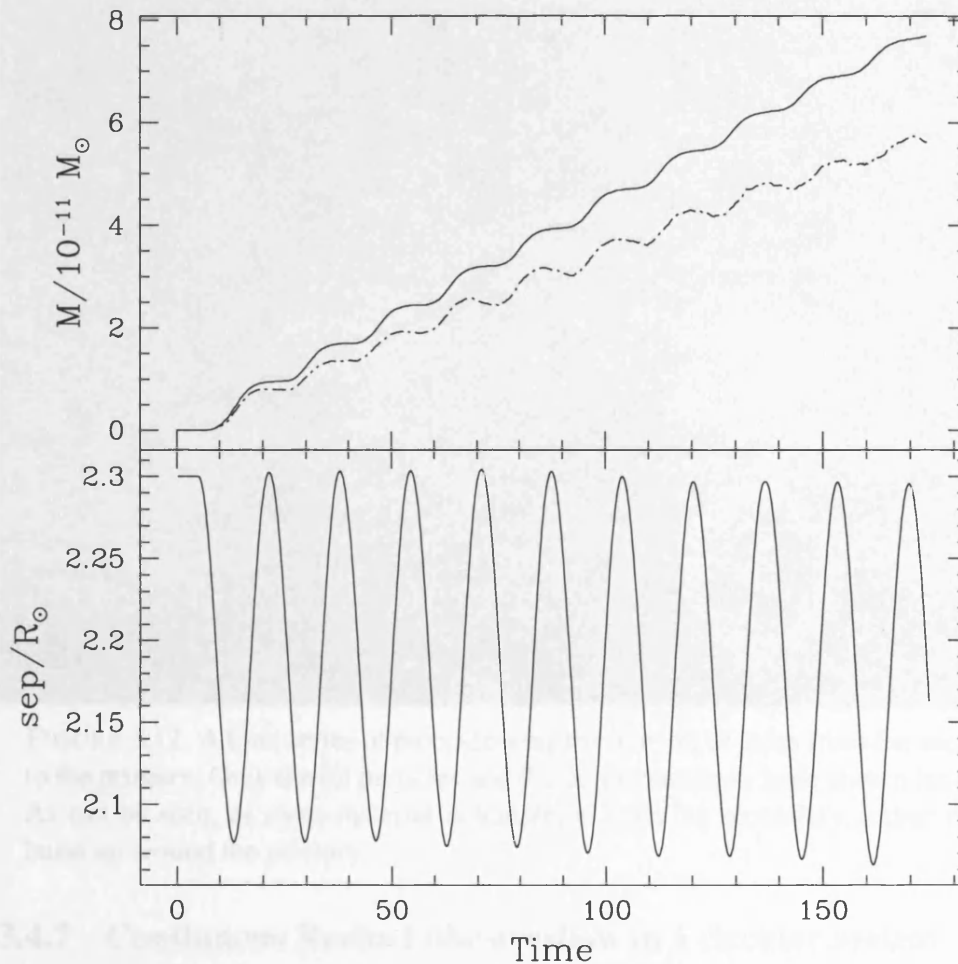


FIGURE 3.11. A plot of the separation of the binary components (in solar units) as a function of time, along with the mass lost from the secondary (solid line, in $10^{-11} M_{\odot}$) and the mass bound to the primary (dashed and dotted line). Unlike Fig. 3.9, in this system the mass transfer never completely turns off at apastron. However, the rate is reduced compared to that of periastron. As expected, given the closer orbit, the overall mass loss rate within this simulation is higher than in the simulation shown in Fig. 3.9.

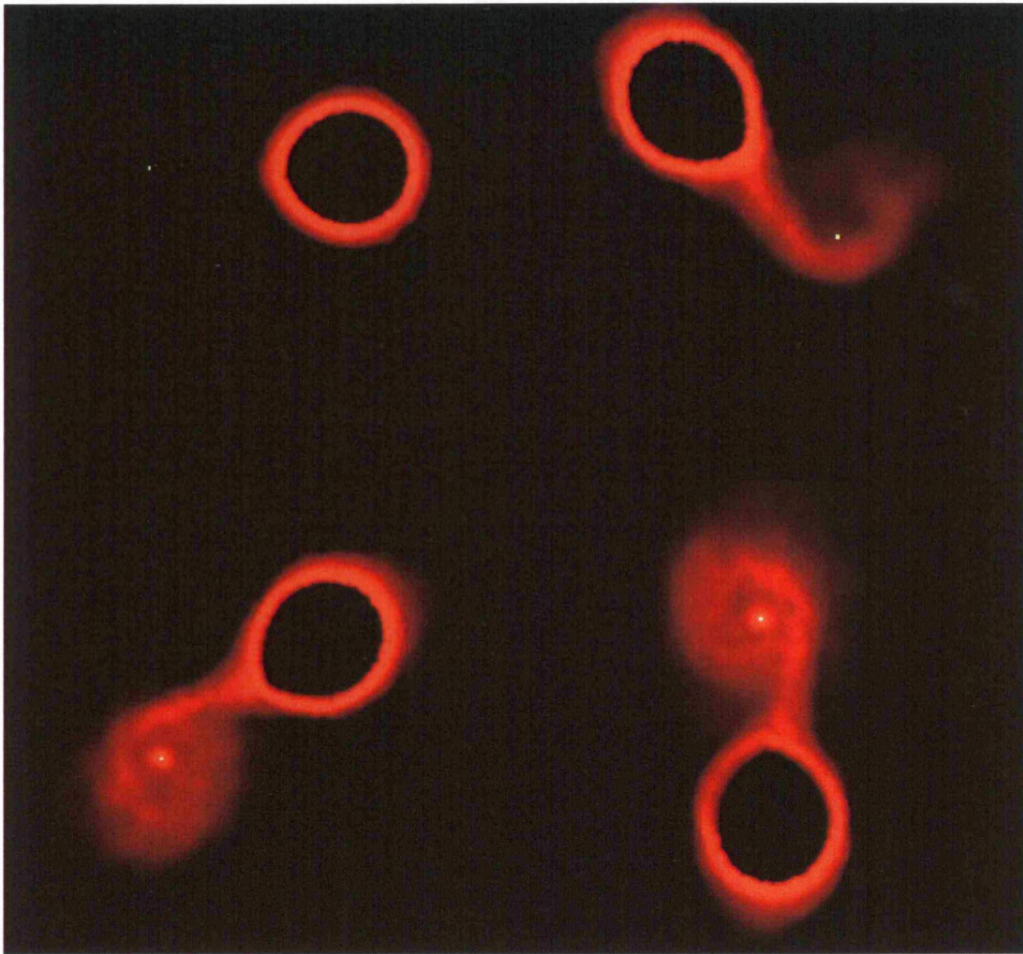


FIGURE 3.12. A time series of plots showing the transfer of mass from the secondary to the primary. Only the oil particles and the point mass have been shown for clarity. As can be seen, as more material is transferred from the secondary, a disc starts to build up around the primary.

3.4.7 Continuous Roche Lobe overflow in a circular system

Having examined system where the mass transfer rate could vary, the next step was to examine the evolution of a binary system where the mass transfer was continuous. A series of binary system separations were examined, from the point where mass transfer just set in at $2.5R_{\odot}$, through to a separation of $2R_{\odot}$. Here I shall concentrate on the simulation with $a=2R_{\odot}$.

The majority of the material that passed through the L1 point became bound to the primary and entered into initially highly eccentric orbits, before finally settling down into a disc structure. In Fig. 3.13 the mass of the disc of material around the primary is

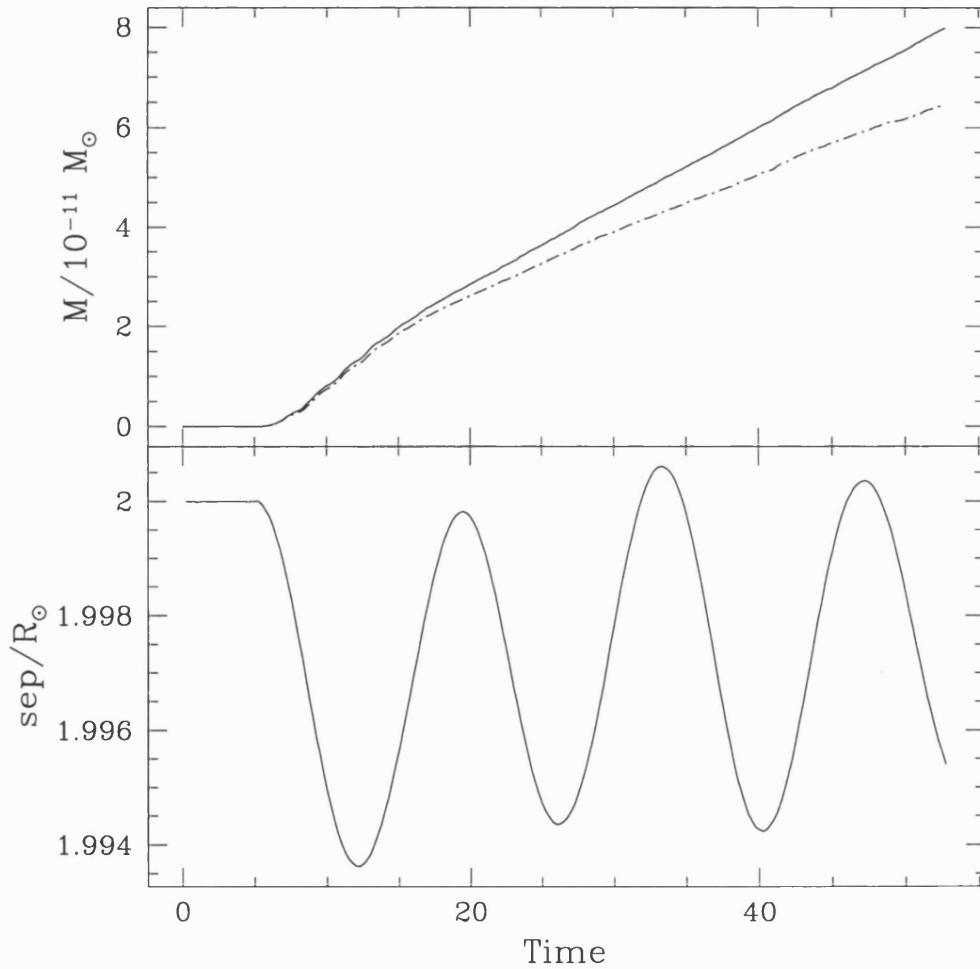


FIGURE 3.13. The lower panel shows the separation as a function of time for the primary and secondary within a circular binary system. As can be seen, there is some slight eccentricity within the orbit, but its effects are at the level of the integrator accuracy and for this particular simulation is inconsequential. In the upper panel the mass which has been lost from the secondary (solid line) and the mass which has become bound to the primary (dotted and dashed line) is plotted as a function of time. As we can see, the mass loss rates are approximately constant after an initial settling period. The majority of the material that is lost from the secondary does become bound to the primary, but there is some mass loss. This plot shows an $\dot{M}_2 = -3.11 \times 10^{-8}$ and $\dot{M}_{disk} = 2.33 \times 10^{-8} M_{\odot} / \text{yr}$.

shown as a function of time along with the separation of the primary and secondary. As can be seen the separation remains virtually constant apart from some small numerical noise, and the mass loss rate (after an initial settling period) remains virtually constant. This is as expected in a circular system. For this binary set up a mass transfer rate from the secondary of $\dot{M}_2 = -3.11 \times 10^{-8} M_\odot / \text{yr}$, whilst the rate that mass is accepted into the disc is $\dot{M}_{disk} = 2.33 \times 10^{-8} M_\odot / \text{yr}$. These transfer rates are resolved by several thousand particles, so we clearly have a good mass resolution, if not high spacial resolution.

The mass transfer rate in a binary has been predicted by Ritter (1988). The rate depends on what the degree the star is filling its Roche lobe and is given by:

$$-\dot{M}_2 = \dot{M}_0 \exp\left(-\frac{R_L - R_2}{H_p}\right) \quad (3.32)$$

where \dot{M}_0 is a scaling factor depending on various physical characteristics of the secondary and the binary system, R_L is the Roche lobe radius of the secondary, R_2 is the radius of the secondary and H_p is the scale height in the atmosphere of the secondary. Thus, the mass transfer rate is determined by how many scale heights the Roche lobe digs into the star. The exponential in the equation results from the exponential nature of a real stellar atmosphere, the scale height in which is of order $10^{-4} R_\odot$. In the current implementation of the oil-on-water code, I do not have sufficient spatial resolution to model the exponential nature of the atmosphere. By comparing the simulations presented in this chapter we do see that slight changes in separation do lead to quite pronounced changes in the mass transfer rate, and this is as expected given the exponential nature of \dot{M}_2 . Increased spatial resolution (i.e. larger particle number) should allow the modelling of the atmosphere more accurately, and we should see more of the details that Eqn. 3.32 predicts.

All the material that passes through the L1 point has the same specific angular momentum:

$$J_{\text{spec}} = b_1 \omega^2 \quad (3.33)$$

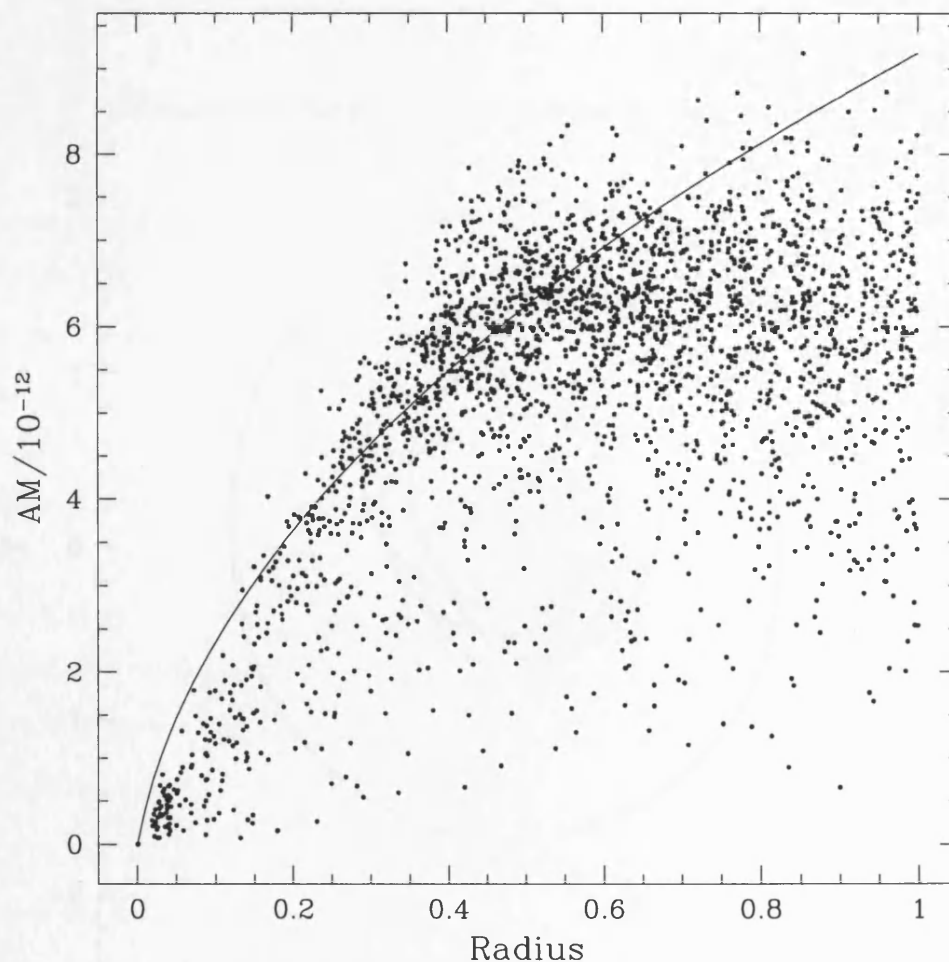


FIGURE 3.14. A plot showing the specific angular momentum (in code units) as a function of distance from the primary for the material which is in a disc around it. The solid line represents the angular momentum of a circular orbit at a particular radius. As can be seen, the angular momentum profile of the particles agrees quite well with the theoretical prediction. At $R \approx 0.5 R_{\odot}$ we see that the angular momentum of the particles starts to follow a fairly flat distribution. This radius corresponds to the circularisation radius of the system, i.e. this is the angular momentum that the particles had when passing through the L1 point.

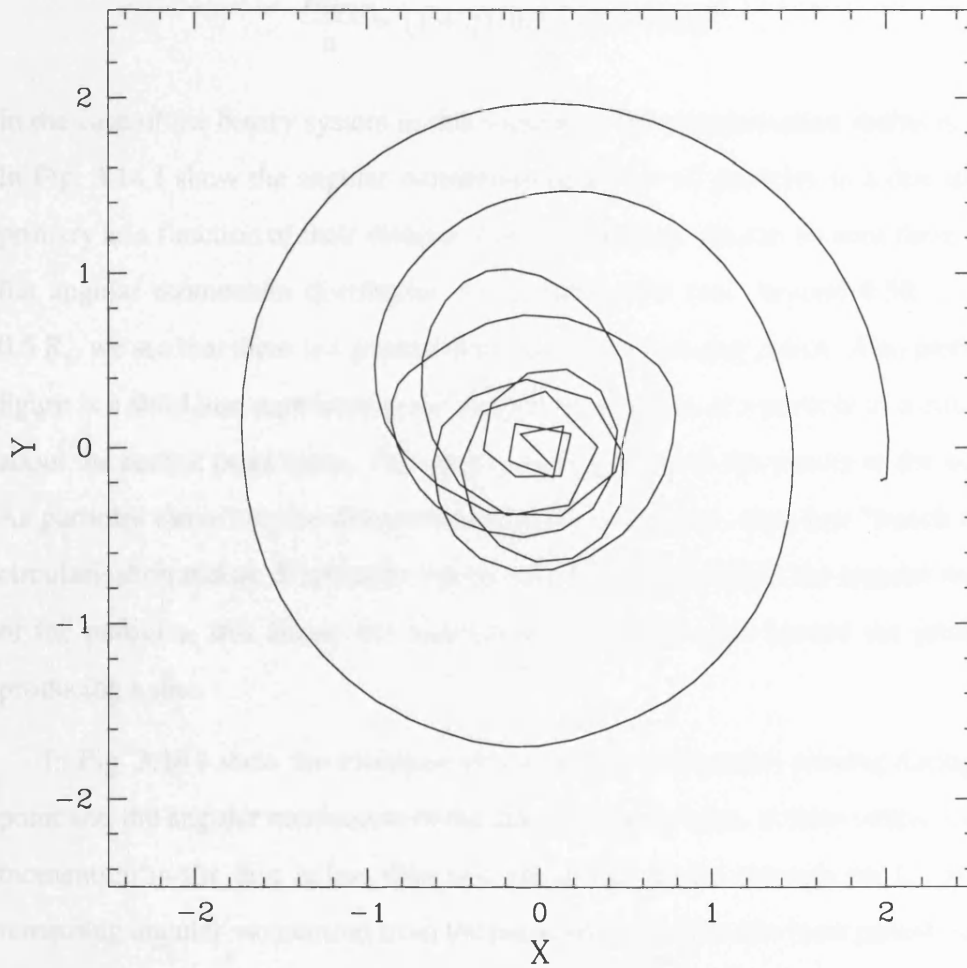


FIGURE 3.15. A plot showing the trajectory of one of the oil particles around the primary (located at 0,0). As can be seen, the particle executes a number of decreasing radii orbits about the central point mass.

where b_1 is the distance of the L1 point from the primary. Having this angular momentum forces the particles to orbit the primary at a distance where a Keplerian orbit would have the same specific angular momentum. This is known as the circularisation radius, given by:

$$\frac{R_{\text{circ}}}{a} = (1 + q) (0.5 - 0.277 \ln q)^4 \quad (3.34)$$

In the case of the binary system in this simulation the circularisation radius is $\approx 0.5 R_{\odot}$. In Fig. 3.14 I show the angular momentum of all the oil particles in a disc around the primary as a function of their distance from the primary. As can be seen there is a fairly flat angular momentum distribution for particles with radii beyond $0.5 R_{\odot}$. Inside of $0.5 R_{\odot}$ we see that there is a gradual drop off with decreasing radius. Also plotted in this figure is a solid line representing the angular momentum of a particle in a circular orbit about the central point mass. This profile closely matches the results of the simulation. As particles move into the disc surrounding the point mass, they first “bunch up” at the circularisation radius. Eventually viscous processes redistribute the angular momentum of the particles, this allows the material to spread in-wards toward the primary, thus producing a disc.

In Fig. 3.16 I show the evolution of the angular momentum passing through the L1 point and the angular momentum in the disc. As can be seen, at later stages, the angular momentum in the disc is less than that which has passed through the L1 point. The remaining angular momentum from the particles in the disc has been passed back to the orbit of the binary system causing it to expand (although not by a measurable amount).



Circular_bin.mpg

A movie of the simulation detailed in this section is contained on the cd-rom. As can be seen, after relaxing in a co-rotating frame, the secondary goes on to fill its Roche lobe and pass material to the primary. This material goes on to form a disc around the primary as it has too much angular momentum to be directly accreted.

3.5. Further work and Astrophysical context

In this chapter I have detailed the development of a new implementation of the Hill technique. With the addition of the new procedure, I have obtained a number of interesting

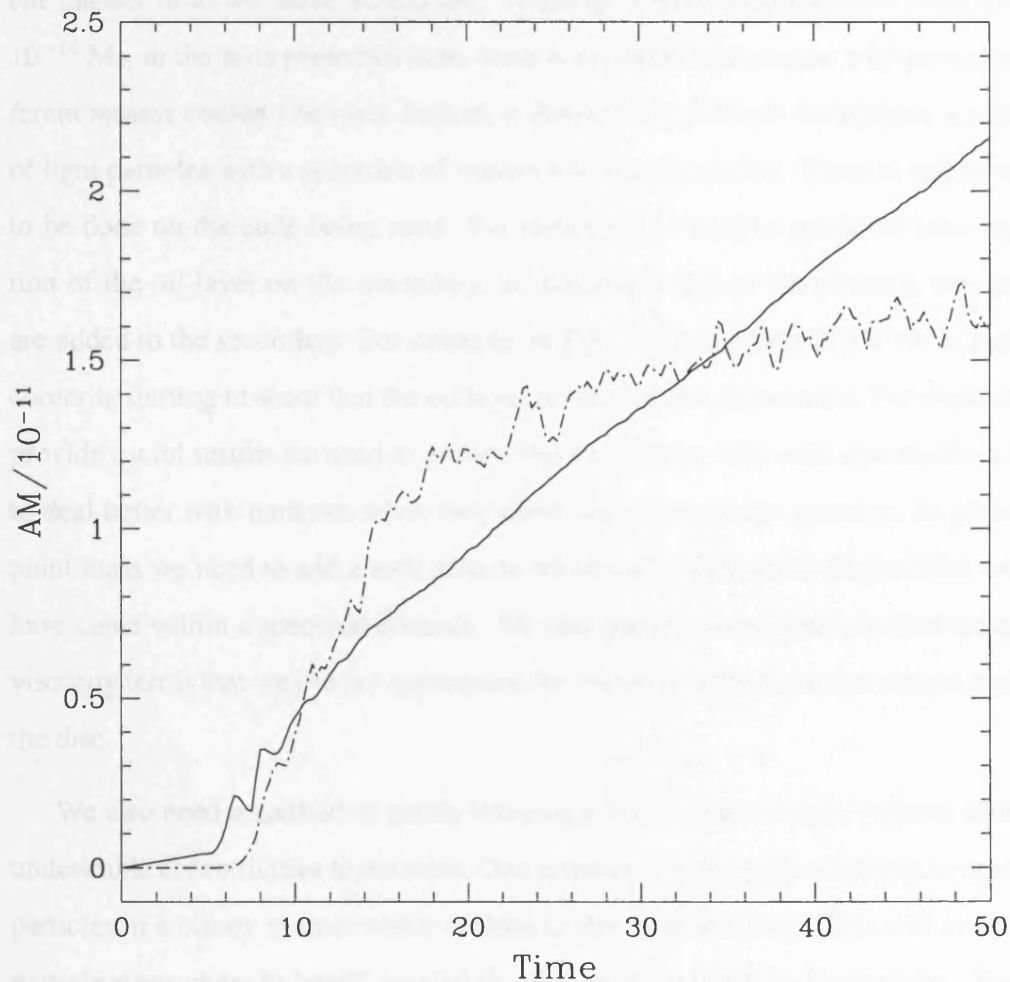


FIGURE 3.16. A plot showing the angular momentum (code units) which passes through the L1 point (solid line) and the angular momentum of the disc around the primary (dashed and dotted line) as a function of time. Of most interest in this plot are the latter portions. Once the disc has built up we see that the angular momentum in the disc is reduced compared to the angular momentum which has passed through the L1 point. The remaining angular momentum would be passed back into the orbit of the binary, forcing it to expand.

3.5 Further work and Astrophysical context

In this chapter I have detailed the development of a new implementation of the SPH technique. With this method it is now possible to incorporate particles of very different masses in to the same simulation. Although I have used particles with a mass of $10^{-14} M_{\odot}$ in the tests presented here, there is no theoretical reason why particles of different masses couldn't be used. Indeed, it should be possible to incorporate a population of light particles with a spectrum of masses into the simulation. There is still some work to be done on the code being used. For instance, it would be useful to have regeneration of the oil layer on the secondary, as material is lost to the primary, new particles are added to the secondary. For example, in Fig. 3.12 the image in the lower right hand corner is starting to show that the oil layer is running out of particles. For simulations to provide useful results we need to prevent this happening. The code also needs to be able to deal better with particles when they move very close to the primary. In place of the point mass we need to add a sink particle which can swallow the oil particles once they have come within a specified distance. We also need to investigate whether the standard viscosity terms that we use are appropriate for material in the accretion stream and within the disc.

We also need a method of gently bringing a binary into contact, without adding any undesirable eccentricities to the orbit. One possibility is to apply a heating term to the oil particles in a binary system which is close to Roche lobe filling. This will cause the oil particle atmosphere to “puff” up slightly and the star will fill its Roche lobe. For this to be useful, we can only do this within a system which is very close to Roche lobe filling anyway.

In terms of an astrophysical context, it will now be possible to explore mass transfer in many binary systems. In particular we now have a method of examining how the mass transfer rate will vary in an eccentric binary system (such as Be binary systems) and what implications this will have on the light curve that we observe from such a system. We will also be able to examine the details of how mass transfer starts within a system and the feedback mechanisms acting along the mass transfer stream.

Some of the systems that we can now examine include:

Common envelopes

The common envelope process is very important in explaining the formation of many close binary systems, such as cataclysmic variables. A common envelope results when mass is transferred from the more massive star in a binary system, as mass is transferred the Roche lobe of the mass losing star shrinks and eats deeper into its surface. As a result the mass transfer is unstable. Too much mass passes through the L1 point for the companion star to accept, and so instead of forming a disc the material smoothes the binary system. Within the enshrouding envelope of gas the two components continue to orbit one another. In moving through the gas, energy and angular momentum are removed from the binary's orbit and passed to the gas. This has the effect of shrinking the binary orbit and expelling gas from the system. Eventually we are left with a close binary system which can then go on to experience a second period of mass transfer when material leaves the main-sequence star and is accreted by the remains of the primary star in the system.

Thus far, whenever a common-envelope has been invoked, it has only really been done so in a parameterised fashion (see for example de Kool (1990)). In chapter 5, I have used the standard parameterisation to explain how a binary system may have its orbital separation shrunk down to the point where it is Roche-lobe filling. Within this parameterisation one assumes that the energy to eject the envelope gas from the binary system has to come from a change in the binary system orbit. It is further assumed that the transfer of energy from the binary orbit to the common envelope happens with some characteristic efficiency α (see Chapter 5 for more details). Thus it is possible to produce a whole range of different final separations by just varying the parameters very slightly.

There have been attempts to model the Common envelope phase. Rasio & Livio (1996) performed some simulations where the secondary star was a giant which was disrupted during the orbit and the two bodies spiralled in toward each other. This work demonstrated that motion through the gaseous material is very dissipative as one would expect. This naturally results in the binary separation grinding down to smaller values.

However, this envelope was made up of relatively heavy particles, so the fine details of the onset of common envelope could easily have been missed.

Using the oil-on-water technique it should be possible to examine the details of what happens at the onset of the common envelope phase. We won't be able to model the entire event, but we should be able to understand the initial onset a lot better than we are currently able to do.

Blue stragglers

Blue stragglers are stars found in globular clusters with masses greater than the turn-off mass. In chapter 4, I conclude that it is likely that the majority of the blue straggler population results from a period of mass transfer occurring in a binary system. If a binary is initially composed of two main-sequence stars, then as one evolves off of the main-sequence, it can fill its Roche lobe and pass material to the less massive star. This will have the effect of increasing the mass of the companion and turning it into a blue straggler.

Using the oil-on-water technique we will be able to examine the onset of this mass transfer. Identifying the regimes where it is stable and the fate of the transferred material.

The understanding that we gain from using the oil-on-water technique can then be combined with the use of stellar evolution codes to allow a full understanding of the blue stragglers formed in such a manner.

White dwarf mergers

Another possible use for the oil-on-water technique is the modelling of the inspiral of two white dwarfs in a binary system. Simulations by Benz *et. al.*(1990) suggests that the final inspiral is very rapid with the two components merging in less than two orbital periods. However, these simulations used relatively massive particles and fine details within the mass transfer process could have been missed. It might be possible that the initial onset of mass transfer could be slower than demonstrated by Benz *et. al.*(1990) and instead of a quick merger we have a disc of material form around the accreting star. This could lead to the passing back of angular momentum to the orbit, offsetting the

angular momentum losses due to gravitational radiation. Possibly we could get nuclear burning within this disc as well. The oil-on-water technique is ideal for examining the start of this process. If the mass transfer really is rapid, the entire population of oil particles should be transferred very quickly. If they are not we will be able to examine the torques being exerted on the orbit of the binary system by measuring the angular momentum in the disc.

In conclusion; the oil-on-water method should allow a much greater understanding and more detailed modelling of the processes which occur within binary systems. Thus far many of the details have been lost in simulations because of the simple fact that each of the SPH particles have simply been too heavy, a single particle in a million particle simulation of a $0.6 M_{\odot}$ star would still represent over $10^{-6} M_{\odot}$ an amount of material transferred in some 10^5 or so orbits in a typical CV.

With increased particle number, we should be able to increase the spatial resolution in the oil layer as well as the mass resolution. The tests presented here typically used 15,000 oil particles and were all performed on a single processor. The code is already set up for use on a shared memory machine, so it should be possible to increase the number of particles up to say 10^6 on computers such as UKAFF.

Chapter 4

Blue stragglers in globular clusters

4.1 Introduction

¹Observations of several globular clusters have revealed the existence of a population of main-sequence stars with masses apparently beyond the cluster turn off mass. Thus far all observations seem to have confirmed that these blue stragglers genuinely do have masses beyond the main sequence limit. For example Shara, Saffer & Livio (1997) measured the mass of a blue straggler in 47 Tucanae and found it to be nearly twice that of the oldest primordial hydrogen burning cluster star. Explaining the formation of these objects has proved troublesome until recently. They cannot be formed through standard single star evolution, and it seems unlikely that a second epoch of star formation could have taken place within these clusters as any free gas should have been swept out of the cluster when the initial stellar population was formed. Instead, given the crowded natures of globular clusters it has been suggested (Fabian, Pringle & Rees 1975) that blue stragglers might be formed via physical collisions between stars. Alternatively they may be formed through some binary evolution mechanism where mass is transferred from one star to another.

If blue stragglers are formed via collisions, then their properties could be an important tool for understanding the dynamics of the cluster. The dynamical state of a globular cluster (its density profile, velocity dispersion, amount of mass segregation etc.) will

¹Evolution of the collision products was performed by Dr Alison Sills.

determine the rate and nature of the collisions which occur in the cluster. As the cluster evolves, the kinds of collision that occur will change. Therefore, the population of collision products in a cluster could be used to probe the history of the cluster (Sills, Bailyn, Edmonds & Gilliland 2000, Hurley et al. 2001).

Simulations of head on collisions between main-sequence stars have shown that the resulting merged object has similar properties to the observed population of blue stragglers, however a head-on collision is a relatively unlikely event. Simulations of off-axis collisions have thus far proved complicated. There has been evidence of an angular momentum problem; the merged object appeared to have too much angular momentum to be able to contract down to the main-sequence.

Most recent simulations of collisions between main-sequence stars have used 10^4 particles (Lombardi, Rasio & Shapiro 1996*b*, Sandquist, Bolte & Hernquist 1997), with the highest resolution simulation using 10^5 particles (Sills, Faber, Lombardi, Rasio & Warren 2001). Here I have increased the number of particles to 10^6 . There are three key reasons for doing this: first and foremost we need to make sure that there is no fundamental change in our understanding of blue stragglers. In earlier work Benz & Hills (1987) performed an SPH simulation using 1024 particles, they concluded that the collision product was fully mixed and so chemically homogeneous. Just 10 years later with simulations containing a factor of 10-50 more particles (Lombardi et al. 1996*b*) showed that in fact the collision products were not fully mixed, but instead some memory of the original parent stars was retained. It seems unlikely that such a huge change in understanding will occur again, but it is good to check, by comparing the results of multiple resolutions of the same runs we should be able to say what the minimum resolution requirement for these simulations are.

The second question to be answered relates to the structure of the outer layers of the collision products. There have been many questions asked as to whether the collision products have a surface convection zone. If such a convection zone were present, then the chemical abundances of the surface could be drastically altered after the collision, in addition the presence of such a convection zone can have implications for the rotation rate of the blue straggler (Leonard & Livio 1995). Previous SPH simulations and sub-

sequent evolution models have shown that no convection zone exists at the end of the collision, nor does it develop during the initial thermal relaxation of the star (Lombardi et al. 1996*b*, Sills, Lombardi, Bailyn, Demarque, Rasio & Shapiro 1997). However, previous simulations have been particularly poorly resolved in the outer edges of the star as they have been done with particles of equal mass. Here I use equally spaced particles with different masses; this provides much better resolution than has been used previously.

The third question to be answered is; what happens to the material thrown off during the collision? Previous simulations have hinted at an angular momentum problem for blue stragglers formed through off-axis collisions (Sills et al. 2001). In simple terms, previous simulations have suggested that the merged object has too much angular momentum to contract down to the main-sequence. One possible method of resolving this problem is that angular momentum may be taken away from the system by escaping mass, and this may not have shown up during previous simulations. Alternatively a disk may form around the merged object and we could have magnetic braking slowing the blue straggler down, in much the same way as T Tauri stars are slowed down as they contract.

There has been an alternative proposal put forward as a creation mechanism for the blue straggler population. Preston & Sneden (2000) describe observations of blue stragglers observed in the field. They conclude that they must be produced by a period of mass transfer within a binary system. Mass from the more evolved star can pass to the less evolved companion as it expands and fills its Roche lobe. I leave further discussion of this mechanism to Section 4.7.

The properties of blue stragglers formed through collisional mergers could be quite different to those produced through binary interactions. Thus, if we are to discriminate between the two populations we need to model the evolution of the blue stragglers formed through both collisional events and binary evolution. In this chapter I limit myself to examining the formation of blue stragglers through collisions between stars. The modelling of blue straggler formation through binary system evolution awaits the development of two or three dimensional stellar evolution codes.

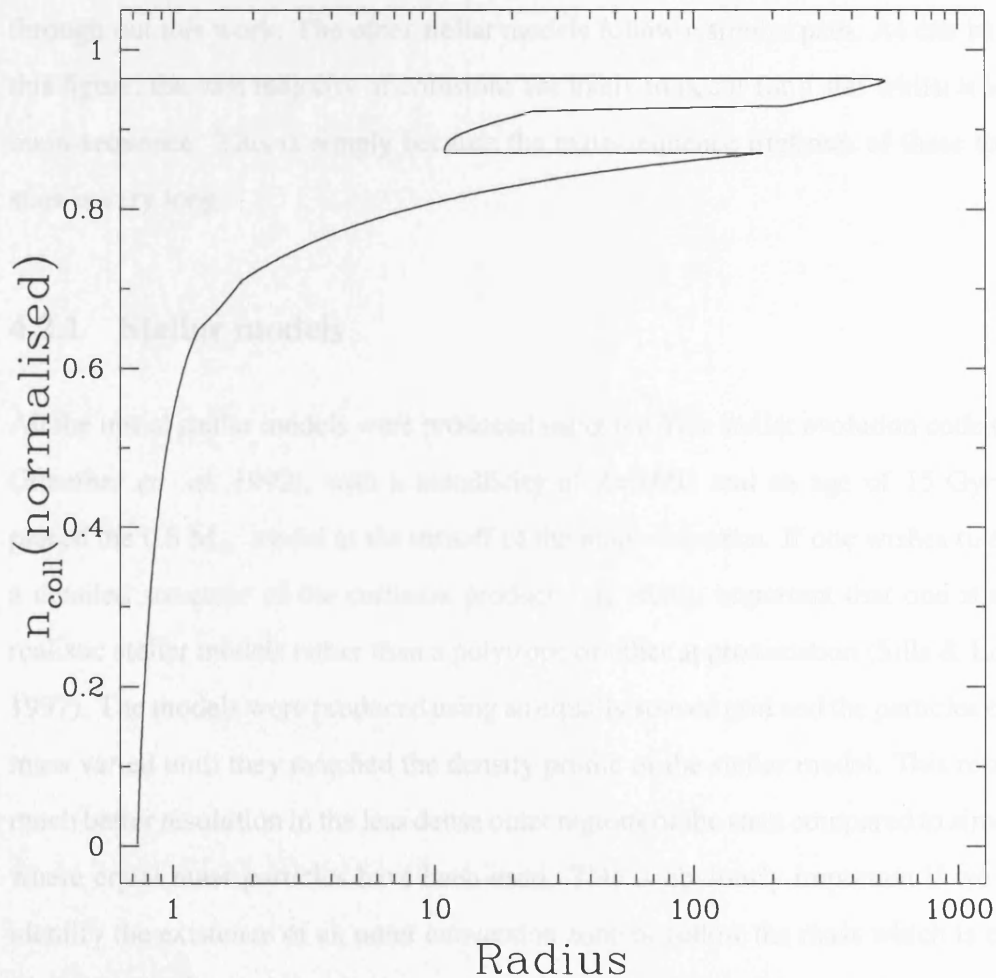


FIGURE 4.1. The normalised collision probability for the $0.4 M_{\odot}$ model used in this investigation as a function of its radius (which is a tracer of its age). As can be seen the star expects to undergo the majority of its collisions whilst it is on the main-sequence. The paths for the $0.6 M_{\odot}$ and $0.8 M_{\odot}$ models are very similar to this.

4.2 Theory

Globular clusters are crowded places, with densities in post-core-collapse clusters up to 10^5 stars/pc³. Within such a crowded environment it is inevitable that collisions will occur between stars. Indeed collisions have been invoked as a possible mechanism of explaining the apparent paucity of red giants in the cores of globular clusters (Adams, Davies & Sills (submitted) or see chapter 5). It seems reasonable that collisions could play a role in the creation of blue stragglers.

In Fig. 4.1 I plot the normalised collision probability for the $0.4 M_{\odot}$ model used through out this work. The other stellar models follow a similar path. As can be seen in this figure, the vast majority of collisions are likely to occur for a star whilst it is on the main-sequence. This is simply because the main-sequence lifetimes of these low mass stars is very long.

4.2.1 Stellar models

All the initial stellar models were produced using the Yale stellar evolution code (YREC, Guenther *et. al.* 1992), with a metallicity of $Z=0.001$ and an age of 15 Gyrs. This placed the $0.8 M_{\odot}$ model at the turnoff of the main-sequence. If one wishes to examine a detailed structure of the collision product it is vitally important that one starts with realistic stellar models rather than a polytrope or other approximation (Sills & Lombardi 1997). The models were produced using an equally spaced grid and the particles had their mass varied until they matched the density profile of the stellar model. This results in a much better resolution in the less dense outer regions of the stars compared to simulations where equal mass particles have been used. This is obviously important if we wish to identify the existence of an outer convection zone or follow the mass which is escaping after the collision.

The merged objects formed during the SPH simulations were converted into one dimensional models that can be used as a starting point for the YREC code. The entropy and chemical abundances of the particles were averaged over surfaces of constant gravitational potential and binned into 100 bins. The structure of the collision product is determined from these profiles using the equation of hydrostatic equilibrium. The temperature profile is calculated using the ideal gas equation of state. For more details of the conversion between SPH results and stellar evolution models, see (Sills *et al.* 1997, Sills *et al.* 2001).

The use of YREC gave an insight to the subsequent evolution of the merged object. It was possible to follow the evolution through the thermal relaxation phase (this may be thought of as the pre-main-sequence of normal stars) along to the main-sequence and the

Run	r_p R_\odot	N_{part}	h_0 R_\odot	M_{min} M_\odot	M_{max} M_\odot	M_{lost} M_\odot
A	0.0	10 162	0.058	2.10×10^{-6}	4.58×10^{-3}	8.14×10^{-2}
B	0.0	29 950	0.0417	3.71×10^{-7}	1.37×10^{-3}	7.76×10^{-2}
C	0.0	100 034	0.028568	4.96×10^{-8}	4.47×10^{-4}	7.49×10^{-2}
D	0.0	299 398	0.02011	5.27×10^{-9}	1.56×10^{-4}	7.41×10^{-2}
E	0.0	999 778	0.0136	2.98×10^{-10}	4.75×10^{-5}	7.47×10^{-2}
F	0.25	10 162	0.058	2.10×10^{-6}	4.58×10^{-3}	3.45×10^{-2}
G	0.25	29 950	0.0417	3.71×10^{-7}	1.37×10^{-3}	3.62×10^{-2}
H	0.25	100 034	0.028568	4.96×10^{-8}	4.47×10^{-4}	3.99×10^{-2}
I	0.25	299 398	0.02011	5.27×10^{-9}	1.56×10^{-4}	4.16×10^{-2}

Table 4.1. A list of the runs performed to identify the optimum resolution for performing collisions between stars. I have examined two specific collisions and performed them at various different resolutions to observe the effects. Both stars had an initial mass of $0.6 M_\odot$ and the distance of closest approach for the simulations is as given in the table. Also listed are the smoothing lengths used for setting up the stars as well as the minimum, M_{min} , and maximum, M_{max} , particle mass. Also listed is the mass no longer bound after the collision, M_{lost} .

subsequent evolution along the red giant branch.

4.3 Finding the ideal resolution

As mentioned in the introduction, one of the goals of this work was to identify the resolution which gave the correct results with the minimum computational effort.

To do this I performed various resolution runs of two separate collisions, these simulations are detailed in Table 4.1.

In Fig. 4.2 I plot some of the important features of the head-on collisional products. The various line styles denote the different resolutions, the solid line represents 10,000 particles, dotted line 30,000 particles, the short dashed line 100,000 particles, the long dashed line 300,000 particles and the dot-dashed line 1,000,000 particles (this is the highest resolution simulation to date). As can be seen, the low resolution simulations give the correct general impression of the results; however, increasing the resolution by just a factor of three does bring about some very noticeable differences. It is when we get to 100,000 particles and above we see that there is very little difference in any of the

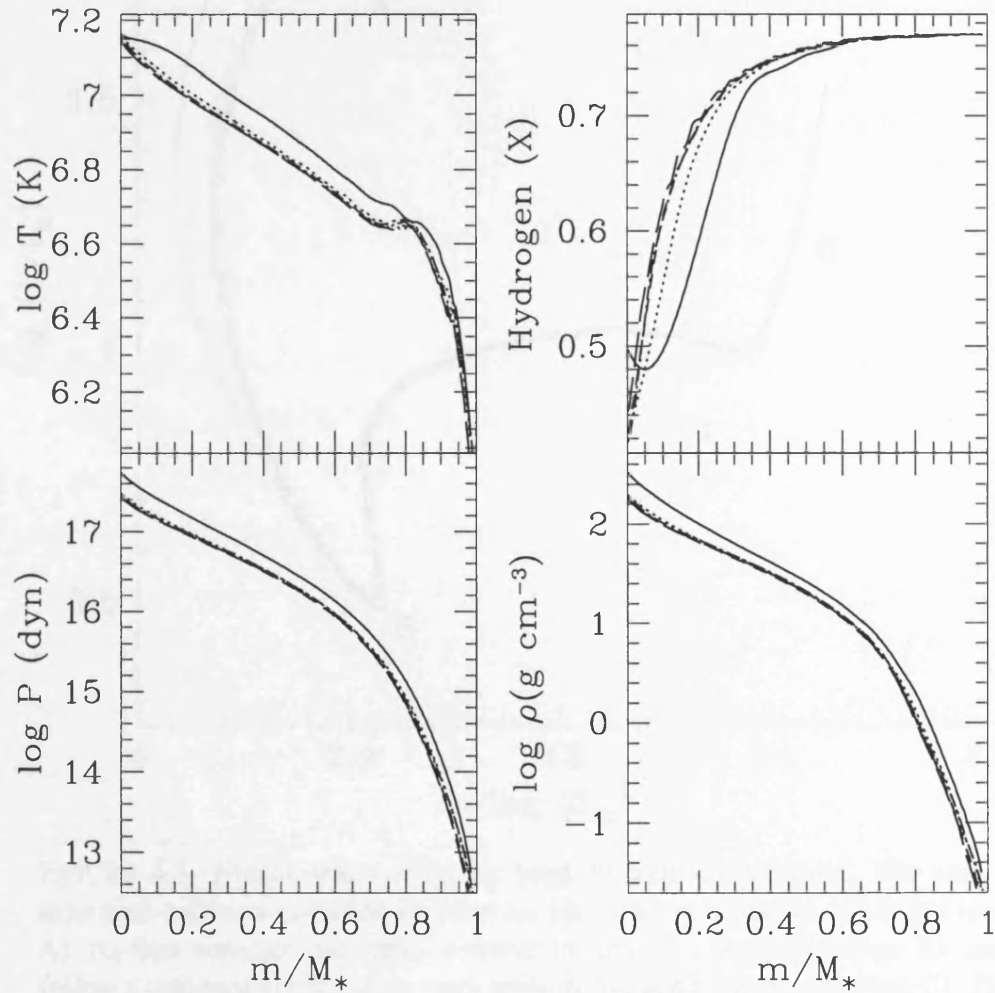


FIGURE 4.2. Structure of head-on collision products resulting from the merger of two $0.6 M_{\odot}$ stars. The main structure parameters of a non-rotating star have been plotted as a function of mass fraction: pressure, temperature, density, and hydrogen mass fraction. The different line styles show the results for different numbers of SPH particles. In increasing order of particles, they are: solid (10 000 particles), dotted (30 000 particles), short-dashed (100 000 particles) long-dashed (300 000 particles), and dot-dashed (1 000 000 particles). The models converge towards the 1 000 000 particle simulation, and there is very little obvious difference between the 100 000, 300 000 and 1 000 000 particle results.

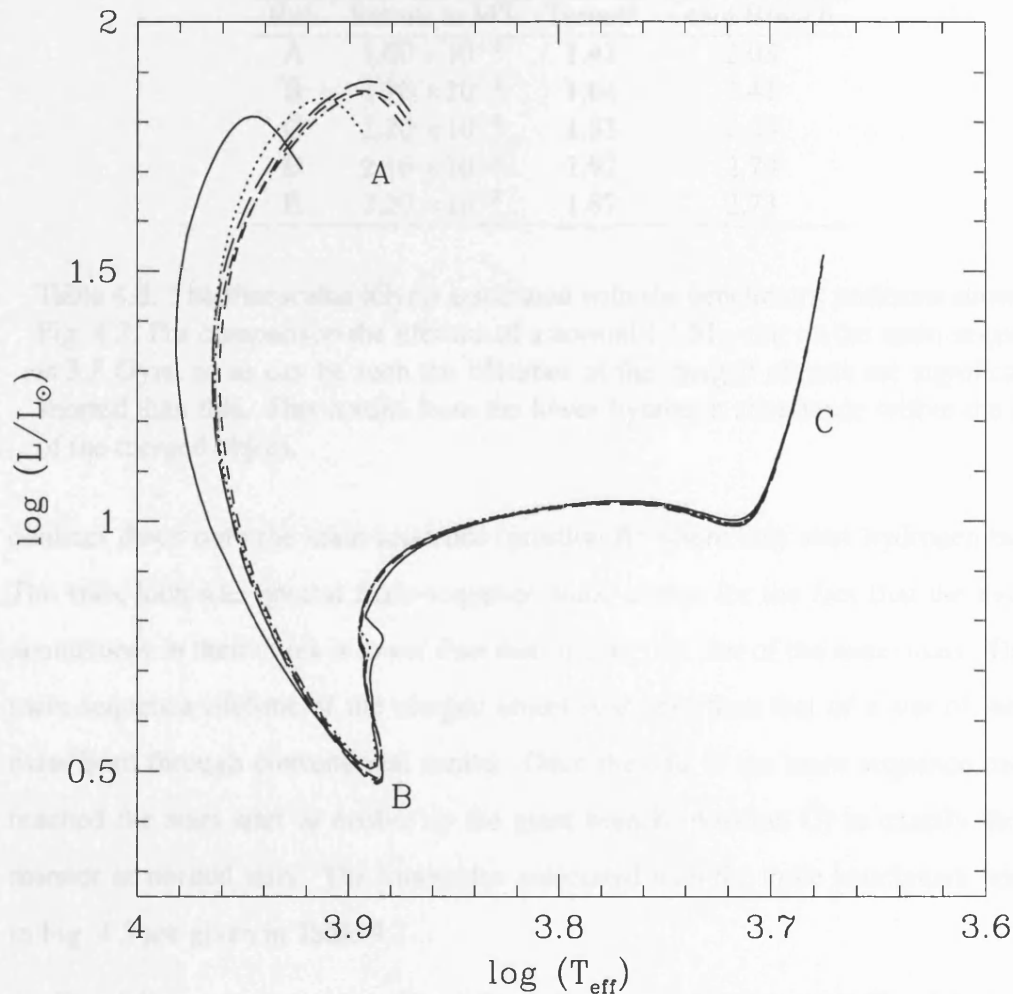


FIGURE 4.3. Evolutionary tracks for head-on collision products. The stars begin their post-collision evolution far from the Hayashi track, but are still bright (position A). As they contract, they move towards the main sequence (position B), and then follow a standard evolutionary track towards the giant branch (position C). The line styles are the same as in Fig. 4.2. The difference in structure between the different resolution simulations manifests itself as a difference in evolutionary track shape. The tracks are most different during their initial contraction, and then again near the turnoff of the main sequence.

key properties of the merged object.

In Fig. 4.3 I show the evolutionary tracks which result from the starting models shown in Fig. 4.2. The blue stragglers begin their lives at position A, a long way from the Hayashi track on the right. All the models are bright as well as being out of thermal equilibrium due to the energy deposited into their envelopes during the collisions. The merged objects

Run	Return to MS	Turnoff	Giant Branch
A	1.60×10^{-3}	1.41	2.08
B	1.90×10^{-3}	1.64	2.41
C	2.20×10^{-3}	1.85	2.69
D	2.16×10^{-3}	1.92	2.79
E	2.20×10^{-3}	1.87	2.73

Table 4.2. The timescales (Gyrs) associated with the benchmark positions shown in Fig. 4.3. For comparison the lifetime of a normal $1.1 M_{\odot}$ star on the main-sequence is 3.3 Gyrs, so as can be seen the lifetimes of the merged objects are significantly shorter than this. This results from the lower hydrogen abundance within the core of the merged object.

contract down onto the main-sequence (position B) where they start hydrogen burning. The stars look like normal main-sequence stars, except for the fact that the hydrogen abundances in their cores is lower than that of a normal star of the same mass. Thus the main-sequence lifetime of the merged object is shorter than that of a star of the same mass born through conventional means. Once the end of the main sequence has been reached the stars start to evolve up the giant branch (position C) in exactly the same manner as normal stars. The timescales associated with the three benchmark positions in Fig. 4.3 are given in Table 4.2.

The different lines styles in Fig. 4.3 are the same as those used in Fig. 4.2. As in the case of the structural properties we see that the evolutionary tracks converge to a common solution at around 100,000 particles, this is not unexpected since the evolution of a star is clearly governed by its internal properties. In Table 4.2 we again see the same pattern of convergence as we reach 100,000 particles. The largest differences come in the period required to reach the main-sequence through the thermal relaxation phase. Once at the main-sequence the majority of the simulations are almost identical. The lowest resolution simulation does differ from the other models by a considerable amount. It begins its main sequence life close to the next lowest resolution simulation (30,000 particles, dashed line), however it develops a hook near the turnoff of the main-sequence. This hook is not seen in any of the higher resolution simulations, thus indicating that 10^4 particles are not sufficient to give an accurate picture of the collisions products.

4.3.1 Convection zones

One of the other questions I wanted to answer with the higher resolution runs was whether there was any indication of a convection zone in the outer layer of the merged object just after the collision.

Whether or not convection is likely to set in is determined by the Schwarzschild criterion:

$$\nabla - \nabla_{ad} \geq 0 \quad (4.1)$$

where ∇_{ad} is the adiabatic temperature gradient in the star, and ∇ is the radiative temperature gradient:

$$\nabla = \frac{d \ln T}{d \ln P} = \frac{3}{64\pi\sigma G} \frac{\kappa L P}{M T^4} \quad (4.2)$$

where σ is the Stefan Boltzmann constant, G is the gravitational constant, and κ, L, P, M and T are the opacity, luminosity, pressure, enclosed mass and temperature at that position in the star. When the radiative temperature gradient is larger than the adiabatic temperature gradient then convection will set in.

The models taken from the SPH results were used as starting models in the stellar evolution code.

The resulting temperature gradients are plotted as a function of the mass fraction in Fig. 4.4. Again I have utilised the same line styling as in Fig. 4.2. It is obvious that these stars have $\nabla - \nabla_{ad} > 0$ in their core regions, giving them a convective core, however, all the models appear to be stable against convection outside of the inner $0.1 M_{\odot}$. The outermost shell in all our stellar models is at a mass fraction $M/M_{*} = 0.99667$. This value is the same regardless of the number of SPH particles because of the way in which the SPH data was converted into the stellar evolution starting model. The total mass of these stars is $1.12 M_{\odot}$, so only the outer $0.004 M_{\odot}$ is not resolved. Therefore, we can say with certainty that this stellar collision product does not have a surface convection zone larger than $0.004 M_{\odot}$. The evolutionary models show that the stellar collision products

do not develop surface compression zones during their thermal contraction in the main sequence.

4.3.2 Effects of rotation

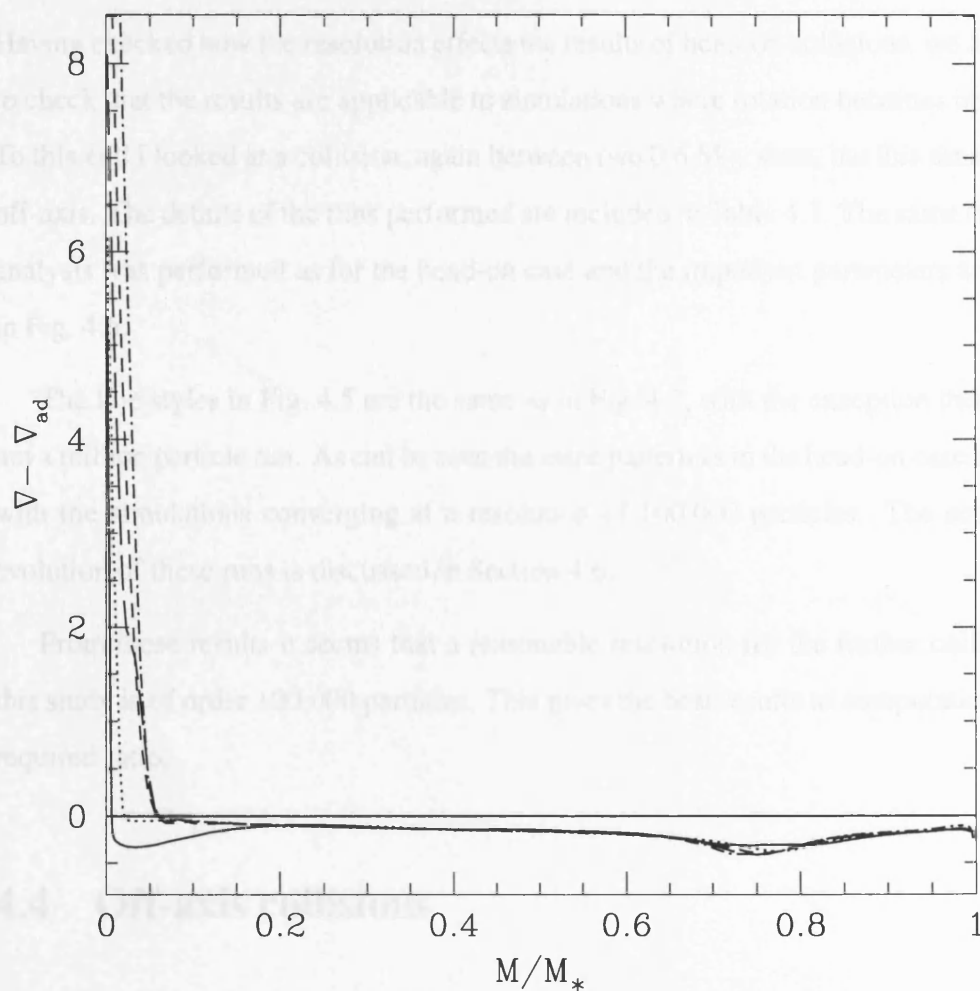


FIGURE 4.4. Convective stability criterion $\nabla - \nabla_{ad}$ as a function of mass fraction for the head-on collision models immediately after the collision. The line styles are the same as in Fig. 4.2. When $\nabla - \nabla_{ad}$ is less than zero (i.e. the adiabatic temperature gradient is larger than the radiative temperature gradient), the region is stable against convection. Except for a small region at the centre of the star, the entire collision product is stable against convection.

do not develop surface convection zones during their thermal contraction to the main sequence.

4.3.2 Effects of rotation

Having checked how the resolution effects the results of head-on collisions, we also need to check that the results are applicable to simulations where rotation becomes important. To this end I looked at a collision, again between two $0.6 M_{\odot}$ stars, but this time slightly off-axis. The details of the runs performed are included in Table 4.1. The same structural analysis was performed as for the head-on case and the important parameters are shown in Fig. 4.5.

The line styles in Fig. 4.5 are the same as in Fig. 4.2, with the exception that there is not a million particle run. As can be seen the same pattern as in the head-on case emerges, with the simulations converging at a resolution of 100,000 particles. The subsequent evolution of these runs is discussed in Section 4.6.

From these results it seems that a reasonable resolution for the further collisions in this study is of order 100,000 particles. This gives the best results to computational time required ratio.

4.4 Off-axis collisions

The evolution of head-on merger objects is now relatively well understood. However, the probability of getting a head-on collision within a globular cluster is vanishingly small and in reality there will always be some off-axis nature to the collision. In this section I examine such off axis collisions in an attempt to understand the properties of the merger remnant and its subsequent evolution. Previous work on high resolution simulations of off-axis collisions between stars have utilised equal mass particles (Sills et al. 2001). This has the unfortunate effect of lowering the resolution in the outer, low density, regions of the stellar models. To ensure consistency, I have performed a series

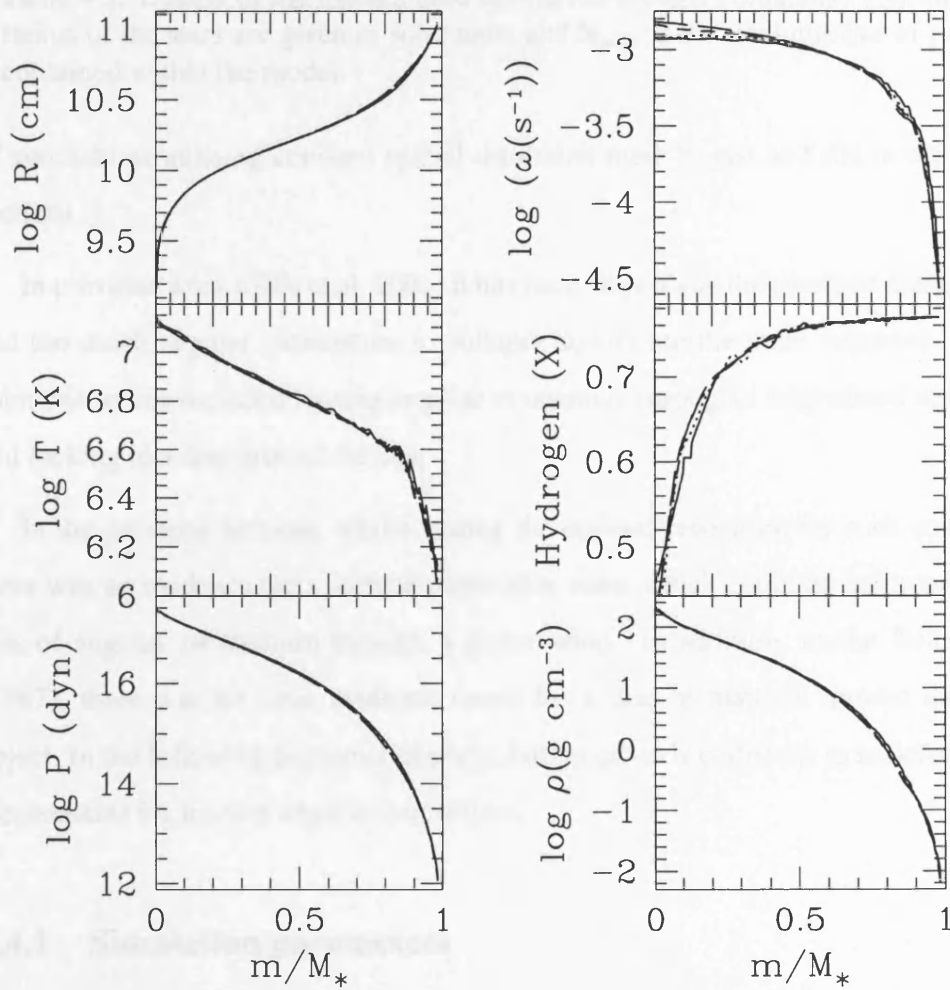


FIGURE 4.5. Structural parameters of the merged object formed after an off-axis collisions. Plotted are the Radius, temperature, pressure, rotational velocity, hydrogen fraction and density as a function of contained mass. The solid line represents a 10,000 particle simulation, dotted (30 000 particles), short-dashed (100 000 particles) and long-dashed (300 000 particles). As in the case of the head-on collisions a convergence in the results is seen as we reach 100,000 particles.

M_{\star}	R_{\star}	N_{part}
0.4	0.41	50019
0.6	0.61	50017
0.8	1.15	50017

Table 4.3. Details of the models used during the off-axis collisions. The mass and radius of the stars are given in solar units and N_{part} is the total number of particles contained within the model.

of simulations utilising constant spatial resolution models, just as I did in the previous sections.

In previous work (Sills et al. 2001) it has been shown that the resultant merged object had too much angular momentum to collapse down onto the main sequence. Possible solutions to this included losing angular momentum through a magnetised stellar wind and locking to a disc around the star.

In the previous sections, whilst finding the optimal resolution for such simulations, there was no evidence for a surface convection zone, which could be detrimental to the loss of angular momentum through a stellar wind. In addition, unlike Benz & Hills (1987), there was no clear evidence found for a disc of material around the merged object. In the following sections I examine further off-axis collisions to look for possible mechanisms for losing angular momentum.

4.4.1 Simulation parameters

I have considered collisions between stars of masses, 0.4, 0.6 and 0.8 M_{\odot} . These were chosen as they were representative of the stellar populations seen in most globular clusters, and collisions between them would create stars with masses beyond the turnoff. The details of the models used are given in Table 4.3.

All the collisions were performed with a relative velocity at infinity of $v_{\infty} = 10$ km/s which, again, is typical for globular clusters. In accordance with the results of the previous section all simulations were performed with 50,000 particles in each star. The minimum distance of approach for the two stars in a collision was set by the equation:

M_1	M_2	X	M_{obj}
0.4	0.4	0	0.756
0.4	0.4	0.25	0.776
0.4	0.4	0.5	0.790
0.4	0.4	1.0	0.791
0.4	0.6	0	0.945
0.4	0.6	0.25	0.976
0.4	0.6	0.5	0.988
0.4	0.6	1.0	0.999
0.4	0.8	0	1.155
0.4	0.8	0.25	1.160
0.4	0.8	0.5	1.193
0.4	0.8	1.0	1.2
0.6	0.6	0	1.120
0.6	0.6	0.25	1.152
0.6	0.6	0.5	1.162
0.6	0.6	1.0	1.185
0.6	0.8	0	1.308
0.6	0.8	0.25	1.368
0.6	0.8	0.5	1.347
0.8	0.8	0	1.467
0.8	0.8	0.25	1.471
0.8	0.8	0.5	1.41

Table 4.4. Details of the off-axis collisions performed. M_{obj} is the mass of the merged object directly after the collision and does not take into account any mass loss which occurs during the subsequent evolution. X relates to the minimum distance of approach as described by Eqn. 4.3.

$$R_{min} = X(R_1 + R_2) \quad (4.3)$$

where X take a value of either 0, 0.25, 0.5 or 1.0. The details of the runs that I have performed are presented in Table 4.4.

4.5 Results

In Fig. 4.6 I show a time series plot from a collision between a 0.6 and a 0.4 M_{\odot} star with a minimum distance of approach of $0.25(R_1+R_2)$. I have plotted the two stars in different colours so that we can see where the mass from the two stars goes during the collision. As was found in previous work, it is the material with the highest entropy (in most cases, this is the material from the most evolved star) which ends up at the centre of the blue straggler. However, there is some mixing of material and some of the material from the less evolved star does make it into the core of the collision product. A similar pattern is found in all of the collisions.

Figs 4.7 and 4.8 help to show this lack of complete mixing again. Fig. 4.7 shows the fraction of mass from a particular star as a function of a mass co-ordinate in the merged object. Clearly we see that at the centre of the merged object the material is mainly from the heavier star, whilst further out the material is more well mixed. This is again present in Fig. 4.8. Here I have plotted a histogram similar to that shown in Benz & Hills (1987). The different levels of shading represent where material has come from within the star. All the stars are split into four bins based on radius from their centres, where the material ends up in the bins of the blue straggler is then shown in the histogram. The heaviest shading represents material from the inner quartile of the parent stars, whilst the lightest shading represents the outermost quartile. Again we can clearly see that the inner regions of the blue straggler are made up of material from the innermost regions of the parent stars, and thus the blue straggler is not well mixed.

In Fig. 4.10 I plot some of the physical characteristics of the merged object formed from the collision shown in Fig. 4.6. In Fig. 4.10 the angular velocity of the resultant merged object is shown, the black line is the actual ω whilst the dashed line is the break up velocity. As can be seen, initially the merged object is far from its break up speed. However, the merged object is considerably out of thermal equilibrium. Over time, the star contracts down toward an equilibrium state. As this occurs to conserve angular momentum the merged object must rotate faster, and it is this which pushes the star toward its break up speed and limits further contraction.

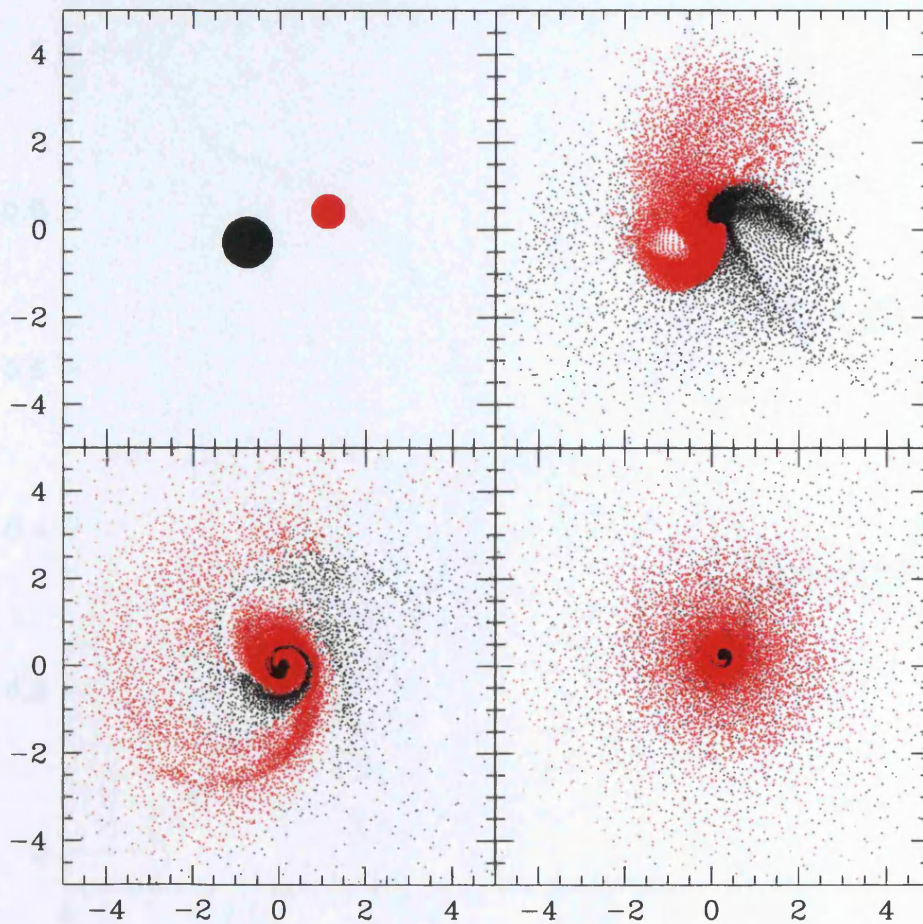


FIGURE 4.6. A time series plot of those particles contained within $2h$ of the $z=0$ plane. This is a collision between a 0.6 (black particles) and a $0.4 M_{\odot}$ (red particles) star, with a minimum distance of approach of $0.255 R_{\odot}$ (i.e. $X=0.25$). As can be seen, it is the material from the heavier star which ends up at centre of the merged object. It is the composition of the core which will determine how long a particular blue straggler will spend on the main sequence compared to a star of the same mass produced through the collapse of the initial gas cloud.

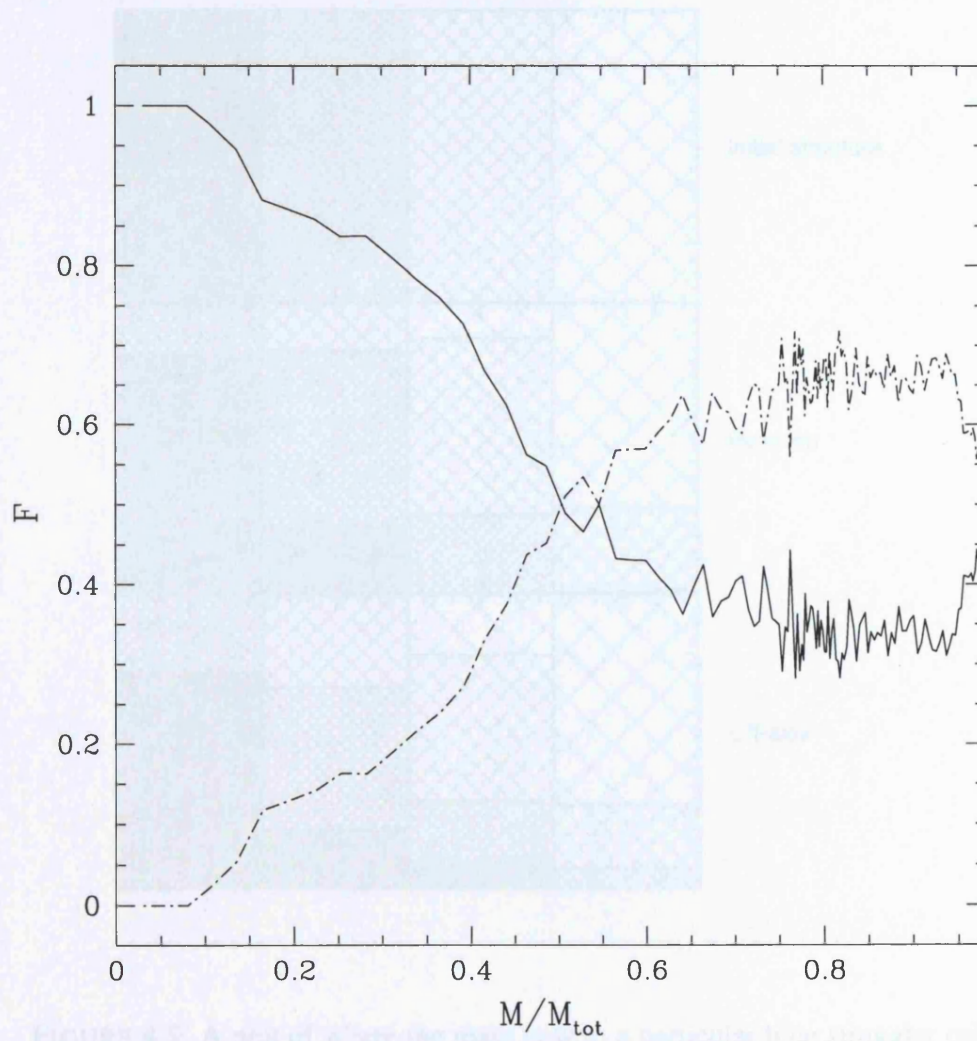


FIGURE 4.7. A plot of the fraction of mass in a shell from a particular star as a function of the total mass of the system. This plot was produced for the same simulation as that shown in Fig. 4.6, the solid line represents the material coming from the $0.6 M_{\odot}$ star, whilst the dashed and dotted line represents that material which originally came from the $0.4 M_{\odot}$ star. As can be seen, within the core of the merged object nearly all the material was originally within the heavier star, this is as predicted from previous work.

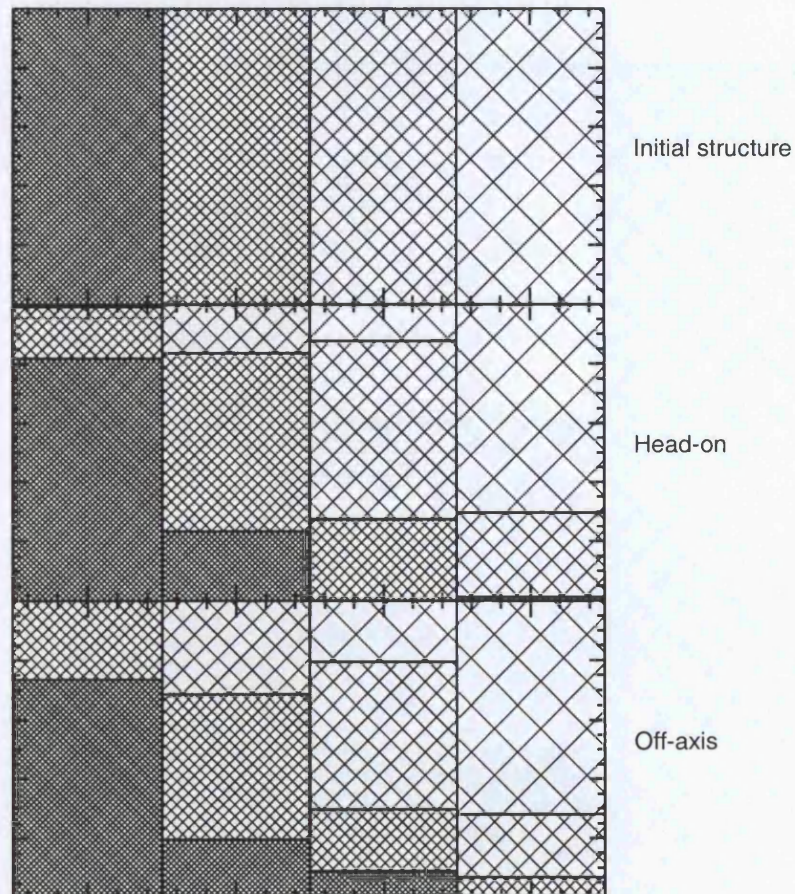


FIGURE 4.8. A plot of where the mass now in a particular blue straggler originally came from. The four columns in each plot represent four equally spaced mass bins. The Darkest hatching represents material that came from the inner quarter of the parent stars, whilst the widest hatching represents material which came from the outer quarter of the parent stars. I have shown two blue straggler models, a head-on collision and the same off-axis collision as has been looked at throughout this section. As can be seen, the inner most quarter of the blue straggler is composed primarily of processed material from the parent stars. This indicates that the blue straggler will have a shorter lifespan than a main-sequence star of equivalent mass. This is even more evident in Fig. 4.9.

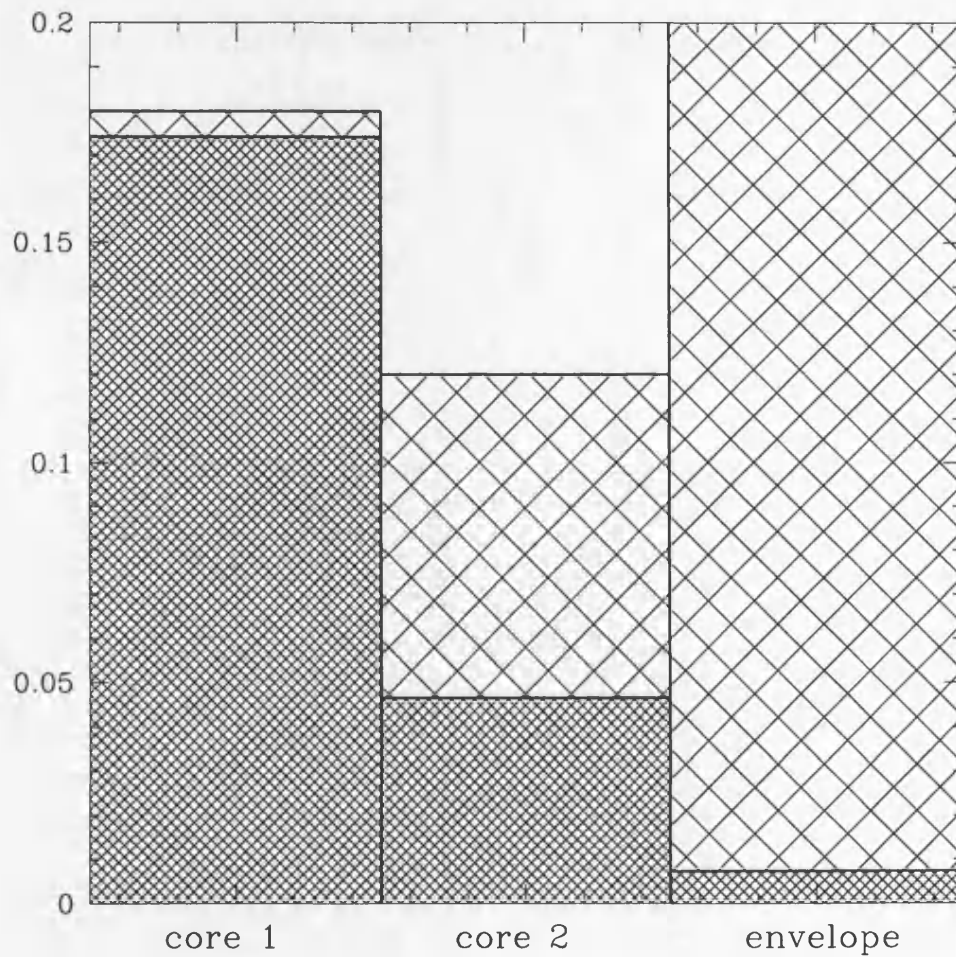


FIGURE 4.9. A plot showing how the mass of the parent star was redistributed in the merged object of the $0.6 - 0.4 M_{\odot}$ $X=0.25$ collision. The first two columns show the mass of the cores of the original stars, the darker hatching represents that mass of material from that core went into the core of the merged object. Clearly we see that the core of the merged object is not well mixed, but is instead composed primarily of processed material. As a consequence it will have a shorter main-sequence lifetime than a star of the same mass produced through conventional means.

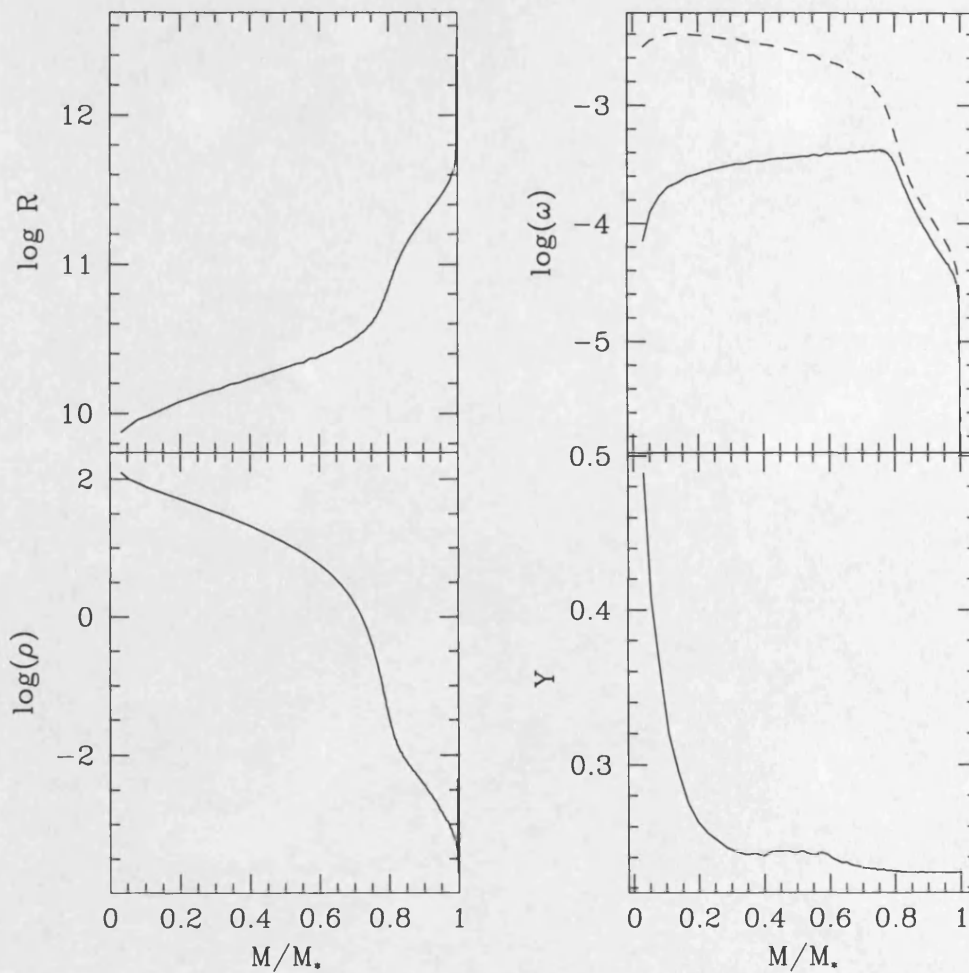


FIGURE 4.10. Some of the physical properties of the merged object formed during the collision shown in Fig. 4.6, at the end of the SPH period of simulation. All units are in cgs. As can be seen, the merged object is quite large in terms of radius, but the majority of the mass is contained in a much smaller region. Also plotted is the helium fraction (Y) as a function of mass. This will be altered dramatically as the star tries to reach a new equilibrium and mixing occurs within the new star.

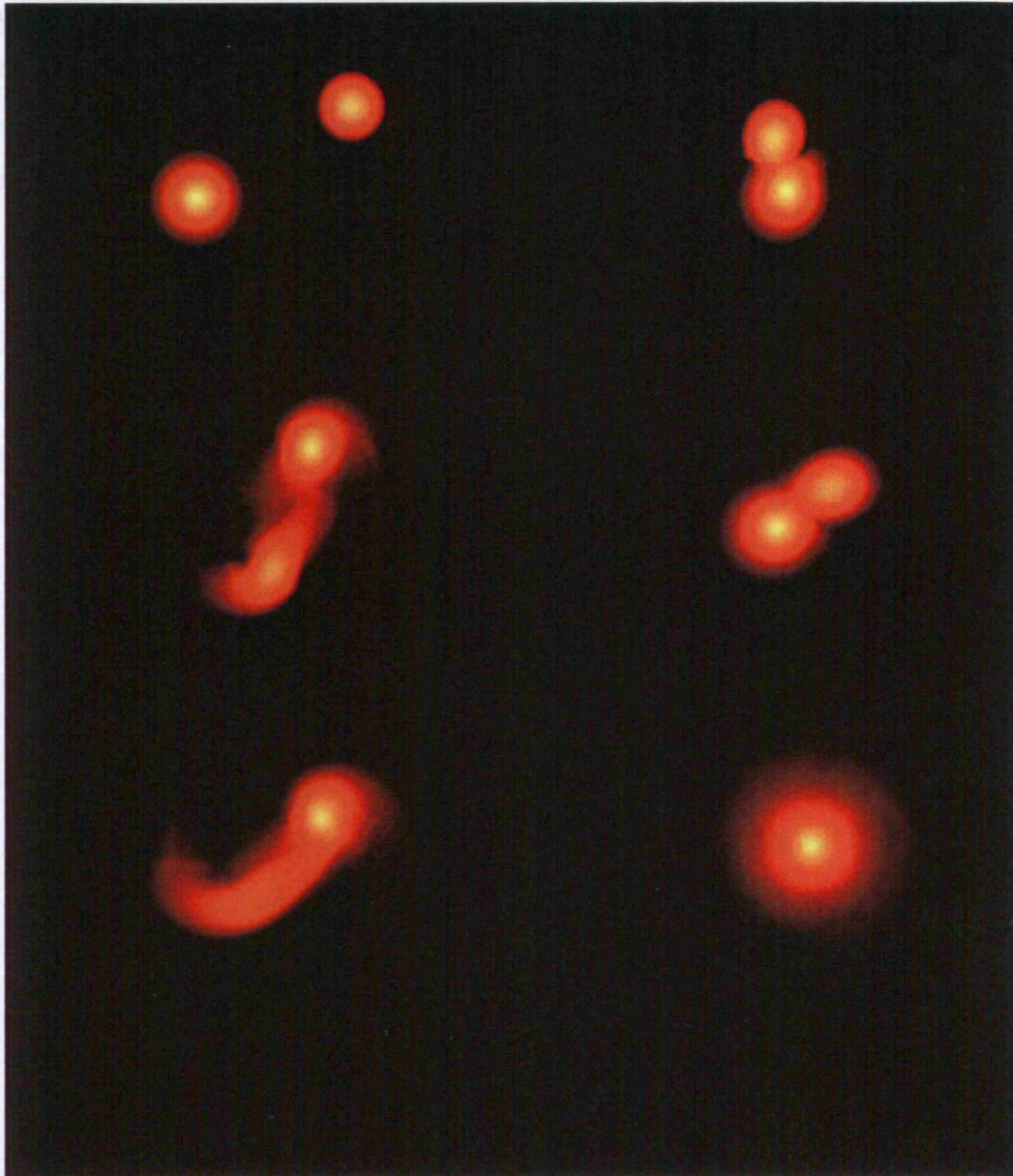


FIGURE 4.11. A time series of snap shots from a collision between a 0.6 and $0.4 M_{\odot}$ star with $X=0.25$. As can be seen the two stars do not merge on the first passage, but instead end up on an eccentric orbit. On subsequent periastron passages the two stars do merge producing a possible blue straggler.

An examination of all the simulations has revealed no strong evidence for the presence of a disc unlike Benz & Hills (1987). There are many possible explanations for this difference; for instance the presence of a disc might have been a numerical artifact caused by the lower resolution. Although I haven't seen direct evidence for a disc around the merged object, there is some material which is bound to the central object, although not apparently part of the blue straggler. Perhaps this material could eventually go on to form a disc around the central object.



blue_stragglers_(1 - 3).mpg

On the cd-rom I have included a number of movies from the simulations performed for this investigation. In all the movies we see that the two objects merge and if there was any off axis nature to the collision the merged object is rapidly rotating.

4.6 Evolution of collision products

With the SPH simulations completed, the next task is to perform the evolution on the models. The evolution of rotating blue stragglers has proved difficult in past work (Sills *et. al.*2001). The YREC code which has been utilised throughout this work is intrinsically one dimensional. The three dimensional SPH models are converted to one dimensional models by averaging over equi-potential surfaces. When a body is rotating this averaging is made more complicated, as a rotating body really needs two dimensions to be represented accurately. To cope with rotation in the YREC code, the potential associated with the Coriolis force is added to the gravitational potential and then properties averaged over the resulting equi-potential surfaces. This is only a compromise, a full understanding of the structure and evolution of rotating bodies will require a two dimensional form of YREC to be developed.

Our SPH models showed, as in previous work, that they had too much angular momentum to contract down to the main-sequence. If these collision products are going

to form some proportion of the blue straggler population seen in globular clusters, they need a method of losing some of this angular momentum.

4.6.1 Mass and angular momentum loss

Let us consider what is likely to happen to the blue straggler as it contracts down toward the main-sequence. As the star contracts it has to conserve angular momentum, thus material is forced to rotate about the rotation axis faster. As this happens the star becomes deformed, becoming somewhat oblate. It is here that a new mechanism might be able to take effect. We know that the star can contract down to the point where it reaches its break up speed, at this point we could get mass loss as surface material becomes unbound from the star. This mass loss could do one of two things, it could take angular momentum away to infinity, thus reducing the angular momentum of the merged object, or alternatively it might form a disc around the star. If the star then has a strong magnetic field (which seems reasonable for most of the stars produced in the collisions detailed here as they are rapidly rotating) then it is possible for the disc and star to become locked, thus spinning down the star. Or the same magnetic field could be locked to the freely flowing material thus providing a torque in the same way as a stellar wind.

We need to examine how these two effects will alter the spin of the star if we are to incorporate their effects in the stellar evolution code.

Disc locking

Let us first look at the effects of disc locking. The prescription that I have used follows on from the work of Armitage & Clarke (1996). The torque on a star from an annulus of a magnetically locked accretion disc, of width ΔR is related to the transfer of angular momentum through magnetic stresses:

$$\Gamma_{\text{annulus}} = B_{\phi} B_z R^2 \Delta R \quad (4.4)$$

where B_z is the vertical component of the magnetic field at a distance R from the star and B_ϕ is the toroidal component of the magnetic field. These two magnetic components may be expressed as:

$$B_z = \frac{\mu}{R^3} \quad (4.5)$$

where μ is the stellar dipole moment. Livio & Pringle (1992) give the toroidal component as:

$$B_\phi = B_z \left(\frac{\Omega(R) - \Omega_\star}{\Omega(R)} \right) \quad (4.6)$$

where Ω is the angular velocity of the Keplerian disc and Ω_\star is the angular velocity of the star².

The torque on the star will produce a change in its angular momentum, thus:

$$\begin{aligned} \frac{dJ}{dt} &= \Gamma_{\text{annulus}} \\ &= \frac{\mu^2}{R^4} \left(\frac{\Omega(R) - \Omega_\star}{\Omega(R)} \right) \Delta R \end{aligned} \quad (4.7)$$

and a change in the angular momentum of the body will alter its rotation rate:

$$\frac{dJ}{dt} = \Omega_\star \frac{dI_\star}{dt} + I_\star \frac{d\Omega_\star}{dt} \quad (4.8)$$

$$\frac{d\Omega_\star}{dt} = \frac{1}{I_\star} \left(\Gamma_{\text{disc}} - \Omega_\star \frac{dI_\star}{dt} \right) \quad (4.9)$$

To get a proper estimate of the torque from the entire disc we have to integrate Eqn. 4.4 over the extent of the disc using the definitions of Eqn.s 4.5 and 4.6. If we assume that it extends from some inner radius R_{in} out to infinity then we get:

²This relation breaks down near the co-rotation radius, at this point $B_\phi \approx B_z$

$$\Gamma_{\text{disc}} = \frac{\mu^2}{3} \left(\frac{1}{R_{\text{in}}^3} - \frac{2\Omega_{\star}}{(GM_{\star}R_{\text{in}}^3)^{\frac{1}{2}}} \right) \quad (4.10)$$

Thus the spin down rate of the star is now given by:

$$\frac{d\Omega_{\star}}{dt} = \frac{1}{I_{\star}} \left[\frac{\mu^2}{3} \left(\frac{1}{R_{\text{in}}^3} - \frac{2\Omega_{\star}}{(GM_{\star}R_{\text{in}}^3)^{\frac{1}{2}}} \right) - \Omega_{\star} \frac{dI_{\star}}{dt} \right] \quad (4.11)$$

This expression indicates that the rate of spin down of the star is independent of the mass of the disc. Once we have a substantial disc we will get a braking torque on the star and it will always lead to the same reduction in the angular velocity of the star. This is in agreement with the results of Armitage & Clarke (1996)

If the material surrounding the merged object that was discussed in Section 4.6 does collapse down to form a disc, then it would have the same effects as the disc that has been postulated in this section.

Locking to out-flowing material

In previous sections I have explicitly stated that we do not have large convection zones on the surface of any of the collisional products. This has thus apparently ruled out a torque associated with stellar wind braking.³ However, we know that the collisional product will contract and spin up. This will eject material from the stars surface, whilst not strictly a wind in the conventional sense, there is no apparent reason why this material cannot become locked to the magnetic field as it moves away from the star and thus produce a braking torque.

To examine how this torque will break the rotation of the star, we first start off with the mass continuity equation:

³In a normal main-sequence star, if we are to lose angular momentum through a stellar wind, we require a deep surface convection zone. This is because angular momentum transport processes within the star are very slow. We rely on dynamical motions in the convection zone to speed up the transport of angular momentum around the star. However, the magnetic field of these merged objects is likely to be very high because of their rapid rotation (see Eqn. 4.21). Thus, it is likely that the star and field are tightly locked. Hence, as a torque is applied to the magnetic field, the whole star suffers the same torque and it is spun down.

$$\dot{m} = 4\pi R^2 \rho v \quad (4.12)$$

where \dot{m} is the mass loss from the star, or equivalently the mass flux of the wind-like material across a surface, v is the wind speed (which will be some multiple of the escape velocity of the star) and ρ is the density of the wind-like material.

We now look for pressure balance between the gas pressure and the magnetic pressure. This will give us the Alfvén radius for the star.

$$\rho_{\text{ra}} v_{\text{ra}}^2 = \frac{B_r^2(R_{\text{ra}})}{8\pi} \quad (4.13)$$

If we look at an open field line configuration, we may replace B_r with:

$$B_r = B_o \left(\frac{R_\star}{R} \right)^2 \quad (4.14)$$

If we now substitute Eqn.s 4.12 and 4.14 into Eqn. 4.13 we get:

$$R_{\text{ra}} = B_o R_\star^2 \dot{m}^{-\frac{1}{2}} v^{\frac{1}{2}} \quad (4.15)$$

then simply setting the velocity of the wind to be the escape velocity from the surface of the star the Alfvén radius may be expressed as:

$$R_{\text{ra}} = B_o R_\star^{\frac{9}{4}} \dot{m}^{-\frac{1}{2}} m_\star^{-\frac{1}{4}} \frac{1}{(8G)^{\frac{1}{4}}} \quad (4.16)$$

If we the equate the angular momentum loss from the star to be the same as the angular momentum carried away by the wind once it has reached the Alfvén radius, one can say:

$$\frac{dJ}{dt} = \dot{m}\Omega_* R_{ra}^2 \quad (4.17)$$

then once we substitute Eqn. 4.16 into the above we get:

$$\frac{dJ}{dt} = B_o^2 R_*^{\frac{9}{2}} m_*^{-\frac{1}{2}} \Omega_* \frac{1}{(8G)^{\frac{1}{2}}} \quad (4.18)$$

This agrees with the results of Verbunt (1984).

Then by using Eqn. 4.9 we can get the spin down rate for the star:

$$\frac{d\Omega_*}{dt} = \frac{1}{I_*} \left[-B_o^2 R_*^{\frac{9}{2}} m_*^{-\frac{1}{2}} \Omega_* \frac{1}{(8G)^{\frac{1}{2}}} - \Omega_* \frac{dI_*}{dt} \right] \quad (4.19)$$

One can make an estimate on the likely evolution of the radius of the blue straggler by using this torque. As we know, the torque will slow the star down and this will allow the star to contract to smaller and smaller radii until an equilibrium is reached. If we assume that the star is initially rotating at some fraction of its maximum rotation rate:

$$\Omega_* = f \sqrt{\frac{2GM_*}{R_*^3}} \quad (4.20)$$

then we can calculate the minimum size that the star can contract down to as a function of time. This is plotted in Fig. 4.12. This figure has assumed a magnetic field that had an initial value of 200 Gauss and varied with time as (Armitage & Clarke 1996):

$$B = B_o \left(\frac{P_o}{P} \right)^2 \quad (4.21)$$

along with a mass loss rate of $10^{-10} M_\odot$ /yr, although the form of the graph is actually largely independent of \dot{m} . In the plot I have shown two sets of lines. The uppermost set represent the evolution of radius if it were solely dependent on the change in angular

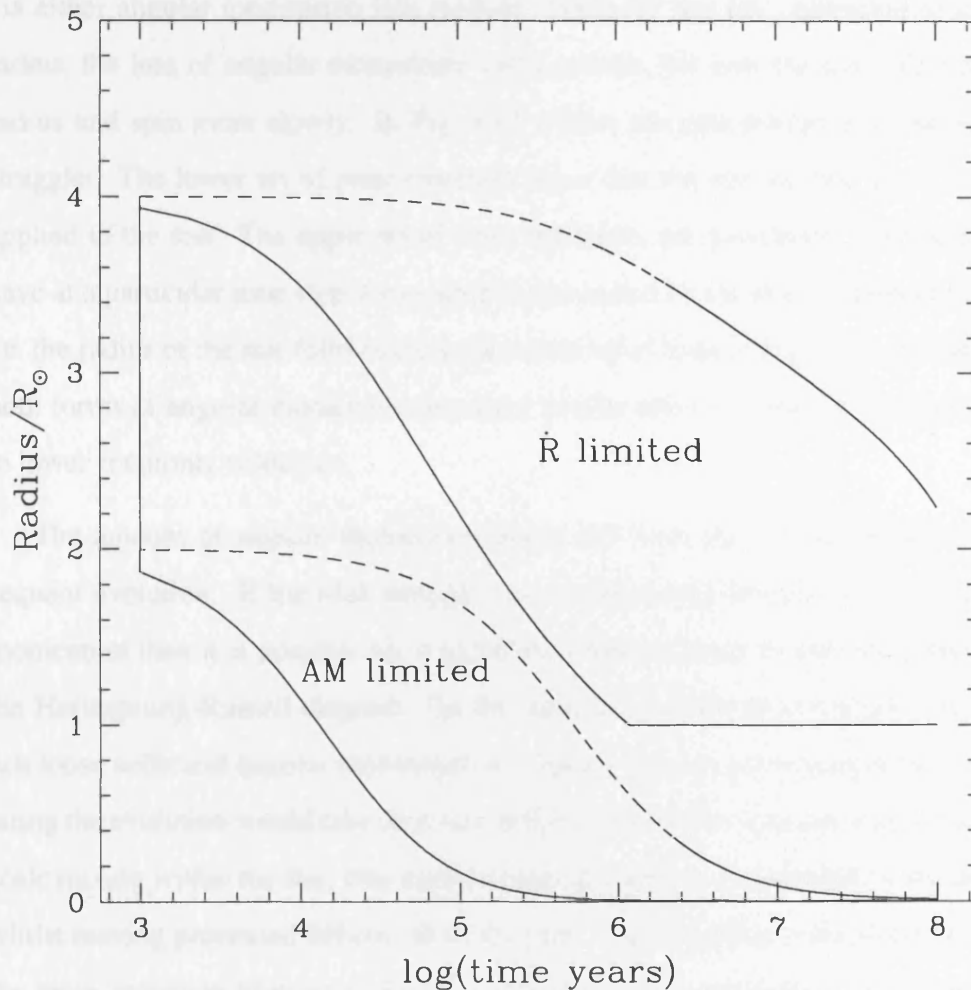


FIGURE 4.12. Evolution of the radius of the blue straggler as a function of time. The first two lines (labelled (\dot{R})) represent how the radius of the blue straggler would evolve if it were solely dependent on the angular momentum losses within the star. The solid line represents angular momentum losses due to wind braking, whilst the dashed line represents the effects of having a disc. In reality the star will shrink by more than this, as its radius is also dependent on the cooling of the star. The point where it can shrink to is limited by its angular momentum. The lower two lines on the plot show the smallest radius that the star can shrink to with the angular momentum that it has at a particular time step. The evolution of a blue straggler will lie somewhere in-between the two encompassing lines.

momentum of the star. The lower set represent the minimum radius that the star can contract to with the angular momentum that it has at a particular time step. As can be seen, we quickly loose sufficient angular velocity to allow the blue straggler to contract down via either angular momentum loss method. Once the star has contracted to its desired radius, the loss of angular momentum will continue, but now the star will maintain its radius and spin more slowly. In Fig. 4.13 I show the spin evolution of the same blue straggler. The lower set of lines represent the ω that the star has because of the torque applied to the star. The upper set of lines represents the maximum ω that a model can have at a particular time step if its radius is dominated by the angular momentum losses, i.e. the radius of the star follows the upper-most set of lines in Fig. 4.12. As can be seen, both forms of angular momentum loss have similar effects on the star, spinning it down to lower rotational velocities.

The amount of angular momentum that a star loses has a huge impact on its subsequent evolution. If the blue straggler lost a substantial amount of its initial angular momentum then it is possible for it to follow a fairly normal evolutionary path through the Hertzsprung-Russell diagram. On the other hand, if the blue straggler were to only just loose sufficient angular momentum to contract and was subsequently still rapidly rotating the evolution would take on a very different form. The rotation would lead to large scale mixing within the star, thus replenishing the supplies of hydrogen in the stellar core whilst moving processed helium out of the core. This would have the effect of extending the main-sequence lifetime of the blue straggler, and would lead to the formation of a helium star. These two extremes are represented by Fig. 5-7 of Sills *et. al.* (2001)

It is not only the helium abundance within the star that is strongly affected by rotation. All the metals that are produced in the core will be redistributed around the rapidly rotating stars. In Fig. 4.14 various atomic abundances (as calculated by the YREC model) are shown as a function of time for a particular blue straggler model with and without strong angular momentum loss during its early life. Clearly the marks of rapid rotation are visible, with very different chemical make ups in the two models.

Thus far there has been very little observational work done on obtaining the rotational velocities of blue stragglers in globular clusters. Thus far only one blue straggler has a

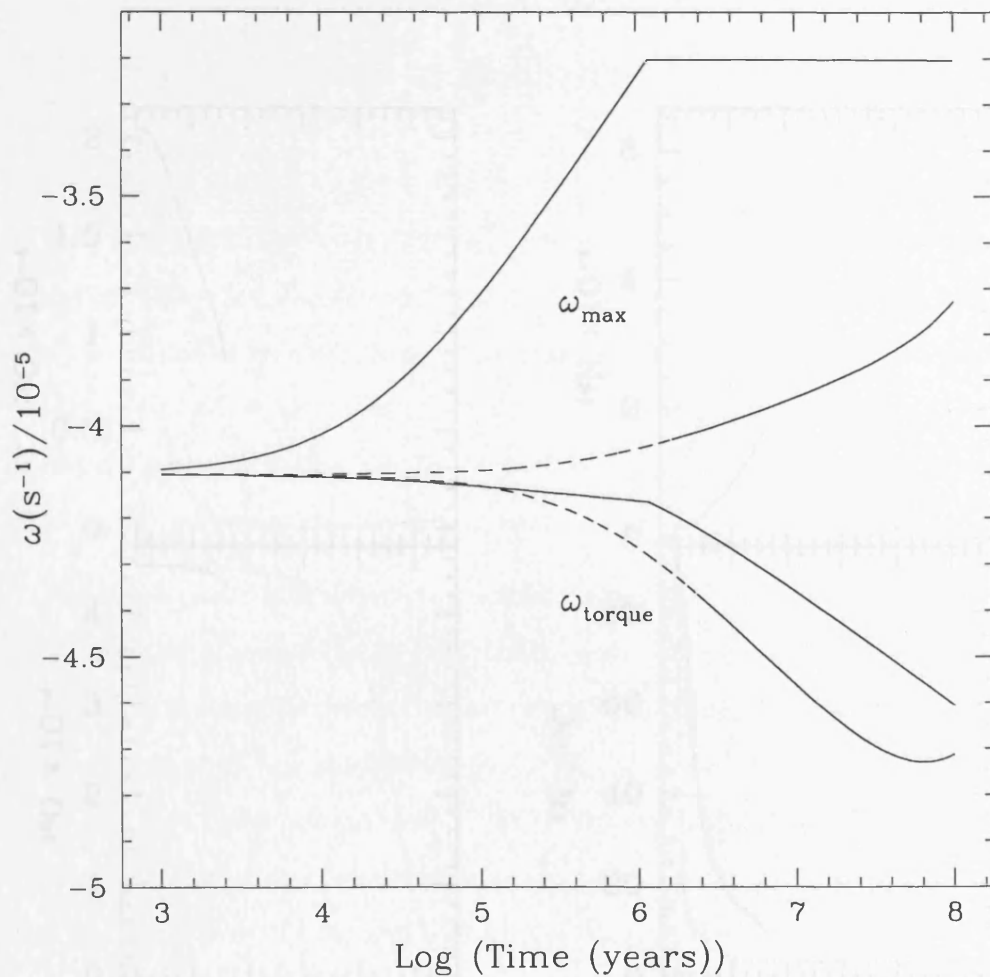


FIGURE 4.13. The spin evolution of one of the blue straggler stars. The solid lines represents the effects of angular momentum loss through a wind, whilst the dashed lines represents angular momentum loss through locking to a disc. The top two lines represent the maximum ω that the model could have at a particular time if its radius was dominated by angular momentum losses (i.e. it followed the upper lines in Fig. 4.12). The lower two lines represent the ω calculated for the models using Eqns. 4.11 and 4.19. As can be seen, both forms of angular momentum loss have very similar effects on the spin of the star, and rapidly take it below its critical velocity.

4.7. Other methods of producing blue stragglers

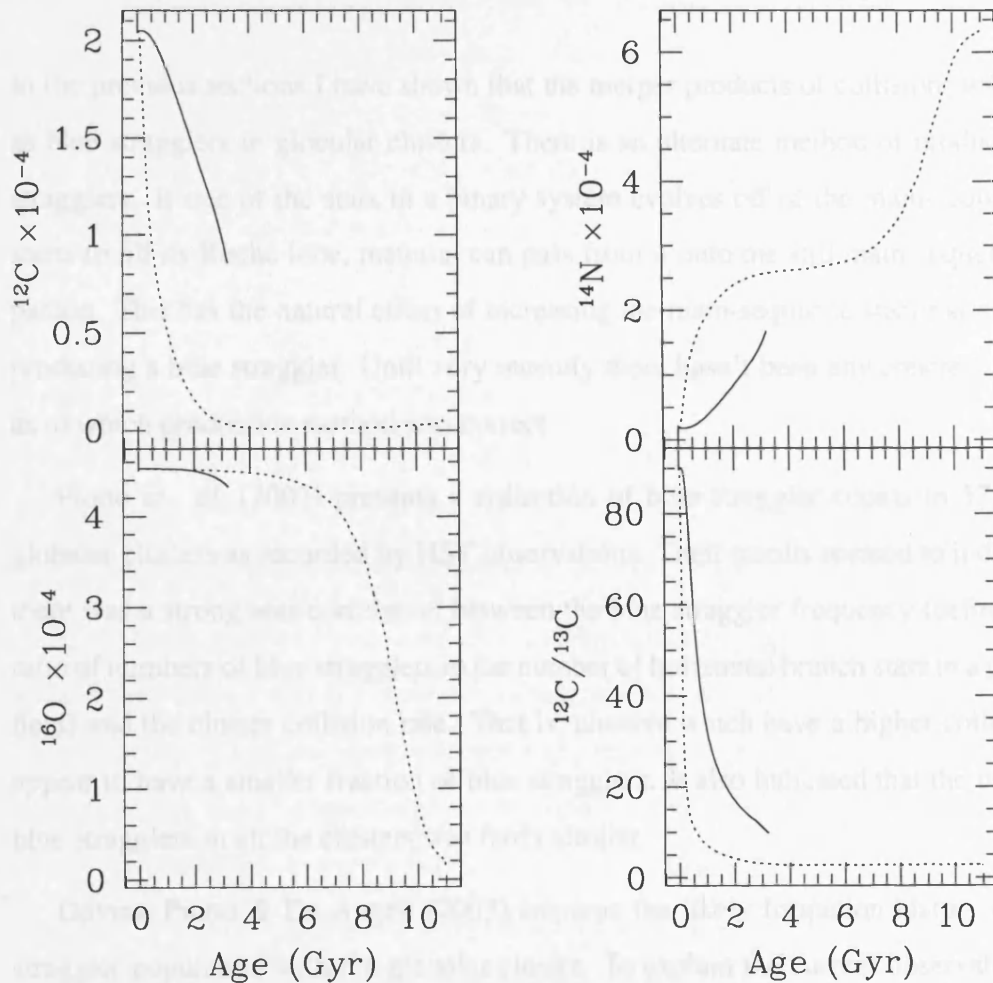


FIGURE 4.14. Surface chemical composition of one of the blue straggler models with (solid line) and without (dashed line) a period of angular momentum loss during their early evolution. The more rapidly star has a significantly altered chemical composition. This results from the movement of material in and out of the core.

stragglers. These are formed through binary evolution, where one star fills its main-sequence phase and the other star is left behind. A combination of the high-mass population is also responsible for the blue stragglers that are seen today.

The principal population of blue stragglers deserves some more details. In any cluster

well determined rotation rate, BBS 19 in 47 Tucanae has a measured $v \sin i = 155\text{km/s}$ (Shara, Saffer & Livio 1997). This fits in well with the models proposed in this chapter, it is rotating fast, but not near its break up speed.

4.7 Other methods of producing blue stragglers

In the previous sections I have shown that the merger products of collisions will appear as blue stragglers in globular clusters. There is an alternate method of producing blue stragglers. If one of the stars in a binary system evolves off of the main-sequence and starts to fill its Roche lobe, material can pass from it onto the still main-sequence companion. This has the natural effect of increasing the main-sequence stars mass and thus producing a blue straggler. Until very recently there hasn't been any concrete evidence as to which production method was correct.

Piotto *et. al.* (2003) presents a collection of blue straggler counts in 57 separate globular clusters as recorded by HST observations. Their results seemed to indicate that there was a strong anti-correlation between the blue straggler frequency (defined as the ratio of numbers of blue stragglers to the number of horizontal branch stars in a particular field) and the cluster collision rate. That is, clusters which have a higher collision rate appear to have a smaller fraction of blue stragglers. It also indicated that the number of blue stragglers in all the clusters was fairly similar.

Davies, Piotto & De Angeli (2003) examine the likely formation history of a blue straggler population within a globular cluster. To explain the current observations they conclude that there must be two sources of blue stragglers. The first source is referred to as the dynamical blue stragglers. These are produced through collisions such as those detailed in this chapter. The second population is referred to as the primordial blue stragglers. These are formed through binary evolution, where one star fills its Roche lobe and passes mass onto the other star in the system. A combination of the these two populations is then responsible for the blue stragglers that we see today.

The primordial population of blue stragglers deserves some more details. In any clus-

ter environment we inevitably get a population of binary systems produced as the cluster is formed. The low velocity dispersion within globular clusters means that the hard soft boundary for a binary system is actually quite large. Thus we can have a population of binary systems with a separation of a few hundred solar radii. As was discussed in chapter 2 interactions within the cluster lead to heavy stars replacing lighter stars within a binary. To produce a blue straggler that we will see today we require that the mass transfer which turned a normal star into a blue straggler to have occurred no more than a billion or so years ago (this is a consequence of the lifetime of the blue straggler). This gives a constraint on the upper mass of the heavier star in the binary system. We require the heavier star to have a mass which would lead to it evolving in the past 1 Gyr or so, in order to produce a blue straggler that we can see today. It is this requirement that means that more massive clusters have proportionally less blue stragglers produced via binary systems. In high mass clusters, the binary collision rate goes up so we are more likely to end up with binary systems which have a very massive component. These will produce a blue straggler, but it would have happened in the past and the resultant blue straggler would have evolved and would no longer be distinguishable within the cluster.

So, in more massive clusters more blue stragglers are produced via collisions between stars, whilst in less massive clusters more blue stragglers are produced via binary system evolution. These two formation methods combine to explain Piotto *et. al.*'s (2003) results. In Fig. 4.15 I show how the two populations of blue stragglers (primordial and dynamical) combine to give a fairly flat distribution in the number of blue stragglers over a large range of absolute magnitudes. In Fig. 4.16 I show the fractions of the blue straggler population that the two production methods provide within a cluster. This figure clearly illustrates that there are two separate regimes where the two different blue straggler methods are individually important.

There is growing direct evidence that binary system evolution is a feasible method of producing a blue straggler population. Preston & Sneden (2000) identified a number of blue stragglers, in the halo of the milky-way, which they believed were in wide binary systems with faint companions. This would be a natural consequence of the binary production method. Rucinski (2000) found that blue stragglers were relatively common in

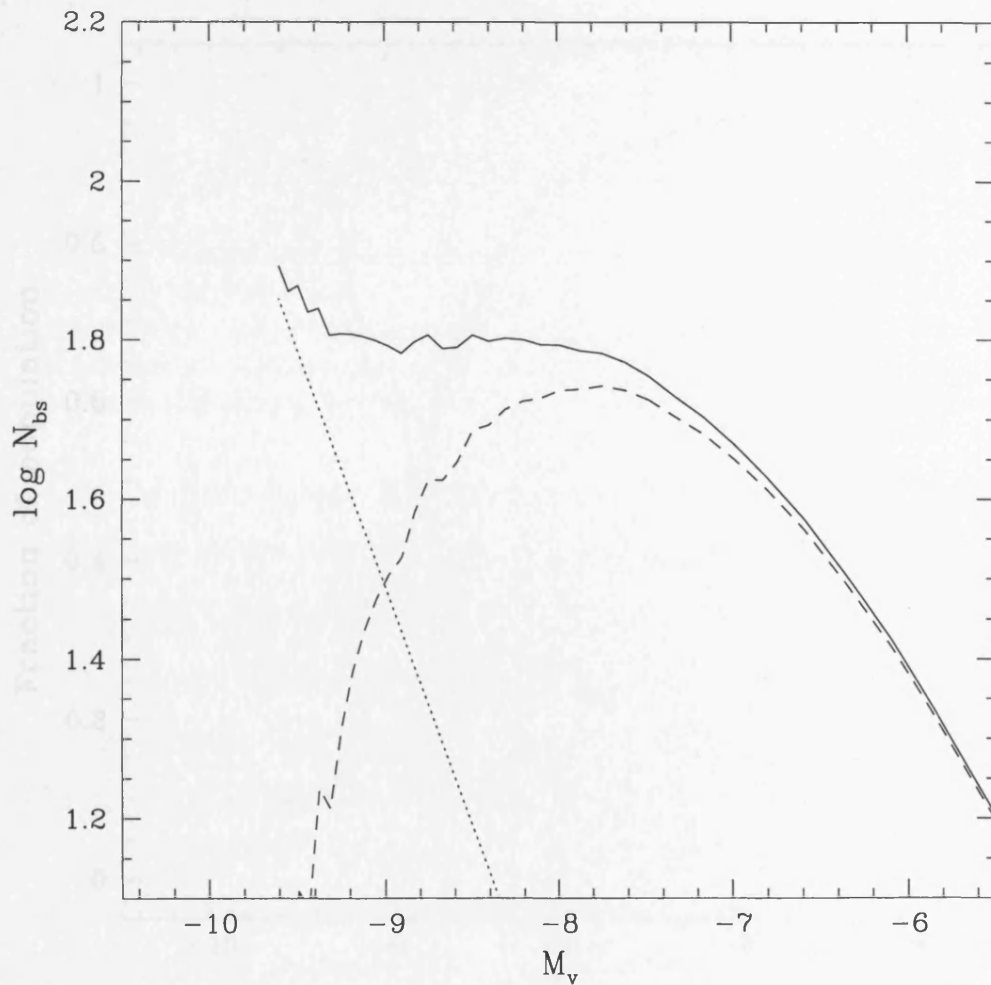


FIGURE 4.15. A plot of the number of blue stragglers produced within a cluster through both dynamical (short dashed line) and primordial (long dashed line) as a function of cluster absolute magnitude. The solid line represents the total population of blue stragglers within the cluster. Clearly, heavier (hence brighter) clusters have the majority of their blue stragglers formed through collisions, whilst at lower cluster masses the majority of blue stragglers result from binary system evolution. Figure courtesy of Davies, Piotto & De Angeli (2003)

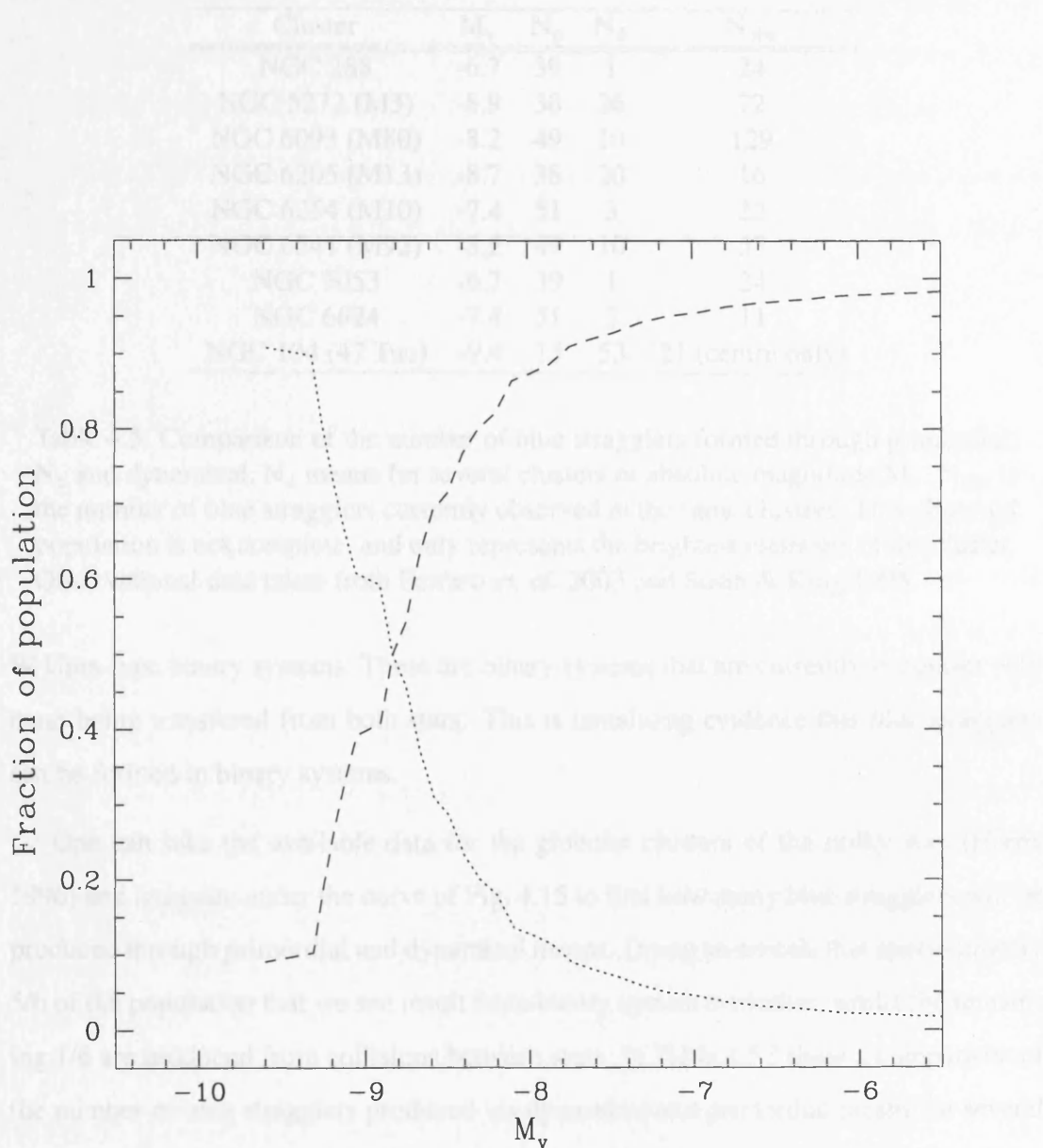


FIGURE 4.16. The fraction of blue stragglers produced through collisions (short dashed line) and binary system evolution (long dashed line) as a function of the clusters absolute magnitude. It is clear from this figure that direct collisions between stars can only be responsible for the blue straggler populations seen in the very heaviest clusters. In the lighter clusters the blue straggler population is made up almost exclusively through the evolution of binary systems.

Cluster	M_v	N_p	N_d	N_{obs}
NGC 288	-6.7	39	1	24
NGC 5272 (M3)	-8.9	30	26	72
NGC 6093 (M80)	-8.2	49	10	129
NGC 6205 (M13)	-8.7	38	20	16
NGC 6254 (M10)	-7.4	51	3	22
NGC 6341 (M92)	-8.2	49	10	53
NGC 5053	-6.7	39	1	24
NGC 6624	-7.4	51	3	11
NGC 104 (47 Tuc)	-9.4	15	53	21 (centre only)

Table 4.5. Comparison of the number of blue stragglers formed through primordial, N_p and dynamical, N_d means for several clusters of absolute magnitude M_v . N_{obs} is the number of blue stragglers currently observed in the same clusters. This observed population is not complete, and only represents the brightest members of the cluster. Observational data taken from Ferraro *et al.* 2003 and Sosin & King 1995.

W Uma-type binary systems. These are binary systems that are currently in contact with mass being transferred from both stars. This is tantalising evidence that blue stragglers can be formed in binary systems.

One can take the available data for the globular clusters of the milky way (Harris 1996) and integrate under the curve of Fig. 4.15 to find how many blue stragglers will be produced through primordial and dynamical means. Doing so reveals that approximately 5/6 of the population that we see result from binary system evolution, whilst the remaining 1/6 are produced from collisions between stars. In Table 4.5 I show a comparison of the number of blue stragglers produced via dynamical and primordial means for several specific globular clusters. For comparison I also show the current blue straggler counts available in the literature for these clusters. As can be seen, there is close agreement between the total number of blue stragglers from theory and observation. The one exception to the close match is M80. This differs from the other clusters in the comparison by having a very high density core. Thus it is likely that it will have a larger population of dynamically produced blue stragglers than has been predicted by Fig. 4.15.

N-body modelling of the old open cluster M67 by Hurley *et al.* (2001) showed that half of the blue straggler population in that cluster would likely be made up of systems

where mass transfer had taken place between two components in a binary system. Performing similar large scale models of globular clusters is still currently beyond the ability of available computers, however this should hopefully change in the near future.

It would seem that future theoretical work on blue stragglers should now move on to looking at the formation of those blue stragglers which are produced within a binary system.

4.8 Conclusions

In this chapter the highest resolution simulations of collisions between main-sequence stars performed to date have been presented. Such high resolution simulations were important to check the validity of slightly lower resolution simulations. I have shown that simulations performed with 100,000 particles are sufficient to understand the details of the mixing during the merger process and gives the same final results after stellar evolution as 1,000,000 particle simulations. The difference in particle number represents a considerable saving in computational effort.

I have confirmed that the blue stragglers produced through off-axis mergers do initially suffer from an angular momentum problem, which would prevent them contracting down to a normal main-sequence position in the Hertzsprung-Russell diagram. It had previously been proposed that the lack of a surface convection zone or a disc formed during the collision, meant that collisionally produced merged objects wouldn't be able to contract down and form a blue straggler. I have detailed two simple methods where the blue straggler can be slowed down, allowing it to contract down to the main-sequence. Utilising the tendency of the blue straggler to eject material as it contracts it is possible for the blue straggler to either become locked to a newly formed disc or to material which flows away from the system.

Thus, it would seem that there is no longer an angular momentum problem associated with collisionally produced blue stragglers.

Further, I have shown (following on from the work of Davies, Piotto & De Angeli

2003) that $5/6$ of the blue straggler population are likely to result from the evolution of binary systems and only $1/6$ of the population will result from dynamical methods. Thus, future work should now focus on studying the properties of blue stragglers produced through the evolution of binary systems.

Chapter 5

On the origin of Red-giant depletion through low velocity collisions

5.1 Introduction

Observations of several post core collapse (PCC) globular clusters have revealed the existence of both population and colour gradients (Djorgovski, Piotto, Phinney & Chernoff 1991). These observations have shown that the clusters become bluer towards the centre and this is believed to be the result of a paucity of red giant stars and/or possibly an increase in the population of faint blue stars. The total effect represents a few per cent of the visible light.

Hubble Space Telescope observations (Bailyn 1994, Shara, Drissen, Rich, Paresce, King & Meylan 1998) have confirmed that there exists a depletion in the red giant population within several PCC clusters with respect to the horizontal branch. In addition within several clusters a population of supra horizontal branch (SHB) stars (stars which are much brighter than the normal horizontal branch and lie as a distinct population within an Hertzsprung-Russell diagram) have been identified. Shara *et. al.* (1998) found a population of SHB stars in NGC6522 which were one and a half magnitudes brighter in the B band than the normal horizontal branch, whilst those found in 47 Tuc (Bailyn 1994) were a magnitude brighter than the local horizontal branch.

An additional interesting population of bright blue objects found in PCC are sub-dwarf B stars (sdB and related sdO/sdOB) (Sargent & Searle 1968). These are believed to be helium core burning objects with a small ($<0.02M_{\odot}$), but hydrogen rich envelope. These stars cannot be formed through standard single main-sequence star evolution. Han *et. al.* (2003) set out three methods for producing these stars through binary system evolution (through the ejection of a common envelope and the creation of a tight binary system, through Roche lobe overflow and through the merger of two helium white dwarfs). I propose the addition of a dynamical source for sdB stars where the core of an old, evolved, red giant is removed from the majority of its envelope.

Within such a dense stellar system it is inevitable that collisions between stars will occur. Indeed collisions have been invoked as one possible mechanism for the creation of blue stragglers (see for example Fabian, Pringle and Rees 1975 or Sills *et. al.* 2002) which are main-sequence stars with mass greater than the turnoff mass of the cluster in question. I now investigate the possibility that collisions between binary systems and red giants could explain not only the depletion of red giant stars but also the existence of some of the more exotic members of the stellar population. I also examine the outcomes of collisions between single bodies and red giant stars.

Previous work on collisions in globular clusters has focused on interactions between single bodies (be they main-sequence stars or degenerate bodies) and red giants. For instance Davies, Benz & Hills (1991) examined collisions between a $0.8 M_{\odot}$ red giant and impactors of mass 0.4 and $0.6 M_{\odot}$ with velocities at infinity of 10 km/s. They found that for impact parameters less than twice the red giant radius the impactor would become bound to the giant and some mass would be lost from the red giant envelope. Closer approaches would lead to more disruptive consequences for the red giant envelope. Rasio & Shapiro (1991) performed a similar set of simulations but found that any material which could go on to form a common envelope system was very quickly disrupted.

The work of Davies *et. al.* (1998) looked at high speed collisions between binary stars and red giants, collisions more pertinent to the galactic centre. They found that the most destructive encounters between binary systems and red giants were those which lead to either the knock out of the red giant core, or those which ended up with a common

envelope system. These two outcomes will be discussed in more detail in section 3.2.

Beer & Davies (2003) have put forward an alternative suggestion to explain the paucity of red giants in PCC clusters. They argue that stars contained within binary systems could go through a double common envelope system as first one star reaches the red giant branch and then the other. During the common envelope stages angular momentum would pass from the orbit of the binary system to the envelope gas causing it to dissipate and the binary to harden. Indeed it is possible that the two compact cores could actually merge in such a scenario.

I investigate interactions between binary systems and red giants in two complimentary fashions. First I examine the time scales of relevance for the collisions utilising an N-body technique. I then follow this up by utilising detailed hydrodynamics to investigate the exact details of the collisions and ensure that the N-body modelling technique is valid.

I also examine the outcomes of collisions between single bodies and red giants in an attempt to understand what impact these collisions can have on the population of red giants in a globular cluster.

5.2 Observations

Observations over the past decade have identified the existence of a colour gradient within many globular cluster cores, in the sense of being bluer inward. Thus far observations have only identified this phenomena within PCC clusters and not within those clusters fitted by the King model (KM).

Two distinct observation techniques have been used. These are not necessarily complementary and a colour gradient which shows up in one need not show up in the other. The first technique is direct surface photometry. Using such a technique, a colour gradient has been identified in, for example, M30 (Djorgovski et al. 1991). The second method is that of creating a colour pixel histogram (Bailyn, Grindlay, Cohn, Lugger, Stetson & Hesser 1989). Two images of the clusters are taken in different bands (typi-

cally U and B) and the cleaned images are then divided. The resulting frame then maps the colour of the cluster rather than the intensity. A statistical analysis of the pixel colour distribution can then be utilised to compare different regions of the cluster. The first method is mainly sensitive to detecting the bright stars within the cluster, whilst the second method is more adept at detecting the fainter population which cover the majority of the cluster.

In Table 5.1 I highlight some of the observations made of globular clusters within our own galaxy.

The two different methods typically result in different interpretations as to the cause of the colour gradient. The direct surface photometry normally suggests that there is an under-abundance of luminous red-giant stars i.e. (Djorgovski & Piotto 1993*b*), whilst the colour pixel histogram technique normally suggests an increased population of faint blue stars, including blue stragglers, toward the centre of the cluster (Bailyn et al. 1989). It is likely that the colour gradient in most clusters actually results from a combination of these two effects (Stetson 1994).

Given that colour gradients have only been confirmed within PCC clusters (3σ or more detection), it is suggestive that there could be some underlying dynamical explanations for their existence. Given the dynamical nature of core collapse, a collisional explanation for the depletion of red giants seems reasonable.

5.3 Theory

5.3.1 Possible outcomes of red-giant binary collisions

Globular clusters are crowded places. In particular, within PCC clusters the number densities of stars reach values in excess of 10^5 stars/pc³. Within such a dense environment it becomes quite likely that collisions of some description will take place. Interactions involving binary systems are used to stave off core collapse (via binary heating) and direct collisions between stars have been proposed as a method of producing the blue straggler population seen within globular clusters.

Cluster	PCC or KM	Giant depletion?	Compared to what?	Colour gradient?	Extreme blue HB?	References
NGC 104 (47 Tuc)	KM	Y	AGB	N	N	Bailyn 1994, Auriere & Ortolani 1988, Cohen <i>et. al.</i> 1997
NGC 2808	KM	N	–	?	Y	Walker 1999
NGC 4147	PCC?	N?	–	Y	Y	Djorgovski 1988
NGC 5272 (M3)	KM	?	–	?	Y	Rosenberg <i>et. al.</i> 2000
NGC 5946	PCC	N	–	?	blue	Davidge 1995
NGC 6093 (M80)	KM	?	–	N	Y	Djorgovski 1988
NGC 6205 (M13)	KM	?	–	?	Y	Rosenberg <i>et. al.</i> 2000
NGC 6284	PCC	?	–	Y	Y	Djorgovski <i>et. al.</i> 1991
NGC 6293	PCC	Y	underlying light	Y	Y	Djorgovski <i>et. al.</i> 1991
NGC 6397	PCC	Y	underlying light	Y	Y,He WDs	Lauzeral 1992, Djorgovski <i>et. al.</i> 1991, Rosenberg <i>et. al.</i> 2000
NGC 6522	PCC	Y	HB	?	Y	Shara <i>et. al.</i> 1998
NGC 6558	PCC	?	–	Y	Y	Djorgovski <i>et. al.</i> 1991
NGC 6624	PCC	?	–	Y	N	Djorgovski <i>et. al.</i> 1991, Rosenberg <i>et. al.</i> 2000
NGC 6626 (M26)	PCC	?	–	Y	Y?	Djorgovski 1988, Rosenberg <i>et. al.</i>
NGC 6715 (M54)	KM	?	–	N	N	Djorgovski <i>et. al.</i> 1991

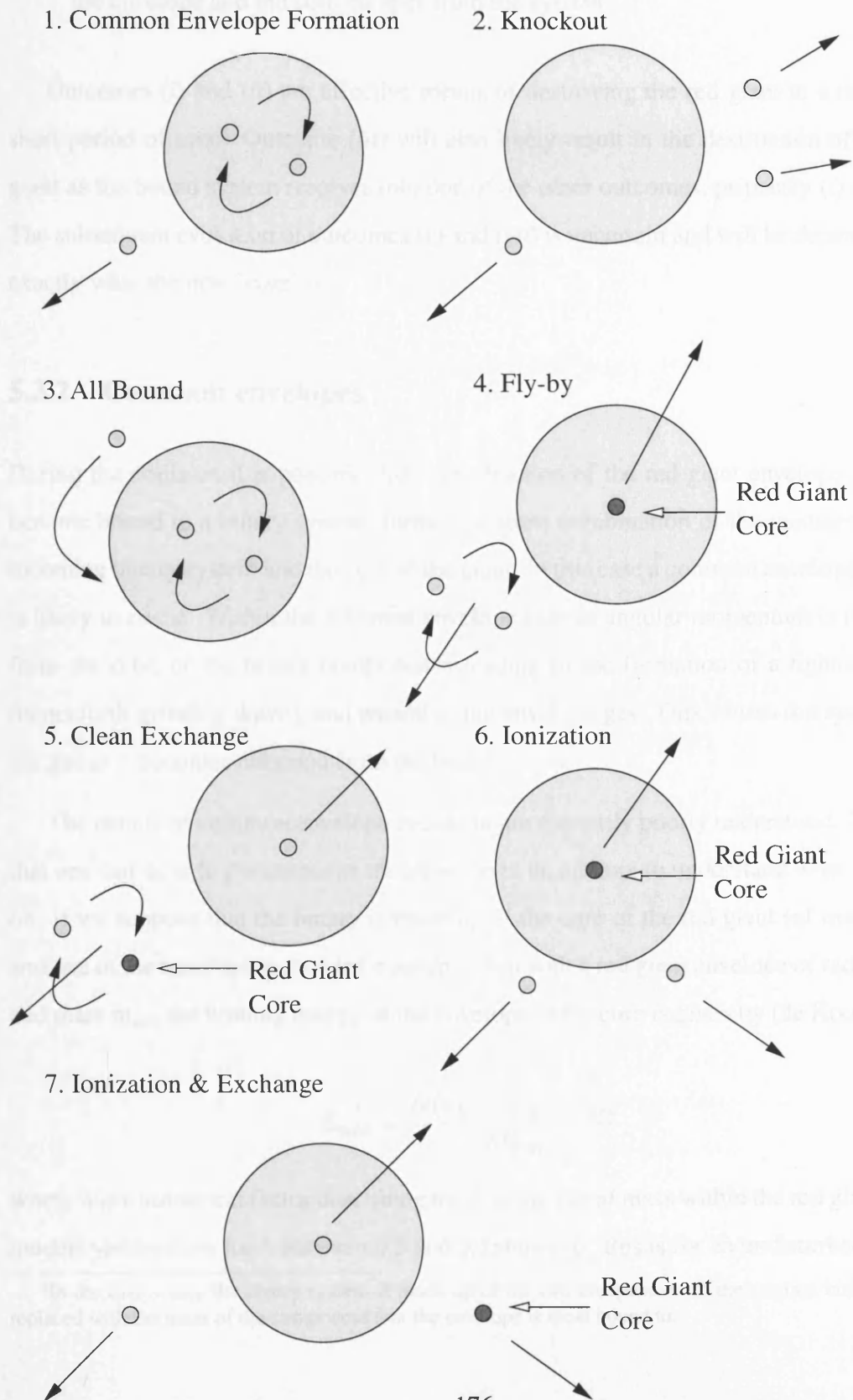
Cluster	PCC or KM	Giant depletion?	Compared to what?	Colour gradient?	Extreme blue HB?	References
NGC 6864 (M75)	KM	?	–	N	Y	Djorgovski <i>et. al.</i> 1991, Harris 1975
NGC 7078 (M15)	PCC	Y	faint RGB, SG	Y	Y	Yanney <i>et. al.</i> 1994, Djorgovski <i>et. al.</i> 1991, Bailyn <i>et. al.</i> 1989, Rosenberg <i>et. al.</i> 2000
NGC 7099 (M30)	PCC	Y	faint RGB, SG, underlying light	Y	N	Guhathakurta <i>et. al.</i> 1998, Davidge 1995, Piotto, King & Djorgovski 1988, Bur- garella & Buat 1996, Djorgovski <i>et. al.</i> 1991

Table 5.1. A table listing some of the globular clusters of our own galaxy and a description of their density profile (i.e. post core collapse or King model) and a description of any observed colour gradient.

In this chapter I am primarily interested in collisions involving binary systems and red giant stars (although in section 5.7 I do consider the outcomes of single star collisions with red giants). Due to the contrast in size between the red giant and the components of the binary system (be they main-sequence stars or degenerate bodies) the binary components have been modelled as point masses in all simulations. In the four-body runs, the red giant has also been approximated as two point masses as well, one for the core and one representing the envelope. The details of this approximation are explained in section 5.4.1

During such an encounter there are a number of distinct possible outcomes. These are detailed in Davies *et. al.* (1998) and I shall only briefly mention the possible outcomes here.

1. A *common-envelope* system may be formed where two of the point masses form a binary within the red giant envelope, whilst the third point mass is ejected.
2. A *knock-out* might occur where the core and envelope of the red giant become unbound. The binary system is also not bound to the envelope. This would completely destroy the giant.
3. All the bodies may become bound in a complex hierarchy. This is likely to be highly unstable and eventually reduce to one of the other outcomes.
4. A *fly-by* may occur where the binary simply passes by the red giant leaving it relatively unperturbed.
5. *Clean exchange*. This is a relatively unlikely event where the core of the red giant replaces one of the binary components. The ejected binary component then becomes the new core of the red giant.
6. *Ionisation*. If the incoming binary is sufficiently soft, then it might be broken up by the encounter with the red giant. The two, now single, components could then remove some small quantity of mass from the red giant envelope.



176
 FIGURE 5.1. Possible outcomes of collisions between red giants and a binary system.

7. *Ionisation and exchange* Again the binary is broken up during the interaction; however, this time one of the components replaces the red giant core at the centre of the envelope and the core escapes from the system.

Outcomes (i) and (ii) are effective means of destroying the red giant in a relatively short period of time. Outcome (iii) will also likely result in the destruction of the red giant as the bound system resolves into one of the other outcomes, primarily (i) and (ii). The subsequent evolution of outcomes (v) and (vii) is uncertain and will be dependent on exactly what the new 'core' is.

5.3.2 Common envelopes

During the collision it is possible that some fraction of the red giant envelope gas will become bound to a binary system, formed of some combination of the members of the incoming binary system and the core of the giant. In this case a common envelope system is likely to ensue. Within the common envelope system angular momentum is removed from the orbit of the binary components, leading to the formation of a tighter binary (henceforth grinding down), and passed to the envelope gas. This causes the ejection of the gas as it becomes unbound from the binary.

The details of common envelope evolution are currently poorly understood. The best that one can do is to parameterise the situation in an attempt to understand what is going on. If we suppose that the binary is made up of the core of the red giant (of mass m_c)¹ and one of the interloping stars (of mass m_2) then with a red giant envelope of radius R_{env} and mass m_{env} the binding energy of the envelope to the core is given by (de Kool 1990):

$$E_{\text{bind}} = \frac{G(m_c + m_{\text{env}})m_{\text{env}}}{\lambda R_{\text{env}}}, \quad (5.1)$$

where λ is a numerical factor describing the distribution of mass within the red giant. Our models yield values for λ between 0.3 and 0.5; however, this is for an undisturbed model

¹In the case where the binary system is made up of the two components of the original binary m_c is replaced with the mass of the component that the envelope is most bound to.

and will change after a collision. As the binary is ground down within the envelope of material its binding energy will change. This change is given by:

$$\delta E_{\text{orb}} = \frac{Gm_2}{2} \left[\frac{m_c}{a_f} - \frac{m_c + m_{\text{env}}}{a_i} \right], \quad (5.2)$$

If we assume that this energy goes into unbinding the envelope with some characteristic efficiency α then:

$$E_{\text{bind}} = \alpha \delta E_{\text{orb}}, \quad (5.3)$$

whereupon a rearrangement for the final radius of the binary system gives:

$$a_f = \frac{m_2 m_c}{2(m_c + m_{\text{env}})} \left[\frac{m_{\text{env}}}{\alpha \lambda R_{\text{env}}} + \frac{m_2}{2a_i} \right]^{-1}, \quad (5.4)$$

In Fig. 5.2 I plot the final separation of a binary against its initial separation (both in solar radii) for a range of α values. As can be seen in this plot we can easily grind down a wide binary system to a tighter system. With less efficient α 's much tighter binary systems can be produced. This could provide a method of grinding down binaries and producing some of the interesting systems seen in globular clusters.

In Fig. 5.3 I plot the ratio of the final separation of a binary system which undergoes a common envelope phase with some fraction, γ , of the total envelope mass of the red giant to the final separation it would have had if $\gamma=1$ as a function of γ . As can be seen, even a modest amount of mass is sufficient to cause a large reduction in the size of the binary orbit. Coupled to this is the effect of α . With less efficient α 's a tighter binary is formed for the same amount of envelope mass.

One might make a comparison between the timescales associated with a binary collecting an envelope and hardening and the time required for scattering events to have the same effect. To do this we first must identify the number of red giants within a cluster. Assuming that all stars within the mass range 0.8 to $0.81M_{\odot}$ (Beer & Davies 2003 submitted) are on the red giant branch, one can integrate a Salpeter type mass function, $dN \approx M^{-2.35} dM$, to find N_{rg} . Assuming that half of this population is contained within

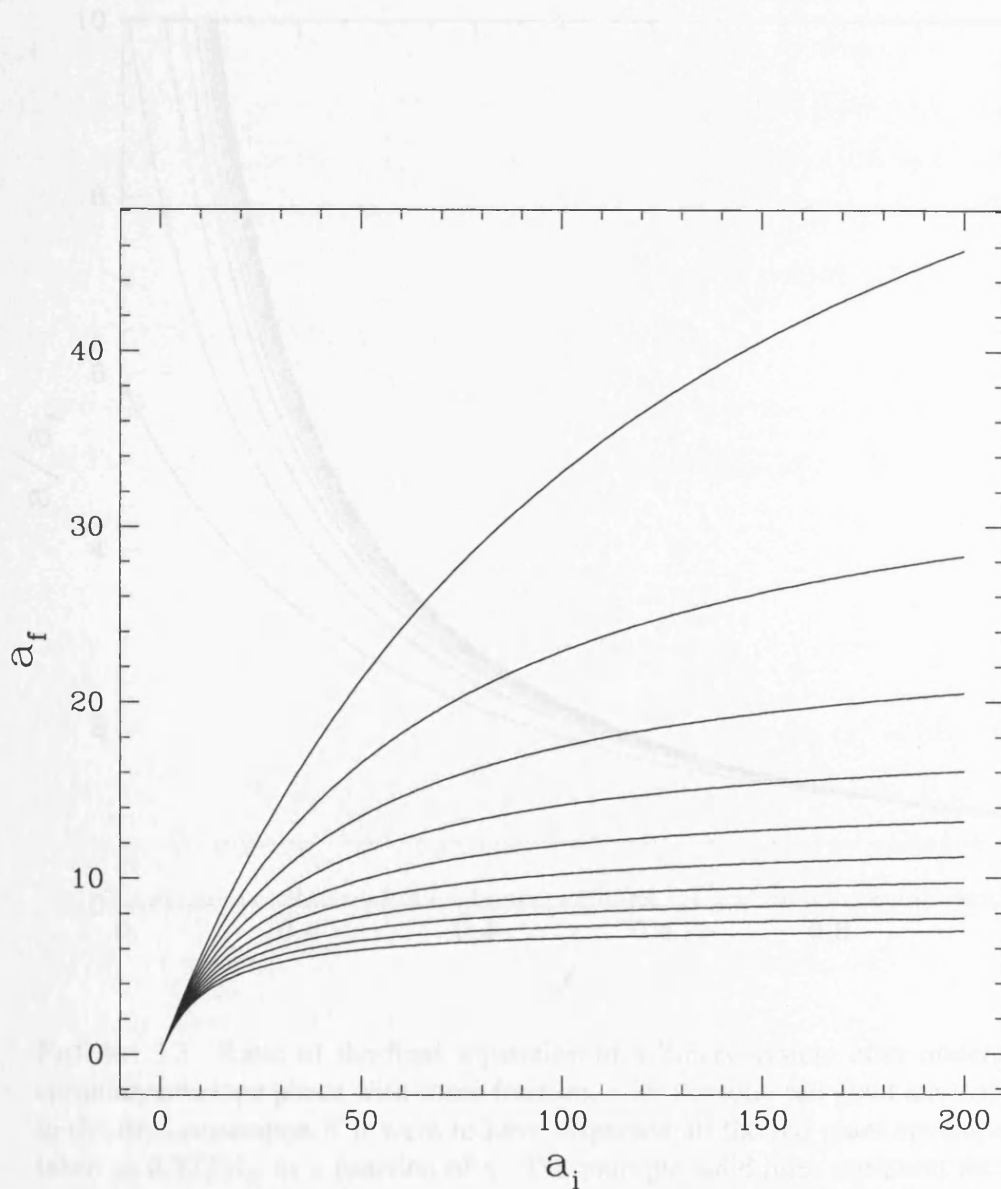


FIGURE 5.2. Final binary separation as a function of initial binary separation, both in solar units. I have plotted multiple curves for various α 's. α decreases monotonically from 1 to 0.1 down the plot. This plot was produced for two equal mass stars, $m_1=m_2=0.8M_{\odot}$, with $\lambda=0.5$, $m_{\text{env}}=0.2$ (i.e. only a fraction of the total red giant envelope mass) and $R_{\text{env}}=100R_{\odot}$.

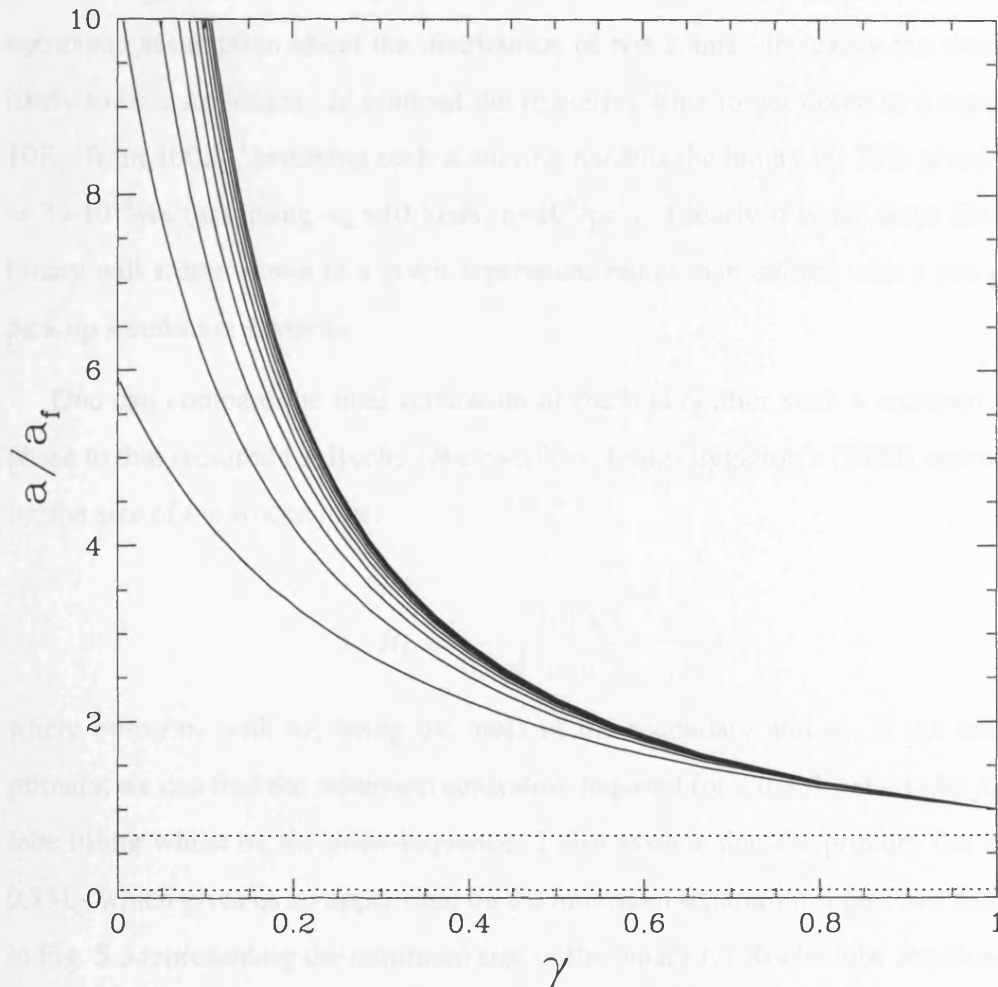


FIGURE 5.3. Ratio of the final separation of a binary system after undergoing a common envelope phase with some fraction, γ , of the total red giant envelope mass to the final separation if it were to have dispersed all the red giant envelope mass, taken as $0.322M_{\odot}$ as a function of γ . The multiple solid lines represent the effects of different values of α , with α increasing monotonically from 0.1 to 1. from top to bottom. The dashed lines represent the ratio of the maximum size of the binary for a $0.8M_{\odot}$ main-sequence star to be just Roche lobe filling to the final separation of the binary if it were to have all the mass of the red giant envelope in the common envelope phase. Again the multiple lines represent the effects of different α 's with α increasing monotonically from 0.1 to 1. from top to bottom. As we can see none of the binary systems quite come into contact through this common envelope phase. However, these calculations assumed an initially circular orbit, the introduction of some eccentricity would serve to bring the two components of the binary system closer to being Roche lobe filling. This plot was produced with $m_1=m_2=0.8M_{\odot}$, with $\lambda=0.5$ and $R_{\text{env}}=100R_{\odot}$.

the central parsec of a globular cluster an approximate timescale for a binary to collide with a red giant is $\approx 3 \times 10^{15}$ yrs. This is clearly a lower estimate given our rather over optimistic assumption about the distribution of red giants. In reality the time scale is likely to be a lot longer. In contrast the scattering time to get down to a separation of $10R_{\odot}$ from $100R_{\odot}$ assuming each scattering hardens the binary by 30% gives a time of $\approx 3 \times 10^{10}$ yrs (assuming $v_{\infty}=10$ km/s, $n=10^5/\text{pc}^3$). Clearly it is far more likely that a binary will scatter down to a given separation, rather than collide with a red giant and pick up a common envelope.

One can compare the final separation of the binary after such a common envelope phase to that required for Roche-lobe overflow. Using Eggleton's (1983) approximation for the size of the Roche lobe:

$$R_L = \frac{0.49q^{\frac{2}{3}}}{0.6q^{\frac{2}{3}} + \ln(1 + q^{\frac{1}{3}})} d, \quad (5.5)$$

where $q=m_2/m_1$ with m_2 being the mass of the secondary and m_1 is the mass of the primary, we can find the minimum separation required for a $0.8M_{\odot}$ star to be *just* Roche lobe filling whilst on the main-sequence. I also assume that the primary has a mass of $0.8M_{\odot}$ which gives us an upper limit on the minimum separation. I plot two dashed lines in Fig. 5.3 representing the minimum size of the binary for Roche lobe overflow divided by the final separation of the binary if it had all the mass of the red giant envelope during the common envelope phase. The different lines represent the effects of different α 's, with $\alpha=0.1$ being the upper line and $\alpha=1$ the lower line. As we can see it is not possible for this binary system to be ground down to a separation where Roche lobe overflow will take place whilst the star is still on the main-sequence. For the binary to come into contact we would require further angular momentum loss to occur. This could be through either gravitational radiation, which would occur on a timescale of:

$$\begin{aligned} \tau_{\text{gr}} &= 1.5 \times 10^8 \left(\frac{M_1}{M_{\odot}} \right)^{-1} \left(\frac{M_2}{M_{\odot}} \right)^{-1} \left(\frac{M_1 + M_2}{M_{\odot}} \right)^{-1} \\ &\times \left[\left(\frac{a_i}{R_{\odot}} \right)^4 - \left(\frac{a_f}{R_{\odot}} \right)^4 \right] \text{yr}, \end{aligned} \quad (5.6)$$

assuming that the eccentricity of the system is negligible, although not necessarily true at the start of the evolution, the evolution of the binary toward a circular orbit is rapid. Alternatively, angular momentum may be lost through magnetic breaking on a timescale of (Di Stefano & Rappaport 1992):

$$\begin{aligned} \tau_{mb} = & 4.3 \times 10^5 \left(\frac{M_1}{M_\odot} \right) \left(\frac{R_\odot}{R_2} \right)^\beta \left(\frac{M_\odot}{M_1 + M_2} \right)^2 \\ & \times \left[\left(\frac{a_i}{R_\odot} \right)^5 - \left(\frac{a_f}{R_\odot} \right)^5 \right] \text{yr}, \end{aligned} \quad (5.7)$$

where a_i and a_f are the initial and final binary separations and R_2 is the radius of the main-sequence star. β is an adjustable parameter used to reflect the uncertainties in the physics behind the process of magnetic breaking, I assume $\beta=2$ (Davies 1997). If we look at the timescales involved when all the bodies have a mass of $0.8M_\odot$ (with one body being a main-sequence star and the other a white dwarf) and an initial separation of $10R_\odot$ the periods required to shrink the binary down to the point where the main-sequence star is just Roche lobe filling are $\tau_{gr}=1.4 \times 10^{12}$ yr and $\tau_{mb}=1 \times 10^{10}$ yr. Clearly whether or not the binary will come into contact will be dependent on how much longer the star will stay on the main sequence, and the final dynamics of the binary system after the common envelope phase. What should be noted however, is that these timescales have been derived for a circular binary system. Clearly in the case of a binary which has undergone some dynamical interaction the binary will have some eccentricity and this could serve to dramatically lower the timescales for bringing the binary into contact. Peters (1964) shows that for the gravitational radiation breaking mechanism, eccentricity can serve to reduce the merger timescales of two bodies by a factor of 10^3 or more with sufficiently large eccentricities compared to a circular orbit. The effects of eccentricity on magnetic breaking and the effects during the common envelope phase are currently unknown but it seems likely that they will reduce the in-spiral time as well. In any event Roche lobe overflow will likely start as the star evolves off the main sequence and starts to expand.

With in-spiral times possibly as short as 10^9 years it is entirely possible that we

could have a mechanism of producing a population of cataclysmic variables from binary systems that otherwise would not come into contact. These are binary systems containing a white dwarf accreting material from a low-mass main-sequence secondary star. Within the cores of globular clusters it has been shown that any primordial population of CVs (i.e. a population of binary systems which will naturally evolve into a CV) will be severely depleted within the core due to collisions with other stars (Davies 1997). Thus having a method of producing a second generation of CVs is important to explain the population within the cores of globular clusters.

5.3.3 Knock outs

To effectively deplete the red giants from the cluster we need to remove the envelope of gas from around the core of the giant. Simply removing some proportion of the envelope gas will not be sufficient to prevent a star becoming a red giant as the expansion of the envelope is driven by the nuclear processes within the core of the star. Examination of our models has suggested that over 50% of the red giant's envelope would have to be removed before the evolution of the red giant was substantially altered. To knock the core out of a red giant star, it needs to receive sufficient energy to escape the potential well of the envelope material. In Table 5.2 I list the escape velocities of the two models used in this paper. These were calculated by integrating over the potential of the red giant envelope.

There are two sources of energy to free the core. The first is the incoming kinetic energy of the collision. In the case of a globular cluster this is likely to be quite small ($v_\infty \approx 10\text{km/s}$). The second source is through a hardening of the incoming binary system. When a binary system undergoes an interaction with a third star it will either break up or get harder, depending on the initial binary separation (Heggie 1972). If the binary becomes harder during an interaction, potential energy is released and can be converted into kinetic energy.

We can simply equate the required kinetic energy for the core to escape from the envelope with a change in the binding energy of the binary system thus:

$$\frac{1}{2}m_c v_{\text{esc}}^2 = \beta E_{\text{bind}}, \quad (5.8)$$

Using the data in Table 5.2 we see that we require the binary to get over 30 per cent harder for any initial binary separation over $60R_{\odot}$. From the work of Heggie (1972) we know that on average interactions between binary systems and single stars result in only a 30 per cent hardening. This indicates that the ejection of the core through a simple hardening of the binary whilst not impossible is none-the-less likely to be a relatively rare event given the wide population of binaries in globular clusters.

5.3.4 Collision probabilities

During the lifetime of a star its radius changes markedly as a result of the nuclear processes going on within the star's core. This variation in stellar radius is of crucial importance when one considers the collision cross-section, σ . Utilising the YREC code (Guenther et al. 1992) I calculated the radius of a $0.8 M_{\odot}$ star as a function of time. The collision cross-section, σ , is related to the stellar radius by:

$$\sigma = \pi R_{\star}^2 \left(1 + \frac{2G(M_{\star} + M_{\text{int}})}{R_{\star} v_{\infty}^2} \right), \quad (5.9)$$

where M_{int} is the mass of the interloping star.

In Fig. 5.4 I plot the integrated collision probability for a $0.8M_{\odot}$ star as a function of its radius, which is indicative of its age, up to the helium flash. As we can see in this figure the vast majority of collisions for the star are likely to occur during its main sequence lifetime. However, we see that roughly 20 per cent of collisions will happen during the red giant phase of the stars life time. In particular we note that 10 per cent of all collisions will occur when the radius of the red giant is between 10 and $100 R_{\odot}$, despite the fact that this actually represents a short period of time. For this reason I have chosen to look at collisions involving red giants of these radii within this paper.

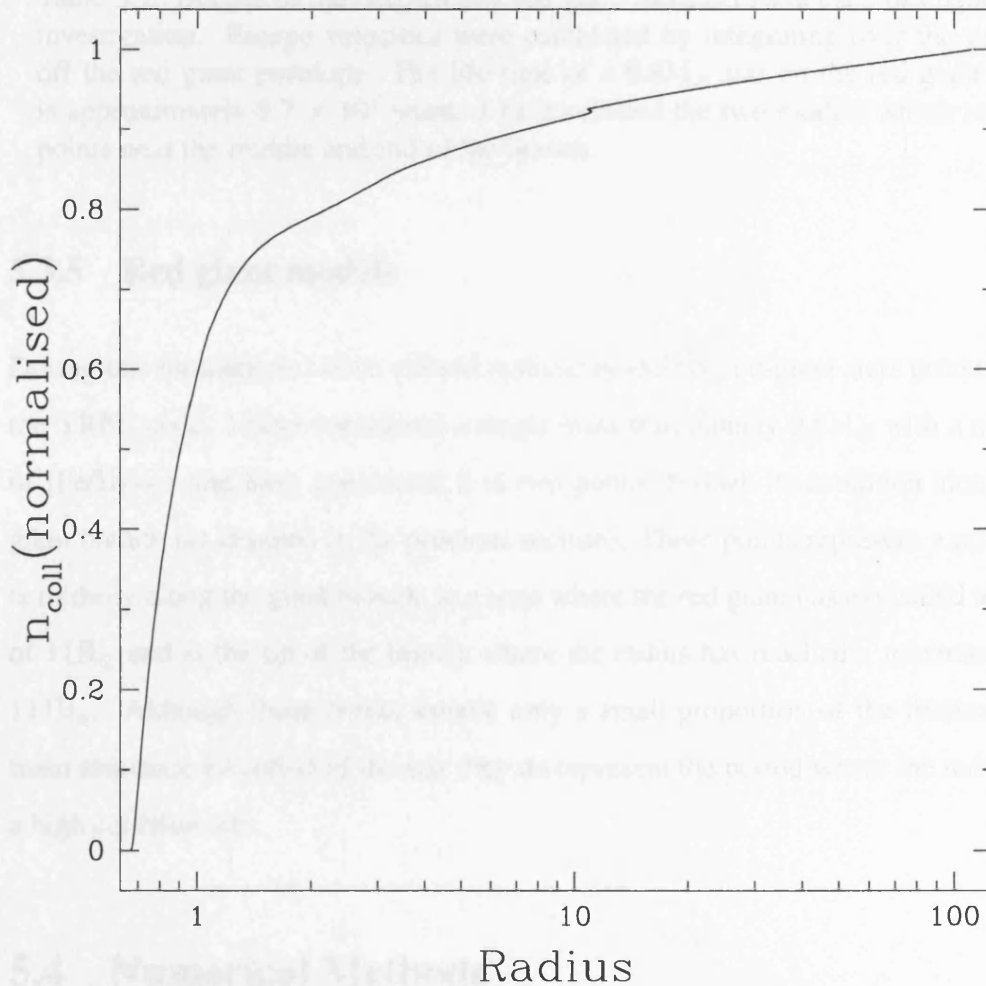


FIGURE 5.4. Integrated, normalised, probability of a $0.8M_{\odot}$ star undergoing a collision as a function of its radius, which is a tracer of the star's age. I have only considered the star up to the helium flash. As can be seen the star will most likely undergo a collision during its main-sequence lifetime, this is due to the long main-sequence lifetime. Although the proportion of collisions occurring for the red giant during the period when its radius is between 10 and $100R_{\odot}$ appears low, it should be noted that the giant only spends of order 10^8 years between these two radii. Thus this period represents the highest collision rate for the red giant.

Model	Time to the He flash (Gyrs)	Core mass (M_{\odot})	Radius (R_{\odot})	Escape speed of core (km/s)
A	0.05	0.284	11.672	249
B	≈ 0	0.478	111.01	53

Table 5.2. Details of the two $0.8 M_{\odot}$ red giant models I have used throughout this investigation. Escape velocities were calculated by integrating over the potential off the red giant envelope. The life time of a $0.8M_{\odot}$ star on the red giant branch is approximately 8.7×10^7 years. I have selected the two models which represent points near the middle and end of the branch.

5.3.5 Red giant models

During our simulations I have utilised realistic models of red-giant stars produced using the YREC code. I have considered a single mass star, namely $0.8M_{\odot}$ with a metallicity of $[\text{Fe}/\text{H}]=-1$ and have considered it at two points through its evolution along the red giant branch (as detailed in the previous section). These points represent a point which is midway along the giant branch, at a time where the red giant has expanded to a radius of $11R_{\odot}$ and at the tip of the branch where the radius has reached a maximum size of $111R_{\odot}$. Although these points sample only a small proportion of the lifetime of post main sequence evolution of the star they do represent the period where the red giant has a high collision rate.

5.4 Numerical Methods

I have taken two distinct paths in performing my simulations. To identify the timescale associated with the collisions in a relatively quick fashion I have utilised a 4 body code (Davies, Blackwell, Bailey & Sigurdsson 1998). Then to check the reliability of our results and to examine the distribution of mass in the post collision system I have performed a number of hydrodynamical simulations.

5.4.1 4-body code

As mentioned in Section 5.3.1 I have modelled the interloping binary components, as well as the core of the red giants, as point masses. I also model the envelope of the red giant as a point mass with the proviso that we take into account that the force on any of the other point masses is dependent on the fraction, f_{enc} , of envelope mass contained between the position of the point mass in question and the envelope centre. Thus, the force between the centre of the envelope, of total mass M_{env} , and the i th point mass, a distance R apart, is given by;

$$\mathbf{F}_{i\text{env}} = -G \frac{M_j M_i f_{\text{enc}}(R)}{|\mathbf{r}_i - \mathbf{r}_j|^3} (\mathbf{r}_i - \mathbf{r}_{\text{env}}), \quad (5.10)$$

For distances larger than the red giant radius this force simply reverts back to being the force due to a point mass. With a functional form for $f_{\text{enc}}(R)$ found for each of our red giant models, with R being the distance between the centre of the envelope and the i th point mass, we may write the equations of motion for the system as;

$$\ddot{\mathbf{r}}_i = -G \sum_{j \neq i} \frac{M_j}{|\mathbf{r}_i - \mathbf{r}_j|^3} (\mathbf{r}_i - \mathbf{r}_j) - G \frac{M_{\text{env}} f_{\text{enc}}(R)}{|\mathbf{r}_i - \mathbf{r}_{\text{env}}|^3} (\mathbf{r}_i - \mathbf{r}_{\text{env}}), \quad (5.11)$$

$$\ddot{\mathbf{r}}_{\text{env}} = -\frac{G}{M_{\text{env}}} \sum_j \frac{M_{\text{env}} f_{\text{enc}}(R) M_j}{|\mathbf{r}_{\text{env}} - \mathbf{r}_j|^3} (\mathbf{r}_{\text{env}} - \mathbf{r}_j), \quad (5.12)$$

The force and potential resulting from the red giant envelope were tabulated and interpolation used to calculate forces and energies at particular separations.

Impact parameters for each collision were chosen at random from within the range 0 to $\rho_{\text{max}}(v_{\infty})$ as defined by Hut and Bachall (1983):

$$\rho_{\text{max}}(v_{\infty}) = \left(\frac{C}{v_{\infty}/v_c} + D \right) a, \quad (5.13)$$

where C and D are numerical parameters (taken as 4 and 0.6 respectively) and a is the binary semi-major axis. The critical velocity, v_c , is the velocity at which the total energy of the system is zero:

$$v_c^2 = G \frac{M_1 M_2 (M_1 + M_2 + M_{\text{rg}})}{M_{\text{rg}} (M_1 + M_2)} \frac{1}{a}, \quad (5.14)$$

For each individual collision within a run I was able to classify the outcome as either one of those detailed in section 5.3.1 or unclassifiable. We started by looking at the energy of the point masses relative to one another:

$$E_{ij} = -G \frac{M_i M_j}{|\mathbf{r}_i - \mathbf{r}_j|} + \frac{1}{2} \frac{M_i M_j}{M_i + M_j} (\dot{\mathbf{r}}_i - \dot{\mathbf{r}}_j)^2 \begin{cases} < 0 & \text{bound} \\ > 0 & \text{unbound} \end{cases} \quad (5.15)$$

with appropriate corrections applied if one of the point masses were within the red giant envelope. The closest binary system was first identified and then this was treated as a single point mass to see if the other point mass was bound to it, this process is iterated over the possible combinations of binary systems until the outcome of the collision is classified.

With the outcomes of the collisions classified it is possible to calculate the cross section of the particular interaction, by assuming it is some fraction of the total cross-section presented by the binary, thus:

$$\sigma_x = \pi \rho_{\text{max}}^2 (v_\infty) \frac{n_x}{n_{\text{tot}}}, \quad (5.16)$$

where n_x/n_{tot} is the fraction of runs which produced the required outcome. Timescales are then trivial to calculate via:

$$\tau = \frac{1}{n \sigma_x v_\infty}, \quad (5.17)$$

For the purpose of our investigation I assume a number density of binary systems, n , of $10^5/\text{pc}^3$ and a velocity at infinity, v , of 10 km/s.

5.4.2 Hydrodynamical simulations

Utilising a modified version of the Benz (1990) 3-D SPH code I performed a set of representative invasive encounters between the binary system and the red giants. To the

standard fluid particles I introduced a number of point masses that interacted with both each other and the fluid particles solely through a gravitational force. The point masses were evolved on either their own unique time-step or on the smallest time-step of the SPH particles within the simulation (which ever was shortest) to ensure accuracy of the integration. I used the standard form of artificial viscosity with $\alpha = 1$ and $\beta = 2.5$, and an adiabatic equation of state. The thermodynamic quantities are evolved by following the change in internal energy. Both the smoothing length and the number of neighbours can change in time and space. The smoothing length is varied to keep the number of neighbours approximately constant at ~ 50 .

For both of the models considered, the central concentration of the giants is sufficient that it becomes increasingly difficult to model them with a reasonable number of SPH particles. Instead I have modelled the highly concentrated core of the giant with a point mass and then having this interact only via gravitational forces with a surrounding envelope of gas modelled with 50,000 SPH particles.

5.5 Results

5.5.1 Determination of interaction timescales

To gain an understanding of the timescales involved in the binary red giant interactions a number of four body simulations were performed. The red giant core and envelope were initially coincident and experienced an interaction with a binary system as described in Table 5.3.

200 collisions were simulated for each of the runs described in Table 5.3. For each run, the phase and orientation of the binary with respect to the red giant is random. In Fig. 5.5 I plot the timescales for knock out events (crosses), common envelope formation (solid triangles) and all bound systems (filled squares). In addition I also plot the timescale for a more general destructive collision to occur (i.e. any of the prior three outcomes) as a filled circle. As can be seen in the figure, there is a trend of decreasing timescale with increasing red giant radii as one would expect. In addition we also see

RunID	M1	M2	M3	M4	$a/R_{\odot}/(R_{rg})$	R_{rg}
1	0.8	0.8	0.27	0.53	5.5 (0.5)	11.0
2	0.8	0.8	0.27	0.53	11.0 (1.0)	11.0
3	0.8	0.8	0.27	0.53	22.0 (2.0)	11.0
4	0.8	0.8	0.49	0.31	56.0 (0.5)	111.0
5	0.8	0.8	0.49	0.31	111.0 (1.0)	111.0
6	0.8	0.8	0.49	0.31	222.0 (2.0)	111.0
7	1.4	0.8	0.27	0.53	5.5 (0.5)	11.0
8	1.4	0.8	0.27	0.53	11.0 (1.0)	11.0
9	1.4	0.8	0.27	0.53	22.0 (2.0)	11.0
10	1.4	0.8	0.49	0.31	56.0 (0.5)	111.0
11	1.4	0.8	0.49	0.31	111.0 (1.0)	111.0
12	1.4	0.8	0.49	0.31	222.0 (2.0)	111.0

Table 5.3. A list of the 4 body runs performed to examine the phase space of the collisions. For each of the runs detailed above 200 simulations of collisions between the red giant and the binary system were performed using a randomly selected set of incoming parameters. M_1 and M_2 are the masses of the binary components, whilst M_3 is the mass of the red giant core and M_4 is the mass of the red giant envelope.

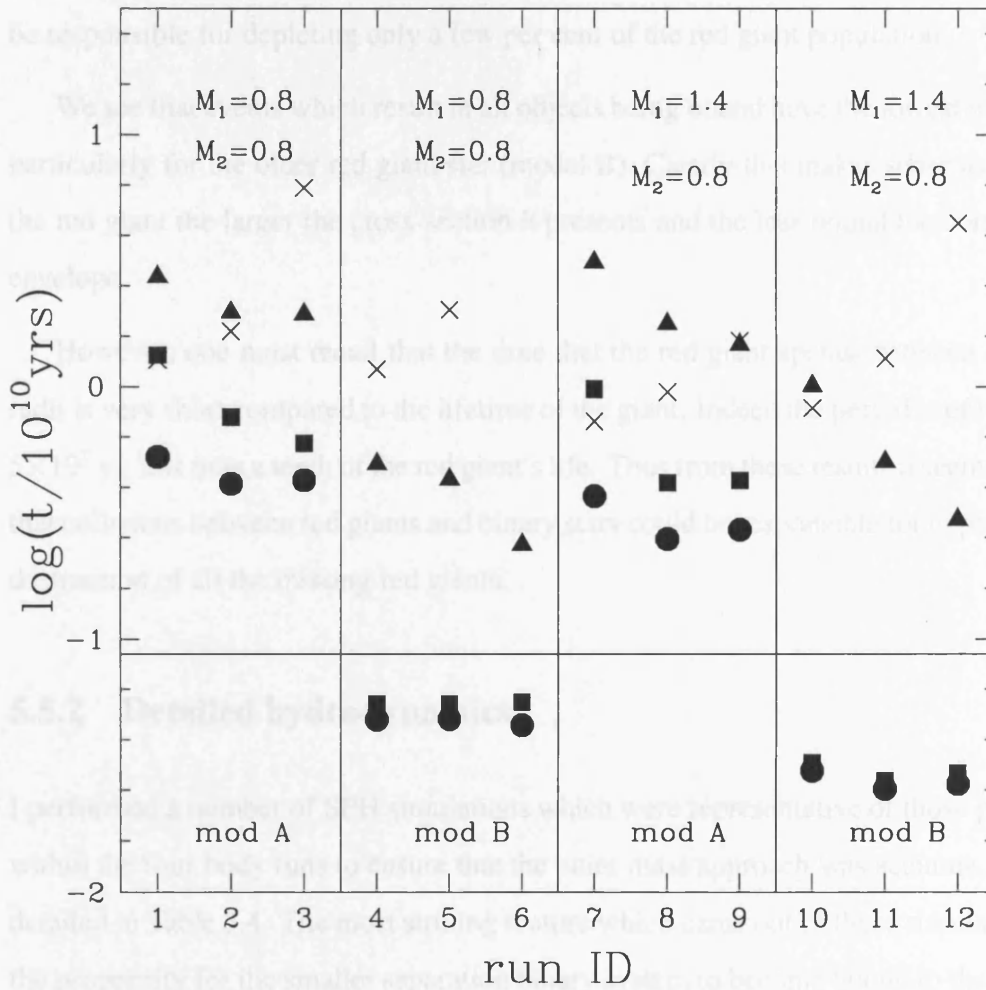


FIGURE 5.5. Plot of the various timescales for events to occur in a cluster with a binary number density of $10^5/\text{pc}^3$ and for a velocity at infinity of 10 km/s. The run ID's are as in Table 5.3. Crosses represent knock out events, solid squares represent all bound events and the solid triangles represent common envelope events. The filled circles represent the *interesting* timescale, i.e. that on which one of the destructive events will happen to the red giants.

a trend of decreasing timescale with increasing mass of the binary component. Again this is as expected due to the gravitational focusing term in the cross-section equation. On the figure I plot a horizontal line representing the lifetime of a $0.8M_{\odot}$ star on the red giant branch. As can be seen this lies below all the other timescales except for the larger giant. This indicates that interactions between binary systems and red giants will at most be responsible for depleting only a few per cent of the red giant population.

We see that events which result in all objects being bound have the lowest timescales, particularly for the older red giant star (model B). Clearly this makes sense as the older the red giant the larger the cross-section it presents and the less bound the core is to the envelope.

However, one must recall that the time that the red giant spends between these two radii is very short compared to the lifetime of the giant. Indeed the period is only of order 5×10^7 yr, less than a tenth of the red giant's life. Thus from these results it seems unlikely that collisions between red giants and binary stars could be responsible for explaining the destruction of all the missing red giants.

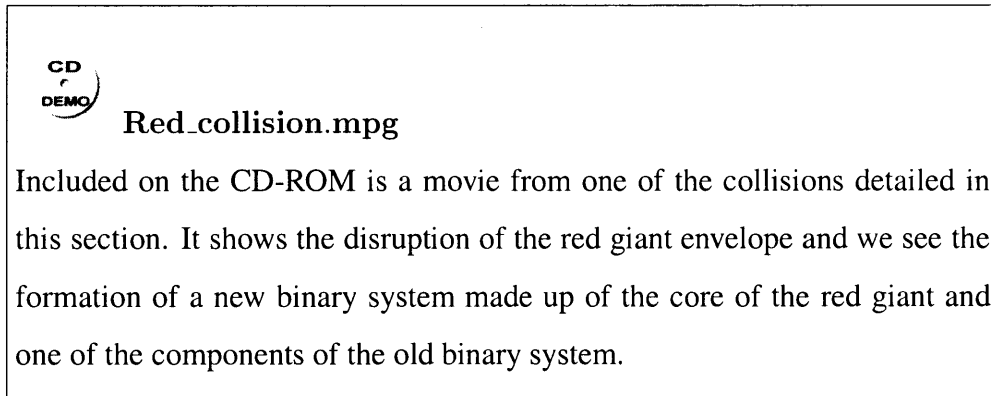
5.5.2 Detailed hydrodynamics

I performed a number of SPH simulations which were representative of those performed within the four body runs to ensure that the point mass approach was accurate, these are detailed in Table 5.4. The most striking feature which came out of these simulations was the propensity for the smaller separation binary system to become bound to the red giant star once one of the stars of the binary started passing through the envelope of the red giant, slightly more so than had been predicted by the four-body simulations. This is not entirely unexpected. The work of Davies, Benz & Hills (1991) centred on collisions between single stars and red giants. They found that once an interloping star came within twice the red giant radius, tides could be raised and energy dissipated resulting in a bound system with an eccentric orbit. If the star came within $1.6R_{\text{rg}}$, it would eventually spiral into the red giant envelope on subsequent periastron passages. Thus in my simulations it is clear that most invasive collisions will result in an all bound system, which will evolve

Run	a/R_{\odot}	R_{\min}/R_{\odot}	M_1	M_2
1	22	0	0.8	0.8
2	22	21	0.8	0.8
3	22	40	0.8	0.8
4	22	80	0.8	0.8
5	56	29	0.8	0.8
6	56	38	0.8	0.8
7	56	80	0.8	0.8
8	56	120	0.8	0.8
9	111	0	0.8	0.8
10	111	61	0.8	0.8
11	111	66	0.8	0.8
12	111	81	0.8	0.8
13	111	120	0.8	0.8
14	222	112	0.8	0.8
15	222	117	0.8	0.8
16	222	137	0.8	0.8
17	222	190	0.8	0.8

Table 5.4. Details of the representative SPH simulations that I performed. I used a model B star made up of 50,000 SPH particles with a point mass at its core as described in section 5.4.2. The minimum distance refers to the distance between the centre of mass of the binary system and the core of the red giant.

to one of the other possible outcomes after some period of time. The exact outcome of the unstable triple is impossible to predict. However, we can make tentative predictions based on previous numerical simulations. It is likely that interactions within the system will eventually result in a kick being given to the lightest member of the hierarchy and it then escapes, carrying away whatever mass is bound to it.



Included on the CD-ROM is a movie from one of the collisions detailed in this section. It shows the disruption of the red giant envelope and we see the formation of a new binary system made up of the core of the red giant and one of the components of the old binary system.

In Fig. 5.6 I plot the mass retained by the core and the mass of the envelope gas which is no longer bound to the system as a function of the ratio of binary semi-major axis to minimum distance of approach (where the minimum distance of approach is measured relative to the centre of mass of the binary system). As can be seen, there is an anti-correlation between the two quantities, as one might expect. For collisions during which the binary system moves deep into the red giant envelope, the chances of a close encounter between one of the binary components and the core is increased. Such an encounter would lead to a much increased velocity for the core and it would rapidly move out of the envelope. This then means that less mass can be bound to the core, thus explaining the increased mass loss from the envelope.

In Fig. 5.7 I plot the mass of envelope gas which has become gravitationally bound to the binary system in a common envelope system, as a function of the ratio of the binary separation and minimum distance of approach. As can be seen there is no discernible pattern within this plot, but what we do see is that it is possible for the binary to pick up a non-negligible envelope of material. This material could be important for grinding down the binary as I have discussed.

In Fig. 5.8 I show a time series plot of one of our SPH simulations. As can be seen, the point masses of the binary system have surrounding envelopes of gas particles, whilst

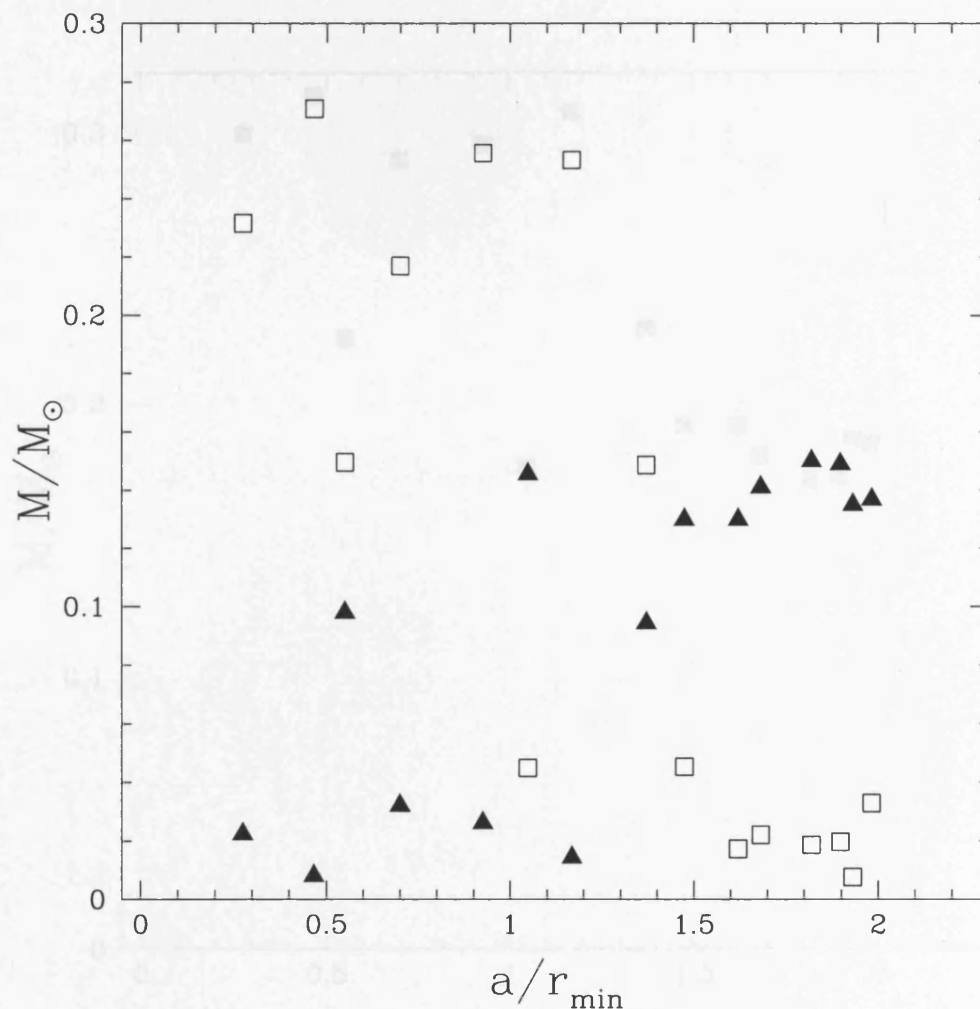


FIGURE 5.6. A combined plot of the mass still bound to the core of the red giant as a function of the ratio of the binary separation and minimum distance at approach (denoted as opened squares), and the total mass no longer bound to any of the point masses or binary systems (filled triangles). As can be seen in the plot, for deeper, more invasive collisions more mass is lost from the system and at the same time less mass remains bound to the core. For less invasive collisions the opposite is true, more mass remains bound to the core of the red giant whilst only a small amount of mass is no longer bound to the system. Initially the total mass of the envelope was $0.322M_{\odot}$.

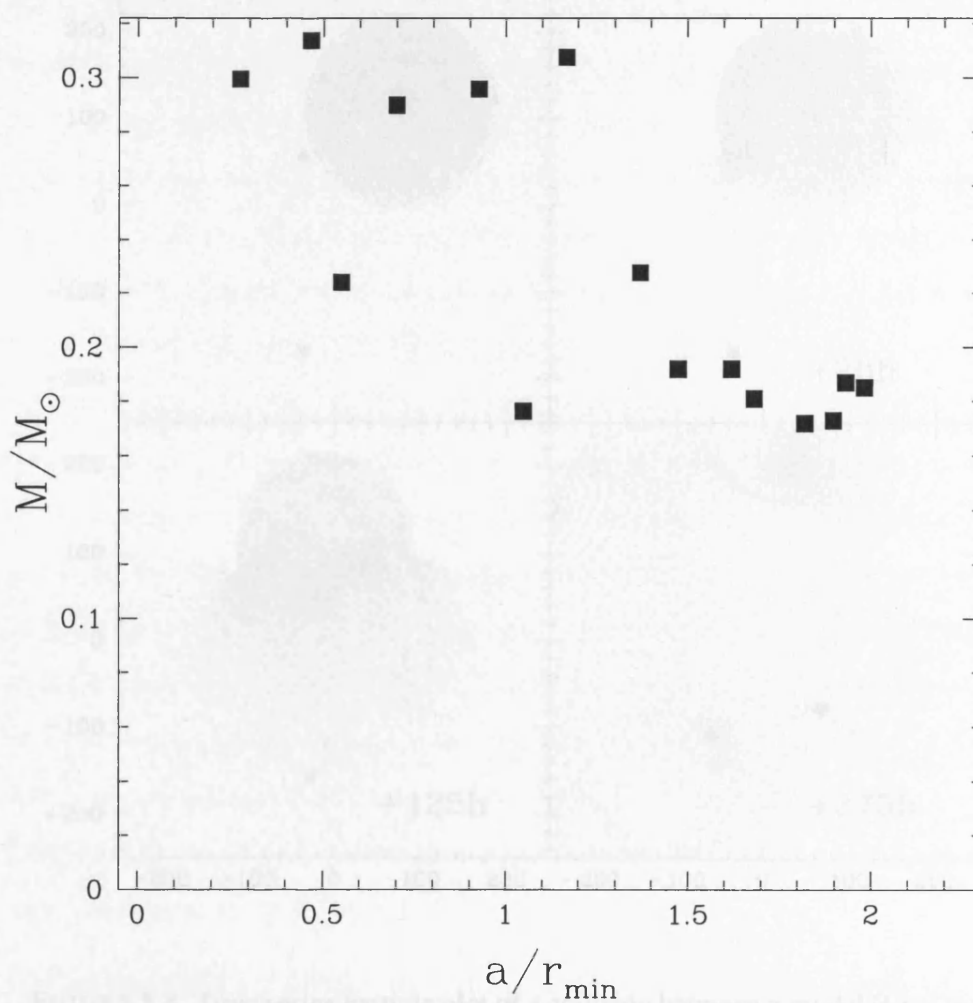


FIGURE 5.7. Common envelope mass as a function of the ratio of binary separation to the minimum distance of approach. As can be seen there is no clear discernible pattern within the figure. The subsequent evolution of the all bound system is likely to add to the mass of gas in the common envelope as close approaches of the three point masses will serve to disrupt their individual gaseous envelopes.

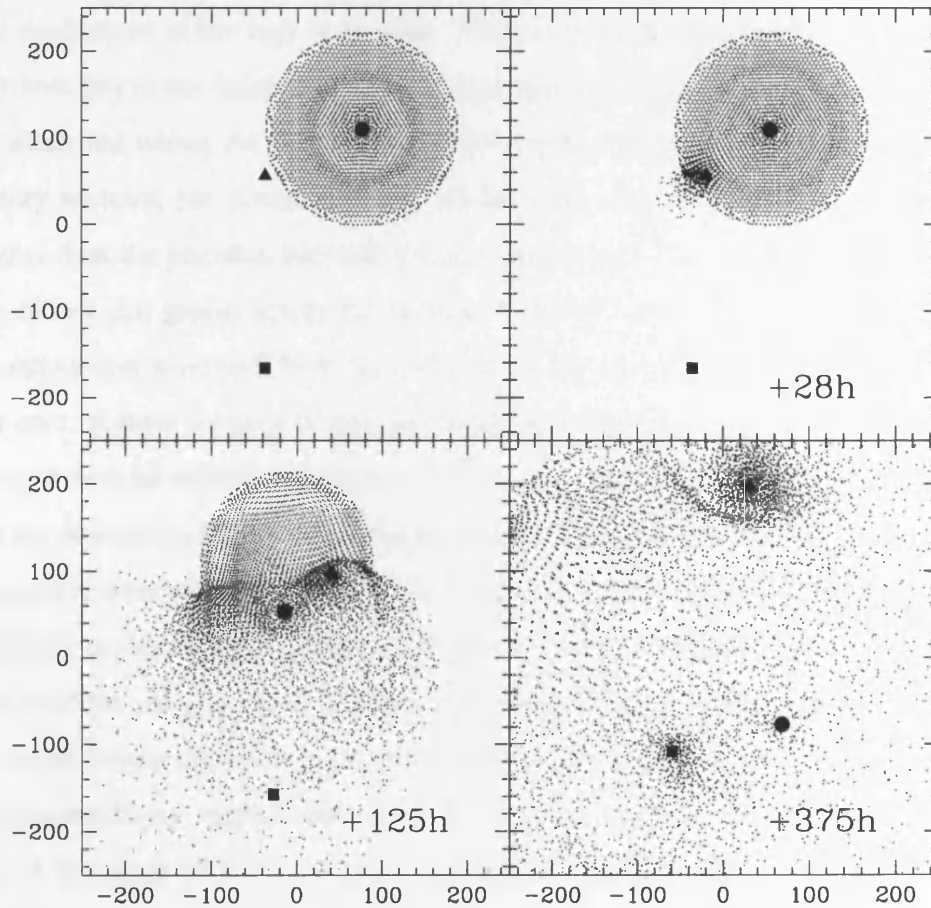


FIGURE 5.8. Time series particle plot of a collision between a model B red giant and a binary system of separation $222R_{\odot}$ with a minimum distance of approach between the core of the red giant and the centre of mass of the binary system of $137R_{\odot}$. The core of the giant is represented by the circle, whilst the square and triangle represent the components of the binary system. The figure shows only those particles within $2h$ of the $z = 0$ plane. All three of the heaviest bodies, the core and binary system components, are bound in the final snapshot. The system will continue to evolve until eventually one of the three bodies is ejected, most probably the light core.

the core of the red giant is in comparison relatively isolated.

As mentioned earlier, from the SPH simulations I found that the formation of an all bound system (i.e. one where all of the point masses are bound together) was somewhat increased for the collisions involving the smaller separation binary systems compared to the predictions of the four body code. There was no increase for the larger systems. I attribute this to the dissipation of the incoming kinetic energy through shocks which can be modelled within the SPH but not in the n-body approach. For the larger separation binary systems, the potential energy between the core and one of the components is higher than the potential between the two components of the binary system, even when the binary just grazes across the surface of the red giant. Thus it is likely that an all bound system will result from the collision. In the case of the smaller systems this isn't the case. Instead we need to dissipate more of the kinetic energy of the collision for the core to become bound to the binary system. To calculate more accurate cross sections for the destructive encounters between the smaller separation binary systems and the red giants I re-examined the collisions performed with the four-body code and selected out all those in which one member of the binary system came within 75% of the red giant radius of the red giant core. These collisions will almost certainly lead to the formation of an all bound system and the subsequent destruction of the red giant. I assumed a binary population number density of $10^5/\text{pc}^3$, and a velocity dispersions of 10 km/s. I found that up to 13% of the red giant population could be destroyed through collisions with binary systems independent of the binary separation.

One can make a prediction of what proportion of the red giant population we would expect to destroy through collisions using the encounter timescale of (Binney & Tremaine 1987):

$$\tau_{\text{enc}} = 7 \times 10^{10} \frac{n}{10^5/\text{pc}^3} \frac{M_{\odot}}{M_{\text{tot}}} \frac{R_{\odot}}{r_{\text{min}}} \frac{v_{\infty}}{10\text{km/s}} \text{yr}, \quad (5.18)$$

if we again assume a number density, n , of $10^5/\text{pc}^3$ along with a $v_{\infty} = 10 \text{ km/s}$ and a total mass of $2.4 M_{\odot}$ (i.e.the masses of the binary components are the same as the mass of the red giant) then for an encounter within $100 R_{\odot}$ we find $\tau_{\text{enc}}=2.9 \times 10^8$ years. Comparing

this to the period that the red giant spends with a radius of approximately $100R_{\odot}$ we find that around 17% of the red giant population will undergo a collision.

5.6 Subsequent evolution

During the majority of the SPH performed collisions we saw the formation of a complex triple system where the two components of the initial binary system and the core of the red giant were bound in some complicated arrangement. Such a system is highly unstable and through further interactions one of the binary systems will harden and the other body will be ejected from the system. It is highly likely that the ejectee will be the core of the red giant as it has a lower mass than either of the initial binary components. During the collision, the envelope of the giant is stirred up and forced to expand as energy is dumped into it. As this occurs the binding energy of the core of the red giant to the envelope is reduced and as a consequence the escape velocity of the core is much lower than in the pre-collision state. The expanded state of the envelope means that it is unlikely that the escaping core will pick up any significant additional material as it passes through it.

The subsequent evolution of the isolated core will be dependent on its mass and the mass of its now small envelope. Cores which are removed from the largest giants are about to start helium burning, so it is entirely possible that these core could form the population of sub-dwarf B stars I discussed in the introduction if they carry away sufficient mass in their envelopes ($<0.05M_{\odot}$). Cores from younger giants (i.e.those which have just moved onto the sub-giant branch) with a non-negligible envelope (40 percent or more of the original envelope) will likely follow a stunted evolutionary path similar to that of a normal giant. There will be obvious differences in the exact evolution but possibly these stars can go on to populate the normal horizontal branch, thereby removing any problem with numbers in the two branches. For the older red giants, their removal from the Hertzsprung Russell diagram requires the core to be stripped of almost all of its surrounding envelope. This is quite likely to occur if the core initially becomes bound to the binary system and is only later ejected, as the core will be moving at the escape speed of the system.

The binary system which remains will be surrounded by at least a cursory common envelope system. Dynamical friction between the components of the binary and the gas in the envelope will transfer angular momentum away from the binary system leading to its shrinkage and the expulsion of the gas. The degree to which the binary shrinks is highly dependent on the mass of the envelope and the efficiency factor α . It is entirely possible that the binary could shrink down to the point where the components come into contact as described in section 5.3.2. This could be useful in explaining some of the more exotic binary systems found within globular clusters. The mass of the envelope may well be increased as the system evolves. It is possible that periastron passages within the triple system may be close enough to disrupt the disc of material surrounding each of the individual bodies, moving mass out of the discs into the common envelope.

As discussed in section 5.3.2 the end of the common envelope phase is not the end of the evolution for the binary system. It will continue to harden through gravitational radiation and magnetic braking. The binaries formed during these interactions are all quite eccentric. If they retain some proportion of this eccentricity past the common envelope phase then the in-spiral time of the binary can be dramatically reduced (Peters 1964). Thus if one of the components of the binary system was a main-sequence star of sufficiently low mass and the other body is a white dwarf then it is entirely possible that the binary could be ground down to the point where the main-sequence star is filling its Roche lobe and thus producing a cataclysmic variable.

5.7 Other methods of depleting giants

Our simulations have shown that whilst collisions between binary stars and red giants can effectively destroy a red giant, the time scales involved suggest that there would have to be an additional depletion method. One possibility is that proposed by Beer & Davies (2003), where the red giant is contained in a binary system and a double common envelope system could occur, effectively destroying the red giant.

Another possible explanation for the paucity of red giants is that collisions with other single stars could lead to their destruction. Rasio & Shapiro (1990) claim through a series

of n-body simulations that the envelope of the giant is almost immediately dissipated during such a collision and a binary system formed. In Rasio & Shapiro (1991) a series of SPH simulations were performed. Instead of dissipating the red giant envelope they find that material goes into forming a large disc around the impacting star. Davies, Benz & Hills (1991) performed SPH simulations of similar collisions and found that whilst the impactor and the core would become bound, the immediate ejection of the envelope didn't occur. Instead a common envelope phase would start and as a result the binary would spiral in and the envelope would be dissipated. In an effort to determine which of these two arguments are correct I performed the collisions detailed in Rasio & Shapiro (1991) utilising our SPH code and models. The details of the collisions performed are in Table 5.5.

Run	r_{\min}/R_{rg}	$v_{\infty}/10\text{km/s}$
1	0.05	10.
2	0.20	10.
3	0.5	10.
4	1.0	10.
5	2.0	10.
6	2.5	10.

Table 5.5. Details of the collisions between a red giant and a single body. The minimum distance of approach in these runs is the same as those in the runs performed in Rasio & Shapiro (1991). I have used my model B red giant.

In all the collisions I found that sufficient energy could be dissipated that the core and the interloping star became bound in eccentric orbits which had periastron passages which were a smaller than the initial distance of closest approach. In the deeply invasive collisions I found that *initially* a large disc (more accurately a flattened spheroid) of material would form around the interloping star, whilst the core retained very little gas mass. However, the disc was sufficiently large that during periastron passages the core would pass through it and the disc would be broken up (I shall discuss this further, later in this section). For less invasive collisions, the core of the red giant would retain most of the mass, but again subsequent periastron passages would result in this material being disturbed. In Fig. 5.9 I show how much mass was lost from the system and how much

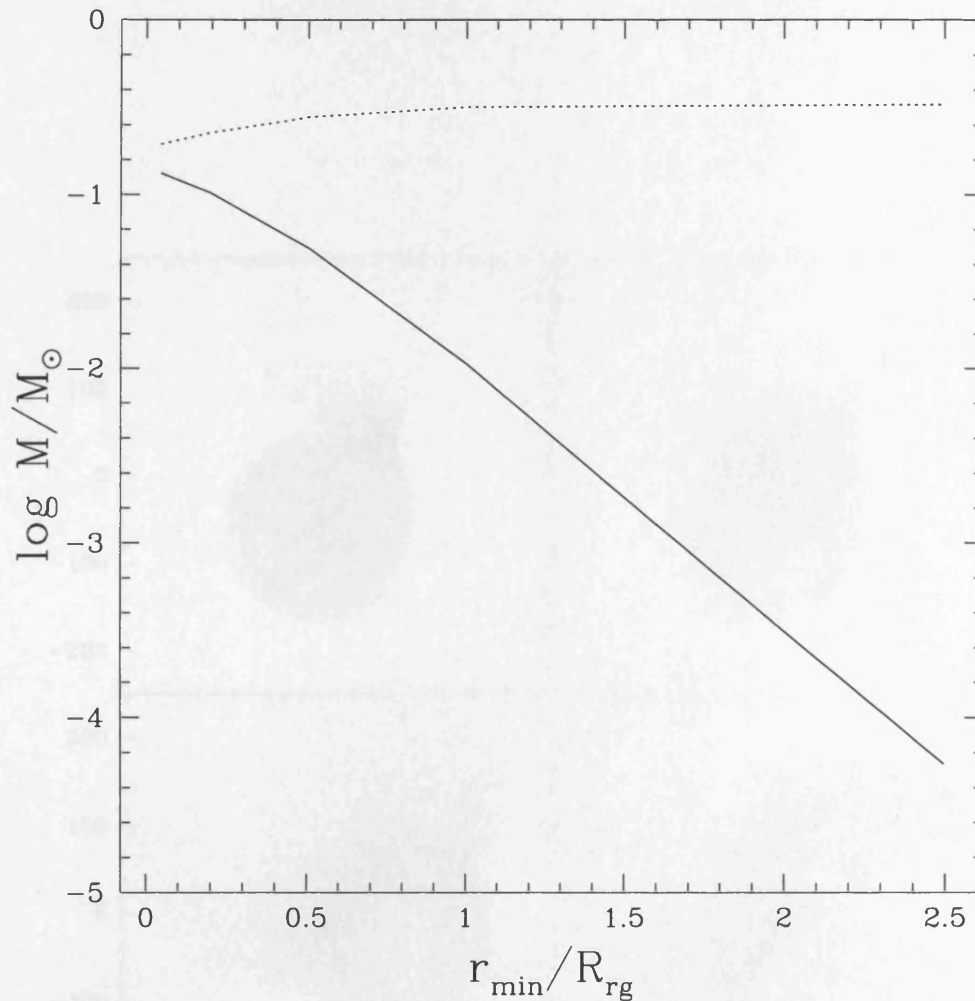


FIGURE 5.9. Mass retained (dashed line) and mass lost (solid line) from the red giant envelope as a function of the minimum separation between the red giant core and the impactor. This plot is produced after the initial impact. As can be seen deeper impacts result in far more mass loss from the system. I have summed all the mass still bound to the system as Fig. 5.11 shows that the system undergoes further mass loss during subsequent periastron passages.

remains bound to it as a function of the minimum distance of approach. As can be seen the mass loss is very sensitive to the minimum distance of approach with very little mass lost for more grazing collisions. In Fig. 5.10 I show a time series plot of the particles laying within $2h$ of the $z=0$ surface for one of the collisions. I can see that initially there is a disc formed around the impacting star. In Fig. 5.11 I show the evolution of the separation of the two point masses for the collision shown in Fig. 5.10, along with the mass loss from the system as a function of time.

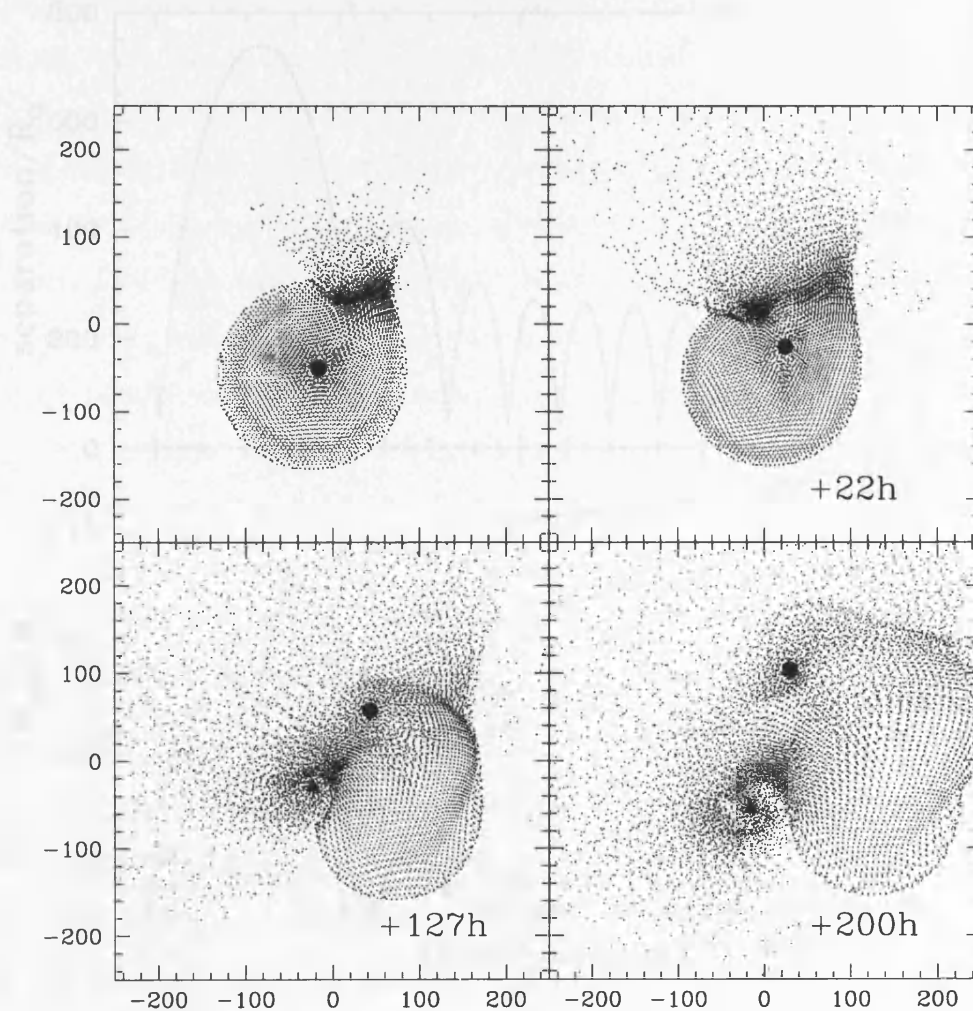


FIGURE 5.10. A collision between a red giant star and a single body. As can be seen initially a disc is formed around the interloping star; however, the core and the interloping star are bound on orbits which bring them back together with a periastron separation which is small enough for the disc of material to be disrupted and the mass redistributed into the common envelope.

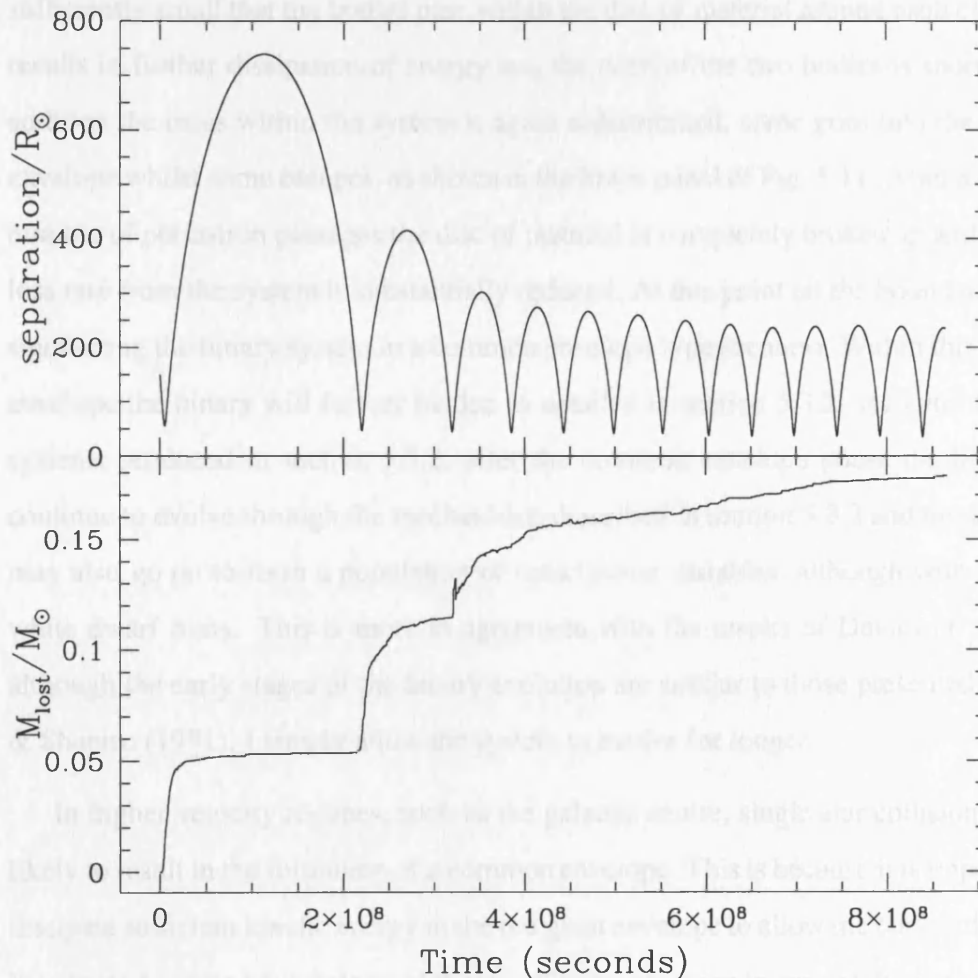


FIGURE 5.11. In the top panel I show the evolution of the separation between the two components of a binary system formed after a collision between a red giant and an impactor with a minimum distance of approach of $0.5 R_{\text{rg}}$. As can be seen each peri-astron passage results in the dissipation of energy and a subsequent decrease in the binary separation. In the lower panel I plot the total mass lost from the system. As we can see, each time there is a peri-astron passage we get a wave of mass loss as the discs of material around the two objects are disrupted. This simulation was performed with 5000 particles. A comparison between the escaping mass fraction for this simulation was made with the initial portions of a 50,000 particle simulation and there were no significant differences.

In the top panel of Fig. 5.11 I show the evolution of the separation of the binary components for one of the simulations ($R_{\min}=0.5R_{rg}$). As can be seen the core and the impactor are initially on large eccentric orbits; however, the periastron separation is sufficiently small that the bodies pass within the disc of material around each other. This results in further dissipation of energy and the orbit of the two bodies is shortened. In addition the mass within the system is again redistributed; some goes into the common envelope whilst some escapes, as shown in the lower panel of Fig. 5.11. After a sufficient number of periastron passages the disc of material is completely broken up and the mass loss rate from the system is substantially reduced. At this point all the bound material is smothering the binary system in a common envelope type scenario. Within this common envelope the binary will further harden as detailed in section 5.3.2. As with the binary systems produced in section 5.5.2, after the common envelope phase the binary will continue to evolve through the mechanisms described in section 5.3.2 and these systems may also go on to form a population of cataclysmic variables, although with a smaller white dwarf mass. This is more in agreement with the results of Davies *et. al.* 1991, although the early stages of the binary evolution are similar to those presented by Rasio & Shapiro (1991). I simply allow the system to evolve for longer.

In higher velocity regimes, such as the galactic centre, single star collisions are less likely to result in the formation of a common envelope. This is because it is impossible to dissipate sufficient kinetic energy in the red giant envelope to allow the core and interloping star to become bound. Instead these collisions are more immediately destructive and close encounters between the core and the interloping stars will result in the core being ejected with only a very small amount of gas. A larger minimum distance of approach will result in large amounts of the envelope gas becoming unbound due to the input of kinetic energy from the interloping star.

5.8 Conclusions

I have shown that collisions between binary systems and red giant stars could be responsible for depleting up to 13 per cent of the red giant population in dense globular clusters.

The passage of one of the components of the binary system through the envelope results in sufficient dissipation of energy that the binary system and the red giant become bound. The subsequent evolution of this triple system is likely to be destructive to the red giant and provides an effective method of removing the giant. During the collision an envelope of material becomes bound to the binary system. This will lead to the binary spiralling in-wards as angular momentum is passed from the orbit of the two stars to the envelope gas. This could play a role in producing some of the very close binary systems, although it should be noted that the timescale for an individual binary to pick up an envelope of gas from a red giant and then shrink through a common envelope phase is much longer than the time required for the same binary to undergo multiple scattering events and harden down to the same separation. These close systems may go on to further harden through angular momentum losses in the form of gravitational radiation or magnetic braking and eventually come into contact thus producing a population of cataclysmic variables.

Djorgovski & Piotto (1993) present evidence suggesting that red giants may be depleted by up to 50 percent in some clusters. Clearly our dynamical method of destroying giants cannot be responsible for all of the observed depletion. Instead it must work alongside other methods, such as that proposed by Beer & Davies (2003).

There are important differences between this and previous work. In Davies *et. al.* (1998) collisions between red giants and binary systems in the galactic centre were considered. There it was found that bound systems were seldom formed. This difference can easily be attributed to the difference in the relative velocities between our work and theirs. Collisions in the galactic centre have a much higher velocity at infinity and during a collision with a red giant it is not possible to dissipate sufficient kinetic energy for the interloper to become bound to the red giant.

In addition I have also looked at low velocity collisions between red giant stars and single stars. I have shown that on the initial impact, a large disc of material can form around the impactor provided the minimum distance of approach is sufficiently small. However, the core and the impactor are on a bound orbit and subsequent periastron passages are sufficiently close that any material which is in a disc around one of the bodies is disrupted.

In conclusion we can say that any physical collision is detrimental for the life expectancy of a red giant. The low velocity dispersion within a globular cluster means that a bound system is a virtual certainty, and the ensuing common envelope phase or disruption of the red giant envelope with each periastron passage will quickly remove the red giant from the cluster.

Chapter 6

Conclusions and future work

6.1 Future work

In this thesis I have considered whether several observational features of stellar clusters could be explained through dynamical events. The answer to this question is, yes- to some extent. The lack of brown dwarf observations in open clusters can in-part be explained by the mass segregation which goes on within a cluster. However, for young clusters, such as the Pleiades, a large proportion of the brown dwarf population should still be contained within the cluster. There are two solutions to this, either our understanding of the IMF is incomplete and the population of brown dwarfs is actually far smaller than has been assumed in this work, or as I have suggested a large proportion of the brown dwarf population could be contained with binary systems. To find out which of these two solutions is correct we will need to ensure that our knowledge of the IMF is accurate, this is no small task. There has been some observational work comparing the IMFs of various open clusters, this has suggested a universality for its form. However, we are still observationally limited as we move toward the brown dwarf end of the mass function. Simulations of collapsing gas clouds forming a small number of stars and brown dwarfs are being done today, but we are still a long way from being able to perform a simulation of a gas cloud which would give birth to an open cluster such as the Pleiades.

In examining the blue straggler population found in globular clusters I have shown that around $5/6$ of the population will most likely result from the evolution of a binary system. It has long been realised that binaries were a possible formation channel, but thus far they have largely been ignored. It would seem that theoretical modelling for the blue straggler population must move on to looking at this channel. This will not be easy. It will require the development of 2 and possibly 3 dimensional stellar evolution codes which in turn require large amounts of computer time to run. There has been some success in the development of a 3D stellar evolution code. Bazan *et. al.* (2003) have completed testing on a 3D stellar evolution code and are promising several papers in the coming months detailing their work. Should this code prove to be reliable, blue stragglers produced in binary system evolution may finally get the attention they have long deserved. With regard to the $1/6$ of the population produced through collisional mergers, I have argued that the angular momentum issues raised by Sills *et. al.* (2001) can be overcome by examining what role the post-collision magnetic field will play. The rapid rotation of the merged object means that the magnetic field is likely to be quite large. This field can lock to either a disc of material or an outflowing wind and spin down the star. Either method can reduce the angular momentum of the star to the point where it can join the main-sequence.

My examination of collisions involving red giants in the centres of post-core-collapse globular clusters has shown that $\approx 17\%$ of the population can be destroyed. Although this is useful, clearly this is not the end of the story. Observations by Djorgovski & Piotto (1993) have indicated that in some clusters nearly 50% of the population is missing. To account for this, either the collision rates need to increase drastically in some clusters or there is an additional depletion method in operation. An additional depletion method has been suggested by Beer & Davies (2003). They outline a scenario where a red giant is contained in a binary system, when the red giant expands to fill its Roche lobe the envelope is removed and goes on to form a common envelope. Inside of the envelope the core of the red giant and the companion spiral in and eventually the envelope is dissipated. A combination of these two effects could explain the depletion of red giants. To gain a full understanding of how the collisions and binary evolution scenarios will effect the

red giant population of a globular cluster, it would seem necessary to include both effects within a model of a globular cluster. The full modelling of a dense stellar environment is the aim of the MODEST group (see [http : //manybody.org/modest.html](http://manybody.org/modest.html)). They are combining n-body modelling, hydrodynamical simulations of collisions and stellar evolution into one all encompassing simulation.

The oil-on-water method developed in this thesis could have great potential. The code itself still requires some work, for instance the replacement of oil particles on the surface of the secondary as they are stripped away by the primary. However, this is just work and shouldn't pose to much of a problem to complete. With improved spatial resolution (by increasing the oil particle number) we should hopefully be able to start modelling the exponential nature of the stellar atmosphere. This will lead to more accurate results for the mass transfer rate in close binary systems. Once fully operational, the oil-on-water method should allow us unprecedented mass resolution simulations of many interacting binary systems and the possibility of answering some old questions.

Appendix A

Fraction of Binary systems which can be resolved

The Binary systems contained within a cluster are all laying at some random inclination to our line of sight. This means that some binary systems can only be resolved in to two separate components at certain points along they're orbit, and other systems we can't resolve at all. The question is, what fraction of the binary systems which have a separation large enough that we could separate them into two components, can be resolved after inclination effects are taken into account?

Let us start by declaring the variable x as the ratio of the apparent binary separation on the sky to the actual spacial separation. The apparent separation is given by:

$$r = d_o \left(1 - \cos^2 \phi \sin^2 i\right)^{\frac{1}{2}} \quad (\text{A.1})$$

where i is the inclination of the binary system, ϕ is the phase angle of the binary and d_o is the space separation of the two components of the binary system. The fraction of the binary orbit that the binary is then visible is:

$$f = \frac{\pi - 2\phi}{\pi} \quad (\text{A.2})$$

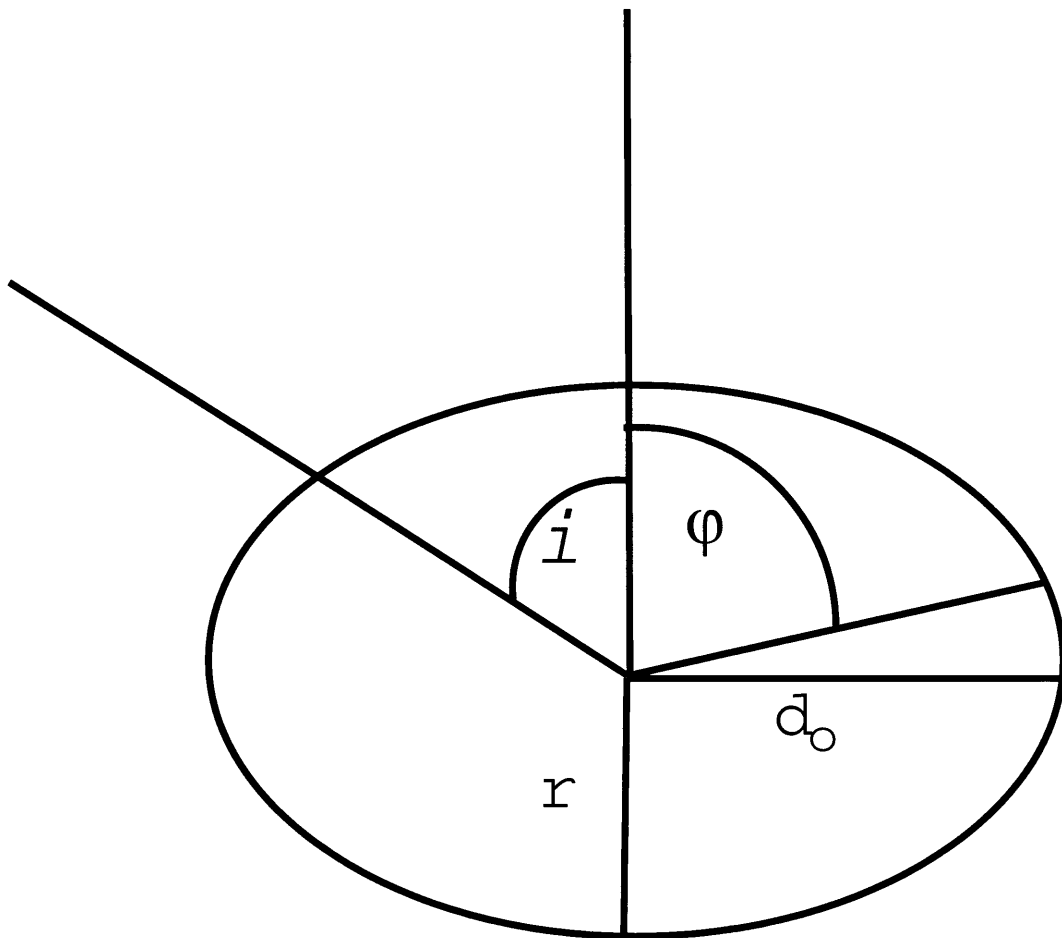


FIGURE A.1. A figure showing the effects of inclination on the binary's separation, and setting up the definitions required for deriving what fraction of the binary population remains visible despite inclination effects.

and integration over all inclinations we get:

$$f(x) = \int_0^{\frac{\pi}{2}} \frac{\pi - 2\phi}{\pi} \sin i di \quad (\text{A.3})$$

where we can limit ϕ using equation A.1:

$$\begin{aligned} \cos \phi &= \frac{(1-x^2)^{\frac{1}{2}}}{\sin i} & \sin i > (1-x^2)^{\frac{1}{2}} \\ \phi &= 0 & \sin i < (1-x^2)^{\frac{1}{2}} \end{aligned} \quad (\text{A.4})$$

If we now take the differential of equation A.3 we get:

$$\frac{df(x)}{dx} = \frac{d}{dx} \int_0^{\frac{\pi}{2}} \frac{\pi - 2\phi}{\pi} \sin i di \quad (\text{A.5})$$

$$\begin{aligned} &= \frac{d}{dx} \int_0^{\sin^{-1}(1-x^2)^{\frac{1}{2}}} \sin i di + \frac{d}{dx} \int_{\sin^{-1}(1-x^2)^{\frac{1}{2}}}^{\frac{\pi}{2}} \sin i di \\ &\frac{d}{dx} \int_{\sin^{-1}(1-x^2)^{\frac{1}{2}}}^{\frac{\pi}{2}} \frac{2\phi}{\pi} \sin i di \end{aligned} \quad (\text{A.6})$$

On application of the limits this reduces to:

$$\begin{aligned} \frac{df(x)}{dx} &= -\frac{2}{\pi} \int_{\sin^{-1}(1-x^2)^{\frac{1}{2}}}^{\frac{\pi}{2}} \sin i di \\ &= -\frac{2}{\pi} \int \frac{\partial}{\partial x} \cos^{-1} \left(\frac{(1-x^2)^{\frac{1}{2}}}{\sin i} \right) \sin i di \end{aligned} \quad (\text{A.7})$$

with sufficient manipulation this becomes:

$$\frac{df(x)}{dx} = -\frac{2}{\pi} \int_0^x \frac{x}{(1-x^2)^{\frac{1}{2}}} \frac{1}{(x^2 - \cos^2 i)^{\frac{1}{2}}} d(\cos i) \quad (\text{A.8})$$

If we allow $u = \cos i$ then

$$\frac{df(x)}{dx} = -\frac{2}{\pi} \int_0^x \frac{x}{(1-x^2)^{\frac{1}{2}}} \frac{1}{(x^2-u^2)^{\frac{1}{2}}} d(u) \quad (\text{A.9})$$

Then allowing $u = x \sin \theta$

$$\begin{aligned} \frac{df(x)}{dx} &= -\frac{2}{\pi} \int_0^{\frac{\pi}{2}} \frac{x}{(1-x^2)^{\frac{1}{2}}} d\theta \\ &= -\frac{2}{\pi} \frac{x}{(1-x^2)^{\frac{1}{2}}} \int_0^{\frac{\pi}{2}} d\theta \end{aligned} \quad (\text{A.10})$$

thus:

$$\frac{df(x)}{dx} = -\frac{x}{(1-x^2)^{\frac{1}{2}}} \quad (\text{A.11})$$

and finally integrating over x gives us:

$$f(x) = (1-x^2)^{\frac{1}{2}} \quad (\text{A.12})$$

which is simply the equation of a circle.

Bibliography

- Adams, T., Davies, M. B., Jameson, R. F. & Scally, A. (2002), ‘Brown dwarf populations in open clusters’, *MNRAS* 333, 547–560.
- Adams, T., Davies, M. B. & Sills, A. I. (submitted), ‘On the origin of red giant collisions through low velocity collisions’, *MNRAS* .
- Anderson, M. (2001), Master’s thesis, University of Copenhagen.
- Armitage, P. J. & Clarke, C. J. (1996), ‘Magnetic braking of T Tauri stars’, *MNRAS* 280, 458–468.
- Bailyn, C. D. (1994), ‘Gradients in giant branch morphology in the core of 47 Tucanae’, *Aj* 107, 1073–1078.
- Bailyn, C. D., Grindlay, J. E., Cohn, H., Lugger, P. M., Stetson, P. B. & Hesser, J. E. (1989), ‘A color gradient in the globular cluster M15’, *Aj* 98, 882–887.
- Baraffe, I., Chabrier, G., Allard, F. & Hauschildt, P. H. (1998), ‘Evolutionary models for solar metallicity low-mass stars: mass-magnitude relationships and color-magnitude diagrams’, *A&A* 337, 403–412.
- Basri, G., Marcy, G. W. & Graham, J. R. (1996), ‘Lithium in Brown Dwarf Candidates: The Mass and Age of the Faintest Pleiades Stars’, *ApJ* 458, 600–+.
- Basri, G. & Martín, E. L. (1999), ‘PPL 15: The First Brown Dwarf Spectroscopic Binary’, *Aj* 118, 2460–2465.

- Bate, M. R., Bonnell, I. A. & Bromm, V. (2003), ‘The formation of a star cluster: predicting the properties of stars and brown dwarfs’, *MNRAS* 339, 577–599.
- Bazán, G., Dearborn, D. S. P., Dossa, D. D., Eggleton, P. P., Taylor, A., Castor, J. I., Murray, S., Cook, K. H., Eltgroth, P. G., Cavallo, R. M., Turcotte, S., Keller, S. C. & Pudliner, B. S. (n.d.), Djehuty, a code for modeling stars in three dimensions, *in* S. Turcotte, S. C. Keller & R. M. Cavallo, eds, ‘3D stellar evolution’, Vol. 239, ASP.
- Beer, M. & Davies, M. B. (2003 submitted), ‘Red giant depletion in globular cluster cores’, *MNRAS* .
- Benz, W. (1990), Smooth Particle Hydrodynamics - a Review, *in* ‘Numerical Modelling of Nonlinear Stellar Pulsations Problems and Prospects’, pp. 269–+.
- Benz, W. & Hills, J. G. (1987), ‘Three-dimensional hydrodynamical simulations of stellar collisions. I - Equal-mass main-sequence stars’, *ApJ* 323, 614–628.
- Binney, J. & Tremaine, S. (1987), *Galactic dynamics*, Princeton, NJ, Princeton University Press, 1987, 747 p.
- Bonnell, I. A. & Davies, M. B. (1998), ‘Mass segregation in young stellar clusters’, *MNRAS* 295, 691–+.
- Casertano, S. & Hut, P. (1985), ‘Core radius and density measurements in N-body experiments Connections with theoretical and observational definitions’, *ApJ* 298, 80–94.
- Cohn, H. (1979), ‘Numerical integration of the Fokker-Planck equation and the evolution of star clusters’, *ApJ* 234, 1036–1053.
- Davies, M. B. (1997), ‘Cataclysmic variable production in globular clusters’, *MNRAS* 288, 117–128.
- Davies, M. B., Benz, W. & Hills, J. G. (1991), ‘Stellar encounters involving red giants in globular cluster cores’, *ApJ* 381, 449–461.

- Davies, M. B., Benz, W. & Hills, J. G. (1992), ‘Stellar encounters involving neutron stars in globular cluster cores’, *ApJ* 401, 246–259.
- Davies, M. B., Blackwell, R., Bailey, V. C. & Sigurdsson, S. (1998), ‘The destructive effects of binary encounters on red giants in the Galactic Centre’, *MNRAS* 301, 745–753.
- Davies, M. B. & Hansen, B. M. S. (1998), ‘Neutron star retention and millisecond pulsar production in globular clusters’, *MNRAS* 301, 15–24.
- Davies, M., Piotto, G. & De Angeli, F. (submitted), ‘Blue Straggler production in globular clusters’, *MNRAS*.
- de Kool, M. (1990), ‘Common envelope evolution and double cores of planetary nebulae’, *ApJ* 358, 189–195.
- de la Fuente Marcos, R. & de la Fuente Marcos, C. (2000), ‘On the dynamical evolution of the brown dwarf population in open clusters’, *Ap&SS* 271, 127–144.
- Djorgovski, S. & Piotto, G. (1993a), Color and Population Gradients in Globular Clusters, in ‘ASP Conf. Ser. 50: Structure and Dynamics of Globular Clusters’, pp. 203–+.
- Djorgovski, S. & Piotto, G. (1993b), Dynamically Induced Stellar Population Gradients in Globular Clusters, in ‘ASP Conf. Ser. 48: The Globular Cluster-Galaxy Connection’, pp. 84–+.
- Djorgovski, S., Piotto, G., Phinney, E. S. & Chernoff, D. F. (1991), ‘Modification of stellar populations in post-core-collapse globular clusters’, *ApJL* 372, L41–L44.
- Eggleton, P. P., Fitchett, M. J. & Tout, C. A. (1989), ‘The distribution of visual binaries with two bright components’, *ApJ* 347, 998–1011.
- Fabian, A. C., Pringle, J. E. & Rees, M. J. (1975), ‘Tidal capture formation of binary systems and X-ray sources in globular clusters’, *MNRAS* 172, 15P–+.

- Giersz, M. & Heggie, D. C. (1997), 'Statistics of N-body simulations - IV. Unequal masses with a tidal field', *MNRAS* 286, 709–731.
- Gingold, R. A. & Monaghan, J. J. (1977), 'Smoothed particle hydrodynamics - Theory and application to non-spherical stars', *MNRAS* 181, 375–389.
- Gingold, R. A. & Monaghan, J. J. (1983), 'On the fragmentation of differentially rotating clouds', *MNRAS* 204, 715–733.
- Gizis, J. E. (2000), 'The Frequency of Brown Dwarfs as Companions', *American Astronomical Society Meeting* 197.
- Gizis, J. E., Kirkpatrick, J. D., Burgasser, A., Reid, I. N., Monet, D. G., Liebert, J. & Wilson, J. C. (2001), 'Substellar Companions to Main-Sequence Stars: No Brown Dwarf Desert at Wide Separations', *ApJL* 551, L163–L166.
- Gizis, J. E., Reid, I. N. & Monet, D. G. (1999), 'A 2MASS Survey for Brown Dwarfs toward the Hyades', *Aj* 118, 997–1004.
- Gnedin, O. Y. & Ostriker, J. P. (1997), 'Destruction of the Galactic Globular Cluster System', *ApJ* 474, 223–+.
- Golimowski, D. A., Burrows, C. J., Kulkarni, S. R., Oppenheimer, B. R. & Brukardt, R. A. (1998), 'Wide Field Planetary Camera 2 Observations of the Brown Dwarf Gliese 229B: Optical Colors and Orbital Motion', *Aj* 115, 2579–2586.
- Grindlay, J. E., Heinke, C. O., Edmonds, P. D., Murray, S. S. & Cool, A. M. (2001), 'Chandra Exposes the Core-collapsed Globular Cluster NGC 6397', *ApJL* 563, L53–L56.
- Guenther, D. B., Demarque, P., Pinsonneault, M. H. & Kim, Y.-C. (1992), 'Standard solar model. II - g-modes', *ApJ* 392, 328–336.
- Gunn, J. E. & Griffin, R. F. (1979), 'Dynamical studies of globular clusters based on photoelectric radial velocities of individual stars. I - M3', *Aj* 84, 752–773.

- Haffner, H. & Heckmann, O. (1937), 'Das Farben-Helligkeits-Diagramm der Praesepe auf Grund neuer Beobachtungen', *Veroeffentlichungen der Universitaets-Sternwarte zu Goettingen* 4, 77–95.
- Hambly, N. C., Hodgkin, S. T., Cossburn, M. R. & Jameson, R. F. (1999), 'Brown dwarfs in the Pleiades and the initial mass function across the stellar/substellar boundary', *MNRAS* 303, 835–844.
- Harris, W. E. (1996), 'A Catalog of Parameters for Globular Clusters in the Milky Way', *Aj* 112, 1487–+.
- Harris, W. E. & Racine, R. (1974), 'A C-M diagram for M80 obtained with a new photographic calibration technique', *Aj* 79, 472–+.
- Harris, W. E. & Racine, R. (1979), 'Globular clusters in galaxies', *ARA&A* 17, 241–274.
- Heggie, D. C. (1972), A Multi-Particle Regularisation Technique, in 'Gravitational N-Body Problem, Proceedings of IAU Colloq. 10, held in Cambridge, England, 12–15 August, 1970. Edited by Myron Lecar. D. Reidel Publishing Company, 1971., p.148', pp. 148–+.
- Heggie, D. & Hut, P. (2003), *The gravitational million-body problem*, Cambridge university press.
- Hurley, J. R., Tout, C. A., Aarseth, S. J. & Pols, O. R. (2001), 'Direct N-body modelling of stellar populations: blue stragglers in M67', *MNRAS* 323, 630–650.
- Hurley, J. & Tout, C. A. (1998), 'The binary second sequence in cluster colour-magnitude diagrams', *MNRAS* 300, 977–980.
- Jeans, J. H. (1902), *Phil. Trans. Roy. Astron. Soc.* 199, 1–5.
- Jeans, J. H. (1929), *The universe around us*, New York, The Macmillan company; Cambridge, Eng., The University press [c1929].
- King, I. (1962), 'The structure of star clusters. I. an empirical density law', *Aj* 67, 471–.

- King, I. R. (1966), 'The structure of star clusters. III. Some simple dynamical models', *Aj* 71, 64–+.
- King, I. R. (1985), Observed surface densities in globular clusters, in 'IAU Symp. 113: Dynamics of Star Clusters', pp. 1–15.
- Klose, S. (1986), 'The Rho Ophiuchi cloud - an overview', *Ap&SS* 128, 135–149.
- Kroupa, P. (1995), 'Inverse dynamical population synthesis and star formation', *MNRAS* 277, 1491–.
- Kroupa, P. (2000), 'Constraints on stellar-dynamical models of the Orion Nebula Cluster', *New Astronomy* 4, 615–624.
- Kroupa, P., Petr, M. G. & McCaughrean, M. J. (1999), 'Binary stars in young clusters: models versus observations of the Trapezium Cluster', *New Astronomy* 4, 495–520.
- Kroupa, P., Tout, C. A. & Gilmore, G. (1993), 'The distribution of low-mass stars in the Galactic disc', *MNRAS* 262, 545–587.
- Lançon, A. & Boily, C. M., eds (2000), *Massive Stellar Clusters*.
- Leinert, C., Zinnecker, H., Weitzel, N., Christou, J., Ridgway, S. T., Jameson, R., Haas, M. & Lenzen, R. (1993), 'A systematic approach for young binaries in Taurus', *A&A* 278, 129–149.
- Leonard, P. J. T. & Livio, M. (1995), 'The Rotational Rates of Blue Stragglers Produced by Physical Stellar Collisions', *ApJL* 447, L121+.
- Livio, M. & Pringle, J. E. (1992), 'Dwarf nova outbursts - The ultraviolet delay and the effect of a weakly magnetized white dwarf', *MNRAS* 259, 23P–26P.
- Lombardi, J. C., Rasio, F. A. & Shapiro, S. L. (1996a), 'Collisions of Main-Sequence Stars and the Formation of Blue Stragglers in Globular Clusters', *ApJ* 468, 797–+.
- Lombardi, J. C., Rasio, F. A. & Shapiro, S. L. (1996b), 'Collisions of Main-Sequence Stars and the Formation of Blue Stragglers in Globular Clusters', *ApJ* 468, 797–.

- Lucy, L. B. (1977), ‘A numerical approach to the testing of the fission hypothesis’, *Aj* 82, 1013–1024.
- Luhman, K. L. & Rieke, G. H. (1998), ‘The Low-Mass Initial Mass Function in Young Clusters: L1495E’, *ApJ* 497, 354–+.
- Luhman, K. L., Rieke, G. H., Lada, C. J. & Lada, E. A. (1998), ‘Low-Mass Star Formation and the Initial Mass Function in IC 348’, *ApJ* 508, 347–369.
- Luhman, K. L., Rieke, G. H., Young, E. T., Cotera, A. S., Chen, H., Rieke, M. J., Schneider, G. & Thompson, R. I. (2000), ‘The Initial Mass Function of Low-Mass Stars and Brown Dwarfs in Young Clusters’, *ApJ* 540, 1016–1040.
- Martín, E. L., Brandner, W., Bouvier, J., Luhman, K. L., Stauffer, J., Basri, G., Zapatero Osorio, M. R. & Barrado y Navascués, D. (2000), ‘Membership and Multiplicity among Very Low Mass Stars and Brown Dwarfs in the Pleiades Cluster’, *ApJ* 543, 299–312.
- Mazeh, T. & Goldberg, D. (1992), ‘On the study of the mass ratio of spectroscopic binaries’, *ApJ* 394, 592–598.
- Monaghan, J. J. & Lattanzio, J. C. (1985), ‘A refined particle method for astrophysical problems’, *A&A* 149, 135–143.
- Nakajima, T., Oppenheimer, B. R., Kulkarni, S. R., Golimowski, D. A., Matthews, K. & Durrance, S. T. (1995), ‘Discovery of a Cool Brown Dwarf’, *nature* 378, 463–+.
- Odenkirchen, M., Grebel, E. K., Rockosi, C. M., Dehnen, W., Ibata, R., Rix, H., Stolte, A., Wolf, C., Anderson, J. E., Bahcall, N. A., Brinkmann, J., Csabai, I., Hennessy, G., Hindsley, R. B., Ivezić, Ž., Lupton, R. H., Munn, J. A., Pier, J. R., Stoughton, C. & York, D. G. (2001), ‘Detection of Massive Tidal Tails around the Globular Cluster Palomar 5 with Sloan Digital Sky Survey Commissioning Data’, *ApJL* 548, L165–L169.
- Ott, F. & Schnetter, E. (2003 submitted), ‘A modified sph approach for fluids with large density differences’, *Journal of Computational Physics* .

- Pinfield, D. J., Hodgkin, S. T., Jameson, R. F., Cossburn, M. R., Hambly, N. C. & Devereux, N. (2000), 'A six-square-degree survey for Pleiades low-mass stars and brown dwarfs', *MNRAS* 313, 347–363.
- Pinfield, D. J., Jameson, R. F. & Hodgkin, S. T. (1998), 'The mass of the Pleiades', *MNRAS* 299, 955–964.
- Portegies Zwart, S. F., McMillan, S. L. W., Hut, P. & Makino, J. (2001), 'Star cluster ecology - IV. Dissection of an open star cluster: photometry', *MNRAS* 321, 199–226.
- Preston, G. W. & Sneden, C. (2000), 'What Are These Blue Metal-Poor Stars?', *Aj* 120, 1014–1055.
- Procter Sills, A., Bailyn, C. D. & Demarque, P. (1995), 'Are Blue Stragglers Mixed during Collisions?', *ApJL* 455, L163+.
- Rasio, F. A. & Livio, M. (1996), 'On the Formation and Evolution of Common Envelope Systems', *ApJ* 471, 366–+.
- Rasio, F. A. & Shapiro, S. L. (1990), 'Encounters between compact stars and red giants in dense stellar systems', *ApJ* 354, 201–210.
- Rasio, F. A. & Shapiro, S. L. (1991), 'Collisions of giant stars with compact objects - Hydrodynamical calculations', *ApJ* 377, 559–580.
- Reid, I. N. & Mahoney, S. (2000), 'Low-mass spectroscopic binaries in the Hyades: a candidate brown dwarf companion', *MNRAS* 316, 827–844.
- Renvoizé, V., Baraffe, I., Kolb, U. & Ritter, H. (2002), 'Distortion of secondaries in semi-detached binaries and the cataclysmic variable period minimum', *A&A* 389, 485–493.
- Richichi, A., Leinert, C., Jameson, R. & Zinnecker, H. (1994), 'New binary young stars in the Taurus and Ophiuchus star-forming regions', *A&A* 287, 145–153.

- Ritter, H. (1988), 'Turning on and off mass transfer in cataclysmic binaries', *A&A* 202, 93–100.
- Rosswog, S. & Davies, M. B. (2002), 'High-resolution calculations of merging neutron stars - I. Model description and hydrodynamic evolution', *MNRAS* 334, 481–497.
- Rucinski, S. M. (2000), 'W UMA-Type Binary Stars in Globular Clusters', *Aj* 120, 319–332.
- Sandage, A. R. (1953), 'The color-magnitude diagram for the globular cluster M 3.', *Aj* 58, 61–+.
- Sandquist, E. L., Bolte, M. & Hernquist, L. (1997), 'Composition Mixing during Blue Straggler Formation and Evolution', *ApJ* 477, 335–.
- Sargent, W. L. W. & Searle, L. (1968), 'A Quantitative Description of the Spectra of the Brighter Feige Stars', *ApJ* 152, 443–+.
- Shara, M. M., Drissen, L., Rich, R. M., Paresce, F., King, I. R. & Meylan, G. (1998), 'Supra-Horizontal-Branch Stars and Population Gradients in the Galactic Center Globular Cluster NGC 6522', *ApJ* 495, 796–+.
- Shara, M. M., Saffer, R. A. & Livio, M. (1997), 'The First Direct Measurement of the Mass of a Blue Straggler in the Core of a Globular Cluster: BSS 19 in 47 Tucanae', *ApJL* 489, L59+.
- Sills, A., Adams, T. & Davies, M. B. (2003), 'Blue stragglers as stellar collision products: The angular momentum question, in prep.', *MNRAS* .
- Sills, A., Adams, T., Davies, M. B. & Bate, M. R. (2002), 'High-resolution simulations of stellar collisions between equal-mass main-sequence stars in globular clusters', *MNRAS* 332, 49–54.
- Sills, A., Baily, C. D., Edmonds, P. D. & Gilliland, R. L. (2000), 'The Formation Rate of Blue Stragglers in 47 Tucanae', *ApJ* 535, 298–303.

- Sills, A., Faber, J. A., Lombardi, J. C., Rasio, F. A. & Warren, A. R. (2001), 'Evolution of Stellar Collision Products in Globular Clusters. II. Off-Axis Collisions', *ApJ* 548, 323–334.
- Sills, A. & Lombardi, J. C. (1997), 'The Importance of Realistic Starting Models for Hydrodynamic Simulations of Stellar Collisions', *ApJL* 484, L51+.
- Sills, A., Lombardi, J. C., Baily, C. D., Demarque, P., Rasio, F. A. & Shapiro, S. L. (1997), 'Evolution of Stellar Collision Products in Globular Clusters. I. Head-on Collisions', *ApJ* 487, 290–+.
- Skrutskie, M. F., Beichman, C., Capps, R., Carpenter, J., Chester, T., Cutri, R., Elias, J., Elston, R., Huchra, J., Liebert, J., Lonsdale, C., Monet, D., Price, S., Schneider, S., Seitzer, P., Stiening, R., Strom, S. & Weinberg, M. (1995), The Two Micron All Sky Survey (2MASS), Vol. 27, pp. 1392–+.
- Spitzer, L. J. (1940), 'The stability of isolated clusters', *MNRAS* 100, 396–+.
- Spitzer, L. J. (1949), 'The Formation of Stars', *Leaflet of the Astronomical Society of the Pacific* 5, 336–+.
- Spitzer, L. J. & Chevalier, R. A. (1973), 'Random Gravitational Encounters and the Evolution of Spherical Systems. V. Gravitational Shocks', *ApJ* 183, 565–582.
- Stauffer, J. R., Hamilton, D. & Probst, R. G. (1994), 'A CCD-based search for very low mass members of the Pleiades cluster', *Aj* 108, 155–159.
- Steele, I. A. & Jameson, R. F. (1995), 'Optical spectroscopy of low-mass stars and brown dwarfs in the Pleiades', *MNRAS* 272, 630–646.
- Stetson, P. B. (1994), 'The center of the core-cusp globular cluster M15: CFHT and HST Observations, ALLFRAME reductions', *PASP* 106, 250–280.
- Terlevich, E. (1987), 'Evolution of n-body open clusters', *MNRAS* 224, 193–225.
- Truss, M. R. (2002), 'Outburst Behaviour of Accretion Discs In Close Binary Systems', *Ph.D. Thesis* .

Verbunt, F. (1984), 'Mass transfer and the period gap of cataclysmic variables', *MNRAS* 209, 227–240.

Verbunt, F. & Hut, P. (1987), The Globular Cluster Population of X-Ray Binaries, *in* 'IAU Symp. 125: The Origin and Evolution of Neutron Stars', pp. 187–+.

Wilking, B. A. & Lada, C. J. (1983), 'The discovery of new embedded sources in the centrally condensed core of the Rho Ophiuchi dark cloud - The formation of a bound cluster', *ApJ* 274, 698–716.